Pocket beach wave processes and current systems investigated via field and numerical modelling studies: A case study of Okains Bay

A thesis submitted in fulfillment of the requirements

for the degree of

Doctor of Philosophy in Environmental Science

at the University of Canterbury

By

Arash Eisazadeh Moghaddam

University of Canterbury

2014

Abstract

Confined coasts in general, and pocket beach environments in particular, are under huge development pressures worldwide, not least due to their sheltered nature and perceived shoreline stability. However, understanding of their physical functioning is poor in comparison to that of open coast beaches. This study aims to improve understanding in terms of the existing gaps in knowledge of wave processes and nearshore currents, and also to examine the importance of local wind and tide factors in generating nearshore currents, in micro-tidal pocket beaches. The boundaries of embayments are generally recognized as important controls of their beach processes and responses, yet little detailed knowledge exists of how the exact embayment dimensions and characteristics influences these processes. One key embayment feature the influence of which is poorly understood is the downcoast headland. In this thesis, field observations plus Zanuttigh and Van der Meer's (2008) approach, and the SWAN wave model were used to evaluate the downcoast headland effects on wave processes within Okains Bay, an example pocket beach environment. The results showed that incident wave heights and directions were significantly influenced by wave reflection processes from the downcoast headland inside the bay. The intensity of reflection effects on wave characteristics inside the pocket beach varied according to approaching wave direction. Reflection effects reduced when waves approached from angles close to parallel to the headlands, increasing towards headland-perpendicular wave approaches.

Field observations and the XBeach model were used to examine whether or not tides can significantly influence nearshore currents within example and model pocket beach environments. Results indicated that tides can be the primary driver of nearshore currents close to the bed inside micro-tidal pocket beaches, depending on incident wave conditions. In areas of micro-tidal pocket beaches exposed to direct approaching waves, currents were wave driven, while in areas further into the bay that experienced headland filtering of their wave environment, currents were mainly tide generated.

The results of this study demonstrated how the current circulation system within micro-tidal pocket beaches is related to the incoming directions of offshore waves. If high energy waves approach oblique or normal to the shoreline (with the assumption that the shoreline is at 90° to the headlands), the current system was found to consist of longshore currents influenced by headlands, plus a rip current in the center of the shoreline or a toporip in proximity to headlands. The location of the rip current or toporip was determined by the direction of

approaching incident waves.

This study also examined the behavior of local winds in a pocket beach environment and their consequent effects on nearshore currents. Results for Okains Bay show that local winds tended to blow in offshore and onshore directions, as the bay is located in a valley, so orographic effects channel and shift the wind directions to angles close to offshore and onshore directions inside the bay. Results also indicated that local winds influence the hydrodynamic currents of pocket beaches that are confined by elevated topography, producing semi-cross shore influences since the winds are topographically channelled to blow in predominantly offshore and onshore directions.

This research significantly refines our understanding of micro-tidal pocket beach wave and current processes, including quantification of the filtering effects of headlands on their wave environments, revealing the various and variable influences of tides and winds compared to in open coast beaches; and, significantly, highlighting the role of downcoast headland wave reflection effects. With regard to the latter, this research elucidates some key process differences between pocket and embayed beaches and clarifies reasons why the application of embayed beach models that include refraction and diffraction but exclude reflection effects to the study of pocket beaches is inappropriate for studying pocket beaches. This research also provides methodological and topic suggestions for future research on pocket beach environments, including how to use the improved hydrodynamic knowledge of this study in future studies seeking to better understand pocket beach sediment systems, a topic that was beyond the scope of the current research.

Keywords: Pocket beach; Reflection; Diffraction; Downcoast headland; Upcoast headland; Wave height; Wave direction; Current systems; Tides; Local winds.

Acknowledgments

This research was made possible through the help and support from everyone, including my wife, my parents, and family and, in essence, all sentient beings. First and foremost, I would like to thank Dr Deirdre Hart, Dr Peyman Zawar-Reza, Mr Derek Todd and Dr Martin Single for their great efforts in supervising and leading me to accomplish this work. I would like to extend my gratitude to Mr Brandon Strong, Senior, from Teledyne RD Instruments, for help with the analysis of the downward-facing ADCP data.

I am also very thankful to Dr Rober McCall, from University of Plymouth, for his precious time in advising me on the XBeach model setup. Also I appreciate Mr Bruce Gabites efforts, from ECAN, for providing the deep water wave buoy data, and Dr Richard Gorman, from NIWA, for providing 40 years wave hindcast. My especial thanks goes to Mr Nicholas Key and Mr Justin Harrison, from the University of Canterbury, New Zealand, for assisting me in accomplishing the field measurements in Okains Bay.

This research was supported by New Zealand Coastal Society PhD scholarship (2009), Department of Geography PhD Research fund and the Coastal and Ocean Engineering Conference fund.

Table of Contents

Part II: NEARSHORE CURRENT PROCESSES IN POCKET BEACHES

LIST OF FIGURES

LIST OF TABLES

Chapter 1: Introduction and research problem

This chapter introduces the research background, highlights the research objectives and the questions that needed to be answered, and outlines the structure of the thesis.

1.1. Thesis statement

This study investigates wave and current processes operating within a micro-tidal pocket beach environment based on fieldwork and numerical modelling, using the SWAN wave model and the two dimensional hydrodynamic, morphodynamic XBeach model. About 80% of coastlines worldwide are confined by one or two headlands, forming headland-enclosed bay beaches (Ojeda and Guillen, 2008). Little research has focused on the wave, current and morphodynamics processes operating in such environments (Dehouck *et al*., 2009). This means that the operation of these processes in headland-enclosed bay beaches, especially for beaches with two long headlands or pocket beaches, is poorly documented. This thesis examines the wave and current processes operating in a case study pocket beach environment - Okains Bay, Banks Peninsula, New Zealand (Figure 1.1). It also evaluates the importance of winds and tides in controlling nearshore currents in pocket beach environments. Note that the bathymetric data were obtained from Land Information New Zealand (LINZ) with a resolution of 3.18 m.

Studies on headland-enclosed bay beaches (Dehouck *et al*., 2009; Klein *et al*., 2002; Short, 1999 and 2010) suggest that net sediment transport is limited, and long-term shoreline changes are minor, despite short-term variations in wave conditions. Hart and Bryan (2008) showed that if the length of the shoreline in embayments is longer and beaches are more connected, sediment transport or bypassing is more likely and this sediment movement can control the planform morphology of headland-enclosed bay beaches. Individual storm events can cause considerable gross sediment transport, thereby altering the shoreline; but observations to date suggest that these shoreline responses to storms are dampened compared to those of open coast beaches (Dehouck *et al*., 2009; Klein *et al*., 2002). Accordingly, the construction of artificial two-headland-bay beaches (e.g. see Cooper and Alonso 2006), such

as embayed (bays enclosed by two short headlands) and pocket beaches (bays enclosed by two long headlands) has recently been recommended as a tool to stabilize shorelines in various coastal settings (Ojeda and Guillen, 2008; Williams and Micallef, 2009) since these structures are perceived as amenity friendly in many parts of the world (Williams et al. 2005). Given that our understanding of the detailed wave and nearshore current processes operating within pocket beach environments is poor, more observations and models elucidating the hydrodynamics of these environments is arguably needed for effective coastal management of both artificial and natural pocket beach settings.

It has been suggested that wind and tides may play a key role in controlling nearshore currents and sediment transport in micro-tidal pocket beaches (Dehouck *et al*., 2009). Incident waves can only approach pocket beach shorelines from a limited directional sector, so the strength of wave-driven nearshore currents inside headland enclosed bays is likely to differ from that of open coast beaches subject to the same offshore wave climate. Thus, the wind and tide effects on the currents and sediment transport might be more accentuated in pocket beaches relative to in adjacent open coast beaches.

Further, the majority of pocket beach research has been conducted in meso- and macro-tidal environments (Dehouck *et al.*, 2009). Scant data exists on the influence of tides in micro-tidal pocket beach environments. The effect of local winds on currents in pocket beaches during different wave conditions, especially under different wave directions, is also poorly documented. This study seeks to examine the importance of local winds and tides on nearshore currents affecting micro-tidal pocket beaches.

The term 'downcoast headland' is used in this thesis to refer to the headland furthest from the wave approach direction while upcoast headland is used to refer to the headland that the approaching waves reach first. As such the downcoast and upcoast designations are not permanently fixed to one of the two pocket beach headlands but rather change based on the direction of approaching waves. Pocket beaches that experience a predominant wave approach also have a predominant upcoast and downcoast headland but these terms may be used without the 'predominant qualifier' when talking about current wave conditions and headland labels.

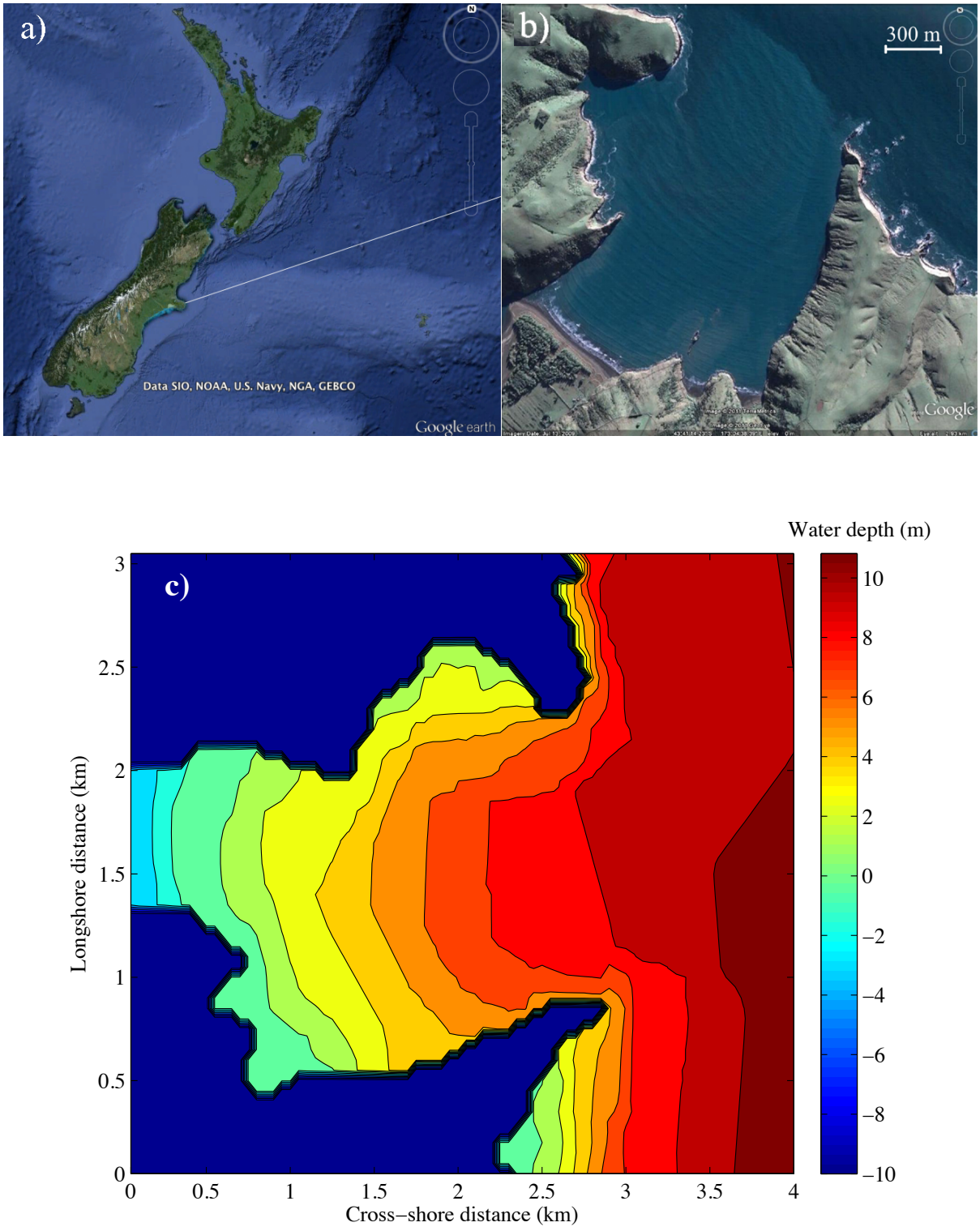

Figure 1.1. Okains Bay is a pocket beach embayed between two rocky headlands and facing east to the Pacific Ocean from Banks Peninsula, Canterbury, New Zealand (Google Earth, 2011) (a and b), Okains Bay bathymetric contours (c).

Figure 1.2. Beaches embayed by rocky headlands on the east coast of Canterbury, New Zealand, 43°43'S and 173°06' E (Google Earth, 2010).

1.2. Significance of this study for understanding natural pocket beaches

Pocket beaches are areas constrained between two long, shore-normal extremes such as rocky headlands, groynes, breakwaters and peninsulas, which are either artificial or natural (Figure 1.2). In such environments, the longshore currents and sediment transport are topographically controlled by the headlands close to which one or two rip currents or megarips might be formed (Short, 1999). In pocket beaches, gross sediment transport is limited and sands are mostly carried from one side of the beach to the other during different wave conditions, a process called beach rotation.

Since natural pocket beaches often have outstanding beauty and natural character values, these areas can be an important tourist attraction. The natural extension of mountains into the sea, with the formation of sandy beaches in between, creates spectacular scenery (Figure 1.3), which is a significantly valuable aspect of any coastal environment (Ergin and Williams, 2006). Many coastlines around the world consist of natural embayed and pocket

beaches, some of which have already been developed; these are renowned as popular beaches for locals and tourists alike. Such beaches include the Tasman region of New Zealand, Alexandra Headland beach in Australia and Kamari beach in Greece. Although New Zealand is a country with a high percentage of natural embayed and pocket beaches, many of these areas have not yet been developed in terms of human habitation and infrastructure. Knowledge about hydrodynamics and sediment transport mechanisms in natural pocket beaches could enable tourism industries to invest wisely in these areas by building infrastructure and basic necessities for tourists that will withstand the test of time in proximity to the coastlal environment.

A better understanding of the nature of pocket beaches can also be an early step in considering the relocation of highways, ports, manufacturing industries, factories and businesses, which need to be built close to the sea, whether in erosional and expensive-to-maintain open coast areas or embayed and pocket beaches. Over half of the world's population lives in close proximity to coastlines (McGranahan *et al*., 2007) and this proportion is growing disproportionately (Nicholls and Mimura, 1998). New Zealand is following this trend of coastal zone population concentration, with an estimated 75% of its residents living within 10 km of the coast (Statistics New Zealand, 2012). This has encouraged many businesses and factories to be run or built in areas close to the sea. Some of these areas have been facing erosion issues due to periodic storms, climate change and sea level rises. Therefore, coastal managers have often had to construct sea defences to protect coast-proximal lands. These constructions not only require regular maintenance, but they typically have significant negative effects on the natural environment and often shift the coastal management issue to adjacent areas. Since the shoreline of natural embayed and pocket beaches is protected by two headlands, which operate as natural sea defences, these environments are usually more sheltered than open coasts and hence their shorelines are often more stable during different wave conditions. Therefore, the shoreline of pocket beaches might experience fewer changes due to sea level rise or climate change, relative to open coast beaches. A better understanding of the nature of pocket beaches and also a detailed examination of long- and short-term shoreline stability are desirable if infrastructure and habitation are to be encouraged to locate in proximity to such environments.

Figure 1.3. Okains Bay, Banks Peninsula, Canterbury, New Zealand.

In the past few decades, artificial pocket beaches, or pairs of parallel hard structures, have also been recommended for many eroding coastlines around the world as a tool to stabilise the shoreline (Ojeda and Guillen, 2008). Some examples of artificial pocket beaches can be seen in the shorelines of: Barcelona, Spain, (Figure 1.4); Chesapeake Bay, USA; and Rayong, Thailand (Hardaway and Gunn, 2010; Iglesias *et al*., 2010; Hsu *et al*., 2010). Erosion is one of the major problems which coastal managers have been facing in a variety of beaches, especially after the occurrence of a severe storm.

Some beaches are popular recreational areas, so tourism industries have invested large sums of money to attract more tourists. Other beaches separate the sea from houses, farms or main roads. Long-term shoreline erosion can, therefore, seriously jeopardise the tourism industry, people's properties or government lands. Construction of breakwaters along the shore, such as bulkheads, groins or stone revetments, or sand nourishment is a traditional method of restoring the beach. These constructions might threaten the beach or sea habitats as a result of bottom scour (Hardaway and Gunn, 2010).

The combination of artificial pocket beaches, sand nourishment, or sometimes wetlands plantings seems could be an effective defensive method for protecting shorelines, and also to enhance the beach and sea habitats (Hardaway and Gunn, 2010). I personally believe that although breakwaters or seawalls might stop or reduce erosion in a particular location, they can also damage the natural environment and shift the issue to adjacent areas. However, coastal managers sometimes face the dilemma of choosing between solutions that offer a minimum of damage to the natural environment and which can save the valuable coastal lands. In order to make such decisions, it is crucial to have the best understanding possible of how they function. Currently our knowledge of pocket beach solutions is very poor.

The purpose of creating artificial pocket beaches is to mirror the apparent shoreline stability and sheltered environment that natural pocket beaches are believed to be characterised by. Little research has quantified these characteristics for natural pocket beaches, or explored their process environments. In order to better understand the nature of artificial pocket beaches and to better design them, it is necessary to improve our knowledge of nearshore current processes in natural pocket beaches under different incident wave conditions, especially storm events.

Figure 1.4. Artificial pocket beaches, La Fonda del Port Olympic, Barcelona, Spain, in August 2003 (a), and in October 2010 (b) (Google Earth, 2011).

1.3. Overview of headland-enclosed bay beach studies, including pocket beaches

Pocket beaches are a subcategory of headland-enclosed beaches, but no research to date has precisely classified the terms of embayed and pocket beaches. Researchers working on headland-enclosed bay beaches have used the terms "embayed" and "pocket" beaches for both one- (Uda *et al*., 2010; Oliveira and Barreiro, 2010) and two-headland bay beaches (e.g. Hardaway and Gunn, 2010; Klein et al., 2010; Dehouck *et al*., 2009; Hsu *et al.,* 2008). The published classification scheme designed for application in headland-enclosed bay beaches is

based on current circulations, developed by Short (1999). This classification indicates whether the current system is topographically controlled by headlands or not. However, pocket beaches can be classified as beaches confined by two headlands with a cellular current system, and embayed beaches can be defined as beaches confined by two headlands with a transitional current system (Prof A. Short, University of Sydney, Coastal scientists, pres. comm. 28/07/2010). According to this classification, the net sediment transport state for a pocket beach might vary from limited to considerable, depending on the size of the bay and length of the headlands. Therefore the shoreline could be either steady or vulnerable to quick changes.

Woodroffe (2002) briefly defines the terms "pocket" and "embayed" beaches. Embayed beaches are defined as areas where the upcoast headland controls the shape of the shoreline and refracted waves form a shadow zone with a long straight shoreline towards the downcoast headland. Pocket beaches are defined as very deep enclosed beaches so that wave crests in the breaker line are often parallel to the shoreline. However, no method is available to determine when deep enclosed beaches are called pocket beaches. Is a deep dissipative enclosed beach with a closure depth outside the bay called a pocket beach? For example, Shelly beach, in Australia, with a short upcoast headland compared to the length of its shoreline, is called an embayed beach according to Woodroffe's (2002) definition, but the degree of updrift curvature is similar to that of the downdrift curvature and there is no shadow zone. Also the beach planform of Shelly beach is very similar to that of Okains Bay, in New Zealand, with two long headlands, which can be defined as a pocket beach according to Woodroffe's (2002) definition. This similarity of the beach planform can be explained by the orientation of beaches to the incident waves. However, in this thesis, the terms pocket and embayed beaches are classified similarly to Woodroffe's (2002) definition, but with some modifications in their definitions.

The major difference between open coast beaches and embayments is the limitation on longshore and cross-shore sediment transport imposed in embayments by the presence of headland(s). This rate could be reduced in beaches with two long headlands, especially for beaches where the closure depth is inside the bay. More studies are needed to clearly morphodynamically distinguish, and thus classify, embayments into pocket and embayed beach types.

The majority of research on embayed coasts has been conducted on beaches enclosed by one headland, such as hooked bay beaches, or on beaches with two short headlands and similar features to hooked bay beaches (Hsu and Evans, 1989; Silvester and Hsu, 1999; Hsu *et al.,* 2008; Klein *et al.,* 2002b, 2010; Hart and Bryan, 2008). In such environments, nearshore current systems and thus sediment transport mechanisms have been studied during different wave conditions (Silvester and Hsu, 1999). These results were then used to develop models based on logarithmic spirals, hyperbolic tangents and parabolic shapes, in order to predict the shoreline planform (or shoreline curvature) that would result in states of stasis or equilibrium (Silvester, 1970; Hsu and Evans, 1989; Moreno and Kraus, 1999; Martino *et al.,* 2003; Hsu *et al.*, 2008). Amongst these models, the parabolic shape model is reportedly the state of the art method to show a best fit for the shoreline of one-headland bay beaches in static equilibrium (Hsu *et al.,* 2008, 2010; Hardaway and Gunn, 2010; Jackson and Cooper, 2010).

Other studies on one-headland bay beaches have focused on the stability of the shoreline and short-term changes in shoreline planform or beach rotation processes (Bryan *et al*., 2013; Klein *et al*., 2002 and 2010; Silva *et al*., 2010; Ojeda and Guillen, 2008; Short 1999 and 1995; Cowell *et al*., 1996). These studies indicated that net sediment transport in such beach environments is very limited with the sediment mostly moving from one side of the bay to another under different wave conditions. Cowell *et al.* (1996) proposed a formula to estimate the amplitude of beach rotation in one-headland bay beaches, and Klein *et al*. (2002) used this formula to study beach rotation in embayed beaches (beaches enclosed by two short headlands).

After the development of hard engineering practices using pairs of parallel hard structures to create artificial pocket beaches, there has been some research produced focusing on beaches with two long headlands (e.g. Short, 1999, 2010; Dehouck *et al.,* 2009; Hsu *et al.,* 2008, 2010). The majority of these studies examined beach morphodynamics and shoreline predictions with the assumption that wave processes, nearshore currents and sediment transport mechanisms in such environments are similar to those of one-headland bay beaches. For instance, Hsu *et al.* (2008) and (2010) applied the parabolic shape equation to both embayed and pocket beaches with their one and two diffraction points respectively. Although developed for one-headland bay environments with only one diffraction point, this method can be applied to beaches with two diffraction points. That is because the parabolic shape model can take into account the effect of each headland on the shoreline separately. If the bay has only one diffraction point, it is recommended that the same approach is used as in studies

of one-headland bay beaches. Despite there being some research that has been conducted on pocket beaches (or two-long-headland bay beaches), their hydrodynamics and morphodynamics are poorly documented, in particular the influence of the length of headlands.

1.4. Summary of research problems and questions

The overarching purpose of this study is to explore wave and current processes operating within a micro-tidal pocket beach hydrodynamic environment. In order to achieve this purpose, the thesis is structured around the following set of aims:

1) To examine the effects on pocket beach wave and current environments of interactions between wave approach and the two headlands, including the filtering of waves entering the bay, and the operation of refraction and diffraction processes;

2) To examine the influence on pocket beach wave and current environments of the reflection of waves off the downcoast headland within a pocket beach bay;

3) To establish whether or not tides and local winds operate as important influences on the wave and nearshore current environment inside pocket beach bays, and

4) To conduct a preliminary review of the applicability to pocket beaches of existing embayed beach shoreline equilibrium shoreline equations and models based on an understanding of the similarities and differences between their hydrodynamic process environments.

Short (1999) and (2010) studied the nearshore current systems, especially rip currents, in embayments. He stated that longshore currents are topographically controlled by headlands. However, information on the actual effects of the length of headlands on longshore currents is poorly documented. My review of pocket beach process research indicates that if the upcoast headland is long enough to shelter a part of, or the entire, shoreline from approaching incident waves, surface water level differences are the main cause of currents being generated in the opposite direction to that of the longshore currents generated by oblique incident waves. This idea will be tested using SWAN and XBeach simulations in Okains Bay, the results of which contribute towards thesis aim 1.

The numbers of rip currents generated depends on the length of the upcoast headland and on the approaching incident wave directions. According to Short (1999), if an embayment has a cellular current system, it shows that headlands topographically control the nearshore current system. Therefore, two rip currents or megarips will form in proximity to the headlands,

depending on wave conditions. However, my review of pocket beach process research indicates that the number of rip currents may drop to one if the waves cannot directly approach the shoreline, thus, longshore currents will be generated by surface water level differences (Figure 1.5). This idea also contributes towards thesis aims 1 and 2.

Since incident waves can only directly approach the shoreline from a limited range of directions, the effect of winds and tides on nearshore currents could be accentuated in such environments relative to the effects that waves have in open coast settings. My review of pocket beach process research indicates that when incident waves cannot directly approach the shoreline, the effect of strong winds and tidal currents could dominate the nearshore current systems. This study will explicitly examine the importance of winds and tides inside pocket beaches. This idea fits into thesis aims 3.

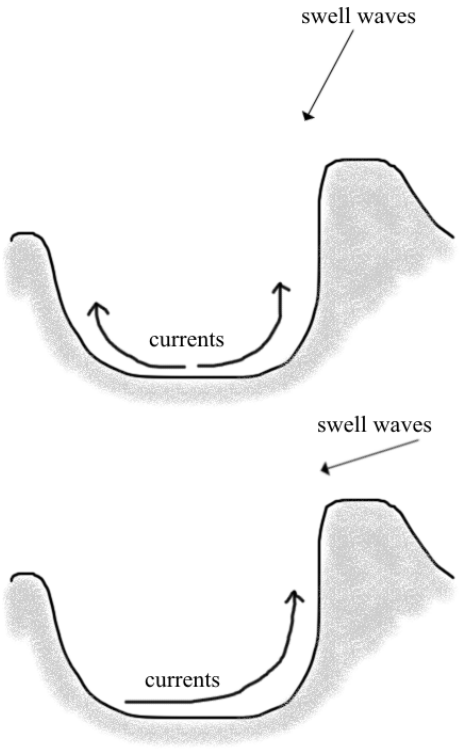

Figure 1.5. Changes in the number of rip currents depending on the direction of approaching swell waves in pocket beaches.

The thesis aims will be achieved using field data and numerical modelling. The different components of this work are outlined in Figure 1.6. As discussed in Chapter 2, the process environments of pocket beaches differ in fundamental ways from those of open coast beaches due to: (a) the limits placed on their wave climate by their confined geometries, and (b) their potentially greater dependence on wind and tide processes to induce sediment transport. Owing to the unique theoretical challenges posed by quantifying sediment transport in pocket beaches, this research has significant potential to contribute to understanding of: how wave processes, including those characterised by low to high energy, could alter when they enter a pocket beach; the current circulation system inside a pocket beach; and the role of wind and tides in controlling pocket beach nearshore currents.

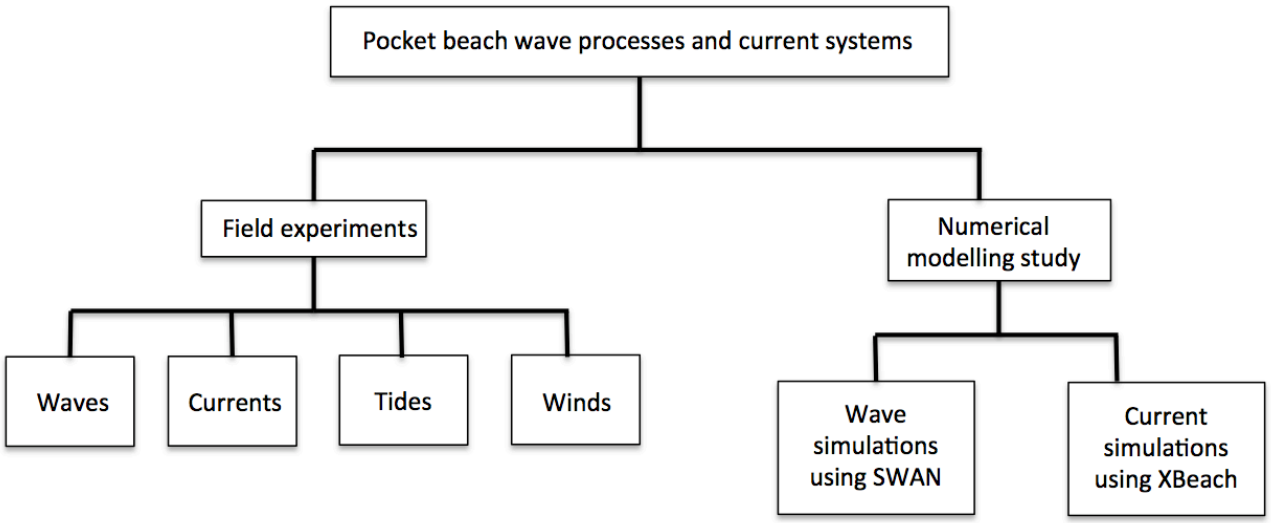

Figure 1.6. Conceptual model of the research approach.

1.5. Organisation of the thesis

This study aims to explore wave and current processes operating within a micro-tidal pocket beach environment. Accordingly the results section of this thesis are structured into two parts. The first part consists of chapters 2 to 4, which discusses wave processes inside and outside

Okains Bay, and also evaluates the importance of reflection in pocket beaches. The second part consists of chapters 5 to 6, which studies nearshore currents under the influence of incident waves, tides and local winds.

These results sections are led into via the current chapter, an introduction to the thesis that explained the importance of doing this research. The literature on headland bay beaches, including pocket beaches was also briefly reviewed. Chapter 2 focuses on the wave processes in more detail within pocket beach bays using three field experiments. In this chapter, wave processes in pocket, embayed and open coast beaches will be discussed.

Chapters 3 concentrates on remapping waves outside Okains Bay using deep water wave data. Since wave data outside the bay were not collected during Field Experiments 2 and 3, it is necessary to predict wave data in this area. In order to find the best approach, linear regression, Linear Wave Theory and the SWAN model were used to predict wave characteristics outside the bay using deep water wave data. Then the results were compared with field data and the best approach was examined for this area.

Chapter 4 focuses on empirical and numerical modeling of wave processes inside Okains Bay. This chapter discusses the importance of reflection in controlling wave processes inside Okains Bay under different deep water wave directions.

Chapter 5 discusses nearshore currents inside Okains Bay using field experiments. This chapter also studies the influence of tides and local winds on nearshore currents during different wave conditions in areas seaward of the breaking zone and also inside the surf zone.

The current system inside the bay is discussed in Chapter 6 using the XBeach model. In this chapter the results of the model were first validated against observations. Then the current system inside the bay was examined during low and high energy waves to better understand the effect of bay characteristics on the current system.

Finally, Chapter 7 is a discussion and conclusion chapter. It is a summary of the main research findings, and it discusses how the results contribute to and, at times, challenge pre-existing views of the workings of pocket beach environments.

Part I: Wave processes in pocket beaches

Chapter 2: Wave observations in Okains Bay

This chapter focuses on wave climates at Okains Bay using field experiments in order to investigate the processes that make pocket beaches unique in terms of wave processes. This chapter contributes towards thesis aims 1 and 2 by starting to investigate the similarities and differences between wave environments inside pocket beach bays and, thus, the effect of headland-wave approach interactions. This chapter also contributes understanding of wave processes towards fulfilling thesis aim 4.

2.1. Introduction

Wave transformation from deep water to shallow water in open coast environments has been widely studied (Eckart, 1952; Cialone and Kraus, 1987; Abreu *et al.*, 1992; Liu, 1994; Davidson-Arnott, 2010). However, wave propagation inside pocket beaches is poorly documented. The majority of research on wave transformation was carried out on embayed beaches or beaches enclosed by one headland (Daly *et al., 2014* ;Woodroffe, 2002; Silvester and Hsu, 1999). Diffraction mainly influences the wave processes inside embayed beaches, and, consequently, it is responsible for the shoreline shape (Klein *et al*., 2002). However, when a shoreline is sheltered by two headlands, in addition to diffraction, reflection could also affect wave processes inside the bay. This chapter examines the important factors in controlling wave processes inside pocket beaches. This chapter discusses observations inside a pocket beach at different depths under a variety of incident wave conditions. Then, the following chapters of Part 1 will numerically evaluate the highlighted factors in controlling wave processes inside pocket beaches.

When a group of ocean waves propagate in deep water, their crests are parallel, and their heights and steepness increase as they travel to shallow water (Bird, 2000). However, when waves enter intermediate and shallow waters, the sea floor influences the wave characteristics, such as wave heights and directions. Generally, when waves move towards the shallow water of open coast beaches, the wave characteristics are modified by a number of processes: dispersion, development of wave asymmetry, shoaling and refraction (Masselink and Hughes,

2003). Note that some of these processes, such as dispersion, could also happen in deep water, but refraction and shoaling are unlikely to influence the wave processes.

A wave field developing in deep water consists of different wave periods (Sorensen, 1997; Masselink and Hughes, 2003). In deep water waves with longer periods travel faster than those with shorter periods. When waves move towards shallow water, long-period waves pass short-period waves and reach the shallow water earlier. The sorting of waves based on wave periods is known as dispersion. This process does not change the wave characteristics; it only sorts waves based on their periods; but other processes alter wave characteristics when waves enter shallow water.

Wave studies in deep water show that the sinusoidal shape of waves change when they move towards shallow water (Peachey, 1986; Abreu *et al*., 1992; Masselink and Hughes, 2003; Holthuijsen, 2007). This process is known as the development of wave asymmetry. Waves in deep water have symmetric crests and troughs. However, when waves move towards intermediate and shallow water, the crest increases and the trough flattens (Stokes, 1847; Holthuijsen, 2007). That is because, in deep water the water particle velocities are symmetric in offshore and onshore directions, but when waves enter into intermediate and shallow water, the onshore water particle velocities become stronger than the offshore water practice velocities. This is an important wave process when waves travel from deep water to shallow water as it changes the shape of the waves, but wave direction is not affected.

Shoaling is another important process controlling the shape of waves in shallow water (Cialone and Kraus, 1987; Bird, 2000; Masselink and Hughes, 2003; Davidson-Arnott, 2010). When waves enter shallow water, the sea floor significantly influences the wave characteristics (Masselink and Hughes, 2003). As a result of shoaling, wave characteristics, such as wavelength, wave group, wave height, and wave velocity are affected. When waves travel from deep water to intermediate water, the ratio between local wave height and deep water wave height (H/H_0) gradually decreases, whereas it rapidly increases in shallow water before breaking as a result of shoaling. However, according to Linear Wave theory, the wave period is the only wave characteristic that is not modified and remains constant when waves travel from deep water to shallow water (Sorensen, 1997; Masselink and Hughes, 2003).

In shallow water, the wave direction is influenced by water depth and decreases the angle between the swell wave and the depth contours (Bird, 2000). This process is known as refraction. When waves enter shallow water, the water depth causes the wave velocity in the

higher part of a wave crest to become faster than the lower part. Therefore, the wave crest rotates to an angle close to the depth contours; that is, when a wave enters into shallow water, the wave direction changes in accordance with the variation of wave velocity (Masselink and Hughes, 2003).

It can be concluded that when waves travel from deep water to shallow water, wave characteristics, such as wave height, direction and velocity will be affected, but according to Linear Wave theory, the wave period remains constant. Four important processes known as dispersion, development of wave asymmetry, shoaling and refraction should always be taken into account in order to transfer waves from deep water to the shallow water of open coast beaches.

However, when waves approach embayed beaches, wave processes could also be influenced by diffraction inside the bay (Klein *et al*., 2002; Woodroffe, 2002; Dehouck *et al*., 2009). Therefore, the shoreline of embayed beaches consists of a highly curved shadow zone formed by diffraction and a straight downcoast shoreline affected by refraction. Diffraction around a headland is discussed more in detail in Chapter 4. However, when waves enter into pocket beaches, this raises the question whether all aforementioned processes are still the main factors in controlling wave characteristics in pocket beaches or other factors such as reflection could prevail in the area?

When waves propagate into transitional and shallow water, local winds could also be a secondary factor in influencing wave characteristics (Whitford and Thornton, 1993). There are two theories to explain wind-generated waves. The first theory is that pressure fluctuations at the sea surface, caused by wind, generate small waves (Eckart, 1953). The second theory is that after small waves are generated, the vertical distributions of wind speed near the water surface will change (Miles, 1957). These variations in wind speed increase close to wave crests and decrease near wave troughs, so the pressure in wave crests differs from wave troughs. This pressure difference causes an increase in wave heights and wave periods.

However, the time taken to increase the wave period is debatable. For instance, Pattiaratchi et al. (1997) compared wave heights before and after the sea breeze and found that wind quickly grows the wave heights and wave periods, whereas Sonu *et al*. (1973) observed that wave periods increase slowly (e.g. 6 hours from 1s to 3s).

Bosserelle *et al*. (2011) also studied the effect of sea breezes on wave characteristics in a embayed beach. Their studies showed the changes in the beachface were mainly influenced by the waves driven during strong sea breezes. They also indicated that when sea breezes decreased by 50%, the currents were reduced as a result of a reduction in wave energies. However, the impact of local winds on waves in pocket beaches is poorly documented. This chapter briefly discusses the effect of local winds on waves, and later in Chapter 5, the importance of winds on nearshore currents will be discussed more in detail.

2.2. Methodology

As explained at its outset, this chapter concerns the measurement and analysis of field observations of wave processes inside and outside of Okains Bay, a case study micro-tidal pocket beach. This approach fits into the left-hand portion of the thesis methodology diagram illustrated in Figure 1.6.

2.2.1. Study site

The study area of Okains Bay is located on the north-eastern side of an extinct and partially eroded volcanic peninsula on the east coast of New Zealand's South Island (Figure 2.1). Beaches in this area, including Okains Bay, are classified as micro-tidal pocket beaches. Tidal information obtained for the nearest harbour, Lyttelton, located about 22 km from Okains Bay, show that the tidal range varied between 1.38 m and 2.35 m during Neap tide and Spring tide respectively (Land Information New Zealand, 2012). The dominant offshore waves at the Canterbury wave buoy [43.75 S 173.33 E] (site B), moored in a depth of 76 m below MSL, around 17 km south east of Okains Bay, approach the outer limits of the bay from the southwest and south (Gorman et al., 2003). Mean significant wave height at this site was reported around 2 m with a maximum significant wave height of 7 m. Mean and maximum wave periods were also reported about 7.39 s and 12.9 s respectively.

Information on local winds in Okains Bay is sparse, but the data are available for larger scale synoptic patterns over Banks Peninsula. This area has prevailing northeast and southwest winds, followed by easterly and southerly winds (NIWA, 2012).

The shoreline of Okains Bay is about 750 m long, and it is enclosed by approximately 2 km of natural rocky headlands. Okains Bay and its shoreline are oriented at 35° to true north, so the bay is relatively exposed to high-energy swell waves from the Pacific Ocean to the east. However, the headlands function to limit the waves that can approach and enter directly into the bay, without consideration of refraction and diffraction, to a directional sector of around 25° to 70° relative to true north. The beach of this bay is classified as dissipative, with a foreshore gradient of 1:60 and a backshore gradient of 1:90 (Dingwall, 1974).

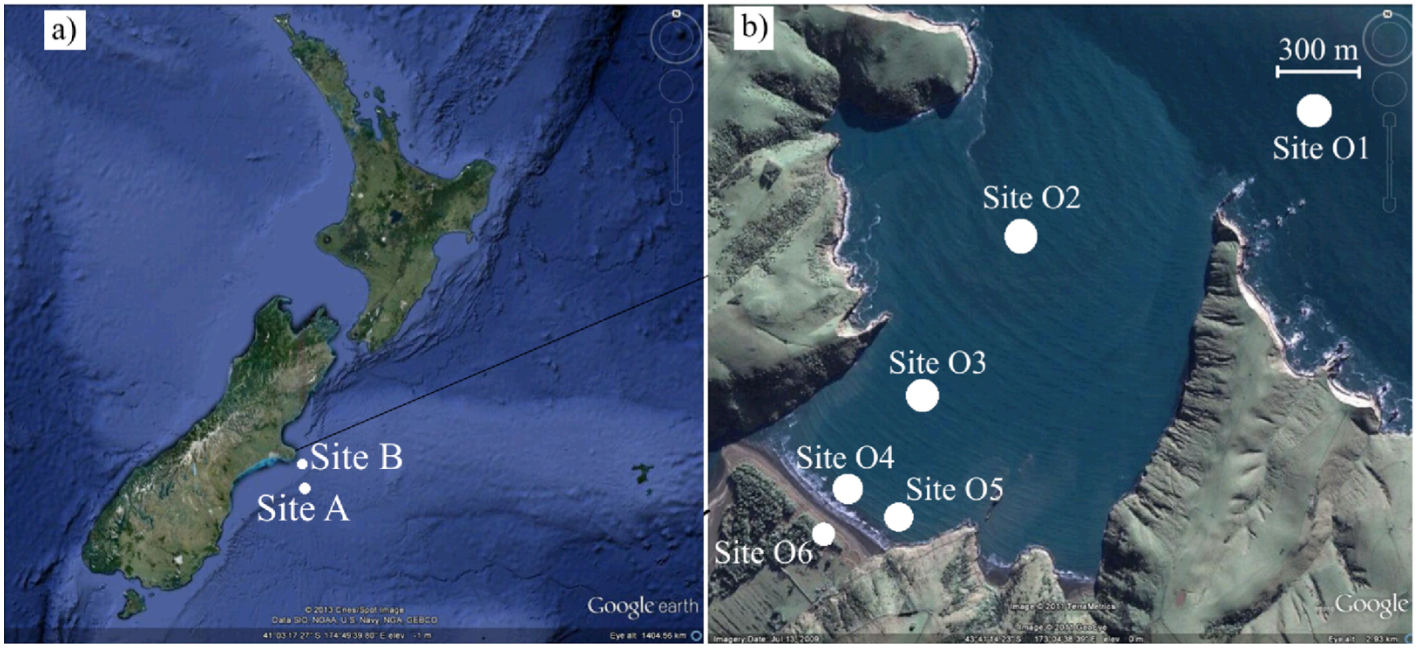

Figure 2.1. Banks Peninsula, New Zealand (a), and field instrument deployment sites in Okains Bay (b), located on Banks Peninsula. Wave hindcast data were obtained for site A (43.50 S 174.00 E), and also wave data were recorded at site B by the Canterbury wave buoy (43.75 S 173.33 E) (modified from Google Earth, 2012).

Table 2.1. Information on instruments' deployment for Field Experiment 1.

Instrument name	Instrument frequency (kHz)	Deployment period	Water depth (Mean Sea Level) (m)	Burst duration (min)	Time between bursts (min)	Site
ADCP	600	20/April/2011 to 11/May/2011	12	20	60	O1
ADCP	1200	20/April/2011 to 11/May/2011	5	20	60	O2
Datawell Mk2 directional	-	20/April/2011 to 11/May/2011	76	30	30	B

Table 2.2. Information on instruments' deployment for Field Experiment 2.

Instrument name	Instrument frequency (kHz)	Deployment period	Water depth (Mean Sea Level) (m)	Burst duration (min)	Time between bursts (min)	Site
Inter Ocean S4	-	19/December/2011 to 22/December/2011	8	20	60	O2
RBR xr-620 CTD	-	19/December/2011 to 21/December/2011	2.8	continuous	n/a	O4
RBR xr-620 CTD	-	21/December/2011 to 22/December/2011	2.8	continuous	n/a	O5
Datawell Mk2 directional	-	21/December/2011 to 22/December/2011	76	30	30	B

Table 2.3. Information on instruments' deployment for Field Experiment 3.

Instrument name	Instrument frequency (kHz)	Deployment period	Water depth (Mean Sea Level) (m)	Burst duration (min)	Time between bursts (min)	Site
ADCP	1200	3/April/2012 to 13/April/2012	12	20	60	O3
RBR xr-620 CTD	-	3/April/2012 to 4/April/2012	2.8	continuous	n/a	O5
RBR xr-620 CTD	-	6/April/2012 to 8/April/2012	2.8	continuous	n/a	O5
Wave hindcast	-	3/April/2012 to 13/April/2012	150	10	10	A

2.2.2. Methods

This study employs field experiments to explore the importance of reflection in controlling wave process in a case study pocket beach, Okains Bay, in Canterbury, New Zealand (Figure 2.1). Field experiments were accomplished in Okains Bay over a period of a year for three individual measurements using an array of instruments. The first field experiment was accomplished between 20th April and 11th May, 2011 in two locations: outside Okains Bay at site O1 [43.66 S 173.08 E] at a depth of 12 m, and inside the bay at site O3 [43.68 S 173.06 E] at a depth of almost 6 m during high tide. In this field experiment, two units of Acoustic Doppler Current Profiler (Teledyne ADCP) (Figure 2.2a) were deployed: an upward-facing 600 kHz ADCP at site O1 (Figure 2.2b), and a downward-facing 1200 kHz ADCP at site O3 (Figure 2.2c). These two instruments collected data for 22 days with a same sampling configuration, as shown in Table 2.1. Deep water wave data were also collected during this deployment by the Canterbury wave buoy, site B, (Figure 2.1 a) (Ecan, 2014). A unit of Datawell Mk2 directional buoy was deployed at this site to collect wave data every 30 min at a rate of 1.28 Hz.

The second field experiment was conducted from 19th Dec to 22nd Dec 2011. An InterOcean S4AWD current meter was deployed at site O2 [43.66 S 173.06 E] at a depth of 8 m during high tide to measure waves (Figure 2.3) (Table 2.2). A RBR xr-620 CTD was also used at a depth of about 2.5 m during high tide at two sites: O4 [43.68 S 173.05 E] and O5 [43.68 S 173.06 E] (Figure 2.4). The RBR was deployed for 35 hours at site O4 and then it was shifted to site O5 for 18 hours (Table 2.2). The RBR continuously collected water levels and then the data were used as an input into a Matlab routine, developed for this study, to extract wave heights and periods based on the zero-up crossing method. Note that RBR is not capable of measuring wave direction. Deep-water wave data were collected during this deployment by the Canterbury wave buoy to represent the wave climates outside Okains Bay. Throughout the measurements, a HOBO H21 weather station was also deployed on the beach at site O6 to collect wind speed and direction inside Okains bay (Figure 2.1b).

In order to compare the wave data calculated from RBR with both ADCP and S4, the first 20 min of RBR water depth data in every hour was selected to calculate the wave data. In this study, ADCP and S4 were configured with a 20 min burst duration and 60 min time between bursts to collect wave data (Table 2.1, 2.2 and 2.3), while the RBR collected water depth continuously at 6 Hz. Since all instruments were configured to start at the same time, the first

20 min of water depth data for each hour was selected to calculate the wave data. For instance, ADCP and S4 collected wave data from 7:00 pm to 7:20 pm and they were idle for 40 min until 7:59 pm when they both started again. However, RBR collected water depth data continuously from 7:00 pm to 8:00 pm, so the first 20 min of collected data were cut and imported into the Matlab routine to calculate the significant wave heights and periods based on the zero-up crossing method.

The third field experiment was carried out between 3rd and 13th April 2012. A 1200 kHz upside-facing ADCP was deployed at site O3 throughout the period of the measurements. An RBR xr-620 CTD was also deployed on two occasions at site O5 for almost 16 hours and 2 days respectively (Table 2.3). Similar to Field Experiment 2, the data extracted from the RBR were used as an input into the Matlab routine in order to calculate significant wave heights and mean periods. Since during the third field experiment, wave data were unavailable from the Canterbury wave buoy, available hindcast wave data for the closest location (site A) to site B was chosen to represent the wave climates outside Okains Bay; site A is located 32 km southeast of Okains Bay [44.50 S 174.00 E]. Wave hindcast data were provided by New Zealand *MetOcean Solutions Ltd* and they were averaged hourly. Similar to Field Experiment 2, the weather station was also deployed on the beach at site O6 to collect wind speed and direction inside Okains Bay.

Throughout this study, regression analysis was used to examine the correlation between wave parameters, tides and local winds. The analysis is based on two assumptions. First data were normally distributed. Second, variables were measured without any errors. In all regression analyses, the time lag for each variable was the same, except for wind variables. The time lag between waves and local wind variables is 10 min. Also based on the assumption, the parameters on both axes are independent of each other.

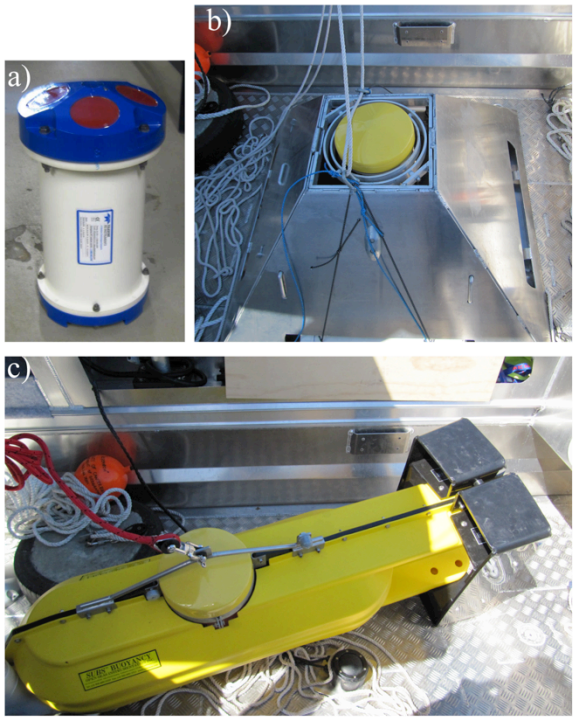

Figure 2.2. Teledyne ADCP used during field experiments in Okains Bay (a), upward facing ADCP frame (b), and downward facing ADCP frame (c).

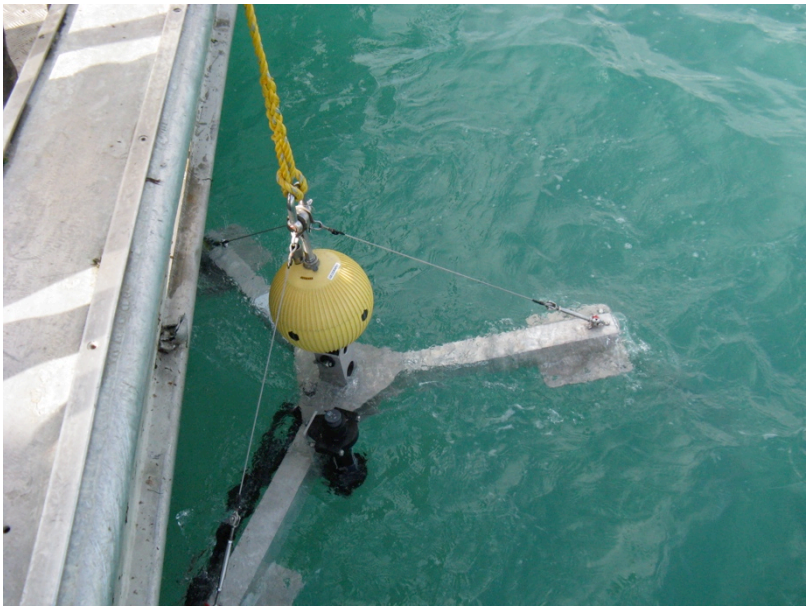

Figure 2.3. InterOcean S4AWD current meter used during Field Experiment 2 (a), and its deployment frame (b).

Figure 2.4. RBR xr-620 CTD used during Field Experiment 2 and 3 (a), and its deployment frame (b).

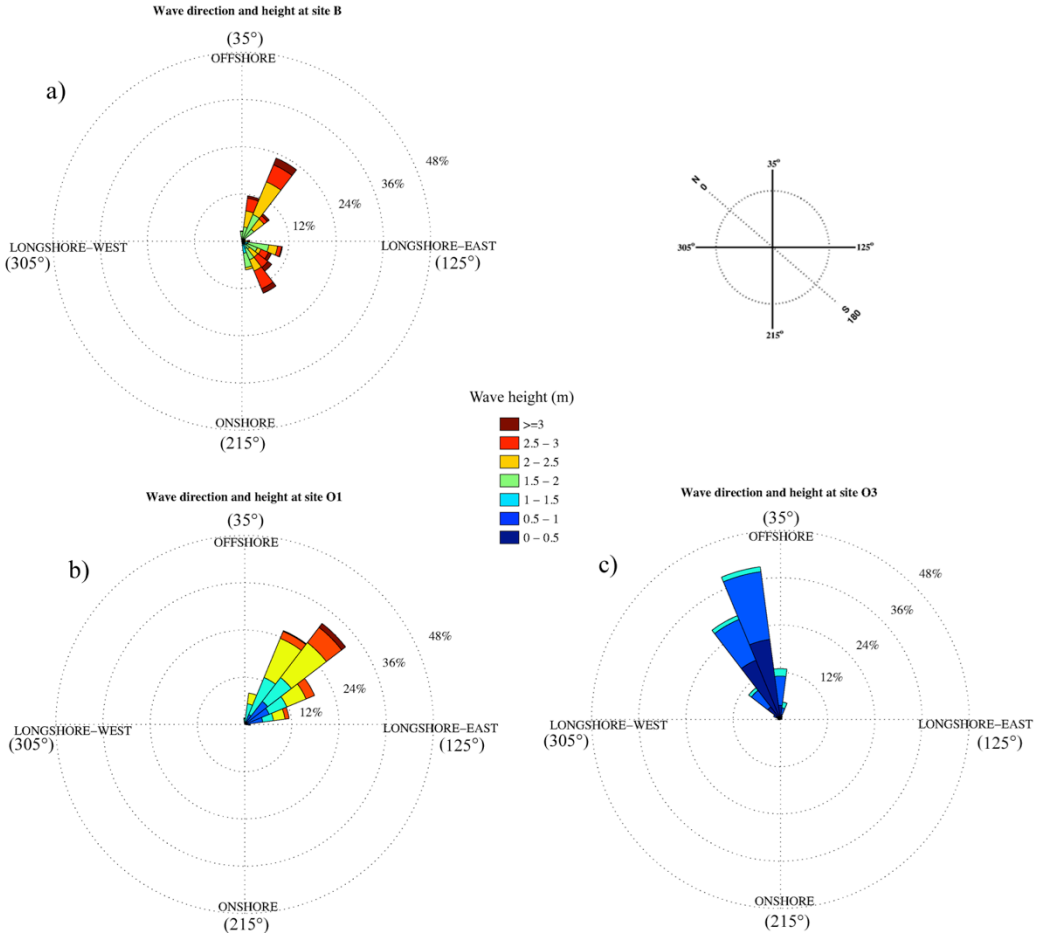

Figure 2.5. Rose plot showing wave heights and directions measured at a depth of 76 m at site B (a), at a depth of 12 m at site O1 (b), and at a depth of 6 m at site O3 (c) during Field Experiment 1. Directions are shown relative to the Okains Bay beach orientation.

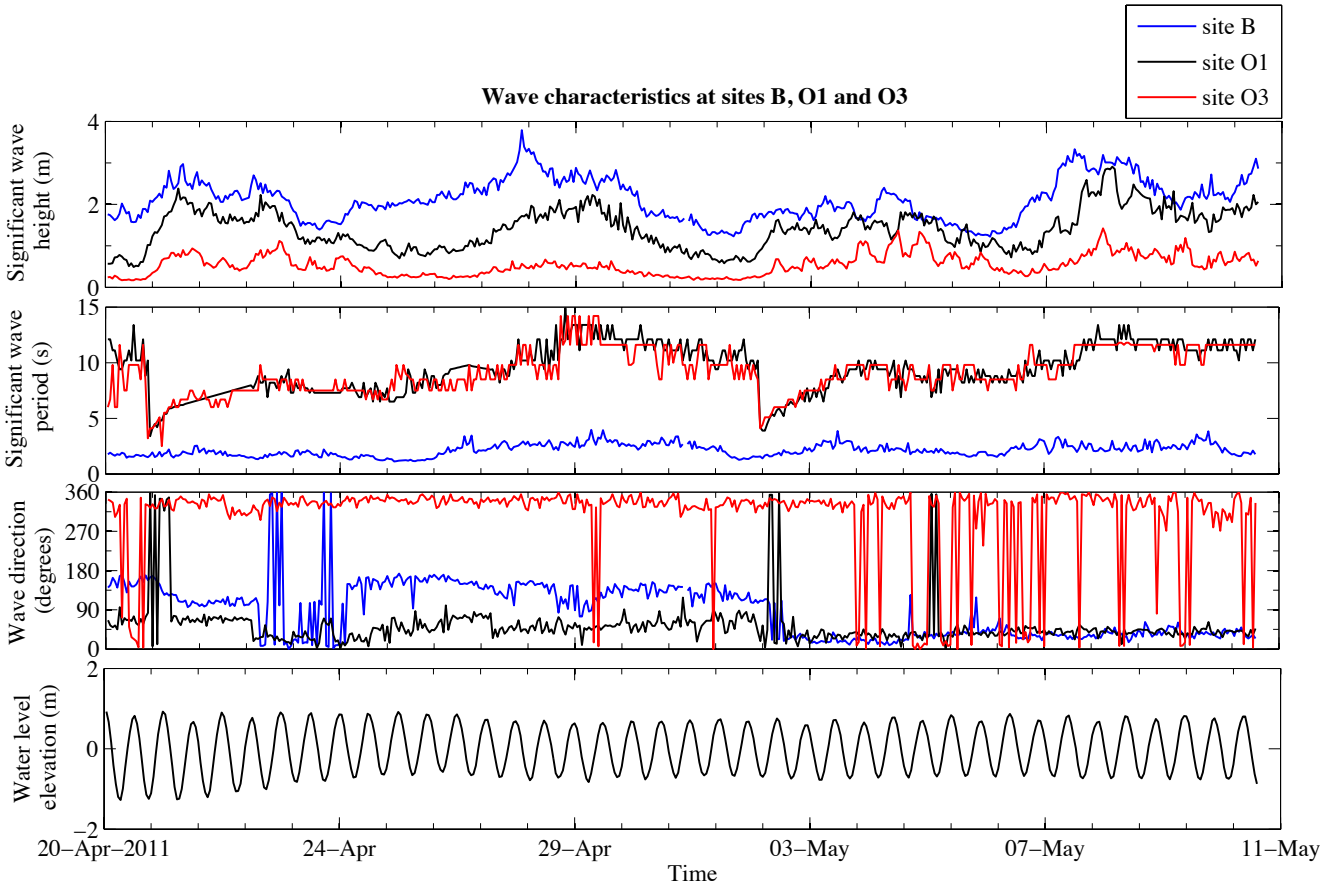

Figure 2.6. Comparison of wave data during Field Experiment 1 at site B, at a depth of 76 m, site O1, in a depth of 12 m outside Okains Bay, and site O3 at a depth of 6 m inside the bay. Directions are given relative to the Okains Bay beach orientation. Water level elevation is given relative to site O3.

2.3. Results of Wave observations at Okains Bay

In this section the raw wave data obtained from an array of instruments at sites O1, O2, O3, O4 and O5 at Okains Bay during three individual experiments between 20th April 2011 and 4th April 2012 are discussed. The section examines wave climates in Okains Bay, an example pocket beach, during different sea conditions with a particular focus on identifying the importance of reflection, in line with the thesis aims 1 and 2. The results serve to accentuate the differences between wave climates of pocket and adjacent open coast beaches.

2.3.1. Field Experiment 1

As discussed earlier, Field Experiment 1 was accomplished between 20th April 2011 and 11th May 2011. Wave data at site B showed that predominant wave directions were from 15° and 30° relative to the shoreline of Okains Bay (or easterly to true north), followed by 140° and 185° (or relatively southerly to the true north) (Figure 2.5 a). Significant wave heights at this site ranged from 1.2 m to 3.8 m, with a mean of 2.12 m, and significant wave periods ranged from 4.7 s to 10.7 s, with a mean of 7 s (Figure 2.6).

Wave data collected at site O1 using an upward-facing 600 kHz ADCP showed that the predominant waves were limited to 30° and 45° relative to the Okains Bay beach shoreline (or easterly to true north) (Figure 2.5 b). Significant wave heights at this site varied from 0.49 m to 2.9 m, with a mean of 1.41 m, and significant wave periods varied from 3.4 s to 16.9 s, with a mean of 10.2 s (Figure 2.6).

Wave data collected at site O3 using a downward-facing 1200 kHz ADCP indicated that the predominant wave direction was from 345° relative to the Okains Bay beach shoreline, (or north-easterly to true north) (Figure 2.5 c). Significant wave heights at this site ranged from 0.17 m to 1.42 m, with a mean of 0.54 m, and significant wave periods ranged from 2.5 s to 14.2 s, with a mean of 9.14 s (Figure 2.6).

The results of Field Experiment 1 reveal that significant wave heights decreased notably when waves travelled from just outside to inside Okains Bay. Figure 2.5 b indicates the variable range of wave heights at site O1 (also see Table 2.4). However, Figure 2.5 c indicates a more limited, lower range of wave heights at site O3. The distance between sites O1 and O3 is about 1.8 km and the water depth changed from 12 m to 6 m, but when waves reached site O3, their heights decreased on average by 0.87 m (Figure 2.6 and Table 2.4). Note that the wave height data at both sites O1 and O3 are normally distributed, indicating that the most-frequent values are clustered around the mean (Figure 2.7). The scatter plot of wave heights at sites O1 versus O3 also shows a positive correlation with an R^2 value of 0.67 (Figure 2.8a). This correlation and the considerable reduction in the wave heights between these two sites could suggest the influence of factors other than wave development via dispersion, development of wave asymmetry, shoaling and refraction in Okains Bay.

Similarly, when waves travelled from site B to O1, wave heights decreased (Figure 2.6 and Table 2.4). As depicted in Figure 2.8 a and c, the point-to-point comparison showed that the

wave height reduction between sites B and O1 was less than that between sites O1 and O3 (see table 2.4). The distance between sites B and O1 was about 14 km and water depth below mean sea level varied from 76 m to 12 m. Therefore, it was expected that the wave height would decrease when waves entered into transitional water owing to dispersion, development of wave asymmetry, shoaling and refraction. However, the distance between sites O1 and O3 was about 1.8 km and water depth decreased from 12 m to 6 m. According to the Linear Wave Theory, wave height cannot considerably change when waves propagate from site O1 to O2, unless they are influenced by other factors such as obstacles or headlands.

The observations also showed that wave directions significantly changed when waves travelled from site O1 to O3 (Figure 2.5 and 2.6). As depicted in Figure 2.5, the waves inside Okains Bay at site O3 predominantly approached at 345° to the shoreline, whereas the predominant wave direction outside the bay at site O1 was 45°. This indicates that the predominant wave direction changed by around 60° between these two sites and waves at site O3 approached from the downcoast headland side due to reflection. This would suggest that reflection from the headland could prevail over other factors, including diffraction and refraction. The scatter plot shown in Figure 2.4 also states that there is a poor correlation between wave directions at sites O1 and O3 with an R^2 of 0.08. This poor correlation could suggest a complex situation resulting from wave processes inside the bay, and waves could be influenced by a combination of reflection, diffraction, shoaling and refraction and bottom friction when waves enter into the bay.

However, when waves approached from site B to O1, the directions at site O1 changed rarely to angles from 216° to 34°. As depicted in Figure 2.5a and b, wave direction predominantly approached from 15° and 30° relative to the shoreline of Okains Bay, followed by 140° and 185°. After travelling about 14 km, when waves reached site O1, the open coast wave transitional factors shifted the wave directions towards normal. The point-to-point analysis shown in Figure 2.8 d, stated that waves with greater angles to the shoreline were more affected and shifted towards normal and they scarcely turned to an angle between 181° to 359° to the shoreline. However, when waves entered the bay, their direction predominantly turned to the opposite quarter. This indicates that other factors, such as reflection, prevailed over open coast wave transitional factors to influence wave processes inside the bay. In Chapter 4, this idea that reflection could play an important role in controlling the wave process inside the bay will be further explored using experimental and numerical modelling tools to build on these field results.

Records from wave period data throughout the first deployment indicated that wave periods collected at site O1 relatively changed when waves moved to site O3. Wave periods are independent of water depth (Sorensen, 1997; Masselink and Hughes, 2003), so without consideration of local winds, it is assumed that when waves travel from deep water to shallow water, the wave period is constant. The observations at site B, O1 and O3 showed that although the trends of wave periods for all sites are the same, the values of wave period mostly increased when waves were propagated from site B to O1 (Figure 2.6). However, wave periods remained relatively constant between sites O1 and O3. These discrepancies in wave period values between sites B and O1 could state the influence of other factors, such as local winds. The distance between these two sites is about 16 km, and this is a reasonable fetch for local winds to influence waves between the sites.

As a result of sheltering, waves with an angle greater than the directional sector of Okains Bay (25° to 70° relative to true north) could be influenced by diffraction, thereby considerably losing the wave energy and, subsequently, decreasing the wave heights inside the bay. The reduction in wave heights would theoretically increase when waves at site O1 approached at an angle closer to longshore (see diffraction coefficient in Wiegel, 1964). For instance, as shown in Figure 2.6, when wave directions at site O1 during the period between 27th April and 2nd May increased to an angle towards longshore with a range between 60° and 120° to the shoreline, the wave heights inside the bay significantly decreased with an average of 0.7 m. This suggests that the process of changes in the wave heights when waves travel from outside to inside pocket beaches could differ from that of open coast beaches, basically because of dispersion, development of wave asymmetry, shoaling and refraction.

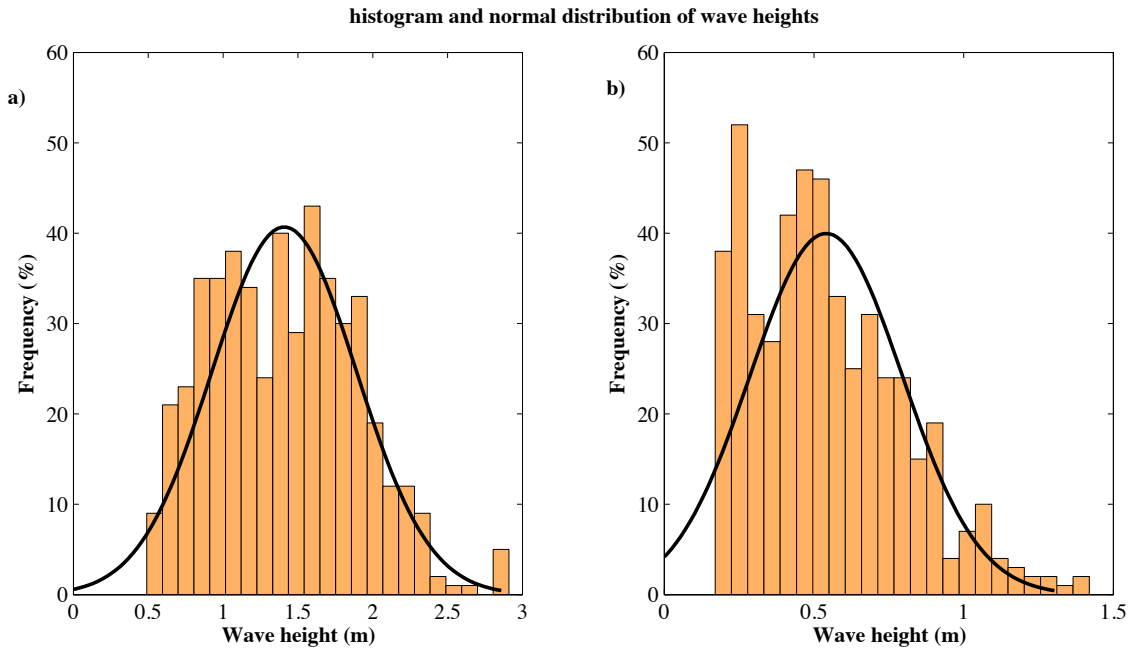

Figure 2.7. Histogram and normal distribution of wave heights at site O1 (a), and site O3 (b) during the Field Experiment 1.

Table 2.4. Min, Max, Mean and Standard deviation of wave heights at site B, O1, and O3, with the difference between each sites when waves travel from site B to O1 and then to O3.

Site	Min (m)	Max (m)	Mean (m)	Standard Deviation (m)
B	1.26	3.8	2.12	0.49
O1	0.49	2.91	1.41	0.48
O3	0.17	1.42	0.54	0.25
Difference between B and O1	0.06	1.71	0.72	0.38
Difference between O1 and O3	0.02	2.15	0.87	0.36

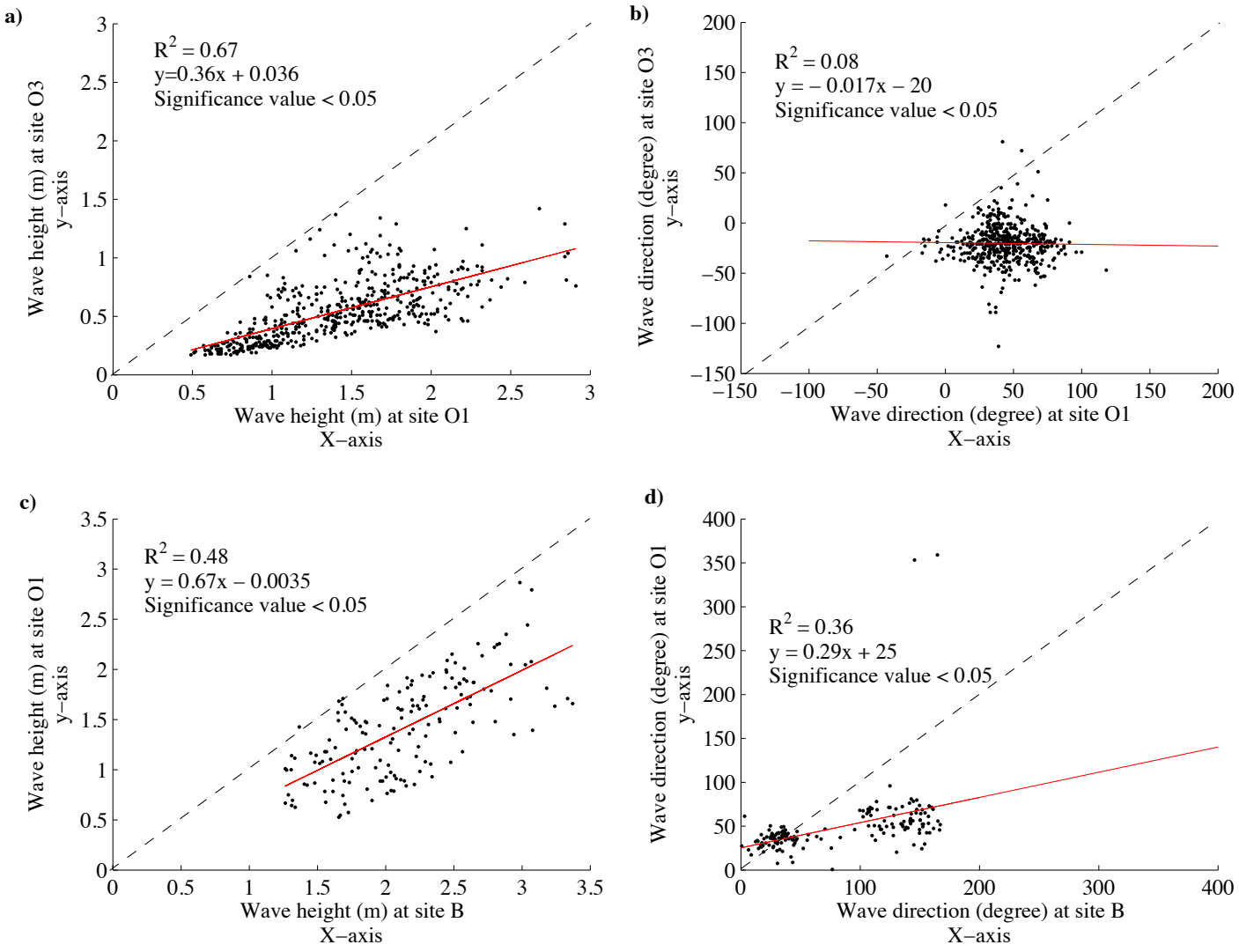

Figure 2.8. Scatter plot of wave height and wave direction for waves measured from site O1, outside Okains Bay, to site O3, inside the bay (a and b), and also for waves measured from site B to O1 during Field Experiment 1. A three hours average was used to compare wave data at site B and O1. Dash lines indicate point-to-point comparison between wave data of each site.

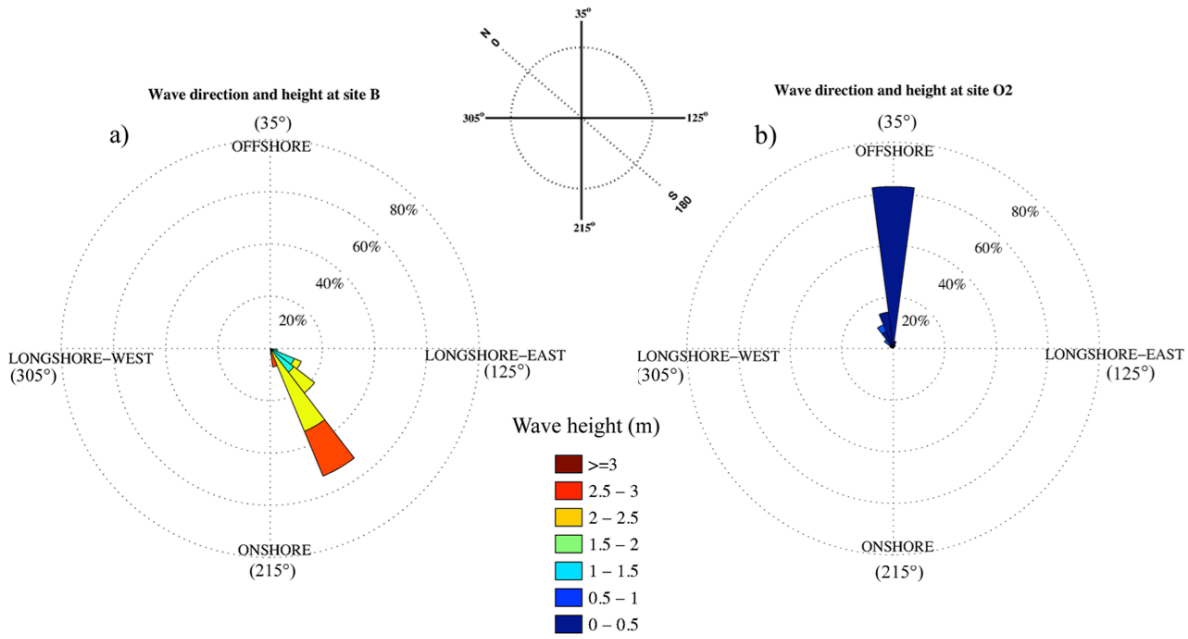

Figure 2.9. Rose plot showing wave height and direction measured during Field Experiment 2 at site B (water depth 76 m) and at site O2 (water depth 8 m). Directions are shown relative to the Okains Bay beach orientation.

2.3.2. Field experiment 2

The second measurements were accomplished between 19th and 22nd Dec 2011. Wave data at site B (Canterbury wave buoy) showed that the predominant waves direction was from 150° relative to the shoreline of Okains Bay (South Westerly to the true North) (Figure 2.9a). Significant wave heights at this site ranged from 1.18 m to 2.25 m with an average of 1.73 m and significant wave periods ranged from 5.84 s to 9.2 s with an average of 7.02 s (Figure 2.10).

Wave data collected at site O2 using an InterOcean S4 indicated that waves predominantly approached normal to the Okains Bay shoreline, (or north-easterly to true north) (Figure 2.9b). Significant wave heights at this site ranged from 0.21 m to 0.6 m with an average of 0.31 m, and significant wave periods ranged from 4.3 s to 8.75 s with an average of 6.49 s (Figure 2.10).

Significant wave heights at site O4 and O5, obtained from the RBR XR-620 unit, ranged from 0.13 m to 0.21 m with an average of 0.17 m and from 0.22 m to 0.36 m with an average of 0.3

m respectively. Significant wave periods ranged from 6.8 s to 8.85 s with an average of 7.72 s at site O4, and from 3.9 s to 5.4 s with an average of 4.9 s at site O5 (Figure 2.10).

Table 2.5. Min, Max, Mean and Standard deviation of wave heights measured during Field Experiment 2 at site B, O2, O4 and O5 and the difference between sites assuming waves move towards the shoreline (negative values indicate that wave height at the starting point is lower than ending point).

Site	Min (m)	Max (m)	Mean (m)	Standard Deviation (m)
B	1.18	2.25	1.73	0.29
O2	0.21	0.55	0.31	0.1
Difference between B and O2	0.78	2.02	1.42	0.36
O4	0.23	0.41	0.32	0.045
Difference between O2 and O4	-0.17	0.03	-0.06	0.053
O5	0.18	0.46	0.39	0.097
Difference between O2 and O5	-0.07	0.17	0.05	0.073

Similar to Field Experiment 1, when waves moved from site B to site O2, inside the bay, significant wave heights were notably reduced (Figure 2.10). During Field Experiment 2, wave data from site O1 was not available, so wave data from site B, outside Okains Bay, was chosen to compare how wave characteristics changed after entering into the bay. A comparison of wave data between site B and O2 showed wave heights decreased with an average of 1.42 m (Table 2.5). Figure 2.9 a indicates a range of wave heights at site B from 1.18 m to 2.25 m (see Table 2.5), whereas Figure 2.9 b indicates small wave heights varied from 0.21 to 0.55 at site O2. Wave heights were found to be normally distributed at site B, so most-frequent wave heights were clustered around the mean. However, they were slightly skewed at site O2, indicating that wave heights frequently occurred near the lower wave height (Figure 2.11). The scatter plot on wave heights at sites B and O2 also shows an average correlation with R^2 of 0.43 (Figure 2.12). Similar to the Field Experiment 1, the poor correlation and the considerable reduction in the wave heights between these two sites

suggests the influence of factors other than dispersion, development of wave asymmetry, shoaling and refraction in Okains Bay.

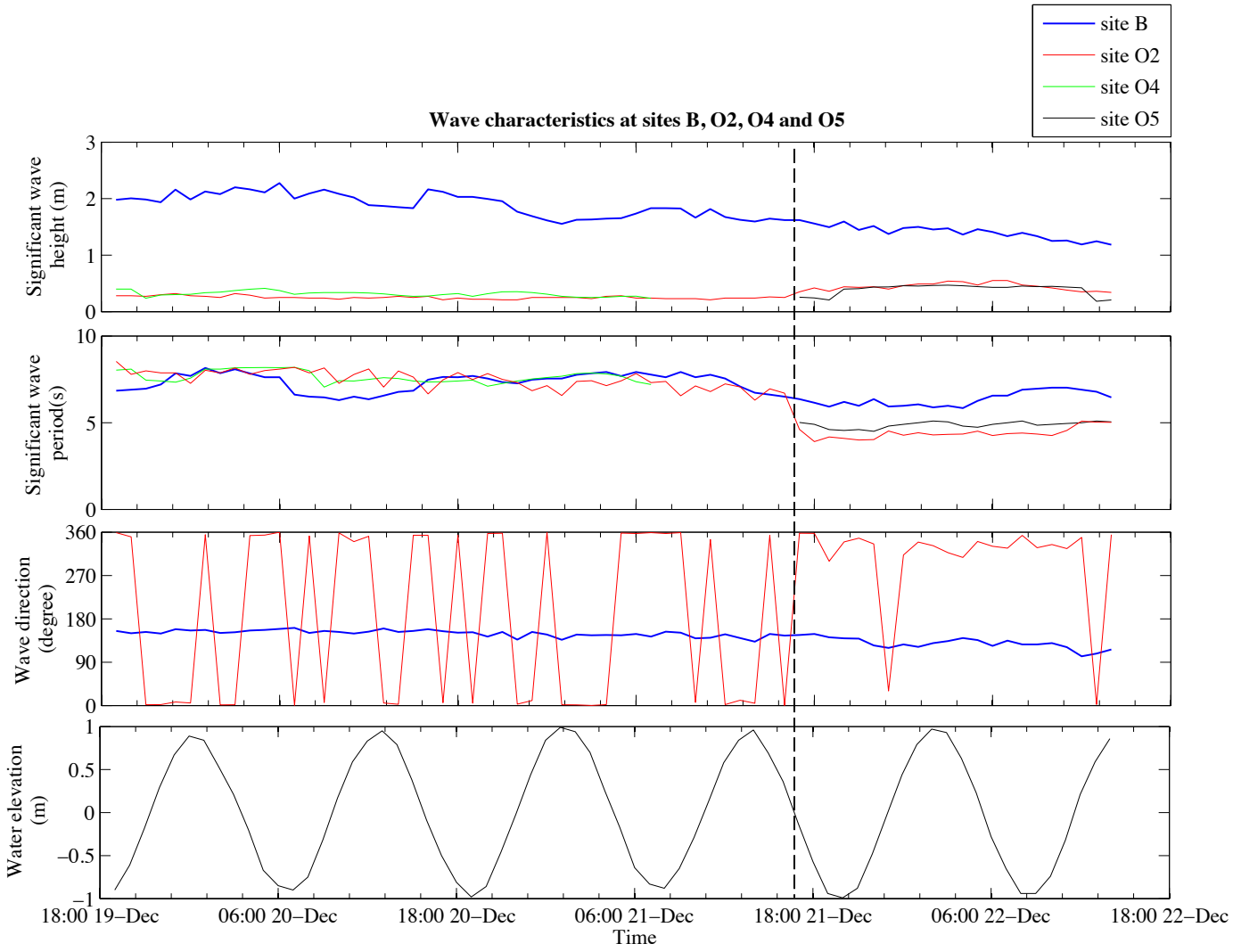

Figure 2.10. Comparison of wave data during Field Experiment 2 at site B (water depth 76 m), site O2 (water depth 8 m), site O4 (water depth 2 m) and site O5 (water depth 72 m). Directions are given relative to the Okains Bay beach orientation. Water elevation is given relative to site O2.

Small changes in the wave heights were observed when waves propagated inside the bay from site O2 to O4 or O5 (Figure 2.10). Observations showed that wave heights slightly increased when reaching the surf zone at site O4 by an average of 0.06 m (Table 2.5). Wave heights were normally distributed at site O4, so most-frequent values were clustered around the mean

(Figure 2.13a). According to wave theories, wave height gradually increases before breaking in the surf zone of open coast beaches (Sorensen, 1997; Masselink and Hughes, 2003). The increase in the wave heights at site O4 relative to at site O2 is similar to that of wave processes in open coasts. This suggests that shoaling and refraction processes prevail over other factors between these sites.

However, observations at site O5 showed that waves could be affected by other factors in areas close to the headlands. Site O5 was at the same depth as site O4, but it is located about 100 m from the upcoast headland (or the headland from where the predominant waves approach) (Figure 2.1b). Note that wave heights are right skewed at site O5, so wave heights frequently occurred near the high wave (Figure 2.13b). As shown in Figure 2.10, the wave heights slightly decreased with an average of 0.05 m, which is different when waves travelled from site O2 to O4. Since wave heights slightly increased at site O2 (Figure 2.10), the breaking zone could be shifted in a seaward direction and wave heights broke before reaching site O5. Therefore, wave heights were slightly reduced when they moved from site O2 to O5. Alternatively, this reduction in the wave heights at site O5 could suggest the influence of the upcoast headland on waves in proximity of the headland.

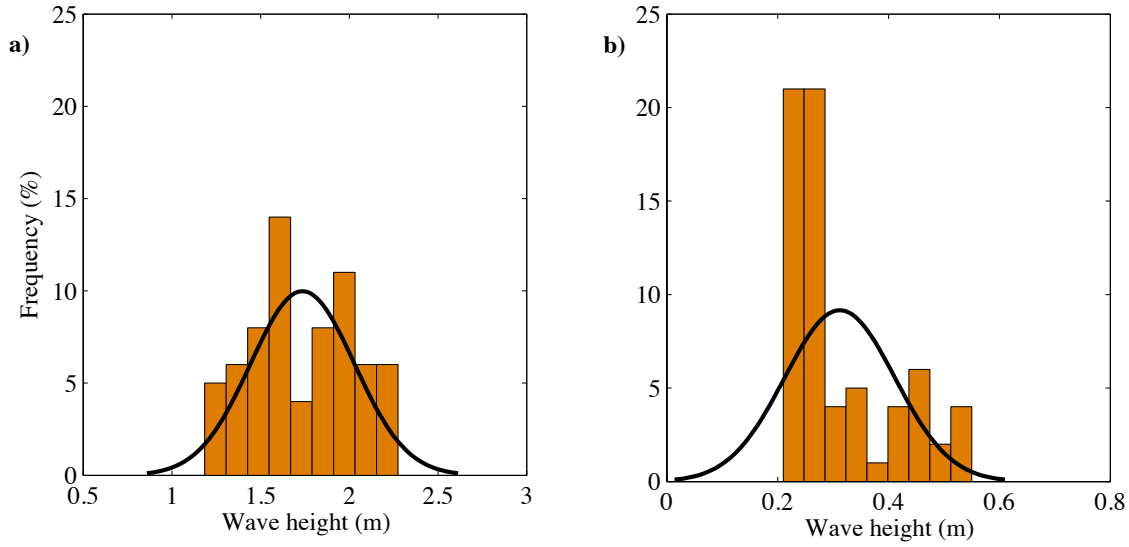

Figure 2.11. Histogram versus normal distribution of wave heights at site B (a), and site O2 (b) during the Field Experiment 2.

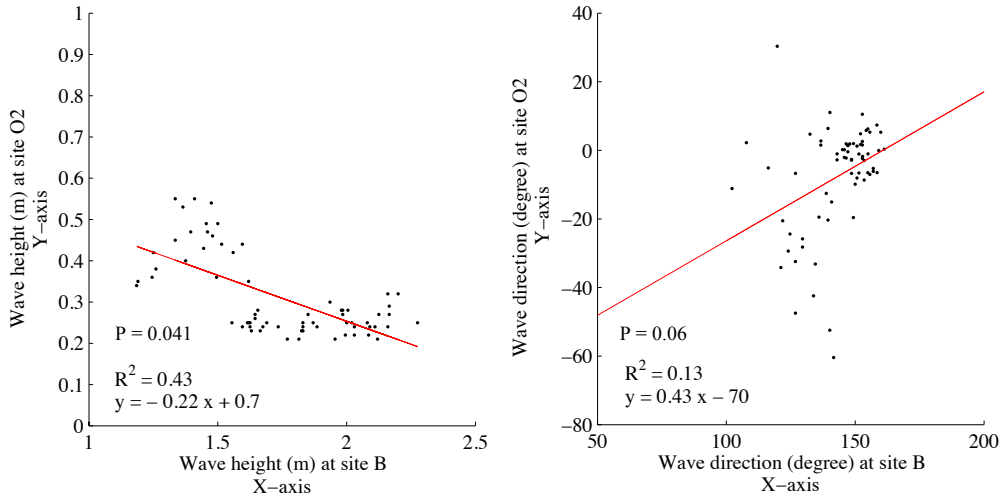

Figure 2.12. Scatter plot of wave height and wave direction when waves travelled from site B, outside Okains Bay, to site O2, inside the bay during the Field Experiment 2.

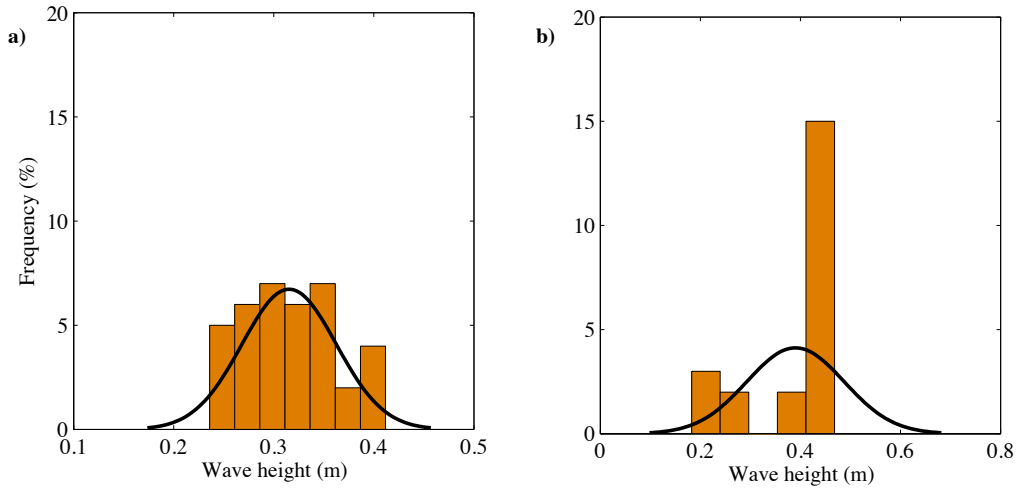

Figure 2.13. Histogram versus normal distribution of wave heights at site O4 (a), and site O5 (b) during the Field Experiment 2.

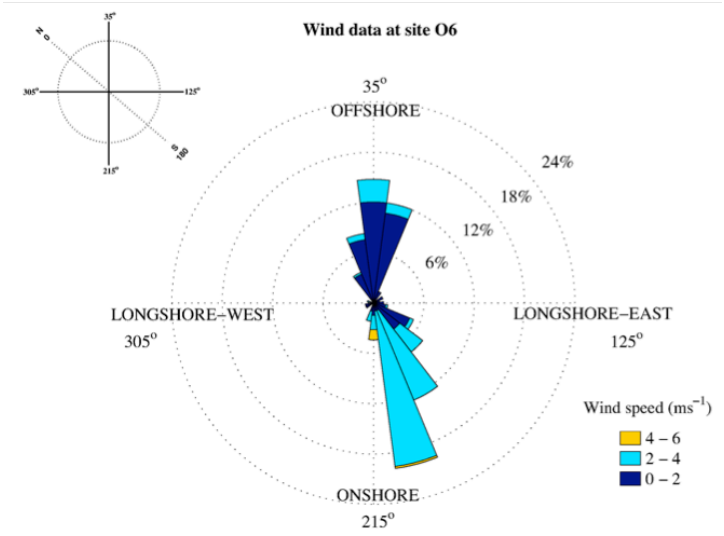

Figure 2.14. Rose plot showing wind data measured during Field Experiment 2 at site O6 inside Okains Bay. Note that wind directions are shown "to" and relative to the Okains Bay beach orientation.

During Field Experiment 2, local wind data were recorded at site O6 (Figure 2.14 and 2.15). The data showed that the predominant wind directions were moving to 0° and 165° relative to the shoreline; that is, winds were mostly blowing in offshore and onshore directions inside the bay. Throughout the measurements, the wind speed varied between 0 and about 4 ms^{-1}. In this study, low to moderate winds are referred to as the winds recorded during Field Experiment 2.

Local winds could slightly influence wave characteristics at some locations inside Okains Bay. The results show that the correlation between wave heights and wind speeds were generally poor (R^2 varied between 0.14 and 0.3 at different sites), indicating local winds insignificantly influence wave characteristics inside Okains Bay (Figure 2.16 and 2.17). The weakest and strongest correlations were observed at site O2 with R^2 of 0.14, and in the surf zone at site O4 with R^2 of 0.3 respectively (Figure 2.16a and c). This correlation was also poor at site O5 with R^2 of 0.25 (Figure 2.16d), but it is stronger than that at site O2. It can be

inferred that the low to moderate local winds could insignificantly impact wave characteristics inside the bay. This could be explained by the length of fetch (about 2 km) for a local wind, which is relatively short inside the bay, as the bay is sheltered by two high headlands.

The results from Field Experiment 2 also showed that wave periods remained fairly constant when waves were propagated inside Okains Bay (Figure 2.15). Similar to Field Experiment 1, wave periods insignificantly changed between sites O2, O4 and O5 with a maximum difference of 0.86 s. The small observed changes could be caused by other factors, such as local winds, tides or the geometry of the bay. However, when waves moved from deep water (site B) to transitional and shallow water (site O2 or O4), the wave periods slightly decreased. For instance, after late 21st Dec (shown by a dashed line in Figure 2.10), wave heights began to increase inside the bay at site O2, while wave heights outside the bay at site B started decreasing. During this period, although wave periods at both sites B and O2 decreased, the differences between them reached its maximum (2.7 s). This indicates the influence of other factors on wave characteristics, such as local winds outside the bay.

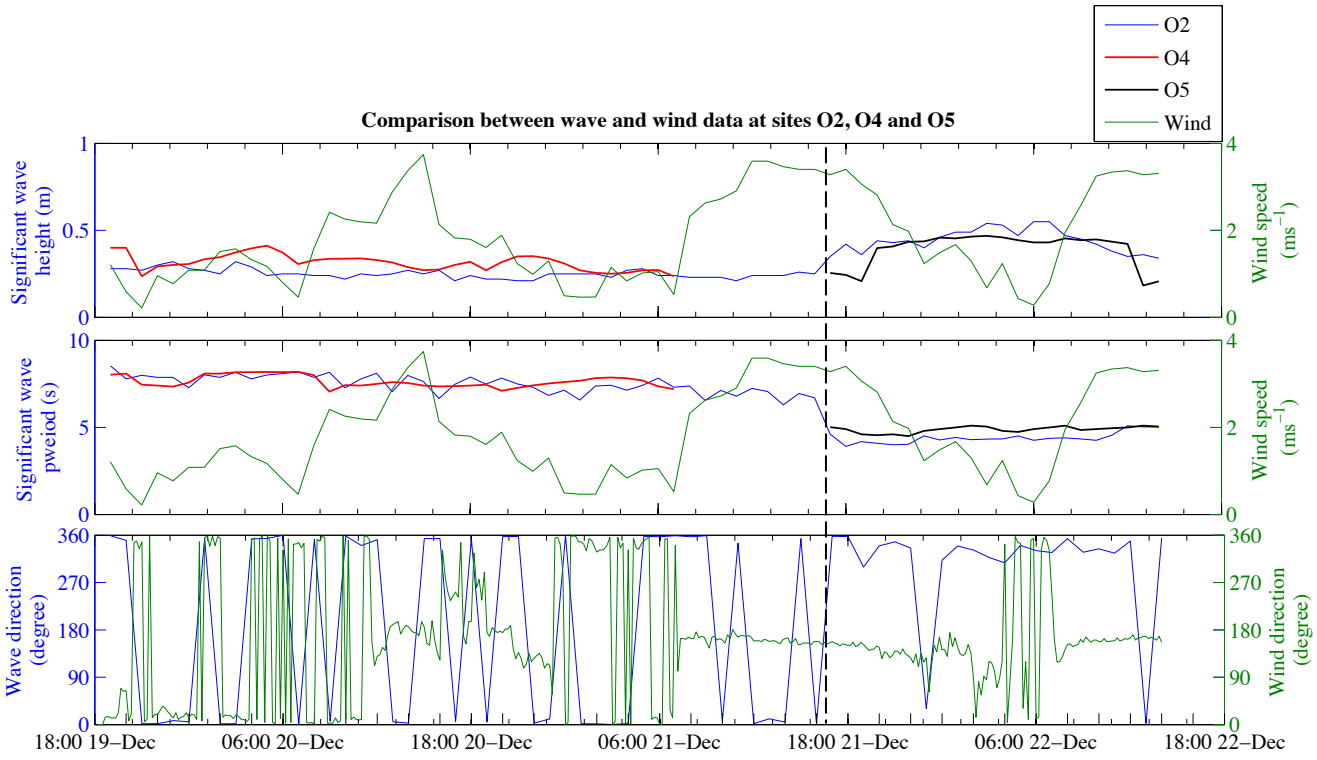

Figure 2.15. Comparison between wind data averaged every hour collected at site O6 during Field Experiment2 and wave data with a 20 min burst at sites O2, O4 and O5. Directions are given relative to the Okains Bay beach orientation.

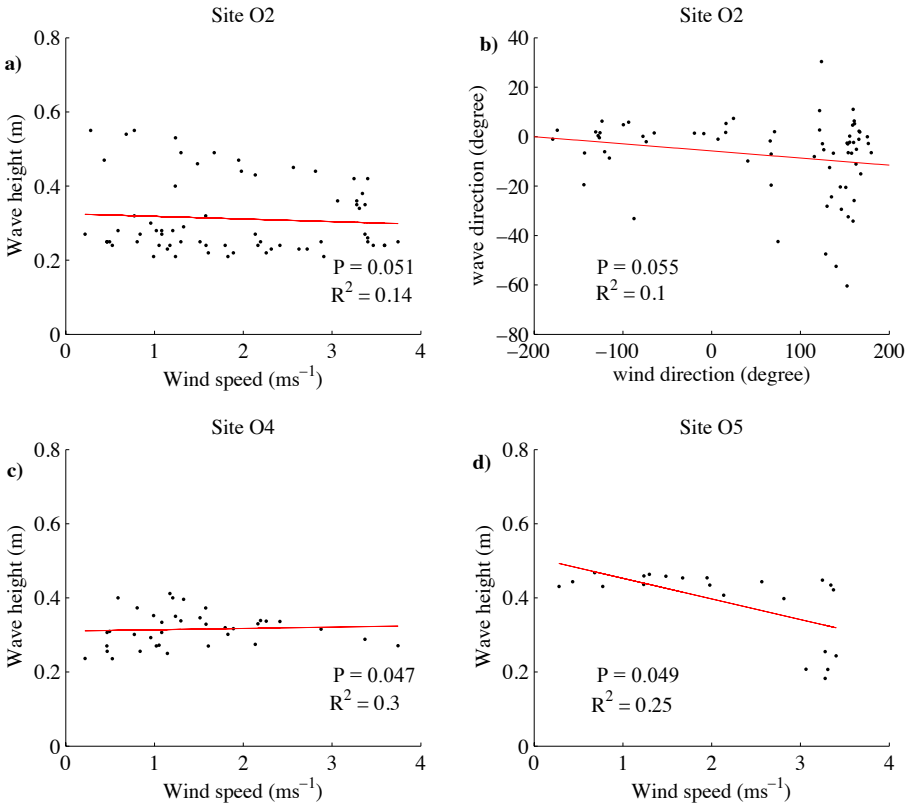

Figure 2.16. Scatter plots of wind speed versus wave height (a, c, d) for sites O2, O4 and O5, and of wind direction versus wave direction inside Okains Bay at site O2 (b) during the Field Experiment 2.

Similar to wave heights, low to moderate local winds (less than 4 ms^{-1}) insignificantly influenced wave periods inside Okains Bay. As shown in Figure 2.17, wind speed and wave period poorly correlated so that the best correlation was observed at site O4 with R^2 of 0.31. The results also indicate that when the wind speed reached its maximum of about 4 ms^{-1} at 1 pm on 20th Dec and at 12 pm on 21st Dec, or reached its minimum about 1 ms^{-1} at 6:45 am on 20th Dec and at 11:45 pm on 20th Dec, maximum wave periods were between 8 s (0.12 Hz) and 11.1 (0.09 Hz) (Figure 2.18). Therefore, it can be concluded that local winds rarely affect wave heights and periods inside Okains Bay.

When waves moved from outside Okains Bay to inside the bay, wave directions notably

changed (Figure 2.10). Wave data indicate that predominant waves approached at 150° to the shoreline at site B and their directions changed to almost normal to the shoreline at site O2 (Figure 2.9). In contrast to the wave direction collected at site O3 during Field Experiment 1, wave directions at site O2 are mostly normal to the shoreline and they did not approach from the downcoast headland. This indicates that waves could be less influenced by reflection but more dominated by dispersion, development of wave asymmetry, shoaling and refraction. That is because site O2 is closer to the entrance of Okains Bay and is more exposed to swell waves, so it is less sheltered by the headlands. However, in order to better evaluate how deep into the bay the effect of reflection and diffraction prevail over other factors, such as refraction and shoaling, SWAN (The Swan Team, 2013) was used to simulate wave processes in Okains Bay; this is discussed in Chapter 4.

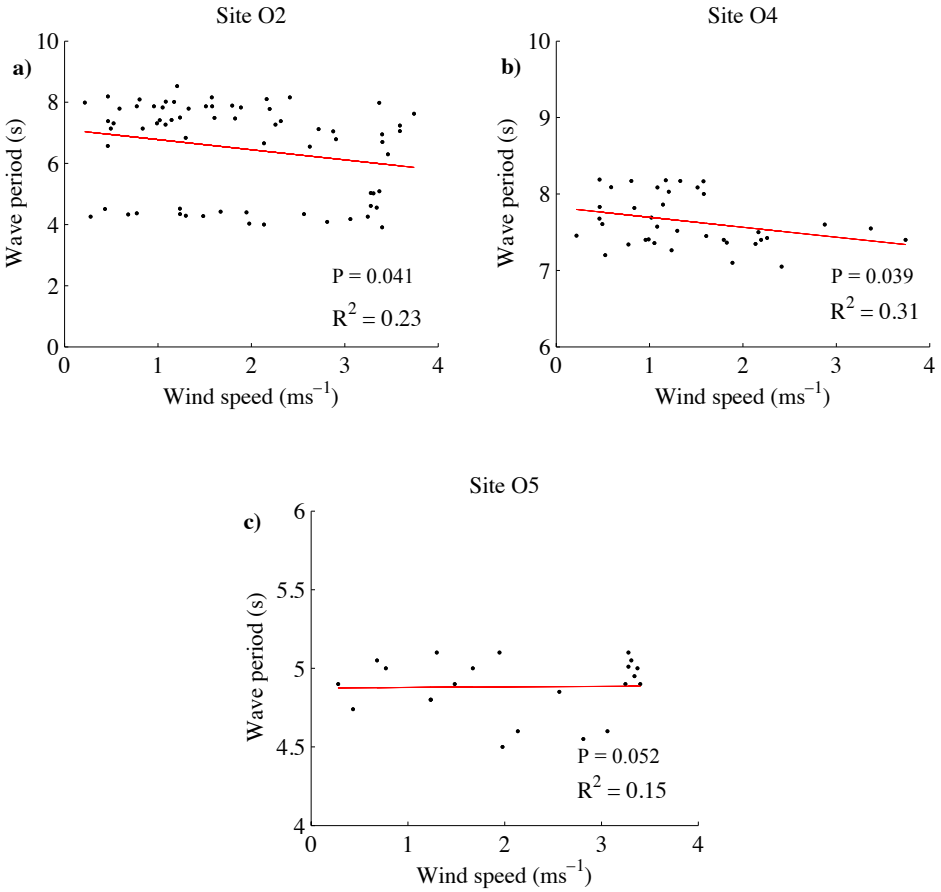

Figure 2.17. Scatter plots of wind speed versus wave period inside Okains Bay at site O2 (a), site O4 (b) and O5 (c) during Field Experiment 2.

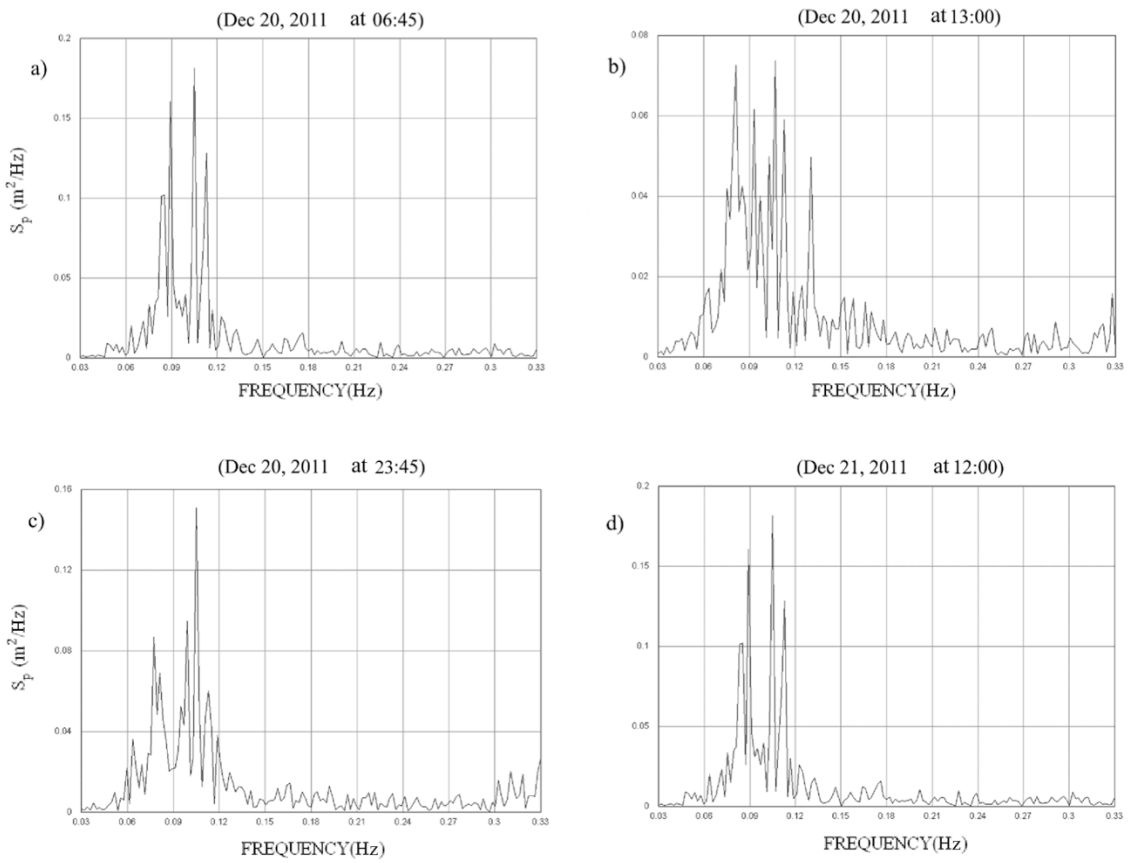

Figure 2.18. Examples of wave spectra versus wave frequency observed during Field Experiment 2, collected at site O2.

Table 2.6. Min, max, mean and standard deviation of wave heights observed during Field Experiment 3 at site A, O3, O5 and the difference between each two sites assuming waves move towards the shoreline (negative values indicates that wave height at the starting point is lower than end point).

Site	Min (m)	Max (m)	Mean (m)	Standard Deviation (m)
A	1.18	4.4	3.54	0.43
O3	0.18	1.57	0.62	0.26
Difference between A and O3	0.63	4.15	1.91	0.51
O5	0.39	1.33	0.81	0.24
Difference between O3 and O5	-0.29	0.56	-0.016	0.2

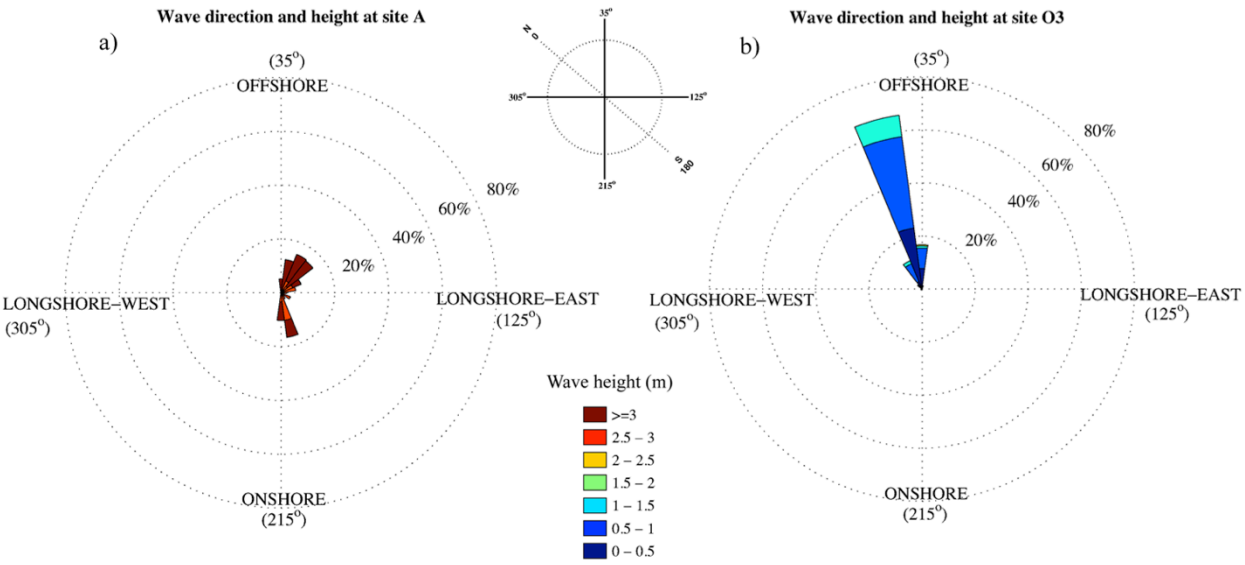

Figure 2.19. Rose plots showing wave height and direction measured during Field Experiment 3 at site A (a) outside Okains Bay, and site O3 (b) inside the bay. Directions are shown relative to the Okains Bay beach orientation.

2.3.3. Field experiment 3

The third experiment was carried out between 3rd and 13th April 2012. Since during that period wave data at site B and O1 were not available due to wave gauge maintenance, hindcast wave data at site A was used as a proxy for the wave climate outside Okains Bay. The hindcast wave data at site A indicate that predominant wave directions approached from 30° and 45° relative to the shoreline of Okains Bay followed by 165° relative to the shoreline (Figure 2.19a). Significant wave heights at this site ranged from 1.18 m to 4.4 m with a mean of 3.54 m, and significant wave periods ranged from 7.1 s to 13.1 s with a mean of 11.3 s (Figure 2.20).

Wave data collected at site O3, using an upward-facing 1200 kHz ADCP, indicated that waves predominantly approached from 345° (Figure 2.19b). Significant wave heights at this site ranged from 0.18 m to 1.57 m with a mean of 0.62 m, and significant wave periods ranged from 4.5 s to 14.9 s with a mean of 8.56 s (Figure 2.20).

Wave data collected at site O5 using a RBR XR-620 unit were split into two periods with a gap of about 40 hours in between. During the first period, significant wave heights at this site ranged from 0.39 m to 0.96 m with a mean of 0.58 m (Figure 2.20); significant wave periods ranged from 4.42 s to 8.9 s with a mean of 7 s. During the second period, significant wave heights ranged from 0.48 m to 1.33 m with a mean of 0.89 m; significant wave periods ranged from 2.9 s to 9.9 s with a mean of 6.26 s.

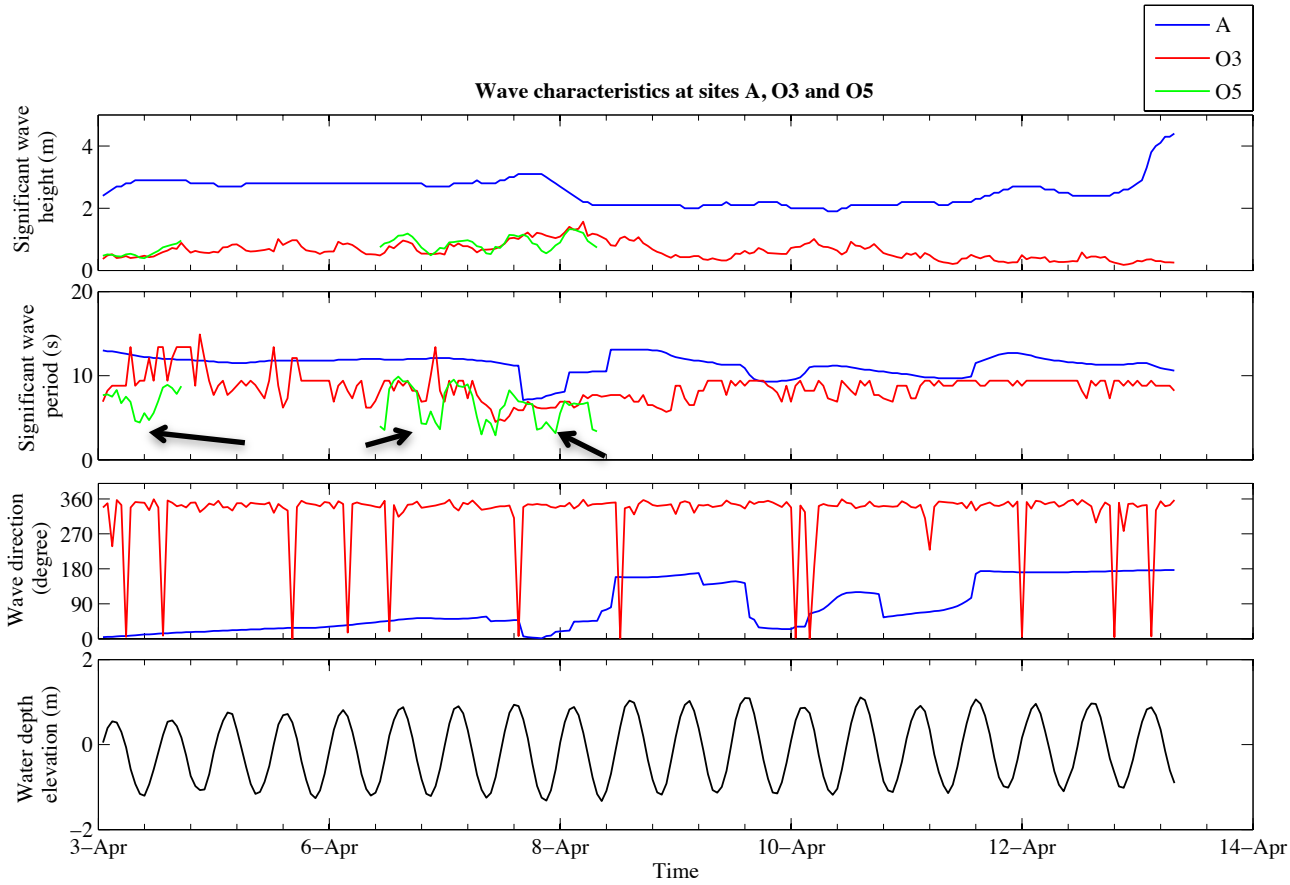

Figure 2.20. Comparison of wave data during Field Experiment 3 at site A, Outside Okains Bay, site O3 inside the bay, and site O5, inside the surf zone of the bay. Directions are given relative to the Okains Bay beach orientation. Water elevation is given relative to site O. Arrows indicates how significant wave periods between sites O3 and O5 notably changed.

The offshore wave hindcast at site A were higher than those observed inside the bay at site O3. (Figure 2.20 and Table 2.6). As depicted in Figure 2.19 a, the majority of wave heights are over 3 m at site A (see Table 2.6), whereas Figure 2.19 b indicates wave heights notably decreased at site O3 with an average of 1.9 m (Table 2.6). Wave heights are normally distributed at site A and O3, so most-frequent wave heights are clustered around the mean (Figure 2.21a and b). The scatter plot on wave heights at sites A and O3 also shows a very weak correlation with an R^2 of 0.05 (Figure 2.22 a). Similar to the Field Experiments 1 and 2, the poor correlation and the considerable reduction in the wave heights between offshore waves and waves inside the bay could suggest that in addition to dispersion, development of wave asymmetry, shoaling and refraction in Okains Bay, other factors, such as diffraction and reflection, could importantly influence wave heights when waves travel from outside to inside the bay.

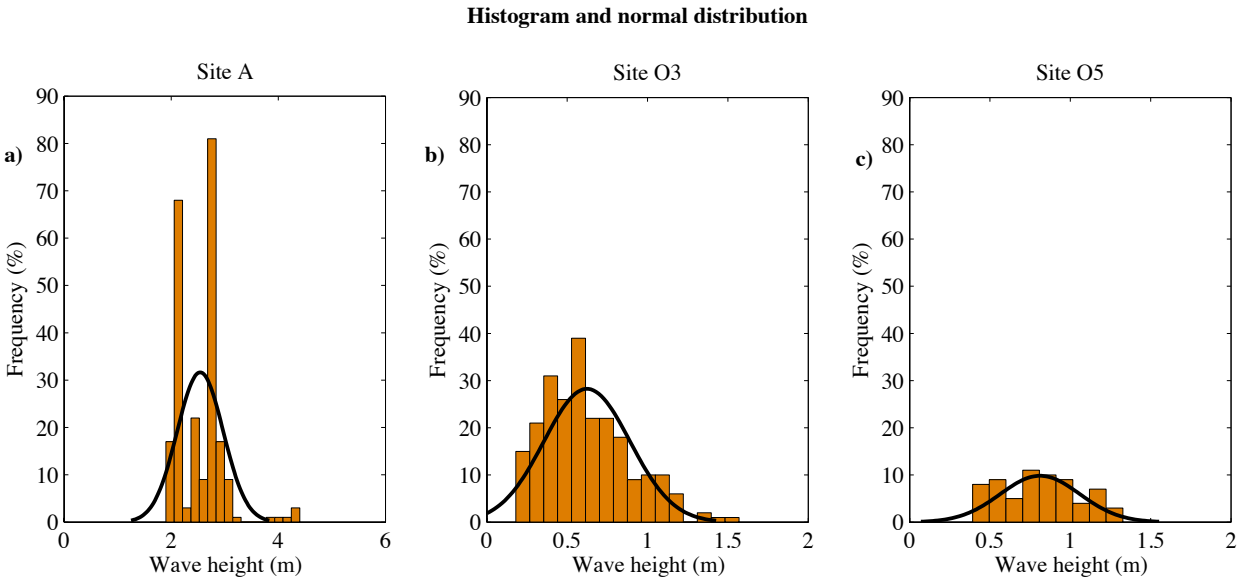

Figure 2.21. Histogram and normal distribution of wave heights at site A (a), site O3 (b), and site O5 during the field experiment 3.

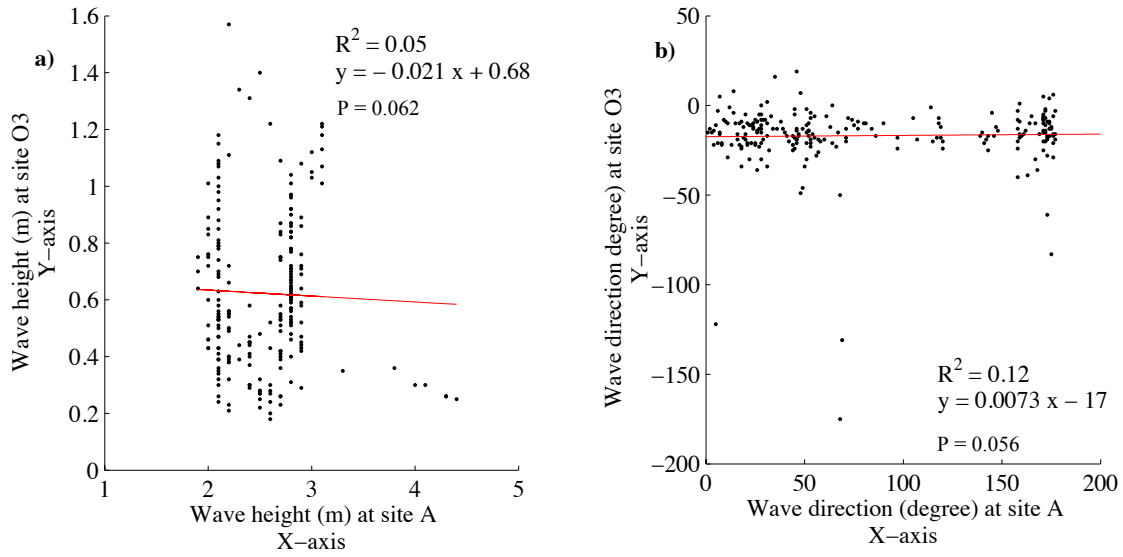

Figure 2.22. Scatter plot of wave height and wave direction when waves travelled from site A, outside Okains Bay, to site O3, inside the bay during Field Experiment 3.

However, the reduction in the wave heights propagating inside the bay from site O3 to O5 was insignificant. Wave heights are normally distributed at site O5, so the most frequent wave heights are clustered around the mean (Figure 2.21c). When waves moved from site O3 to O5, the wave heights insignificantly increased with an average of 0.016 m (Table 2.6). As discussed earlier, the wave height gradually increases before breaking in the surf zone of open coast beaches without consideration of friction (Sorensen, 1997; Masselink and Hughes, 2003). The slight increase in the wave heights at site O5 is similar to the wave processes in open coasts, suggesting that shoaling and refraction prevail over other factors inside the bay.

Similar to the other two experiments, in Field Experiment 3 the observations indicated that wave directions also changed significantly when waves travelled from outside to inside Okains Bay. Waves outside Okains Bay at site A predominantly approached from 30°, 45° and 165° relative to the shoreline, while the waves collected at site O3, inside the bay,

exhibited a predominant wave direction 345° to the shoreline (Figure 2.19). Figure 2.19 b shows that waves at site O3 approached from the downcoast headland side. This would suggest that reflection from the headland prevailed over other factors, including diffraction, shoaling and refraction during this experiment. The scatter plot shown in Figure 2.22 b also indicates that there is a poor correlation between wave directions at sites A and O3 with an R^2 of 0.12. This poor correlation could suggest a complex situation for wave processes inside the bay where waves are influenced by a combination of reflection, diffraction, shoaling and refraction once they enter into the bay. Wave processes inside Okains Bay are numerically explored further in Chapter 4 using SWAN Wave Model.

During Field Experiment 3, local wind data were recorded at site O6 (Figure 2.23). The data showed that the predominant wind directions moved to 15° and 225° relative to the shoreline; that is, winds were mostly blowing in offshore and relatively onshore directions inside the bay. Throughout the measurements, the wind speed varied between 0.2 ms^{-1} and about 6.8 ms^{-1}. In this study, low to moderate winds are referred to as having a wind speed less than 4 ms^{-1}, and moderate to strong winds are referred to as having a wind speed over 4 ms^{-1}.

In Field Experiment 3, wave heights at site O3 inside Okains Bay poorly correlated with the observed local winds (Figure 2.24). In contrast to Field Experiment 2 (Figure 2.14), local winds were reasonably stronger with an average speed of 2.62 ms^{-1} and with a maximum of 6.8 ms^{-1}. Nevertheless, the correlation between wind speed and wave height at site O3 was still weak with an R^2 of 0.32 (Figure 2.25 a).

However, the correlation between observed wave heights and wind speeds was reasonable at site O5 with an R^2 of 0.56 (Figure 2.25 c). It can be inferred that moderate local winds with speeds less than 6.8 ms^{-1} could possibly impact wave characteristics inside the breaking zone of Okains Bay. Since waves deeper into the bay are more sheltered due to the presence of the headlands, moderate to strong local winds could influence wave characteristics in the breaker zone of Okains Bay.

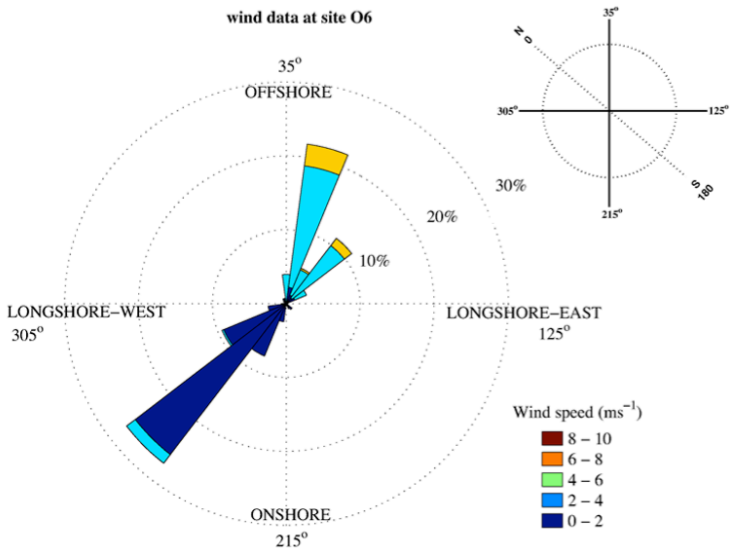

Figure 2.23. Rose plot showing wind data measured during Field Experiment 3 at site O6 inside Okains Bay. Note that wind directions are shown "to" and relative to the Okains Bay beach orientation.

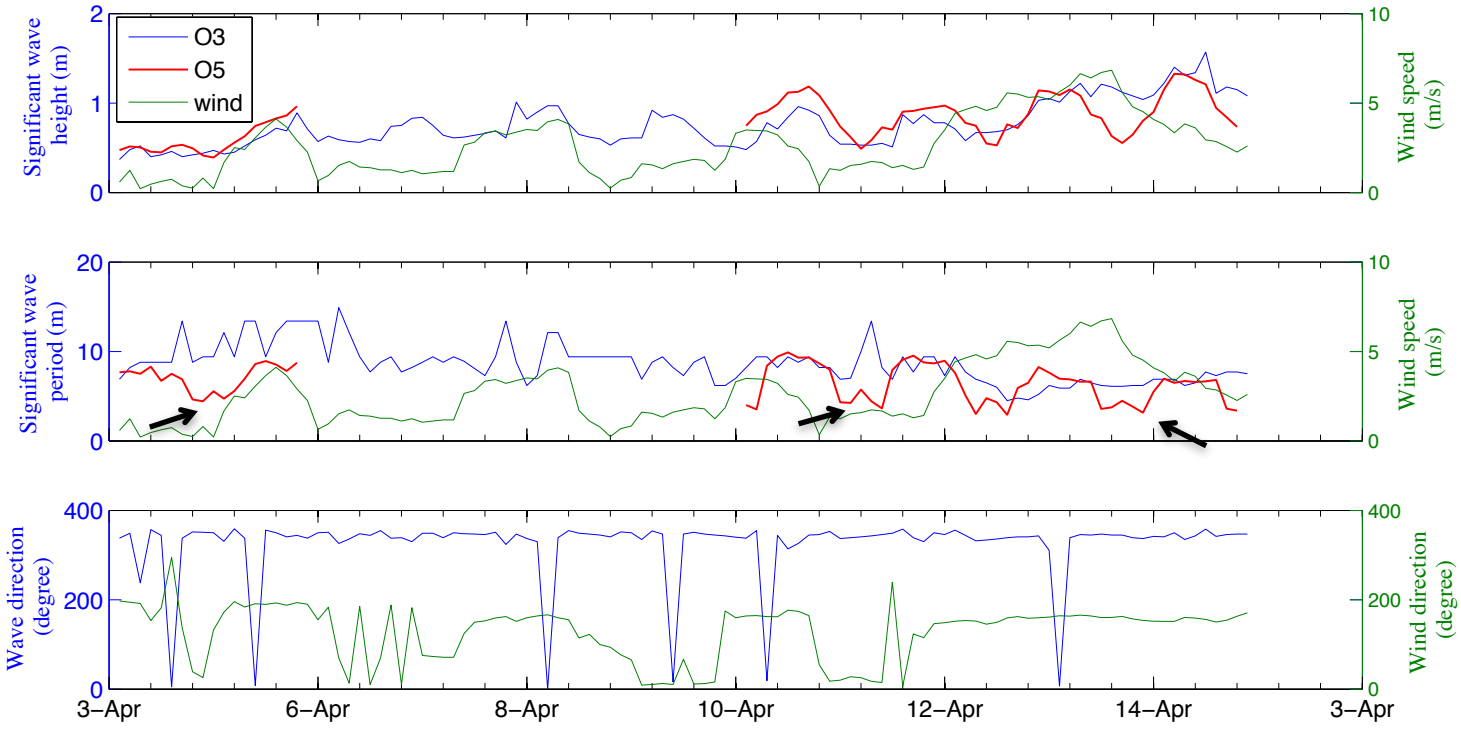

Figure 2.24. Comparison between wind data averaged every 10 minutes collected at site O6 and wave data with a 20 minutes burst at sites O3 and O5 during Field Experiment3. Directions are given relative to the Okains Bay beach orientation.

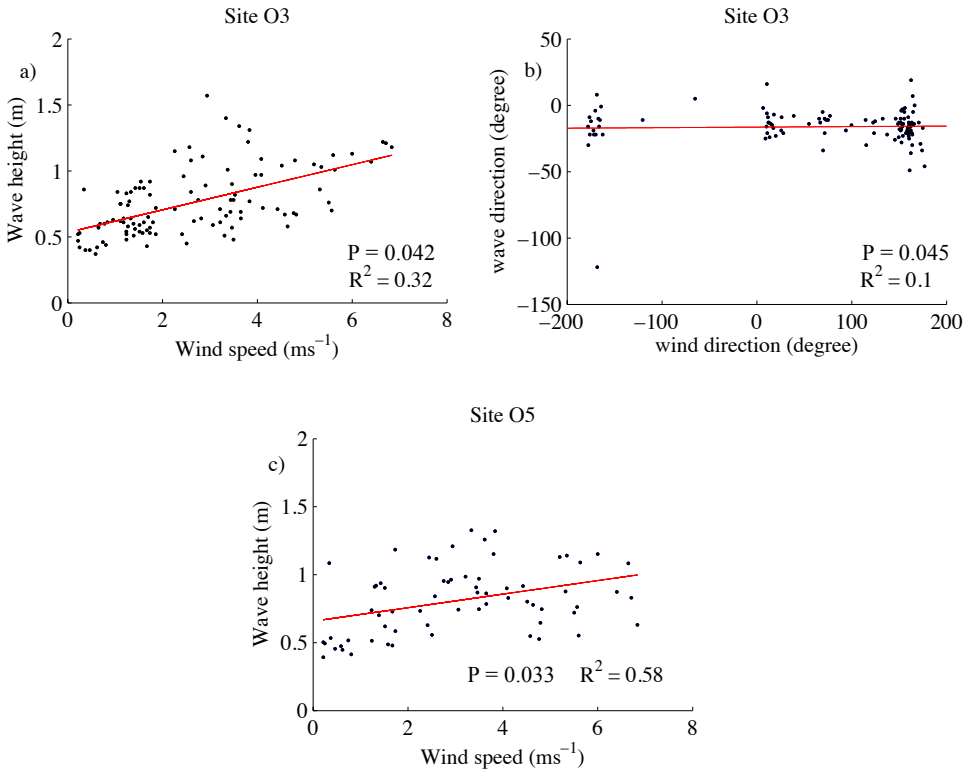

Figure 2.25. Scatter plot of wind speed and wave height and also wind direction and wave direction recorded during Field Experiment 3 inside Okains Bay at site O3 (a, b), and O5 (c).

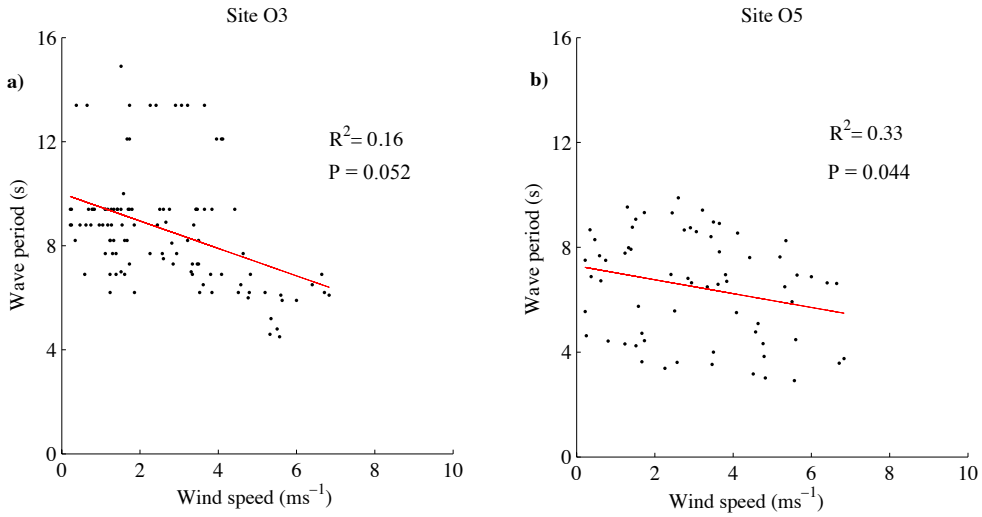

Figure 2.26. Scatter plot of wind speed and wave period inside Okains Bay at site O3 (a), and site O5 (b) during Field Experiment 3.

Wave data on wave periods from Field Experiment 3 indicate that wave periods could change when waves enter into shallow water (Figure 2.24). Similar to Field Experiment 2, the wave periods between sites O3 and O5 inside the bay slightly changed, except for some situations as shown by arrows in Figure 2.24. Local winds could be the main reason that wave periods changed from site O3 to O5. Correlation between local winds and wave periods were weak with an R^2 of 0.16 (Figure 2.26 a). However, as expected, the correlation was stronger at site O5 with an R^2 of 0.33 (Figure 2.26 b). This suggests that the moderate to strong local winds with speeds less than 6.8 ms^{-1} could be one reason that wave periods changed from nearshore site O3 relative to site O5 inside the breaking zone.

Water depth could be another reason that possibly changed the wave periods at site O5. The water level at site O5 varies between about 0.8 m to 2.9 m, causing the location of the breaking to shift across the shore. As shown by arrows in Figure 2.20, during low tide, wave periods only at site O5 dropped considerably. However, when the water level relative to sites O3 and O5 rose, wave periods at site O5 gradually increased so that during high tide the difference of wave periods between both sites reached their minimum of about 0.75 s. The reason this effect was not observed during Field Experiment 2 could be related to the variation of wave heights. Breaking water depth can be calculated by (Komar, 1998):

$$\gamma = \frac{H_d}{h_d} \tag{2.1}$$

where γ is breaking index, which could vary between 0.6 and 1.7 (Weggel, 1972), H_d and h_d are breaker wave height and breaker water depth. Okains Bay beach is classified as dissipative, with a foreshore gradient of 1:60. According to Weggel's (1972) breaking index classification, the breaking index for Okains Bay is about 0.78. During Field Experiment 2, water depth at site O5 varied between 0.8 m and 2.9 m and wave heights varied between 0.18 m and 0.46 m. According to Eq. 2.1 and the Okains Bay breaking index, the critical breaking water depths calculated for these wave heights would be 0.23 m and 0.58 m respectively. That is, during low tide and high tide, site O5 was always seaward of the breaker line.

However, during Field Experiment 3, the incident wave heights increased and varied between 0.39 m and 1.33 m, indicating higher energy waves compared to those collected during Field Experiment 2. According to Eq. 2.1 and the Okains Bay breaking index, the critical breaking water depths for these wave heights would be 0.5 m and 1.7 m respectively. This suggests that during low tide, site O5 was shoreward of the breaker line. As a result, wave periods can significantly change when waves break and propagate in the swash zone. This feature could also happen in open coast beaches, but what makes this feature unique in pocket beaches is the way the headlands filter deep-water high-energy waves. Accordingly, waves lose considerably energy when they enter the bay and, therefore, the tidal effect on wave characteristics may be accentuated.

2.4. Discussion

The wave observations outside and inside Okains Bay showed a complex wave process inside the bay. Once waves entered into the bay, the wave heights significantly decreased. The reduction in the wave height could be caused by open coast wave processes as well as reflection and diffraction that is the result of sheltering of the bay. A comparison of wave directions between offshore waves and shallow water waves inside the bay also showed that wave directions significantly changed inside the bay. The observations of waves in areas deep enough into the bay showed that waves approached from the downcoast headland. This suggests that reflection from the downcoast headland could prevail over other factors, such as diffraction, refraction and shoaling.

A deep look into the planforms of pocket and embayed beaches would suggest the importance of reflection in controlling waves in pocket beaches besides diffraction, shoaling and refraction. The planform of embayed beaches consists of a highly curved shoreline close to the headland, followed by a gentle curvature in the middle of the shoreline, and a straight shoreline towards the downcoast limit of the beach (Klein et al., 2010) (Figures 2.27a and b). However, in pocket beaches like Okains Bay, the shoreline is gently curved in proximity to

both headlands, while the middle section of the shoreline is approximately straight. That is because in embayed beaches, waves are diffracted from the headland and form a highly curved shoreline or a shadow zone in proximity to the headland. Diffraction gradually disappears towards the middle of the shoreline so that waves are mainly influenced by refraction and shoaling. Therefore, the downcoast shoreline becomes almost parallel to the predominant approaching wave crest.

Figure 2.27. Example shorelines of embayed beaches (a and b) versus pocket beaches (c and d). Note that the shoreline of embayed beaches consists of a highly curved shoreline and a shadow zone close to the upcoast headland, while pocket beaches exhibit a simple shadow zone with a gentle curve in proximity to both downcoast and upcoast headlands.

However, pocket beaches exhibit a simple shadow zone plus a shoreline that is parallel to the predominant approaching wave crest (Figures 2.27 c and d). Inside pocket beaches, waves propagate normal to the shoreline or at an angle close to normal regardless of offshore wave direction (see Woodroffe, 2002). In this study, observations showed that waves inside the bay approached either normal to the shoreline or at an angle close to normal from the downcoast headland, while offshore waves approached in a variety of directions to the shoreline. The predominant normal wave direction indicates different wave processes inside the bay than embayed and open coast beaches. This wave process inside pocket beaches could form a simple shadow zone plus parallel shoreline to the predominant approaching wave crest, which could be caused by reflection as a result of the presence of the downcoast headland.

Okains Bay, an example pocket beach, is embayed between two long natural headlands, which limit the in-bay wave directional sector (Figure 2.1b). Waves with directions greater than the directional sector could be influenced by diffraction from the upcoast headland and possibly reflection from the downcoast headland. Wave observations at different sites outside and inside the bay indicate that waves also changed considerably once they were propagated towards the shoreline. Wave heights shoreward of the breaker line were relatively low, while a greater range of wave heights were collected outside of Okains Bay. This suggests that wave heights inside the bay in areas close to the shoreline could be influenced by diffraction as a result of sheltering.

However, a comparison of the wave height reduction at different sites inside Okains Bay showed that wave heights changed less in areas closer to the entrance of the bay, which is more exposed to ocean waves. The results of Field Experiment 2 indicate that even though wave height changed after entering into the bay, the reduction in the wave height is less than that when waves propagate further into the bay towards the shoreline. Since areas closer to the entrance of the bay have a greater directional sector, waves are less influenced by headlands. Therefore, refraction and shoaling prevail over other factors in areas closer to the entrance of the bay.

The effect of reflection on wave directions was clearer than that on wave heights, when waves travelled into Okains Bay. During Field Experiments 1 and 3, waves at site O3 had predominant approach directions from the downcoast headland, while observed wave directions outside Okains Bay predominantly approached from the upcoast headland. This

considerable difference in the wave direction could be mainly caused by reflection from the downcoast headland.

However, this effect was not observed in areas closer to the entrance of Okains Bay at site O2, which is more exposed to ocean waves. Results of Field Experiment 2 indicate that wave direction changed to normal once waves entered into the bay. However, since this area is more exposed to the open ocean, the directional sector is greater. Thus, waves are less influenced by diffraction and reflection, and consequently, refraction and shoaling prevail in the area.

Sheremet et al. (2002) used cross-shore velocity spectral density to decompose the infragravity waves into seaward and shoreward components in order to examine the importance of shoreline-reflected waves. However, in this current study, both reflected waves from the downcoast headland and infragravity waves propagated towards the shoreline, so it would be very difficult to differentiate the reflected waves from infragravity waves. Since approaching wave characteristics, including wave period, change after reflection (Goda and Suzuki, 1976), velocity spectral density could be used to examine the changes when the area is dominated by either reflected or infragravity waves.

The velocity spectral density analysis suggests that depending on the approaching wave direction, reflection could dominate the wave processes inside Okains Bay. As indicated in Figure 2.28, for a cycle between low tide and high tide (the first 12 hours), when waves approached from angles within the Okains Bay directional sector (from 20° to 70° relative to true north), the highest frequency was about 0.09 Hz.

However, after 12 hours when approaching wave direction increased over 70° to the true north, it was expected that the reflected waves dominate the area over the infragravity waves. The velocity spectral density analysis indicated that the highest frequency increased around 0.12 Hz to 0.19 Hz (Figure 2.29) for a period from high tide to low tide. These results suggest that when deep water waves cannot approach the bay directly, the frequency of velocity spectral density increases notably, indicating the importance of reflection on wave characteristics inside the bay.

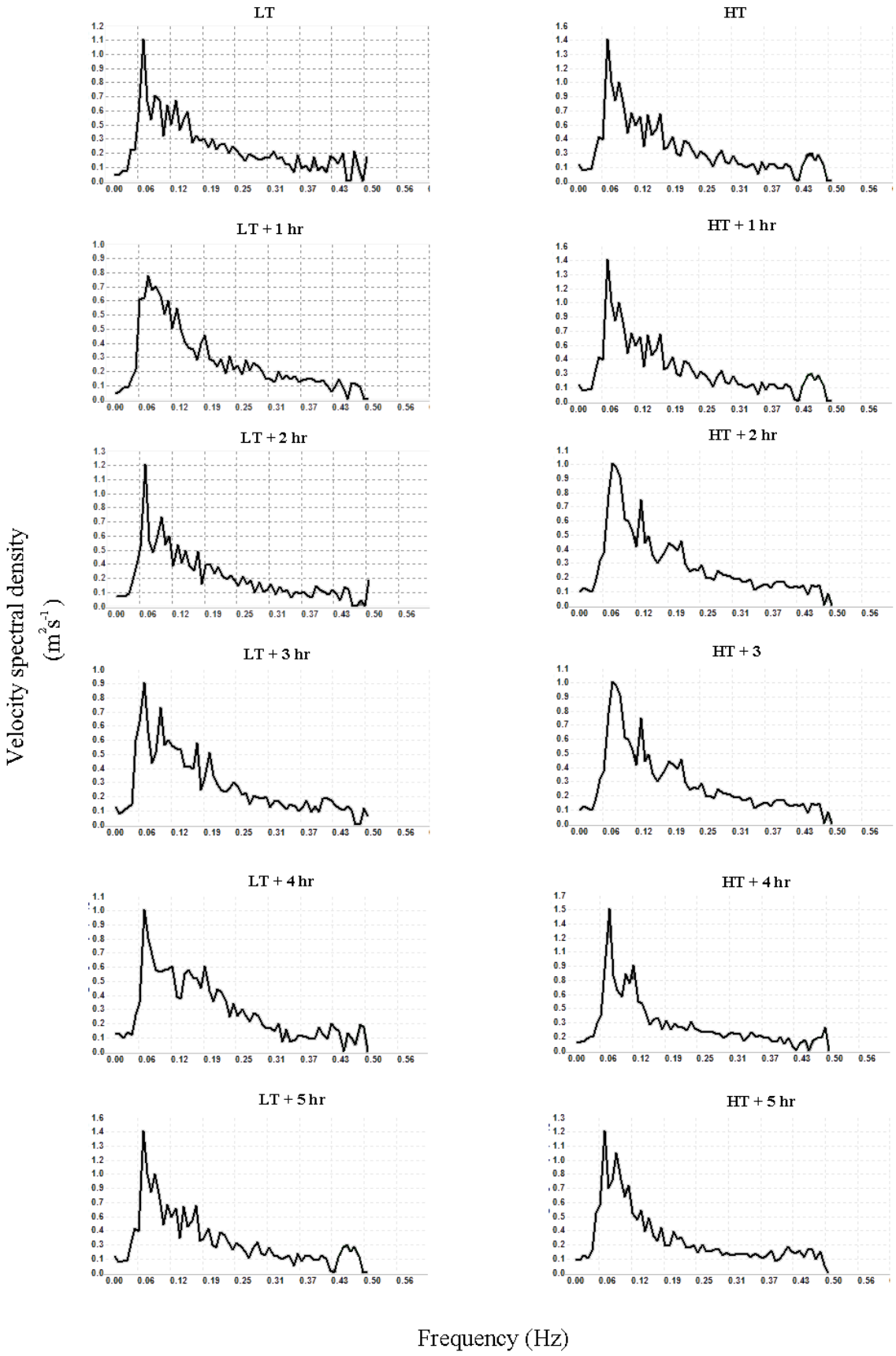

Figure 2.28. Velocity spectral density for a duration of 12 hours from low tide to high tide when waves approached from an angle within the directional sector of Okains Bay during Field Experiment 1.

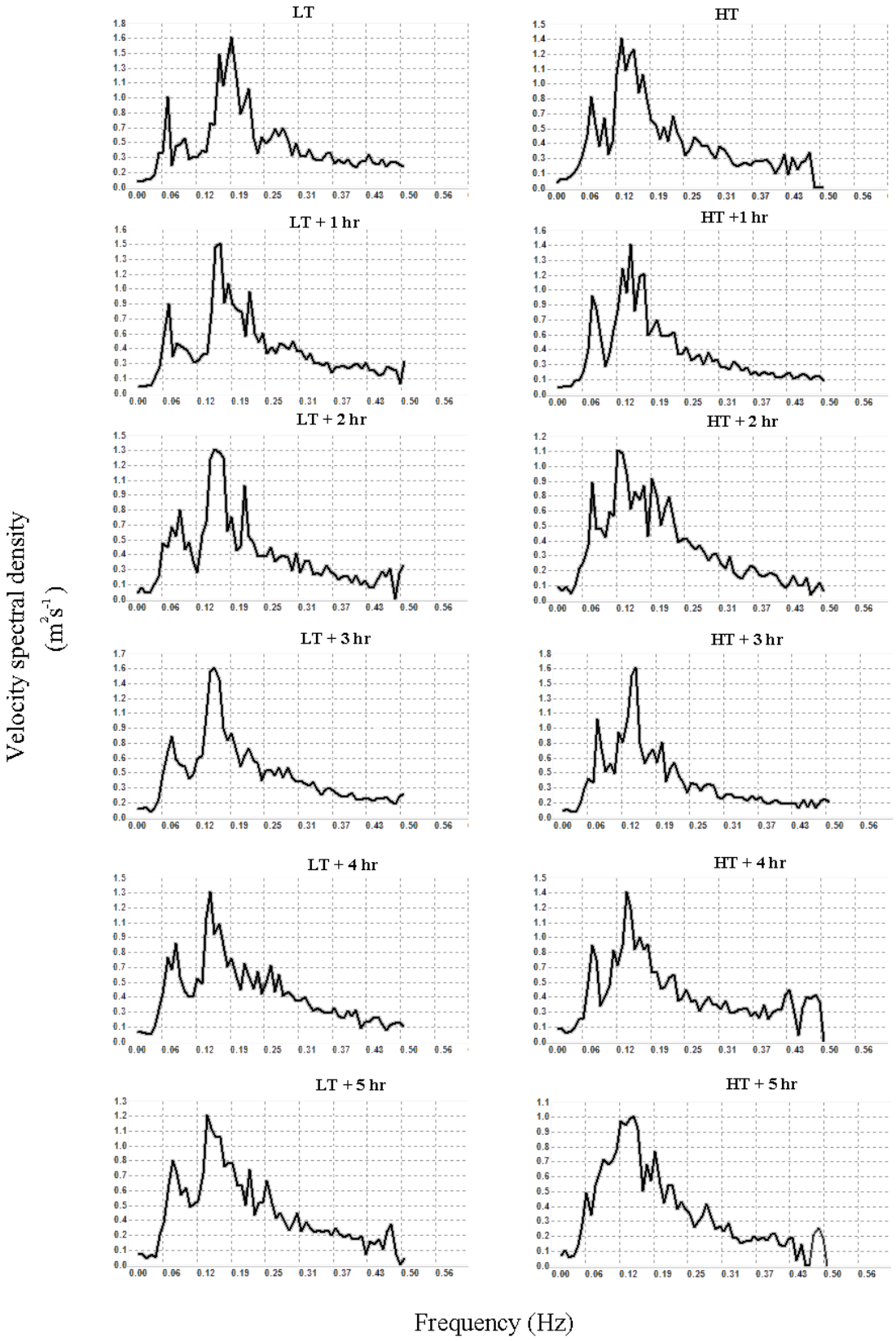

Figure 2.29. Velocity spectral density for a duration of 12 hours from high tide to low tide when waves approached from an angle greater than the directional sector of Okains Bay during Field Experiment 1.

Literature on wave processes in open coast beaches show that waves are mainly influenced by dispersion, development of wave asymmetry, shoaling and refraction (Sorensen 1997; Masselink and Hughes, 2003). When one headland is added to the open coast beaches, like embayed beaches with one headland, diffraction is added into the aforementioned factors (see Wiegel, 1964; Abul-Azm and Williams, 1997; Lin and Demirbilek, 2012). In pocket beaches with two headlands, in addition to other factors, the results of the Okains Bay field experiments suggest that reflection could be an important factor in controlling wave processes inside the bay. However, this idea needs more in depth studies to evaluate the influence of reflection in pocket beaches. In chapter 4, first a simple experimental model is used to show the importance of reflection in Okains Bay. Afterwards, the SWAN will be applied to simulate waves outside and inside the bay in order to quantify the importance of each factor, including reflection, in controlling wave processes when waves enter into the bay from different directions.

2.5. Conclusion

In this chapter, wave climates at Okains Bay were studied in order to investigate the processes that make pocket beaches unique in terms of wave processes. Results from three field experiments indicate that significant wave heights decreased notably from outside compared to inside Okains Bay. This reduction reached its maximum when waves approached at an angle close to a longshore direction. The changes in wave height could suggest that waves could be influenced by other factors, including diffraction and reflection rather than dispersion, development of wave asymmetry, shoaling and refraction.

Literature shows that wave period is independent of water depth (e.g. Sorensen 1997). This means that the wave period remains constant when waves travel from deep to shallow water. Observations on wave periods throughout all three deployments indicated that wave periods collected outside Okains Bay changed compared to wave periods collected at sites O2, O3, O4 and O5, except for the wave periods of the third experiment collected at site O5 at low tide.

The comparison between wave heights collected at site O5 during Field Experiments 2 and 3 showed that small waves would break in a shallower depth according to the breaking index, γ. Therefore, changes in water depth from low tide to high tide could re-locate the position of the breaker line and, subsequently, site O5 would be landward of the breaker line during low tide, thereby exhibiting a significant decrease in wave periods.

Wave directions varied significantly between outside versus inside Okains Bay. Wave data collected at site O3 showed waves approached from the downcoast headland side, suggesting the effect of reflection on wave directions. However, observations at site O2 showed waves approached normal to the shoreline. This could suggest that other factors, such as refraction and shoaling, prevail over diffraction and reflection in areas closer to the entrance of the bay.

In the next chapter, Linear Wave Theory and also linear regression analysis will be used to transfer waves from deep water (site A and B) to transitional water at site O1, outside Okains Bay. The reason for finding the best approach to transfer waves from deep water to site O1 is that wave data were not collected at this site during the Field Experiment 2 and 3, but wave data at site O1 are needed for the numerical modelling studied in chapter 4.

Chapter 3: Wave transformation

This chapter focuses on transferring waves from deep water to areas outside Okains Bay in a depth of 12 m. This task fills the gap in wave data for site O1 during Field Experiments 2 and 3 and contributes towards thesis aim 1 by starting to theoretically test the similarities and differences between wave environments outside and inside pocket beach bays and, thus, the effect of headland-wave approach interactions.

3.1. Introduction

Wave transformation from deep water to shallow water of open coast beaches has been studied widely (Liu and Losada, 2002; Sorensen, 1997; Dean, 1974; Skjelbreia, 1959; Eckart, 1952). Some of these studies were based on numerical modelling (Lv *et al*., 2013; Gorman et al., 2003a; Liu, 1994) and the others applied wave theories to transfer waves from deep water to intermediate or shallow waters (Sobey, 2012; Craik, 2005; Le Méhauté, 1969; Stokes, 1847). This chapter concerns the transfer waves from deep water to areas outside Okains Bay in a depth of 12 m in order to fill the gap in wave data for site O1 during Field Experiments 2 and 3. The SWAN model, Linear Wave Theory and also statistical correlation were used to evaluate the best prediction method for estimating wave characteristics at site O1.

3.1.1. Linear Wave Theory

This study is based on waves with periods less than 30 s which are classified as short period gravity waves (Sorensen, 1997). Different wave theories were developed for short period waves such as Linear Wave Theory (or Airy theory), Stoke, Cnoidal and Solitary. In this study both Linear Wave and Stokes theories are applied to transfer waves from a depth of about 76 m to 12 m, and then to 6 m. Linear Wave Theory is the simplest wave theory; it is based on mass balance and momentum balance equations, developed for deep waters (Holthuijsen, 2007). If deep-water linear waves are fully developed, the Linear Wave Theory can be extended to shoaling waves up to the breaking point with the assumption that wave steepness is relatively small (less than 0.00004) (Le Roux, 2008).

In Okains Bay, the wave steepness varied between 0.001 and 0.0042 with a relative depth (h/gT^2) varying between about 0.0043 and 0.1. According to Le Méhauté (1969), both second-order Stokes and Linear Wave theories can be used to transfer waves from deep water to site O1. Note that the calculation of wave velocity using these two theories is similar, especially for deeper areas (see Sorenson 1997). The wave velocity, C, and wave length, L, extracted from Linear Wave Theory and used in this study, are shown as (Sorensen, 1997):

$$C = \sqrt{\frac{gL}{2\pi}\tanh\frac{2\pi h}{L}} \tag{3.1}$$

$$L = \frac{g}{2\pi}T^2\tanh\frac{2\pi h}{L} \tag{3.2}$$

where g is the gravitational acceleration (ms^{-2}), T is wave period (s) and h is water depth (m).

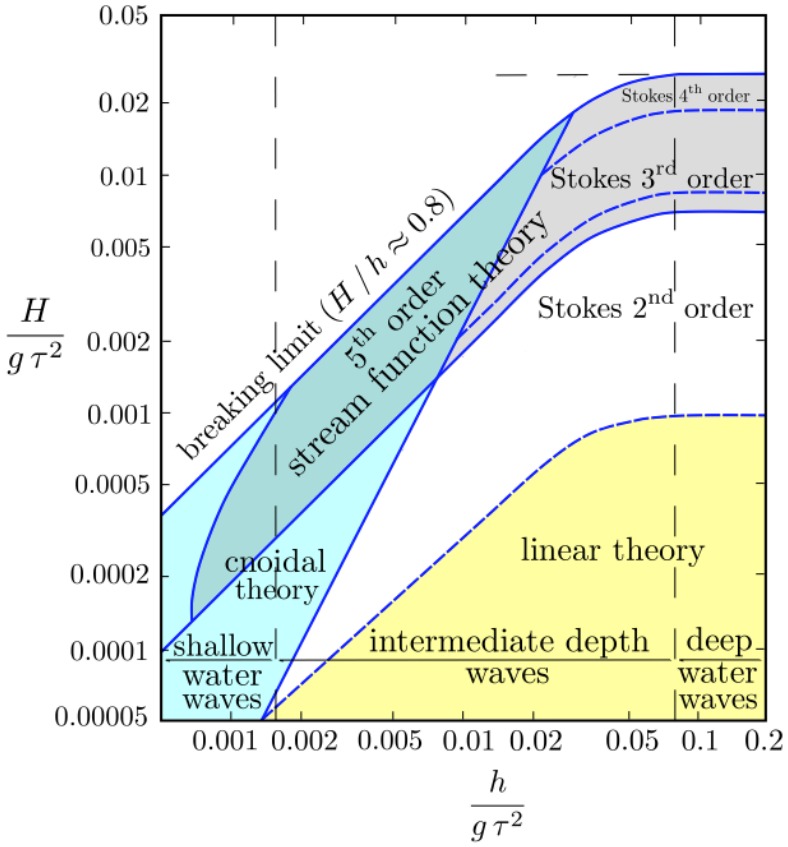

Figure 3.1. The ranges of the applicability of wave theories based on relative depth (x-axis) and wave steepness (y-axis) (Le Méhauté, 1969).

Linear Wave Theory, which has been widely used to analyse ocean waves, is known as the basic theory for ocean waves (e.g. Finnegan and Goggins, 2012; Le Roux, 2008; Holthuijsen, 2007; Abbott et al., 1978; Airy, 1845). Several studies have been conducted to determine the limit of each wave theory's application based on some basic factors such as wave height (H), wave period (T), wave length (L) and water depth (h) (Holthuijsem, 2007; Dean and Dalrymple, 1991; Le Mehaute, 1969). For instance, Le Méhauté (1969) classified the ranges of applicability of each wave theory based on h/gT^2 and H/gT^2 ; the results are shown as a graph (Figure 3.1). The Linear Wave Theory can be used from deep waters to shallow waters, depending on the wave steepness, although its applicability to shallow waters is very limited.

Dean (1974) also studied the application of each theory from deep waters to shallow water based on h/L_0 and H/ H_b (where H_b is breaking wave height) and presented the results as a table. A similar study was also carried out by Dean and Dalrymple (1991). Their studies showed the ranges of applicability of Linear Wave Theory based on h/T^2. According to Dean and Dalrymple (1991), the Linear Wave Theory can also be applied to shallow waters for some specific values of h/T^2, but these are very limited. The main reason is that in Linear Wave Theory the crest and trough of a wave are always equal, while in reality, when a wave enters shallow waters, the trough becomes flatter. It can, therefore, be inferred that the Linear Wave Theory is not applicable to steep waves or waves in very shallow waters. However, once waves enter shallow waters, other theories, such as higher order Stokes or Cnoidal theories, are more appropriate.

Another well-know method widely used to determine the ranges of applicability of wave theories is the Ursell number (Sorensen, 1997). However, the applicability of this method is limited to Stokes and Cnoidal theories. The Ursell number is a dimensionless parameter given as (Holthuijsen, 2007):

$$N_{Ursell} = \frac{steepness}{(relative\ depth)^3} = (\frac{H}{L})/(\frac{h}{L})^3. \quad (3.3)$$

If the N_{Ursell} > 26, Cnoidal theory is applicable and if N_{Ursell} < 10, the Stokes theory is applicable. For a range of 10 < N_{Ursell} < 26, both theories are applicable.

3.1.2. SWAN Wave Model

SWAN (Simulating WAves Nearshore) is a third-generation wave model based on the wave action balance equation with source and sinks (The Swan Team, 2013):

$$\frac{\partial N}{\partial t} + \frac{\partial}{\partial x}(U + c_x)N + \frac{\partial}{\partial y}\big(V + c_y\big)N + \frac{\partial}{\partial \sigma} c_\sigma N + \frac{\partial}{\partial \theta} c_\theta N = \frac{S_{tot}}{\sigma} \qquad (3.4)$$

where N is the wave action spectral density function, σ and θ are the component wave angular frequency and direction, c_x and c_y are the group velocities in the x and y directions, U and V are the current velocities in x and y directions, c_σ and c_θ are the characteristic velocities in σ and θ directions, and S_{tot} is the source term. The first term in this equation states the local variation rate in wave special action density over time (Anastasiou and Sylaios, 2013). The second and third terms represent the propagation of wave energy in two-dimensional Cartesian geographic space and the fourth and fifth terms express the depth and current induced wave refraction. Finally, the right hand side term in Eq. 3.4 expresses the processes of wave energy generation, dissipation and redistribution, given as:

$$S_{tot} = S_{in} + S_{wc} + S_{nl4} + S_{bot} + S_{brk} + S_{nl3} \qquad (3.5)$$

where S_{in} is the transfer of wind energies to waves, S_{wc} is wave energy dissipation due to whitecapping, S_{nl4} is nonlinear transfer of wave energy due to quadruplet interaction, S_{bot} is dissipation caused by bottom friction in shallow water, S_{brk} is depth-induced breaking and S_{nl3} is nonlinear triad interaction.

SWAN is designed to give realistic estimates in different environments such as coastal areas, lakes and estuaries. The model can be applied for coastal scales (e.g. 800x1000 m) and scales even larger than the coastal scales (e.g. 30x40 km). However, this model is not recommended for ocean scales in order to achieve realistic estimates. The WAN and WAVEWATCH III are developed for ocean scales and achieve more accurate estimates than SWAN for such scales (The Swan Team, 2013).

The SWAN model has been widely used to simulate waves in different water depths at coastal scales or in larger areas (Anastasiou and Sylaios, 2013; Lv *et al*., 2013; Huang et al., 2013; Hargreaves *et al*., 2002; Booij *et al*., 1996). Ou *et al*. (2002) studied the simulation of typhoon waves using field experiments and SWAN in coastal areas of Taiwan. Their studies demonstrated how the SWAN model can reasonably predict waves in nearshore regions. They also indicated that the SWAN nested grid scheme could be used to boost the accuracy of the predictions in shallow waters.

Gorman *et. al*. (2003) also applied SWAN model to transfer a 20-year wave hindcast from deep water to shallow water in the outer Hauraki, New Zealand. The results of the model were validated against wave observations at a depth of 30 m in Mangawhai on the northeast coast of the North Island. Gorman et al. (2003) concluded that the SWAN model can be reliably applied to remap wave information for most New Zealand coastlines. However, the effect of local winds on simulated waves was not considered in their study.

Lv *et al*. (2013) studied short-term and long-term wave processes using field experiments and the SWAN model in the Bohai Sea north of China. The results of measurements showed that wind, whitecapping, bottom mechanism of wave source function and tidal currents were four main factors in controlling wave processes. The comparison between the results of measurements and those from the SWAN model indicated that the latter model results accurately estimated wave characteristics in this area over both short and longer terms. Similar studies were also carried out by Booij *et al*. (1999) and van der Westhuysen *et al*. (2007). Their comparisons between the model results and observations indicated that the SWAN model was able to predict wave characteristics in deep water and shallow water with acceptable accuracy.

However, other studies have shown that the SWAN model may overestimate wave heights in deep waters. Huang *et al.* (2013) applied the SWAN model to study the Gulf of Mexico hurricane waves. In their study, hurricane wind data were used as an input into the model. The comparison between the results of the model and observations showed that the model overestimated significant wave heights by about 2 m in deep water (i.e. the estimations exceeded the observations by 20%). Despite the overestimation of the waves in deep water, simulated waves that were transferred to depths shallower than 20-30 m showed a reliable prediction of wave heights. That is because a shallow water dissipative effect was added to

the model, so the overestimated wave height at deep water had limited effects on wave heights in shallower depths.

SWAN has proved over numerous studies to be a reliable model with realistic estimates of wave characteristics. This model was used in this study to simulate waves at both deep water and shallow water. In order to predict shallow water waves using deep water wave data, SWAN was used at a scale larger than coastal, but smaller than an ocean scale, as detailed in the methodology section.

3.2. Methodology

This chapter focuses on transferring waves from deep water to areas outside Okains Bay in a depth of 12 m. This approach fits into both left-hand and right-hand portions of the thesis methodology diagram illustrated in Figure 1.6.

3.2.1. Study site

The study area is offshore Okains Bay, located on the north-eastern side of the volcanic peninsula on the east coast of New Zealand's South Island (Figure 3.2); this area is exposed to the South Pacific Ocean. In this study, the offshore area is divided into two rectangular domains. The smaller rectangle, shown in black in Figure 3.2, has a length of 15 km and a width of 17 km. The water depth in the eastern boundary at site A is approximately 150 m. The larger rectangle, shown in white in Figure 3.2, has a length of 20 km and a width of 14 km. The water depth in the eastern boundary at site B is about 17 m. Wave climates for areas outside Okains Bay at sites A and B were discussed earlier in section 2.2.1.

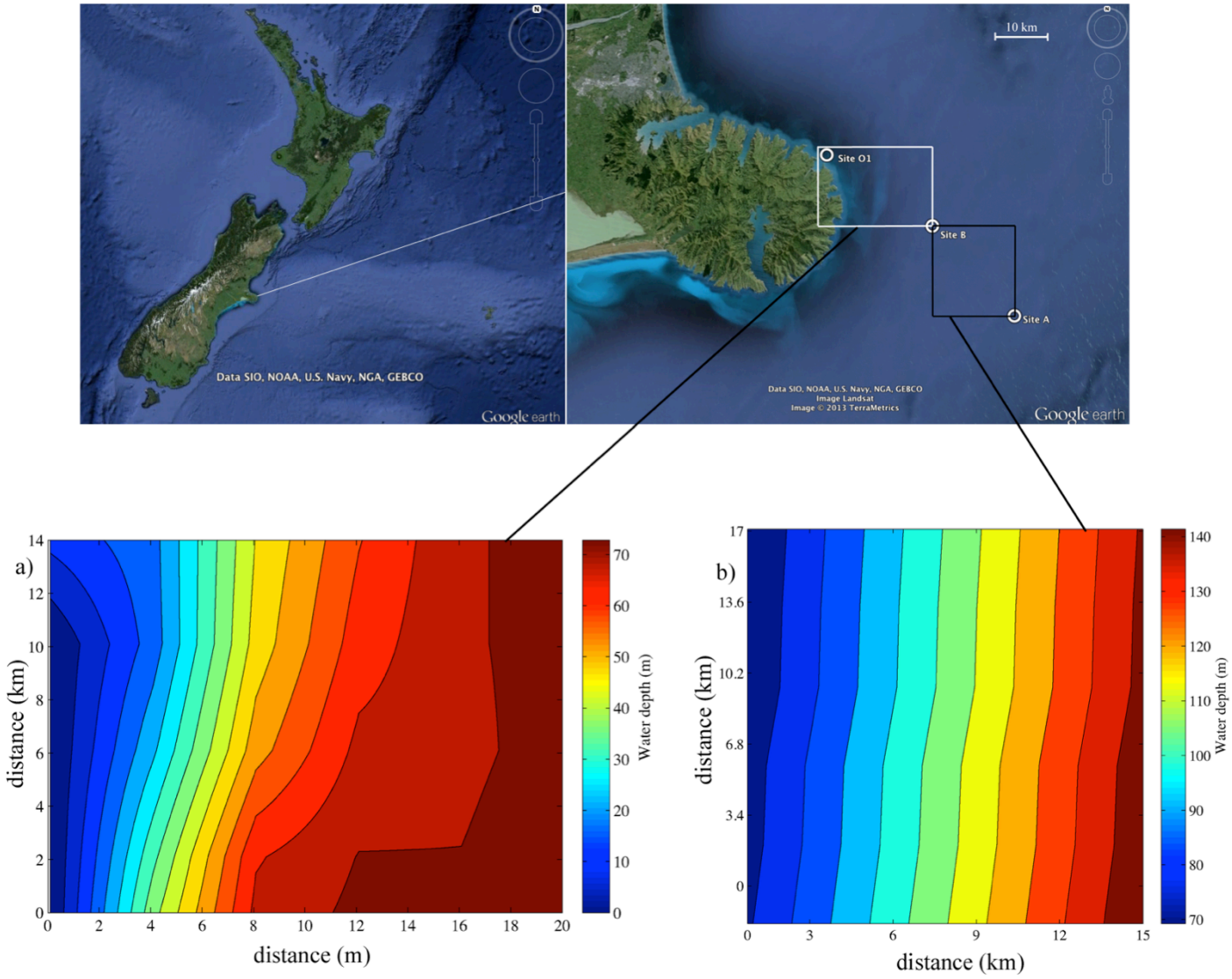

Figure 3.2. Study sites at three locations offshore Okains Bay, Banks Peninsula; Site A is located at about 30 km east of Peninsula, site B is located at about 17 km and site O1 is 200 m outside Okains Bay. Black and white rectangles represent the model domain of wave simulations with bathymetry used in the SWAN model.

3.2.2. Methods

This study employs the SWAN model, Linear Wave Theory and linear regression to investigate the most accurate technique to generate site O1 wave predictions based on input wave data from sites A and B. Wave data collected during Field Experiment 1 between 20th April and 11th May 2011 at site O1 and at site B (see Chapter 2, Table 2.1 for more details on the deployment) were used to validate the best approach to transferring waves from site

B to O1 (Figure 3.3). This approach was then applied to fill the gap in wave data for site O1 during Field Experiment 2 using available wave data at site B.

As discussed in Chapter 2, during Field Experiment 3, wave data were not available at both sites O1 and B. The only available wave data in Banks Peninsula in proximity to site B were the wave hindcast at site A throughout 2012. However, there is no wave data simultaneously available at both sites A and O1 during all three experiments in order to validate the best approach to predicting waves at site O1 (Figure 3.3). Therefore, the available wave data at sites A and B were first used to investigate the best technique to generate wave predictions at site B. Afterwards, the approach used during Field Experiment 2 was applied to fill the gap in wave data for site O1 during Field Experiment 3 based on input wave data from site B. Note that the hindcast wave data at site A were only available for the entire 2012 and only Field Experiment 3 was accomplished in this year. Since wave data recorded during Field Experiment 3 at site B were not available, a period between 10th and 30th Jan 2012 was chosen to cover the availability of both observed waves at site B and hindcast wave data at site A.

The first method applied to transfer waves from site A to B, and then B to O1, was the SWAN model. The simulated areas were divided into two rectangles, shown in Figure 3.2. In order to simulate wave characteristics offshore of Okains Bay, the SWAN model (version 40.91) (The Swan Team, 2013) was implemented with the nominal formulations of the physical processes. JONSWAP bottom friction is used to run the model and whitecapping dissipation, depth-induced breaking and triad wave-wave interaction are also included in the model configuration. The configuration grid for SWAN is shown in Table 3.1 and bathymetry used for these simulations are shown in Figure 3.2a and b. The time step of each simulation was the same as the duration of observations (Table 3.1).

Linear Wave Theory, discussed in section 3.1.1, was also applied to transfer waves from site A to B, and B to O1, during the same experiments used in the SWAN model (Figure 3.3 and Table 3.1). Equations 3.1 and 3.2 were used for each individual significant wave height and direction obtained at site A in order to estimate the significant wave height and direction at site B. The bathymetric data were obtained from Land Information New Zealand (LINZ) with a horizontal resolution of 3.18 m. The same method was also applied to transfer waves from site B to O1. In this approach, according to Sorensen (1997), the wave period was assumed constant between each site.

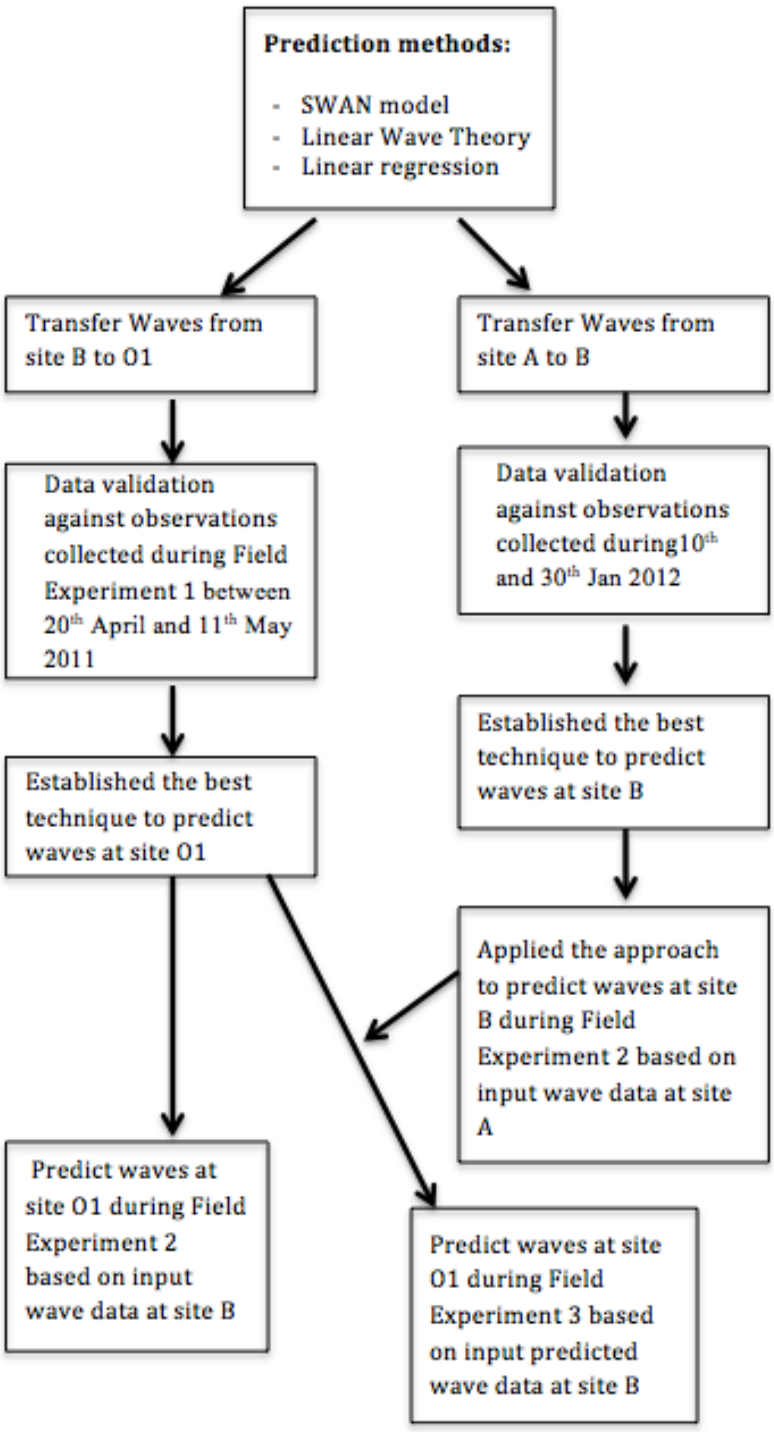

Figure 3.3. Wave prediction diagram showing the technique and data used to generate site O1 wave predictions based on input wave data from sites A and B.

Finally, linear regression was applied to find the best correlation between wave heights and directions at sites A and B, and then B and O1. To this end, linear regression was implemented in SPSS (version 20.0.1) (Argyrous, 2011). Correlations were examined between wave characteristics measured simultaneously at different sites. As in Linear Wave Theory, it was assumed that wave period remains constant when waves travel between each site A, B and O1. In reality, wave period could be influenced by local winds, but this assumption in the study is more related to the influence of the variation of water depth on wave periods.

The results of each approach at sites B and O1 were validated against the observations. Index of Agreement (IOA) and Mean Absolute Error (MAE) were used to compare the results of predictions with observations:

$$MAE = \frac{1}{n}\sum_{i=1}^{n}|P_i - y_i| \tag{3.6}$$

$$IOA = 1 - \frac{\sum_{i=1}^{n}(p_i - y_i)^2}{\sum_{i=1}^{n}[(|p_i| - |\bar{y}|) + (|y_i| - |\bar{y}|)]^2} \tag{3.7}$$

where p is prediction, y is observation, $\bar{y}$ is mean of observations and n is the number of observations. In additional to IOA and MAE, the coefficient of determination, R^2, is also used to indicate how well predicted waves fit the observation and the results shown as scatter plots. A classification of values for IOA, MAE and R^2 used in this study is shown in Table 3.2. These values indicate the accuracy level of a method applied to predict wave characteristics.

3.3. Wave transformation analysis

According to the Linear Wave Theory, when waves propagate from deep waters to shallow waters, their wavelengths begin to slightly decrease (Sorensen, 1997). This effect will be significant when waves approach intermediate and shallow water. A reduction in the wavelength causes the wave speed to decrease and, accordingly, the wave heights and direction change. However, changes in the water depth do not affect wave periods; that is, wave periods are independent of water depth (Sorensen, 1997). This section evaluates three methods to find the best correlation between wave data at sites A and B, and then B and O1, in order to fill the gaps in wave data for site O1 during Field Experiments 2 and 3: Linear

Wave Theory, the SWAN wave model and linear regression analysis. Figure 3.2 shows a classification of values for IOA, MAE and R^2 used in this study to indicate the accuracy level of a method applied to predict wave characteristics.

Table 3.1. Configurational grid for SWAN simulations.

Grid location	Simulation duration	Grid description	Grid (Easting x Northing)	Cell grid size (m)	
				dx	dy
Between sites A and B	20th April 2011 to 11th May 2011	Medium resolution grid	150 x 170	100	100
Between sites B and O1	10th June 2012 to 30th June 2012	Medium resolution grid	200 x 140	100	100

Table 3.2. A classification of values for IOA, MAE and R^2 used in this study to indicate the accuracy level of a method applied to predict wave characteristics.

Statistical tool	Wave characteristics	Strong	Moderate	Weak
IOA	Wave height, period and direction	0.7 - 1	0.4 – 0.69	0 – 0.39
MAE	Wave height	0 – 0.4	0.41 – 0.8	> 0.8
	Wave period	0 - 1	1.1 - 3	>3
	Wave direction	0 - 25	26 - 35	> 35
R^2	Wave height, period and direction	0.7 – 1	0.4 – 0.69	0 – 0.39

3.3.1. Wave transformation from site A to B

During Field Experiment 3, wave data were not available from site B (Canterbury wave buoy), so the hindcast wave data for the closest location to site B was chosen to predict the wave data. In order to establish a correlation between wave data at sites A and B, 20 days wave data available in each site throughout the period of 10th January to 30th January 2012 were used (Figure 3.4). In this correlation, two basic assumptions were made: 1) wave periods are constant and are not affected by the variation of water depth; 2) waves are not affected by local winds.

The statistical analysis, using SPSS tool, showed that the wave directions, as a dependent value, at site B are correlated to the wave directions and periods (as independent values) at site A (Figure 3.5 and 3.6b). A linear regression analysis indicated that there is a strong correlation between the dependent and independent values with an R^2 of 0.81 (Figure 3.6b). IOA and MAE, calculated for this approach, were 0.89 and 25, which indicate reliable estimations using regression analysis (Table 3.3). The resulting linear regression equation is given as:

$$Dir_b = 0.733Dir_a + 2.084T_a + 11.034 \quad (3.8)$$

Also wave heights, as a dependent value, at site B are correlated to the wave heights, directions and periods (as independent values) at site A. A linear regression analysis showed dependent value is reliably correlated to independent values with an R^2 of 0.78 (Figure 3.6a). IOA and MAE, calculated for this approach, were 0.93 and 0.33 (Table 3.3), suggesting regression correlation can accurately predict the wave heights at site B. The resulting linear regression equation is shows as:

$$H_b = 0.51H_a + 0.002Dir_a - 0.088T_a + 1.266. \quad (3.9)$$

where *Dir* is wave direction, *T* is significant wave period, *H* is significant wave height and subscript *a* shows wave characteristics at site A.

Table 3.3. Comparison of IOA and MAE of equation established using linear regression, Linear Wave Theory and the SWAN model for wave characteristics at site B.

Wave Characteristics	Method	IOA	MAE	Significance Value	R^2
Wave height	Eq. 3.9	0.93	0.33	<0.05	0.78
	SWAN model	0.8	0.71	<0.05	0.7
	Linear Wave Theory	0.78	0.73	<0.05	0.67
Wave period	SWAN model	0.96	0.66	<0.05	0.9
Wave direction	Eq. 3.8	0.89	25	<0.05	0.81
	SWAN model	0.79	36.1	<0.05	0.76
	Linear Wave Theory	0.7	51	<0.05	0.72

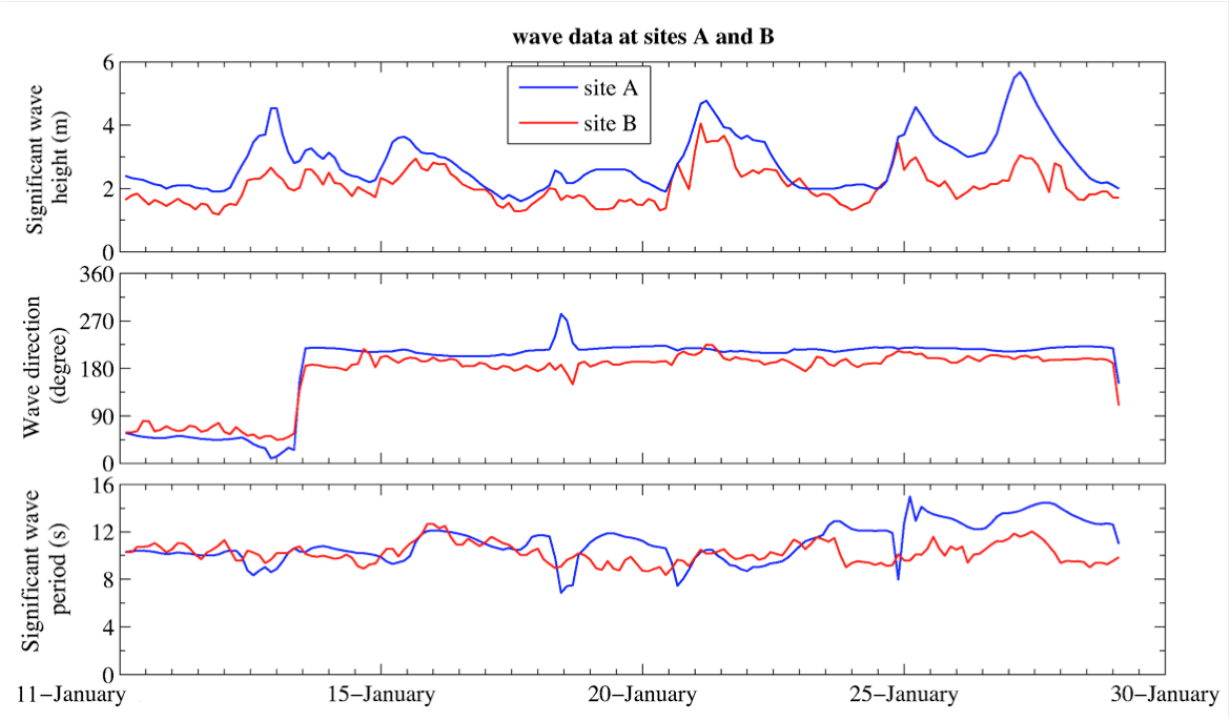

Figure 3.4. A comparison between hindcast wave data averaged hourly, at site A, in a depth of 150 m, and observed wave data at site B, in a depth of 76 m, offshore of Okains Bay during 11 January and 30 January 2012. Directions are shown relative to true north.

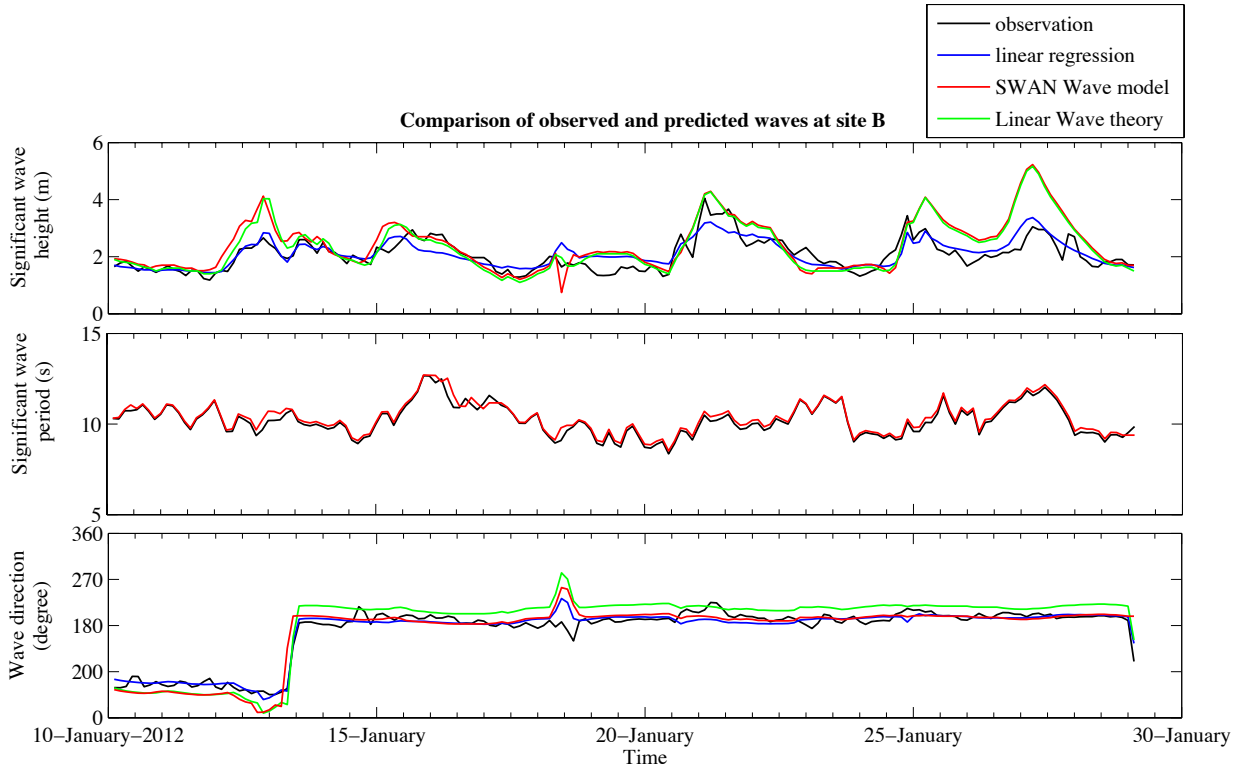

Figure 3.5. A comparison between the various predicted and observed wave data, averaged hourly, in a depth of 76 m at site B offshore of Okains Bay during 11 January and 30 January 2012. Directions are shown relative to true north.

The SWAN model was also applied to transfer waves from sites A to B (Figure 3.5). The results indicated that SWAN overestimates wave heights by about 25% at site B when observed wave heights are over 2.3 m at site A. The maximum overestimation was 2.1 m at site B on 27th January 2011 when observed wave height was about 2.8 m (Figure 3.5). However, this discrepancy reached its minimum when wave heights were about 2.2 m throughout the measurements. Although the correlation between SWAN-estimated wave heights and observations at site B was weaker than that of those predicted using linear regression derived from Eq. 3.9, results indicate that SWAN can be used to generate reasonable estimates of wave height at site B with an R^2 of 0.7 (Figure 3.7). The IOA and MAE calculated for this approach were 0.8 and 0.71 (Table 3.3), further confirming that the SWAN estimates are acceptably accurate.

In contrast to wave height, SWAN can precisely estimate wave periods at site B (Figure 3.7). The results showed that the SWAN-estimated wave period and observations at site B were strongly correlated with an R^2 of 0.9 (Figure 3.7). The IOA and MAE calculated for this approach were 0.96 and 0.66, suggesting the SWAN model is able to generate reasonable prediction of wave period (Table 3.3).

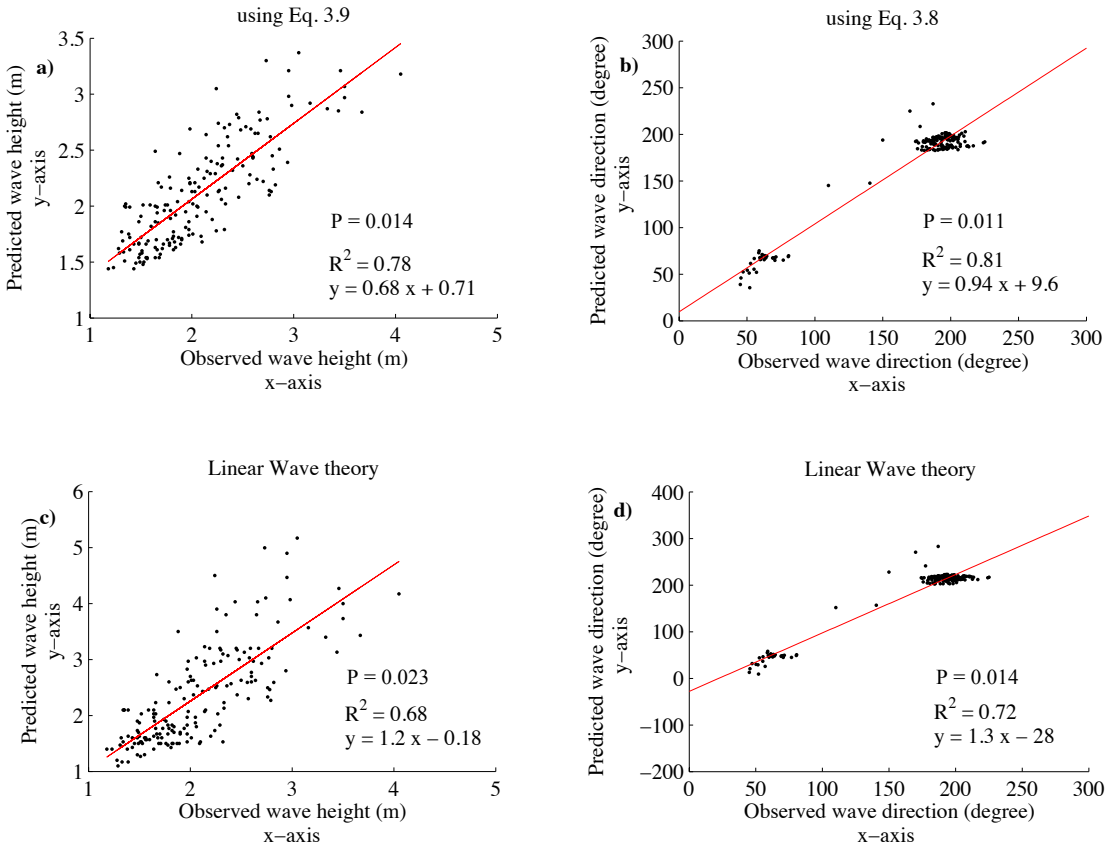

Figure 3.6. Scatter plots of predicted wave height and directions using Eq. 3.8 and 3.9 and Linear Wave Theory versus observations recorded during 10 January and 30 January 2012 at site B.

Wave directions at site B can also be reasonably estimated using the SWAN model. The results indicated that SWAN underestimates wave direction at site B when wave direction is below 50°, while it generates overestimates when wave direction is above 150° (Figure 3.5). The overall correlation between prediction and observation was reasonable, with an R^2 of 0.76. The IOA and MAE calculated for this approach were 0.79 and 36.1, suggesting that the SWAN model can reliably predict wave directions at site B (Table 3.3).

Linear Wave Theory was also used to transfer waves from sites A to B (Figure 3.5). The results indicated that estimated wave heights using Linear Wave Theory were similar to those generated using the SWAN model. However, Linear Wave Theory estimations were slightly higher than those of SWAN. As shown in Figure 3.6c, there is an average correlation between predicted wave height using Linear Wave Theory and observations at site B, with an R^2 of 0.68. The IOA and MAE calculated for this approach were 0.78 and 0.73 (Table 3.3).

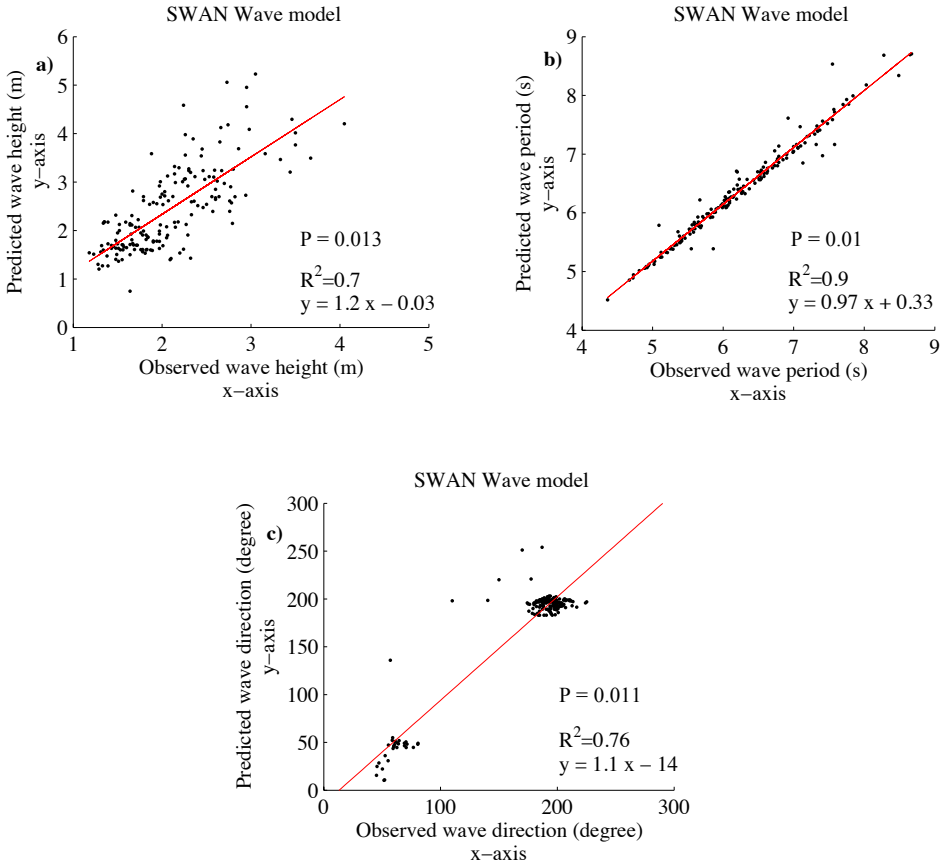

Figure 3.7. Scatter plots of the SWAN-predicted wave height, period and directions versus observations recorded during 10 January and 30 January 2012 at site B.

Linear Wave Theory can moderately estimate wave directions at site B (Figure 3.5). Similar to the results of SWAN, Linear Wave Theory underestimates wave direction at site B when the approaching wave direction is less than 50°, whereas it overestimates directions greater than 150° (Figure 3.5). The correlation between Linear Wave Theory prediction and observation is reasonable with an R^2 of 0.72 (Figure 3.6d). However, the IOA and MAE calculated for this approach were 0.7 and 51, showing a moderate level of estimation accuracy using Linear Wave Theory at site B (Table 3.3).

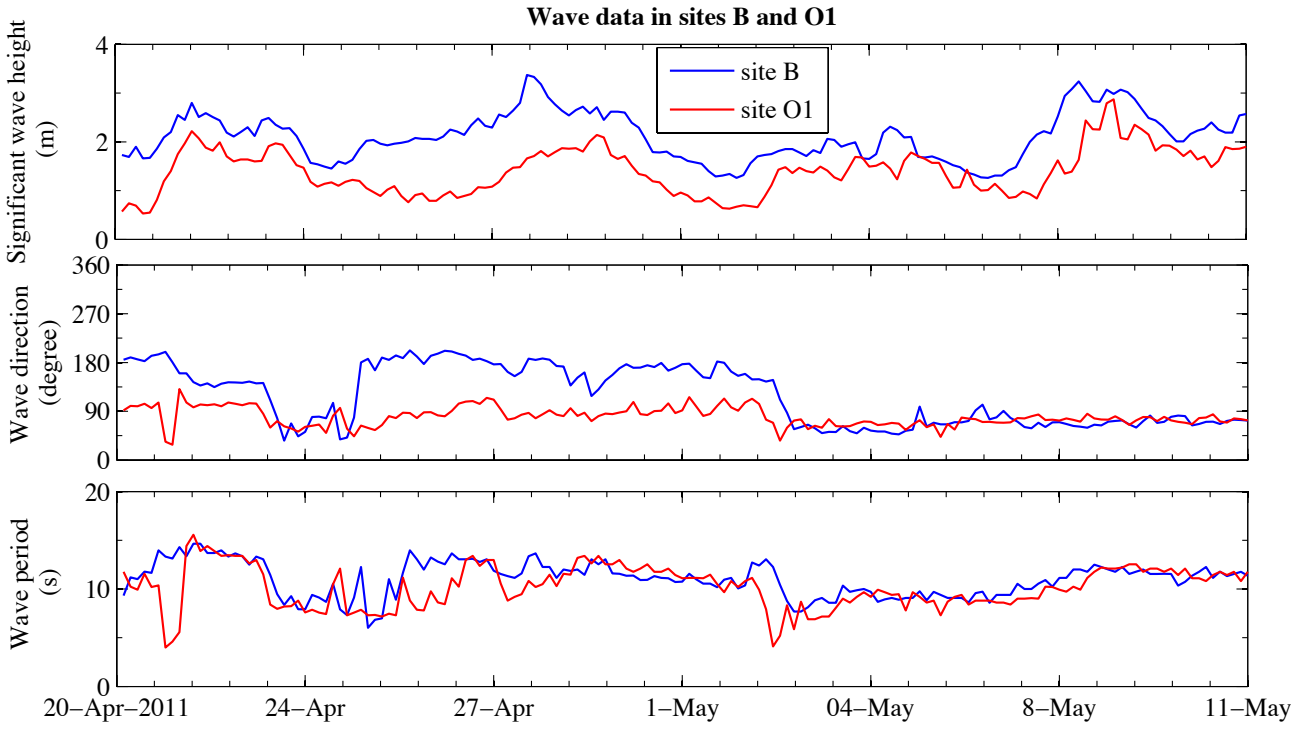

Figure 3.8. A comparison between wave data, averaged hourly, at site B, in depth of 76 m, and site O1, in depth of 12 m, outside Okains Bay during Field Experiment 1. Directions are shown relative to true north.

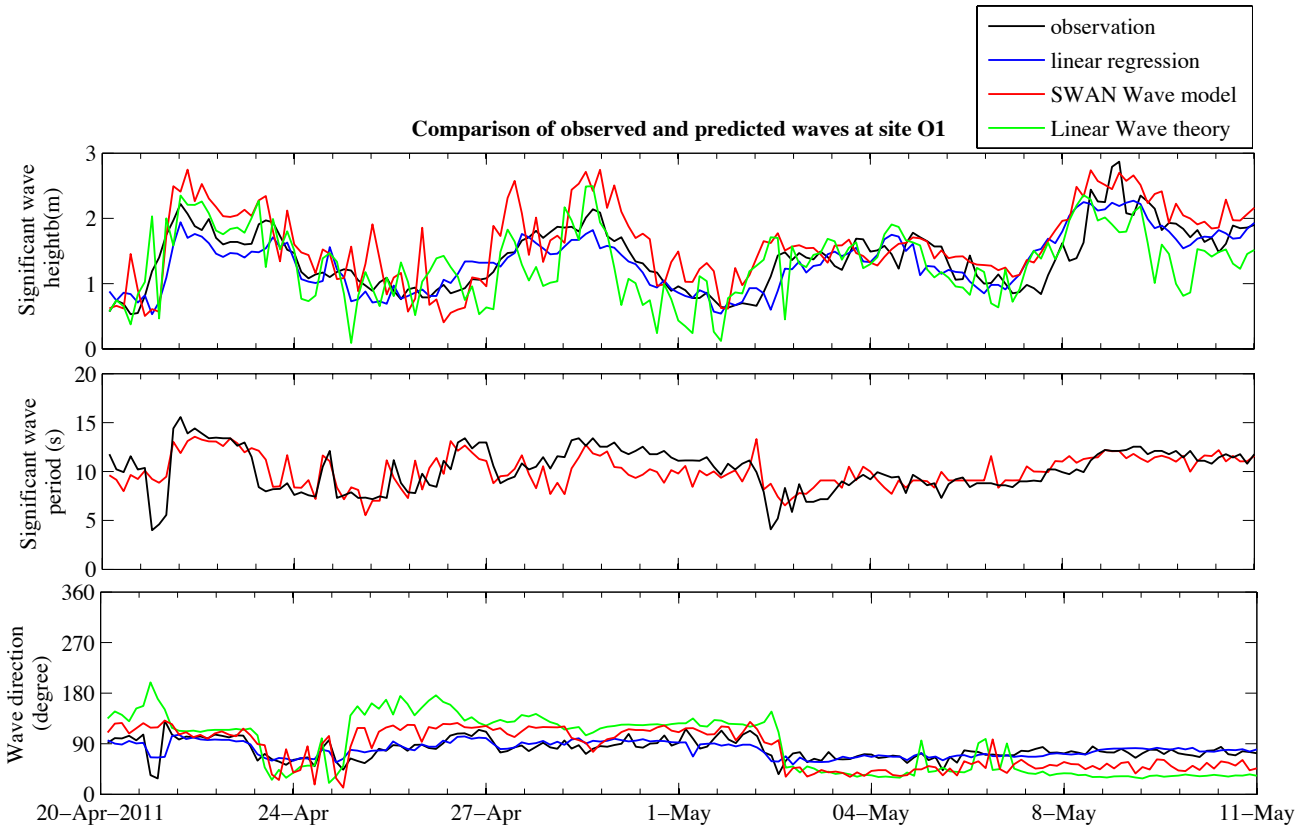

Figure 3.9. A comparison between various predicted wave data averaged hourly, versus observations recorded during Field Experiment 1 in depth of 12 m at site O1 outside Okains Bay. Directions are shown relative to true north.

3.3.2. Wave transformation from site B to O1

As discussed earlier, wave data at site O1 were not available for the periods of the second and third field experiments. Therefore, the wave data for this site were predicted using deep-water wave data at sites A and B. In order to transfer waves from Site B to O1, it is necessary to establish a correlation based on the available wave data in both sites during the period of the first field experiment, which lasted 22 days from 20th April to 11th May 2011 (Figure 3.7). In this correlation – the same as the previous approach – it was assumed that the wave period remained constant and waves were not affected by local winds.

The statistical analysis, using the SPSS tool, showed that the wave directions, as a dependent value, at site O1 were correlated to the wave directions and periods (as independent values) at site B. A linear regression analysis indicated that there is a reliable

correlation between the dependent and independent values with an R^2 of 0.74 (Figure 3.9 and Figure 3.10b). The IOA and MAE calculated for this approach were 0.83 and 11.12, suggesting strong estimations using regression analysis (Table 3.4). The resulting linear regression equation is given as:

$$Dir_{o1} = 0.143Dir_b + 4.189T_b + 20.363 \quad (3.10)$$

where subscripts *b* and *o1* show wave characteristics at sites B and O1.

Table 3.4. Comparison of IOA and MAE of equation established using linear regression, Linear Wave Theory and the SWAN model for wave characteristics at site O1.

Wave Characteristics	Method	IOA	MAE	Significance Value	R^2
Wave height	Eq. 3.11	0.89	0.35	<0.05	0.79
	SWAN wave model	0.74	0.43	<0.05	0.72
	Linear Wave Theory	0.65	0.49	<0.05	0.58
Wave period	SWAN wave model	0.71	1.39	<0.05	0.65
Wave direction	Eq. 3.10	0.83	11.12	<0.05	0.74
	SWAN wave model	0.7	32.52	<0.05	0.6
	Linear Wave Theory	0.51	47.31	<0.05	0.4

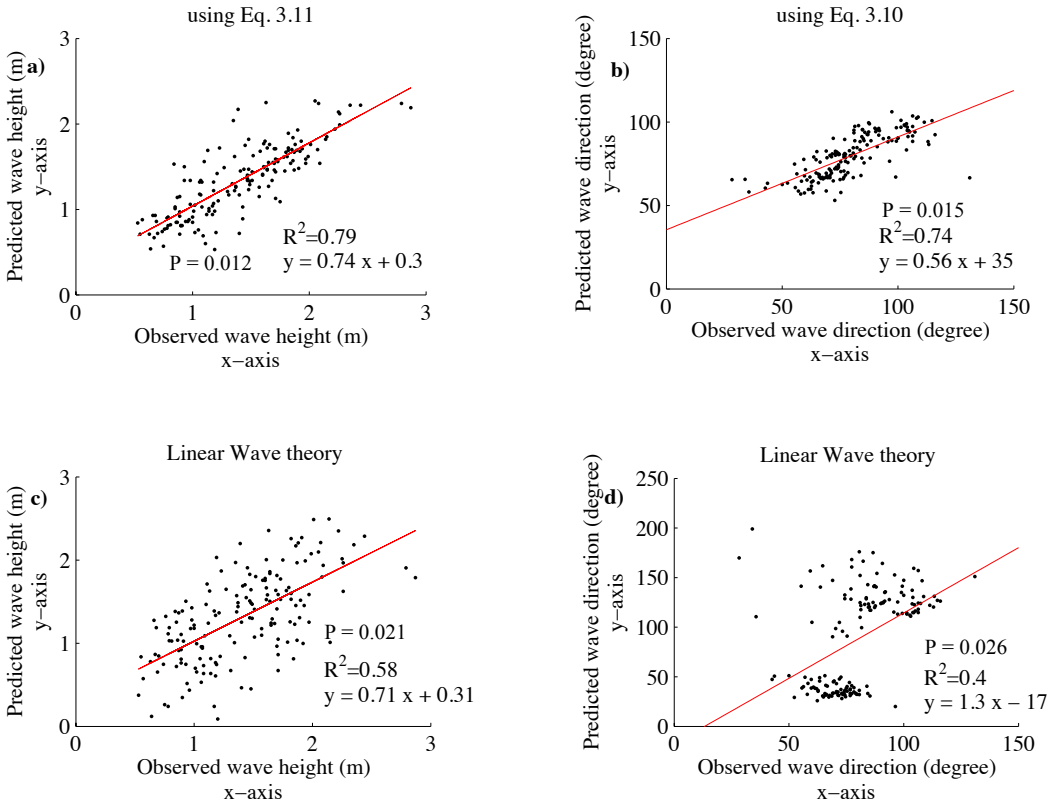

Figure 3.10. Scatter plots of predicted wave height and directions using Eq. 3.8 and 3.9 and Linear Wave Theory versus observations recorded during Field Experiment 1 at site O1.

Also wave heights, as a dependent value, at site O1 are correlated to the wave heights, directions and periods (as independent values) at site B. A linear regression analysis showed that there is a strong correlation between dependent and independent values with an R^2 of 0.79 (Figure 3.9a). The IOA and MAE calculated for this approach were 0.89 and 0.35 (Table 3.4), suggesting regression correlation can strongly predict the wave heights at site B. The resulting linear regression equation is shows as:

$$H_{o1} = 0.573H_b - 0.005Dir_b + 0.063T_b + 0.077 \qquad (3.11)$$

Linear Wave Theory was also used to remap waves at O1 using observed wave data at site B (Figure 3.9). The results indicated there is a poor correlation between predicted wave height using Linear Wave Theory and observations at site O1 with an R^2 of 0.58 (Figure 3.9c). The IOA and MAE calculated for this approach were 0.65 and 0.49 (Table 3.4). This indicates that Linear Wave Theory cannot be used to accurately predict wave height at site O1. As discussed in the literature, Linear Wave Theory has some limitations in shallow water and that could be the main reason that Linear Wave predictions are not reasonable at site O1. The influence of local winds could also be a key reason why the use of Linear Wave Theory was unsuccessful in predicting wave height with an acceptable level of accuracy.

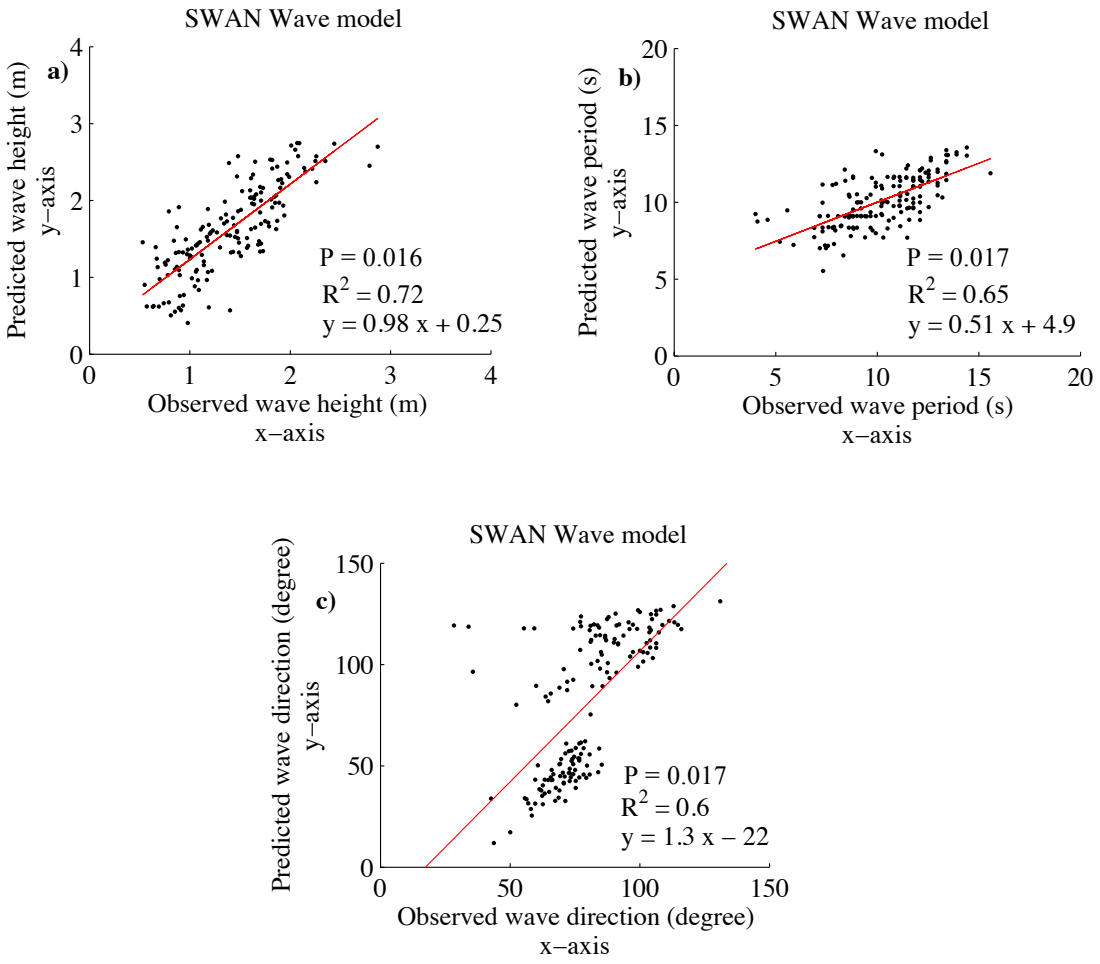

Figure 3.11. Scatter plots of SWAN-predicted wave heights, periods and directions versus observations recorded during Field Experiment 1 at site O1.

Similar to the results of Linear Wave Theory on wave heights, the wave theory cannot be used to accurately estimate wave directions at site O1 (Figure 3.9). Snell's law was applied to estimate wave directions (for more details see section 4.1.1). This approach was found to have underestimated wave direction at site O1 when approaching wave direction was less than 90°, whereas it overestimated directions greater than 90° (Figure 3.9). The correlation between Linear Wave predictions and observations is poor with an R^2 of 0.5 (Figure 3.10d). The IOA and MAE calculated for this approach were 0.51 and 47.31, showing weak estimations using Linear Wave Theory at site O1 (Table 3.4).

The SWAN model was also applied to predict waves from site B to O1 (Figure 3.9). In contrast to the SWAN-predicted wave height at site B, the results indicated that the SWAN model was found to not overestimate wave heights at site O1 for peak values of wave height at site B and the predicted values are more realistic (Figure 3.9). That is because the dissipation effect was activated in shallow water. Nevertheless, the correlation between SWAN-estimated wave heights and observations at site B (R^2 of 0.72) was weaker than that predicted by Eq. 3.11 (R^2 of 0.79) (Table 3.4 and Figure 3.11). IOA and MAE calculated for this approach were 0.74 and 0.43, indicating that SWAN estimates wave height at site O1 with an acceptable level of accuracy.

However, SWAN was found to not produce accurate estimates of wave periods at site O1 compared to wave periods at site B (Figure 3.9). The results showed that the SWAN-estimated wave periods and observations at site B were moderately correlated with an R^2 of 0.65 (Figure 3.11). IOA and MAE calculated for this approach were 0.71 and 1.39 respectively, suggesting that the SWAN model predicts wave periods with a moderate level of accuracy at site O1 (Table 3.4).

The SWAN model was found to not produce satisfactory prediction of wave directions at site O1 (Figure 3.9). Similar to the SWAN-predicted wave direction at site B, the results at site O1 showed that SWAN underestimates wave direction at site O1 when wave direction is less than 90° to the shoreline of Okains Bay, while it produces overestimates when wave direction is greater than 150° (Figure 3.9). The correlation between prediction and observation is moderate with an R^2 of 0.6 (Figure 3.11c). The IOA and MAE calculated for this approach were 0.7 and 32, suggesting that the results of the SWAN model cannot be

used to fill the gaps in wave direction for site O1 with an acceptable level of accuracy (Table 3.4).

A key reason why SWAN was found to not reasonably predict wave period and direction at site O1 could be the influence of local winds that affect the dependent data at site O1. The distance between site B and O1 is about 17 km, so this could give enough fetch for local winds to alter wave characteristics before reaching site O1. Local wind data for that area were not available during the measurements to enter as an input to SWAN to evaluate the effect of local winds on wave characteristics.

Linear regression equations can predict the wave characteristic at sites B and O1 with an acceptable level of accuracy compared to all studied approaches. After comparison of wave data between observations and the predictions using linear regression equations, SWAN and Linear Wave Theory, it can be concluded that linear regression equations are the best approach to estimates of wave heights and directions at both B and O1. Therefore, these equations were used to fill the gap in wave data for site O1 during Field Experiment 2 using wave data observed at site B, and during Field Experiment 3 using wave hindcast at site A.

3.3.3. Predicted wave characteristics at site O1 for Field experiment 2 and 3

As concluded from section 3.3.1 and 3.3.2, the linear regression method was deemed suitably accurate and the best of three tested methods to fill the gap in wave data for site O1. Eq. 3.10 and 3.11 were used to remap wave height and direction at site O1 using deep water wave data recorded at site B for Field Experiment 2. Wave data at site B (Canterbury wave buoy) showed that the predominant wave direction was from 150° to the shoreline of Okains Bay (Figure 3.12a) (Table 3.5). The observed significant wave heights at this site ranged from 1.12 m to 2.27 m, with a mean of 1.74 m and observed significant wave periods ranged from 5.84 s to 9.2 s, with a mean of 7.02 s.

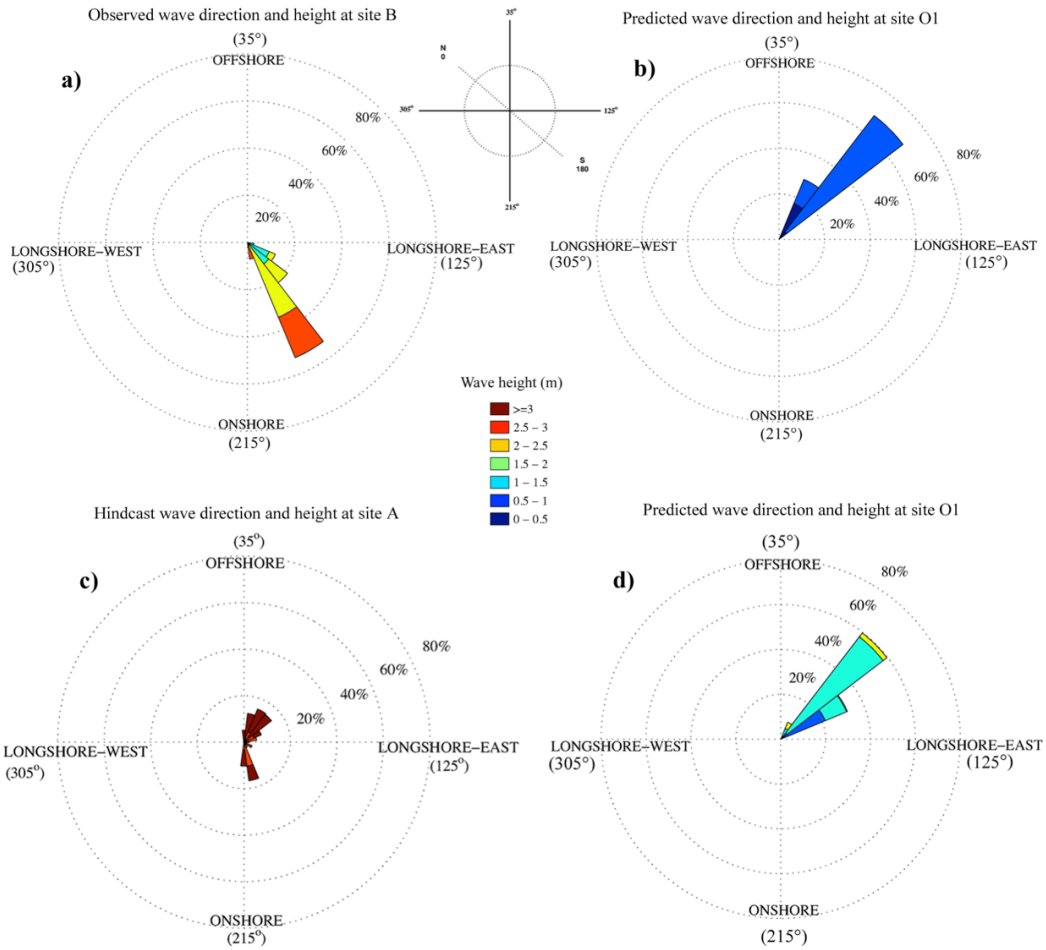

Figure 3.12. Rose plot showing wave height and direction observed at site B and predicted for site O1 during Field Experiment 2 (a and b) and wave height and direction hindcasted for site A and predicted for site O1 Field Experiment 3 (c and d). Directions are shown relative to the Okains Bay beach orientation.

Table 3.5. Maximum, minimum and mean predicted significant wave height and predominant predicted wave direction for site O1 using linear regression equations 3.10 and 3.11 during Field Experiment 2 and 3. Directions are shown relative to the Okains Bay beach orientation.

Experiment	Site	Description	Maximum wave height (m)	Minimum wave height (m)	Mean wave height (m)	Predominant wave direction (degree)
Field Experiment 2	O1	prediction	0.92	0.35	0.62	45
	B	observation	2.27	1.12	1.74	150
Field Experiment 3	O1	prediction	1.58	0.85	1.22	45
	A	hindcast	4.4	1.18	3.54	30, 45, 165

The predicted wave data for site O1 using Eq. 3.10 and 3.11 indicated that the predominant wave direction was 45° to the shoreline (Figure 3.12b) (Table 3.5). The predicted significant wave heights for this site varied from 0.35 m to 0.92 m, with a mean of 0.62 m. Wave periods were assumed constant from sites B to O1 as they are independent of water depth but in reality local wind could influence wave periods.

During Field Experiment 3, wave data at sites B and O1 were not available due to wave gauge failure maintenance. Therefore, first, Eq. 3.8 and 3.9 were used to remap waves for site B using wave data at site A. Then, Eq. 3.10 and 3.11 were applied to predict waves for site O1 using predicted wave data at site B. The wave data at site A indicate that the predominant wave directions approached from 30° and 45° to the shoreline of Okains Bay followed by 165° to the shoreline (Figure 3.12c) (Table 3.5). The hindcast significant wave heights at this site ranged from 1.18 m to 4.4 m, with a mean of 3.54 m. The hindcast significant wave periods ranged from 7.1 s to 13.1 s, with a mean of 11.3 s.

Similar to the predictions for Field Experiment 2, the predicted wave data for site O1 showed that the predominant wave direction was 45° to the shoreline (Figure 3.12d) (Table 3.5). As discussed in the literature of chapter 2, Okains Bay is dominated by southerly and south easterly waves (or a range of directions between about 35° and 80° to the shoreline). Therefore, it was expected that predicted wave directions predominantly approach from an angle between 35° and 80° to the shoreline. The predicted significant wave heights at this site varied from 0.85 m to 1.58 m, with a mean of 1.22 m. Wave periods were assumed constant as they are independent of water depth but in reality local wind could influence wave periods.

In chapter 4, the predicted wave data at site O1 is used as an input into the SWAN model to simulate the wave propagation inside Okains Bay. The results are also used in chapter 6 as an input into the XBeach model to simulate nearshore currents inside Okains Bay with consideration of reflection and diffraction caused by headlands.

3.4. Discussion

A comparison between observation and predicted wave data using (a) linear regression analysis, (b) the SWAN model and (c) Linear Wave Theory revealed that linear regression analysis was found to produce the most accurate estimates of waves for site O1 outside Okains Bay. The distances between site O1 and the deep water sites A and B were about 32 km and 17 km respectively, so local winds have enough fetch between sites to potentially alter the wave characteristics at site O1.

Bathymetry is also another important factor in controlling wave characteristics in intermediate and shallow waters; that is, more accurate bathymetry data could result in more precise predicted wave data for site O1. Using the linear regression approach takes into account all these factors, even though they are not directly provided for the analysis. That is because regression analysis will find the best correlation between wave data collected at different sites and influenced by all possible factors. This is a statistical approach and it does not have any physical explanations. This approach was found successful to give the best fit during different sea conditions, with waves varying from low to high energies (Figures 3.5 and 3.9). However, other methods used in this study take into consideration the water depth. More accurate bathymetry could result in more precise estimations of wave characteristics, especially once waves move from deep water to shallow water.

The SWAN predictions can also be used to reasonably simulate wave transformation from deep water to intermediate or shallow waters. The SWAN model is more developed for shallow water transformation than deep water with larger scales than coastal scales, so the predictions might not be as accurate as its estimation for shallow water. As discussed earlier, SWAN overestimated wave heights for site B when waves at the boundary of the model were over 4 m. Gorman et al. (2003) also applied SWAN to predict waves in shallow water of New Zealand coastlines and the results showed that the model was found to slightly overestimate wave characteristics at a depth of about 30 m. Similarly, Huang et al. (2013) used SWAN to simulate hurricane waves in the deep water of Gulf of Mexico and the model was found to overestimate wave heights. However, for low energy waves, SWAN was found successful to estimate wave characteristics more realistically at deep water sites.

However, in the present study, SWAN predictions at transitional to shallow water were slightly weaker than its predictions in deep water. When waves reached site O1 outside Okains Bay, SWAN was found to not produce reliable estimations of wave height and direction compared to linear regression analysis, even though the dissipation effect was activated. This effect removes the wave height overestimation for high energy waves in intermediate to shallow water, similar to the findings of Huang et al. (2013). However, the use of SWAN was unsuccessful to accurately estimate wave characteristics for this area. The effect of local winds on wave characteristics could be a key reason why the SWAN predictions for site O1 were less reliable than the linear regression equations.

As discussed in section 3.3.2, local winds could potentially change wave characteristics at site O1. A distance of 17 km between sites B and O1 will give enough fetch to local wind to alter wave characteristics when they travel from deep water to intermediate to shallow water. If local wind data for simulated area were available, SWAN could give better predictions at site O1.

SWAN may also overestimate wave directions in deep water or intermediate to shallow water. As shown in the results, once waves were approaching from an angle greater than 150°, predicted wave directions were overestimated. This overestimation reduced when the waves travelled to shallower depths. The dissipation effect added to the model could rectify the overestimation. Additionally, when waves enter into intermediate or shallow water the effect of bathymetry on wave directions will be more accentuated and this effect is taken into account in the model.

Linear Wave Theory, the well-known basic theory for ocean waves, is more accurate at predicting wave characteristics in deep water than in transitional or shallow water. Wave data collected at site B had a minimum and maximum wave steepness of 0.00016 and 0.00029, and also a minimum and maximum relative depth of 0.05 and 0.12. According to Le Méhauté (1969), waves with these values of wave steepness and relative depth would be grouped in Linear Wave Theory. Therefore, Linear Wave Theory could be successfully applied to predict waves for site B. The results produced using the Linear Wave Theory in this study were similar to those generated using the SWAN model. That is, the theory produced overestimates of wave heights for high energy waves and gave more accurate estimations for low energy waves.

However, the use of this theory was unsuccessful to produce reliable predictions of wave characteristics in intermediate to shallow water. Wave data collected at site B had a minimum and maximum wave steepness of 0.00017 and 0.0002 and also minimum and maximum relative depth of 0.005 and 0.048. According to Le Méhauté (1969), waves with these values of wave steepness and relative depth would be grouped in the border of Linear Wave Theory and Stokes second-order (Figure 3.1). Therefore, it is expected that Linear Wave Theory could be applied to reliably predict waves for site O1. However, if local winds tend to play an important role in changing the incident wave characteristics at site O1, the theory would be found unsuccessful to produce estimates of waves for this site, similar to the results of the SWAN model.

Although linear regression analysis is not based on any physical explanations, it was found successful to predict wave height and direction at site O1 using the data collected in this study. This correlation was based on a variety of sea conditions, including low to high energy waves and also could cover different weather conditions during the 22 days of measurements. Therefore, the correlation equations (Eq. 3.10 and 3.11) could potentially be used to successfully predict wave data for site O1 using wave input data from sites A and B.

3.5. Conclusion

In this chapter, the accuracy of prediction approaches for wave transferring from deep water to transitional and shallow water outside of Okains Bay was discussed. Linear regression analysis, SWAN wave model and Linear Wave Theory were used to first estimate waves for site B using wave input data from site A. Then, these approached were applied to predict waves for site O1 outside Okains Bay using wave input data from site B. The most accurate approach found was then used to fill the gaps in wave data for site O1 during Field Experiment 2 and 3.

The results indicated that linear regression analysis could reliably predict wave data for both sites B and O1. The 22 days observations during January 2012 were used to first estimate waves for site B using wave input data from sites A. The wave data included low

to high energy waves with waves approaching from different directions to the shoreline of Okains Bay. In this analysis, it was assumed that wave periods were constant and were not affected by the variation of water depth, but in reality waves could be affected by local winds. A linear regression analysis showed a strong correlation between predicted wave characteristics (i.e. wave height and direction) and observations at site B. Although this approach is not based on physical terms, it could be used to produce wave heights and directions for site B with a high level of acceptance using wave input data from site A.

Linear regression analysis was also used to remap wave height and direction at site O1 using wave input data from site B. The observations collected during Field Experiment 1 at sites B and O1 were used to establish linear regression equations in order to predict wave data for site O1. The results indicated that this approach could reliably predict wave height and direction for site O1 using wave input data from site B.

The second approach used to transfer waves from deep water to shallow water was the SWAN model. Although the results showed that SWAN could reasonably predict wave height for deep water, it was found to overestimate them once wave height at the boundary of the model is above 4 m; adding the dissipation effect in shallow water rectified the overestimation. However, transferring waves from deep water to transitional water (site O1) was not as accurate as the linear regression equations and that could possibly be caused by the effect of local winds on wave height between sites B and O1.

The SWAN predictions also indicated that the model could reasonably predict the wave directions for site B in deep water and for site O1 in transitional water. The deep water results showed that SWAN underestimated wave direction for site B when wave direction was less than 50°, while it overestimates it when wave direction was above 150°. Similarly, SWAN overestimated the wave directions for site O1, but this overestimation was less than that of deep water predictions as the dissipation and bathymetry effects were more accentuated in shallower waters.

Linear Wave Theory was also applied to estimate wave data for site O1 using wave input data from the site. According to relative depth and wave steepness calculated for observations recorded during Field Experiment 1 and also collected during January 2012, Linear Wave Theory could be reliably applied to predict waves for deep water and transitional water. The results showed that this method reasonably predicted wave characteristics in deep water for site B. However, Linear Wave Theory was found to

produce moderate estimates of wave height for site O1, but poor estimates of wave direction. A key reason that could potentially weaken the estimations was the influence of local winds on wave data between sites B and O1.

It can be concluded that the linear regression equations had the best predictions among other approaches studied in this chapter. Therefore, the regression correlation equations were used to fill the gap in wave data for site O1. These equations were used to transfer waves from site B to site O1 during Field Experiment 2. However, during Field Experiment 3, wave data were not available at site B, so Eq. 3.8 and 3.9 were first used to remap wave data for site B using wave input data from site A and then Eq. 3.10 and 3.11 were applied to produce wave data for site O1.

In order to better understand wave processes inside Okains Bay, the next chapter will focus more on wave simulations inside Okains Bay using the SWAN model. Chapter 2 suggested that reflection and diffraction could be two main factors in controlling wave processes inside Okains Bay. Therefore, the SWAN model is applied to examine the wave processes inside the bay with and without consideration of reflection and diffraction. The observations at site O1 and predicted wave data for site O1 using the linear regression equations will also be used as wave input data to the SWAN model in order to simulate wave processes inside Okains Bay during Field Experiments 1, 2 and 3.

Chapter 4: Experimental and numerical studies of wave processes in Okains Bay

This chapter outlines numerical modelling of wave processes within Okains Bay using the SWAN wave model. This chapter also examines the importance of reflection from the downcoast headland on wave characteristics in pocket beach bays. First, the results of model were validated versus observations, then, the model were used to evaluate the effect of reflection on wave processes inside the bay. This task contributes towards the thesis aims 1 and 2 and, with regard to better understanding the role of wave reflection off the downcoast headland, the chapter also ultimately contributes evidence needed to address thesis aim 4.

4.1. Introduction

In pocket beach environments, waves can approach the shoreline from only a narrow range of directions without considerable loss of energy due to sheltering by the longshore barriers. For the purposes of this chapter, these longshore barriers will be referred to as headlands. One key parameter influencing the degree of sheltering, and thus the range of direct shoreline approach angles for waves, is headland length. In addition to the filtering effect of headlands on wave angles, some incident waves undergo significant reflection and diffraction around headlands (Figure 4.1) (Dehouck et al., 2009). This chapter mainly focuses on the importance of reflection from the downcoast headland and its effect on wave processes inside Okains Bay, an example pocket beach. First, the methods developed by Zanuttigh and Andersen (2010) and Zanuttigh and Van der Meer (2008) will be used to highlight the importance of reflection in controlling wave processes inside the bay. Later, the SWAN model will be applied to numerically examine the effect of reflection on wave characteristics, especially wave direction inside the bay.

Knowledge about wave processes, including refraction, diffraction and reflection, can help us to understand the nearshore currents and most importantly, the planform shape of beaches (Woodroffe, 2002). This variation in the shoreline is basically attributable to the direction of waves. Depending on the beach type: open coast, embayed or pocket beaches, the direction

of waves can be influenced by the beach topography, thereby having different shoreline planforms. This chapter starts with the wave processes studied by others in open coast and embayed beaches. Then experimental equations and numerical models are used to highlight the importance of reflection in pocket beaches.

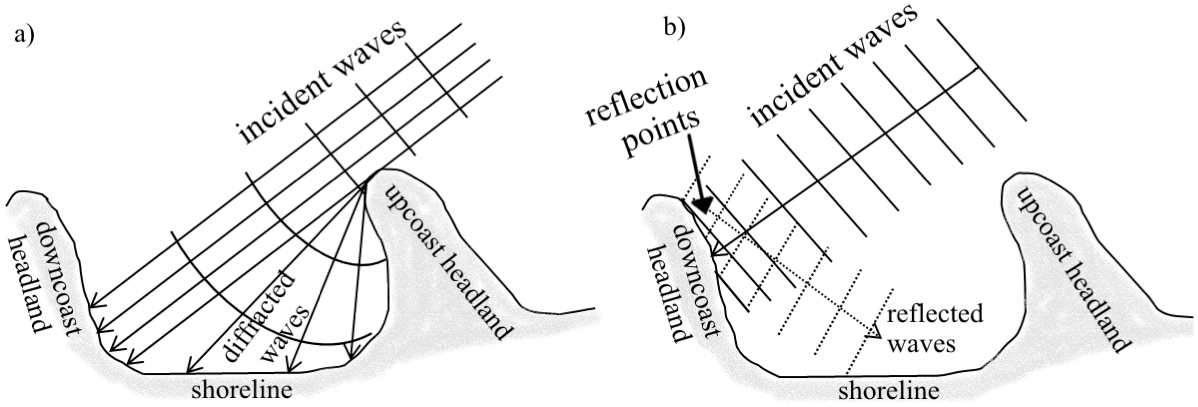

Figure 4.1. Wave diffraction (a) and wave reflection (b) processes inside a pocket beach environment, without consideration of shoaling and refraction. Arrowlines indicate the wave crests while solid lines indicate wave orthogonals.

4.1.1 Wave characteristics in open coast beaches

With the absence of headlands in open coast beaches, the main factor influencing wave processes, particularly wave direction, is the water depth, known as shoaling and refraction. Once waves propagate towards shallow water, the wavelength and wave velocity decrease (Nielsen, 2009). Subsequently, the wave crest direction becomes closer to normal with respect to the orientation of bottom contours. In this case, Snell's law is used to estimate the wave direction influenced by the water depth:

$$\frac{\sin \emptyset_1}{\sin \emptyset_2} = \frac{C_1}{C_2} = \frac{L_1}{L_2} \tag{4.1}$$

where $\emptyset$ is wave direction, C is wave velocity (ms^{-1}), L is wave length (m) and the subscripts 1 and 2 show the wave propagation time order.

Depending on the orientation of bottom contours, wave energy, and thus wave height, could either increase or decrease (Sorenson, 1997). If wave orthogonals converge, the energy per unit crest length rises, whereas a divergence in wave orthogonals results in a decrease in the wave energy and thus in the wave height. In order to estimate the wave height transmitting to different depths, it is necessary to calculate the shoaling and refraction coefficients as:

$$k_r = \sqrt{\frac{\cos \emptyset_1}{\cos \emptyset_2}} \tag{4.2}$$

$$k_s = \sqrt{\frac{L_1}{(1+\frac{2kd}{\sinh 2kd})L_2}} \tag{4.3}$$

$$H_2 = k_s k_r H_1 \tag{4.4}$$

where k_r and k_s are refraction and shoaling coefficients respectively, k is wave number (m^{-1}), d is water depth (m) and H is wave height (m) (Sorenson, 1997).

4.1.2 Wave characteristics in embayed or one headland enclosed bay beaches

One headland enclosed bay or embayed beaches are areas sheltered by one headland. In such environments, waves are both diffracted and refracted before approaching the shoreline (Thomas *et al.,* 2013; Woodroffe, 2002; Short 1999; Rea and Komar, 1975). As a result, the shoreline of embayed beaches consists of a highly curved shadow zone formed by diffraction and a straight downcoast shoreline affected by refraction. It can be concluded that one main feature differentiating embayed beaches from open coast beaches is the occurrence of diffraction from the headland.

Wave characteristics in embayed beaches are importantly influenced by diffraction around upcoast headlands (or updrift headlands), resulting in the propagation of waves into the headland's shadow zone. Daly *et al.,* (2014) studied wave distribution inside an embayed beach using Delft3D. The results indicated that diffraction process plays an important role in defusing wave energy in the bay, particularly in areas around the shadow zone. They also

indicated that the diffraction effect increases when the incoming wave directions relative to the embayment control line is greater than 30°.

The process of diffraction from natural or artificial headlands is similar to that of semi-infinite barrier. In order to better understand wave diffraction, Penny and Price (1952) applied the idea of light diffraction to linear waves on constant depth diffracted from a semi-infinite impermeable barrier. Then Wiegel (1964) used the method of Penny and Price (1952) and classified the diffracted coefficients according to some basic parameters: wave length, the angle between the incident wave and the barrier, the angle between the barrier and the point of interest behind the barrier, and the distance between the diffraction point and the point of interest. In his study, the comparison between predictions and observations in a wave tank showed this approach to be capable of accurately predicting the diffracted waves.

Dalrymple and Martin (1990) analyzed wave diffraction from in-line segmented breakwaters. Later Abul-Azm and Williams (1997) developed Dalrymple and Martin's (1990) approach and showed that it can reasonably predict diffracted waves.

Diffraction analysis based on Green's function approach for segmented breakwater was studied by Williams and Crull (1993) and Williams *et al*. (1995). Even though the latter and Dalrymple and Martin's (1990) approaches give satisfactory results, Wiegel's (1964) approach has been widely used and recommended as an accurate and popular approach for coastal engineering applications (McCormick and Kraemer, 2002; Coastal Engineering Manual, 2002; Bocotti, 2000; Shore protection Manual, 1984). In this study, Wiegel‘s (1964) approach is applied to calculate diffracted wave heights inside the bay.

4.1.3. Wave characteristics in pocket beaches

As discussed in chapter 2, reflection from the downcoast headland could be an important factor in controlling wave processes. Although there is little published research on the operation of wave reflection in natural pocket beach environments, research examining this process on artificial coasts with merged impermeable coastal structures can be used to predict reflected waves inside natural beach pockets. A number of studies have attempted to establish reflection coefficients for waves reflected from rubble mound structures, permeable breakwaters or impermeable structures (Van der Meer, 2005; Davidson, 1996;

Postma, 1989; Seelig and Ahrens, 1981). Battjes (1974a) defined a reflection coefficient, Cr, for regular waves based on the Iribarren number or the surf similarity parameter, Ir, which was then refined and extended for application to monochromatic and irregular waves, based on laboratory investigations by Seelig (1983) and Allsop and Hettiarachchi (1989), given as:

$$C_r = \frac{aI_r^2}{b+I_r^2} \tag{4.5}$$

$$I_r = \frac{\tan\alpha}{\sqrt{\frac{H_i}{L_0}}} \tag{4.6}$$

where α is the angle of the structure face to the horizontal axis, H_i is the wave height at the structure and L_0 is deep water wave length. a and b are constant values which depend on the type of structure and whether the waves are monochromatic or irregular. The values of a and b are 0.75 and 15 for permeable structures, and 0.8 and 10 for impermeable structures. In Eq. 4.6 only the surf similarity parameter was considered. However, there are a few studies on reflected waves that take into account other parameters, such as relative depth (Muttray et al., 2006; Davidson *et al*., 1996).

Zanuttigh and Van der Meer (2008) used extensive data sets and developed an experimental equation to predict the reflection coefficient for coastal structures with a high level of accuracy, shown as:

$$C_r = \tanh(a.I_r^b) \tag{4.7}$$

where values of a and b are 0.14 and 0.90 for impermeable rock structures and can be calculated simply from a roughness factor acquired from a wave overtopping discharge formula (Pullen *et al*., 2007). Zanuttigh et al. (2009) evaluated Eq. 4.7 using 127 tests in a flume and a tank and showed that the equation can be used to accurately predict wave reflection.

However, none of the above equations takes into account the effect of oblique wave approaches on the reflection coefficient. There are few published approaches for calculating reflected waves for oblique short-crested waves (Zanuttigh and Andersen, 2010; Van der Meer *et al*., 2005; Wang *et al*., 2005). Zanuttigh and Andersen (2010) stated that incident wave direction could substantially influence the reflection coefficient. Therefore, these authors took into account the angle of incident waves to modify the reflection coefficient, $C_{rm,}$ given as:

$$C_{rm} = C_r(1 - 0.0077\beta) \quad \text{for short-crested waves} \tag{4.8}$$

$$C_{rm} = C_r(1 - 0.0058\beta) \quad \text{for long-crested wave} \tag{4.9}$$

where β is the approaching wave direction to structure (If β = 0, wave is perpendicular to the structure). Zanuttigh and Andersen (2010) also compared the performance of the formulae described by Postma (1989), Muttray *et al*. (2006), Zanuttigh and Van der Meer (2008), and Calabrese et al. (2009) by comparing Eq. 4.8 and 4.9 against 736 tests carried out in a wave basin. Their results indicated that Zanuttigh and Van der Meer (2008) and Muttray *et al*. (2006) could be used to predict the reflection coefficient with a reasonable level of accuracy for both short- and long-crested waves.

Another important aspect in predicting reflected waves is to calculate the direction of reflected waves from the approaching incident wave direction (Figure 4.2). Van der Meer *et al*. (2005) demonstrated that the ratio between the wave direction reflected from rubble mound structures and incident wave direction is 0.8. For smooth structures, however, this ratio changes according to the incident wave direction. If incident waves approach at an angle less than 45° to the headland, the directions of reflected and incident waves are equal and if incident waves approach at an angle greater than 45° to the headland, the reflected wave direction is 45° (Van der Meer *et al*., 2005).

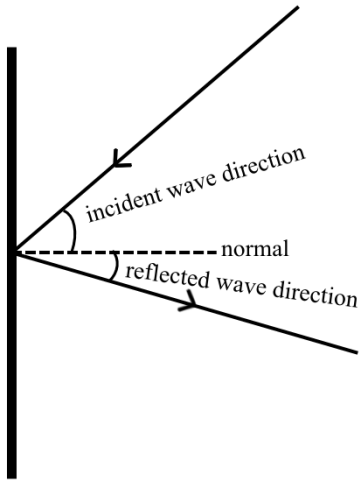

Figure 4.2. Definition sketch of incident and reflected wave directions.

4.1.3.1. Short-crested waves

The combination of diffracted and reflected waves can generate a complex wave pattern known as short-crested waves (Silvester and Hsu 1999; Hsu *et al*., 1993; Roberts, 1983). Silvester and Hsu (1999) studied short-crested waves and assumed that diffracted and reflected waves had equal heights and periods. Under this scenario, when a combined reflected and diffracted wave crest increased in height, there was a reduction in the wave trough. For instance, if the angle between reflected and diffracted waves was 120°, the combined wave crest increased by 70% and the trough decreased by approximately 20%. However, in reality, reflected and diffracted wave heights are not equal, so finding their combined wave height is more complicated.

The majority of published studies analyzed combined waves based on either laboratory data (Silvester and Hsu, 1999; Fenton, 1985) or results obtained from numerical modelling (Zhang *et al*., 1999; Roberts, 1987). In Chapter 2, the importance of reflected waves on incident waves inside Okains Bay was highlighted. This chapter examines the importance of reflected waves in a pocket beach using experimental equations and numerical modelling.

4.2. Methodology

As explained at its outset, this chapter concerns the analysis of numerical modelling of wave processes inside Okains Bay, a case study micro-tidal pocket beach. This approach fits into the right-hand portion of the thesis methodology diagram illustrated in Figure 1.6.

4.2.1. Study site

The study area is inside Okains Bay, located on the north-eastern side of the volcanic peninsula on the east coast of New Zealand's South Island (Figure 4.3a). The wave climate in this area was discussed earlier in sections 2.2.1 and 3.2.1. For the purpose of this study, the study area is shown by a rectangle with a length of 4 km and a width of 3 km (Figure 4.3). Water depth at the offshore side of the rectangle at site O1 is about 12 m during high tide and about 10 m during low tide. The bathymetry of Okains Bay is also shown in Figure 4.3b. This bathymetry data is later used to simulate waves inside Okains Bay using the SWAN model.

4.2.2. Method

This study employs experimental equations developed by Zanuttigh and Andersen (2010), and Zanuttigh and Van der Meer (2008) to highlight the importance of reflection in controlling wave travel in a case study pocket beach, Okains Bay. The SWAN model is also applied to examine this effect on wave processes in Okains Bay using data from field experiments collected inside Okains Bay.

In the first part of this study, a model experiment using Zanuttigh and Van der Meer's (2008) and Zanuttigh and Andersen's (2010) approaches was applied to examine the effect of downcoast headlands on wave reflection in the surf zone of a simplified model pocket beach (Figure 4.4). This experiment examined a 2 m monochromic wave approaching at 20°, 40° and 70° to the model pocket beach. This experiment was repeated for different downcoast headland lengths: 160, 280 and 340m. For the purpose of this experiment, it was assumed that reflection from the rocky headland resembles that from an impermeable rock structure.

In order to evaluate the importance of reflection in the model pocket beach, reflected waves were compared to diffracted waves calculated using Wiegel's (1964) approach (US Army Corps of Engineers, 2002). Additionally, in order to consider refraction and shoaling, Eq. 4.1 to 4.4 were also applied to transfer waves from outside the pocket beach to reflection and diffraction points and then to the surf zone.

This analysis for the model pocket beach was complemented by two field experiments to examine waves observed in the case study pocket beach, Okains Bay. Field Experiment 1 was used to examine reflection in areas further towards the shoreline where incident waves could only reach directly from a limited directional sector. Field Experiment 1 was accomplished between 20th Mar and 11th Apr 2011 outside and inside Okains Bay at sites O1 and O3 respectively (see section 2.3.1 for more details).

Field Experiment 2 was used to examine reflection in an area close to the entrance of Okains Bay which is more exposed to incident waves. This experiment was accomplished between 19th and 22nd Dec 2011 inside Okains Bay at site O2 (see section 2.3.2 for more details). Since wave data were not available at site O1 during the deployment, the linear regression equations developed in chapter 3 (see section 3.3.3) were used to fill the gap in wave data for site O1 using wave input data from site B.

The Zanuttigh and Andersen's (2010), and Zanuttigh and Van der Meer's (2008) approaches were applied to predict the wave reflection for sites O2 and O3 using the wave input data from site O1 during Field Experiments 1 and 2. Shoaling and reflection were employed to remap waves to areas close to the downcoast headland. In this study, it was assumed that the natural headlands have a similar behavior on waves as rubble mound structures. Eq. 4.7 to 4.9 were applied to calculate reflected wave heights from a rubble mound structure. The approach of Van der Meer et al. (2005) was then used to calculate reflected wave direction from rubble mound structures, which the ratio between the wave direction reflected from rubble mound structures and incident wave direction is 0.8. Afterward, shoaling and refraction were again employed to estimate waves for sites O2 and O3 using reflected waves data predicted from wave input data collected at site O1. Finally, the O2 and O3 predictions (based on O1 wave heights) were then compared via linear regression to measurements from site O2 and O3 collected during Field Experiments 1 and 2.

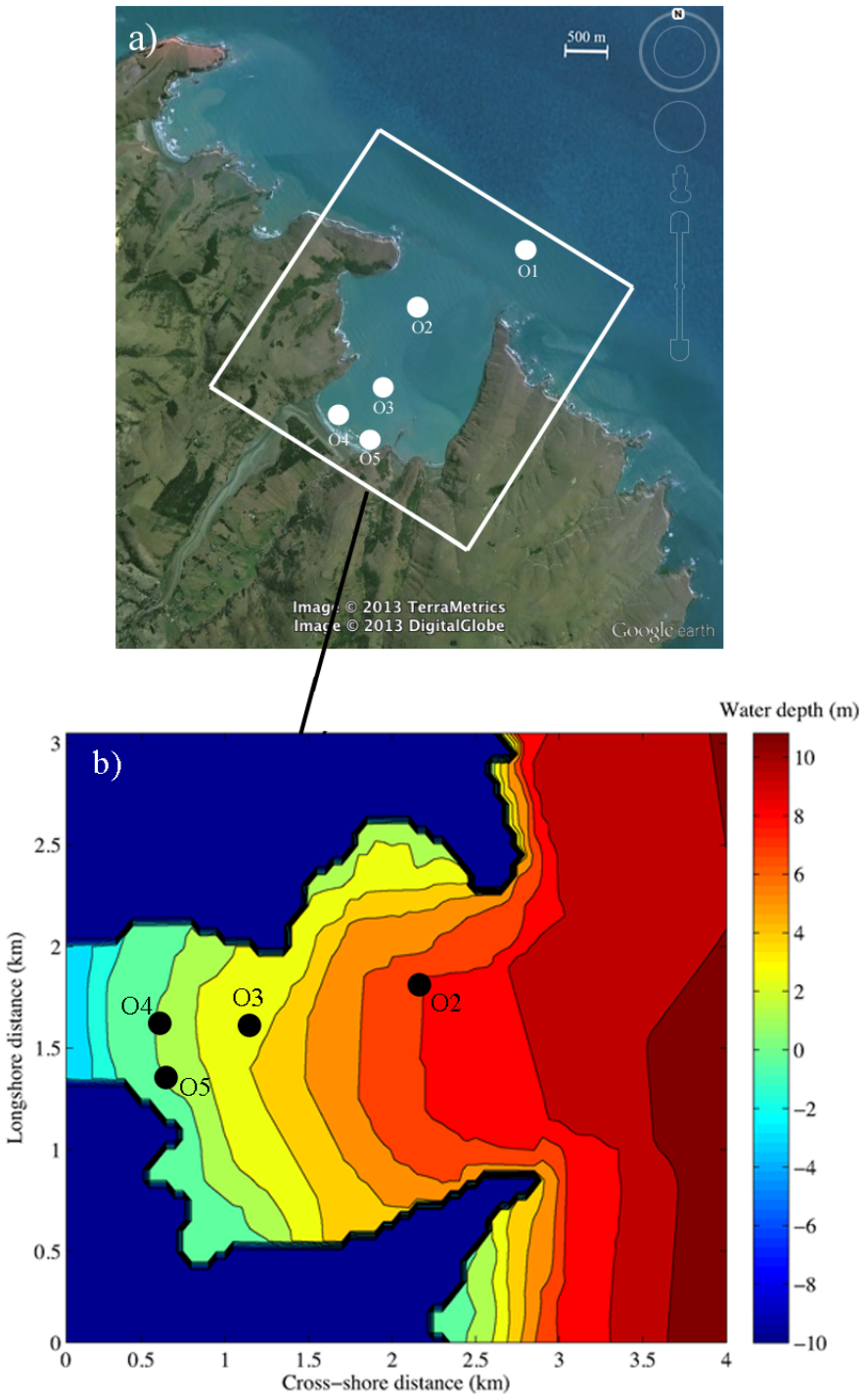

Figure 4.3. Field instrument deployment sites in Okains Bay and the simulated area shown by a white rectangle (a), and Okains Bay bathymetry used in the SWAN model (b). Note that site O1 was used as input wave data into SWAN simulations, so this site is located in the boundary of this bathymetric map.

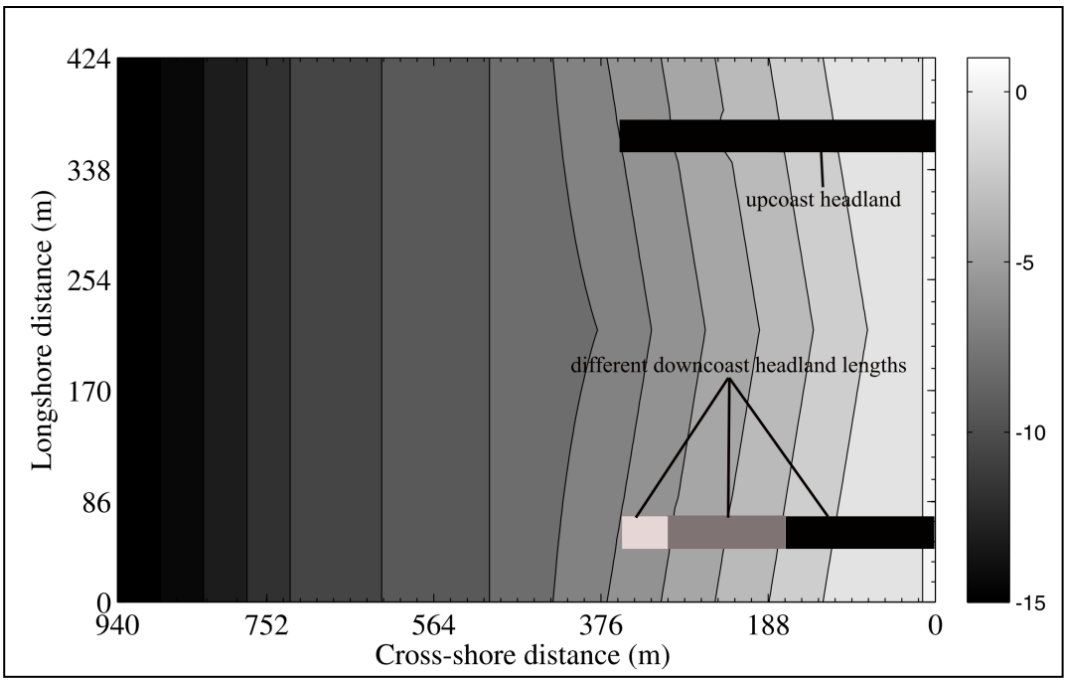

Figure 4.4. Bathymetry map, including different downcoast headland lengths.

The SWAN model was also used to demonstrate the importance of reflected waves in Okains Bay for different wave conditions. The simulated area is shown in Figure 4.3a as a rectangle 4 km in the cross-shore direction and 3 km in the longshore direction. In order to simulate wave characteristics inside Okains Bay, the SWAN model (version 40.91) (The Swan Team, 2013) was implemented with the nominal formulations of the physical processes. JONSWAP bottom friction is used to run the model and whitecapping dissipation, depth-induced breaking, triad wave-wave interaction, and more importantly reflection (d' Angremond *et al.,* 1996) and diffraction (Holthuijsen *et al*., 2003) are also included in the model configuration. In these simulations, uniform and rectangular grids were chosen. Grid configuration used in this model is shown in Table 4.1, and bathymetry is depicted in Figure 4.3b. The time step of each simulation was the same as the duration of each field experiment as discussed in Chapter 2 (Table 4.1).

Wave heights, periods and directions were simulated at sites O2, O3, O4 and O5 for all three field experiments. The purpose of these simulations was to validate the accuracy of the SWAN wave model to predict waves in Okains Bay. For these simulations, wave data at site

O1 were used as the wave boundary in the model. Since wave data at site O1 were not available during the Field Experiments 2 and 3, wave data at site O1 were predicted by the linear regression equations found in chapter 3 using wave input data from sites A and B. Wind data collected during experiments 2 and 3 were also used as an input to SWAN to take into account the effect of local winds on wave characteristics inside the bay.

Finally, in order to examine the importance of reflection in Okains Bay, two more model experiments were run. The same bathymetry and initial conditions were used for these model experiments. In the first experiment, the reflection effect was deactivated in the model to examine how wave characteristics would change without reflection in different locations inside the bay, particularly, in areas close to the downcoast headland. Then the results were compared with simulations which included reflection and diffraction.

In the second experiment, both reflection and diffraction were deactivated in the model. The purpose of this simulation was to examine whether diffraction could influence wave characteristics inside Okains Bay, especially in areas close to the downcoast headland where reflection could significantly affect wave characteristics.

Table 4.1. Configurational grid for SWAN simulations.

Simulation duration	**Grid description**	**Grid (Easting x Northing)**	**Cell grid size (m)**	
			dx	dy
20/April/2011 to 11/May/2011	small resolution grid	80 x 60	50	50
19/December/2011 to 22/December/2011	small resolution grid	80 x 60	50	50
3/April/2011 to 13/April/2011	small resolution grid	80 x 60	50	50

4.3. Reflected waves in pocket beaches using an experimental method

As depicted in Figure (4.5), waves from only a narrow range of directions, ß, can approach the downcoast headland before being reflected into the bay, given by

$$\tan^{-1}\left(\frac{h_u - h_d}{L}\right) < \beta < 90 \tag{4.10}$$

where h_u and h_d are the upcoast and downcoast headland lengths respectively, and L is the length of the shoreline. In this equation, the shoaling and refraction effects were not considered, while in reality, waves could propagate towards the downcoast headland from a wider range of directions than ß. However, Eq. 4.10 can still be applied to determine the minimum range of wave directions that can be reflected into the bay. That is because even if waves with an angle smaller than ß can approach the downcoast headland after refraction, the wave directions at the reflection point will be either equal to or greater than ß.

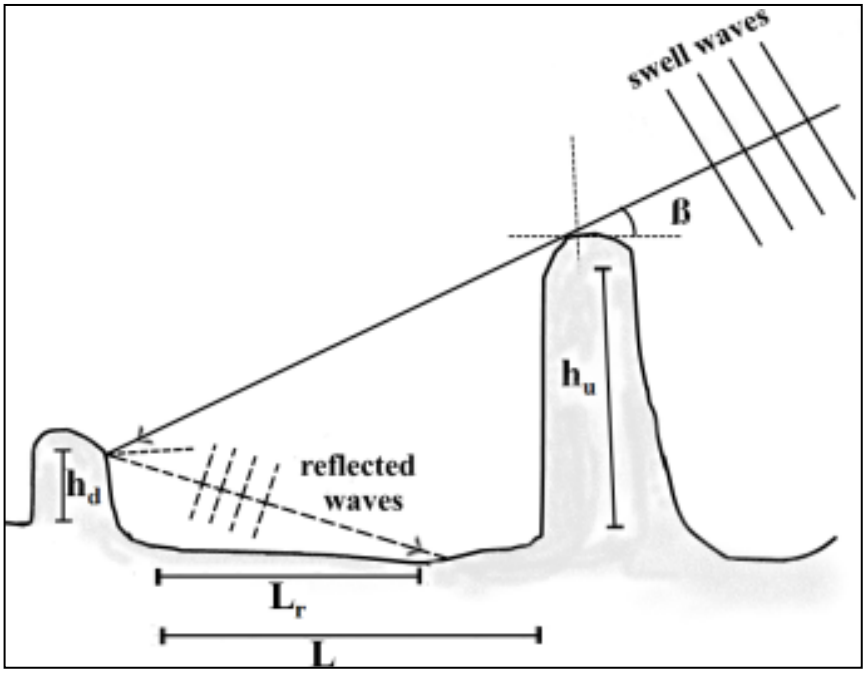

Figure 4.5. Definition sketch of pocket beach characteristics.

Once groups of swell waves are reflected from the downcoast headland, they propagate towards the shoreline and will be combined with refracted waves and with waves diffracted from the upcoast headland and generate a complex wave pattern called short-crested waves (Silvester and Hsu 1999). Depending on the reflection angle and the length of the downcoast headland, reflected waves could dominate a small part of the entire shoreline. The minimum incident wave angle to the shoreline, θ, causing reflected waves from rubble mound structures to possibly propagate into the entire shoreline is shown as

$$\theta = 0.8 \tan^{-1}(\frac{h_d}{L}) \tag{4.11}$$

From Eq. 4.10 and 4.11, it can be also concluded that the downcoast headland length plays an important role in controlling wave reflection. If the length of the downcoast headland decreases, the range of approaching wave directions that can be reflected to the entire shoreline will be reduced.

4.3.1. Simple test experiment for a reflected wave

In order to examine the effect of downcoast headlands on wave reflection, a simple experiment was set up to evaluate monochromic wave behavior after reflection. To this end, a simplified model pocket beach with a different length of rocky downcoast headland was considered (Figure 4.4). For the purpose of this experiment, a 2 m monochromic wave approaching at 20°, 40° and 70° to the model pocket beach was used. It was assumed that reflection from the rocky headland resembles that from an impermeable rock structure. Zanuttigh and Van der Meer's (2008) formula was applied to calculate the reflection coefficient. Then, Zanuttigh and Andersen's (2010) approach was applied to consider the effect of oblique monochromic waves on reflection coefficient. It was also assumed that the reflected wave direction is equal to 0.8 of incident wave direction, shown by Van der Meer et al., (2005). The diffraction waves were calculated using Wiegel's (1962) approach; the results are shown in Table 4.2 to 4.4.

Table 4.2. Comparison of reflected and diffracted wave heights for a 2 m wave approaching at 70° to the shoreline for different downcoast headland lengths.

Downcoast headland size (m)	Length of shoreline affected by reflected waves (m)	Wave height at reflection point (m)	Wave angle at reflection point (°)	Reflected wave height at reflection point (m)	Reflected wave height at 2 m depth (m)	Diffracted wave height at 2 m depth (m)
340	238	1.26	53	0.71	0.62	0.4
280	181	1.22	47.5	0.65	0.56	0.44
160	111	1.2	39	0.6	0.5	0.48

Table 4.3. Comparison of reflected and diffracted wave heights for a 2 m wave approaching at 50° to the shoreline for different downcoast headland lengths.

Downcoast headland size (m)	Length of shoreline affected by reflected waves (m)	Wave height at reflection point (m)	Wave angle at reflection point (°)	Reflected wave height at reflection point (m)	Reflected wave height at 2 m depth (m)	Diffracted wave height at 2 m depth (m)
340	196	1.59	33	0.7	0.65	0.52
280	148	1.61	30	0.69	0.62	0.57
160	93	1.7	25	0.68	0.57	0.8

Table 4.4. Comparison of reflected and direct wave heights for a 2 m wave approaching at 20° to the shoreline for different downcoast headland lengths; note that waves will not be difracted at the studied 2 m depth with a wave approaching at 20°.

Downcoast headland size (m)	Length of shoreline affected by reflected waves (m)	Wave height at reflection point (m)	Wave angle at reflection point (°)	Reflected wave height at reflection point (m)	Reflected wave height at 2 m depth (m)	Diffracted wave height at 2 m depth (m)
340	72	1.65	17	0.62	0.6	2.08
280	57	1.7	15.5	0.62	0.58	2.08
160	35	1.78	13	0.61	0.53	2.08

The length of the downcoast headland plays an important role in controlling the reflected wave heights inside the model pocket beach. The results showed that if the length of the downcoast headland extended to the offshore, the reflected waves could propagate to a larger area. For instance, for a 2 m wave approaching at 70° to the shoreline, the wave directions at the reflection points were 53° and 39° for longest and shortest downcoast headlands respectively (Table 4.2). Therefore, the largest downcoast headland could reflect waves to a larger area of the shoreline at about 238 m of the shoreline, whereas the shortest downcoast headland reflected waves to approximately 111 m of the shoreline. This distance on the shoreline would change according to the wave direction. The reflected waves of those incident waves approaching at an angle closer to normal dominated smaller areas.

Wave heights before and after reflection at the reflection point could change depending on approaching incident wave directions. As can be seen in Tables 4.2 to 4.4, with consideration of refraction and shoaling, a wave with a direction closer to normal, had a greater height at the reflection point. However, reflected wave height at reflection point decreased once the wave approached the downcoast headland at a direction close to normal. For instance, when a wave approached at an angle of 70° to normal, the wave height at the reflection point of the 340 m headland was 1.26 and the reflected wave height was 0.62 (Table 4.2). However, for a wave with an angle of 20°, the wave height at the reflection point was 1.65 m and reflected wave height was 0.6 (Table 4.4). It showed that reflected wave heights decreased when waves approached at a direction close to normal.

Reflected wave heights could be greater than those of diffracted waves inside the shallow water of the model pocket beach. Depending on the approaching waves, the reflected waves could dominate the area. For example, once a wave approached the 340 m downcoast headland at 70° to normal, in 2 m depth, reflected wave height was 0.62 m, while the diffracted wave height was 0.4 m (Table 4.2). This difference between reflected and diffracted waves would be reduced if waves approached at an angle closer to normal. For example, when waves approached at 50° to normal, in 2 m depth, reflected wave height was 0.7 m, while the diffracted wave height was 0.65 m (Table 4.3).

However, if waves can directly approach the surf zone, the refracted waves dominate the pocket beach (Table 4.4). For instance, when waves approached the 340 m downcoast headland at 70° to normal, in 2 m depth, reflected wave height was 0.62 m, while the diffracted wave height was 0.4 m (Table 4.2). In contrast, for a 20° wave, reflected wave

height was 0.6 m, while wave height after shoaling and refraction was 2.08 m, dominating the area (Table 4.4).

As discussed earlier, this test experiment was used to evaluate the effect of reflection on wave characteristics inside pocket beaches. In chapter 2, it was concluded that reflection could play an important role in controlling wave characteristics inside the bay. The results of this simple experimental test were used to highlight the importance of reflected waves in Okains Bay.

4.3.2. Wave reflection in Okains Bay using an experimental method

As discussed in chapter 2, the wave heights collected during Field Experiment 1 at site O1 varied from about 0.49 m to 2.9 m. The incident waves predominantly approached 30° and 45° to the shoreline (Figure 4.6a). According to Eq. 4.10, without consideration of refraction, waves with directions within 355° to 25° to the shoreline could directly approach site O3. If refraction is taken into account, the limited directional sector does not change considerably. That is because the distance between these two sites is about 1.5 km and the water depth changed from 12 m to 6 m according to the refraction coefficient, this much variation in the water depth can only shift wave directions a few degrees to normal.

Since the predominant incident waves approach at angles greater than the wave directional sector of Okains Bay, waves collected at site O3 were expected to be a combination of diffracted and reflected waves. Based on the geometry and the bathymetry of the bay, wave directions approaching from 270° to 355° to the shoreline were considered as reflected waves. The predominant wave directions during Field Experiment 1 at site O3 were from 330° and 345° to the shoreline (Figure 4.6b). This suggests that reflection had a great influence on combined waves (short crested-waves) at site O3 compared to diffraction, once incident waves approached at an angle greater than the approaching directional sector. This finding is similar to the results of the section 4.3.1, for the model pocket beach with 340 m downcoast headland (Table 4.2 and 4.4), where reflection dominated the surf zone compared to diffraction.

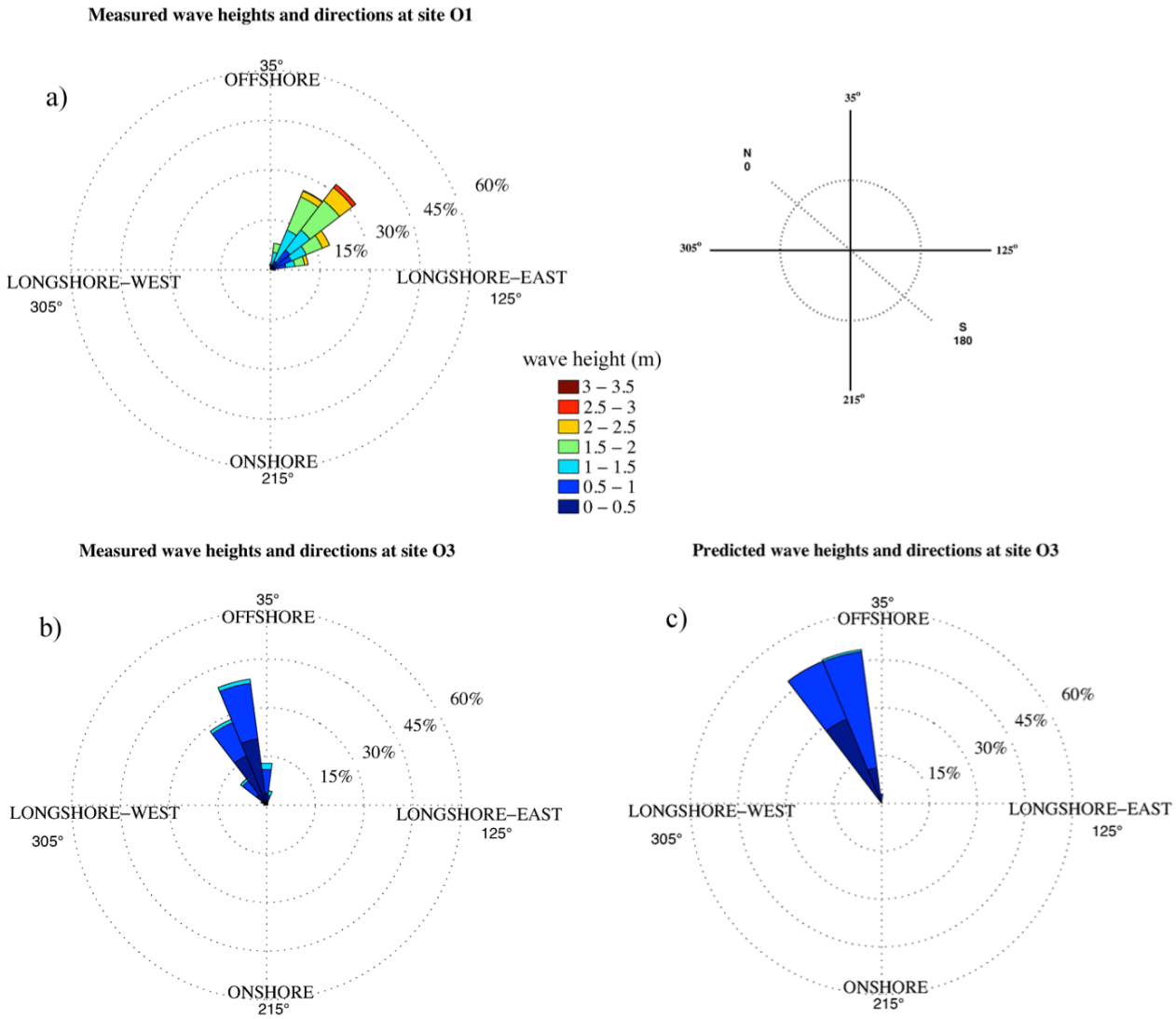

Figure 4.6. Predicted reflected wave data for site O3 versus observations collected during the Field Experiment 1 at sites O1 and O3. Directions are shown relative to the Okains Bay beach orientation.

Similar to the model pocket beach analysis, Eq. 4.7 to 4.9 were used to remap the reflected wave for site O3 using the wave input data collected during Field Experiment 1 from site O1. As depicted in Figure 4.6c, the predicted wave reflection predominantly approached 330° and 345° to the shoreline. The predominant directions were similar to the observations, but with different frequencies (Figure 4.6b and c). A scatter plot analysis indicated that predicted and observed wave directions were poorly correlated with an R^2 of 0.37. However, the MAE and IOA of the predicted wave directions against observations at site O3 were

about 13.29° and 0.6 respectively. This suggests that reflection had a great influence on combined wave directions inside the bay where incident waves cannot directly reach. Note that Eq. 4.7 to 4.9 were not used to predict wave directions for site O3; they were applied to remap the reflected waves for site O3. However, in reality waves could reach site O3 after being mainly influenced by reflection, diffraction and refraction.

The results also indicate that there is good agreement between the predicted reflected wave height and the observations at site O3 with an R^2 of 0.64 (Figure 4.7b). The MAE and IOA calculated for the predicted and observed wave heights were 0.15 and 0.83 respectively (Table 4.5). The differences between predicted and observed wave heights were basically attributed to the influence of diffraction. For instance, the combination of diffraction and reflection may cause the wave height to increase if the waves are in the same phase, or to decrease if they are in a different phase.

Table 4.5. Comparison of IOA and MAE, P-value and correlation coefficient (R^2) for predicted wave height and direction versus observations recorded during Field Experiment 1 at sites O3 and during Field Experiment 2 at O2.

Method	Wave parameter	Site	IOA (H)	MAE (H)	P-Value	R^2
Eq. 4.7, 4.8 and 4.9	Height	O2	0.1	0.13	<0.05	0.3
	Direction	O2	0.07	30.1	<0.05	0.16
	Height	O3	0.83	0.15	<0.05	0.64
	Direction	O3	0.6	13.29	0.079	0.37

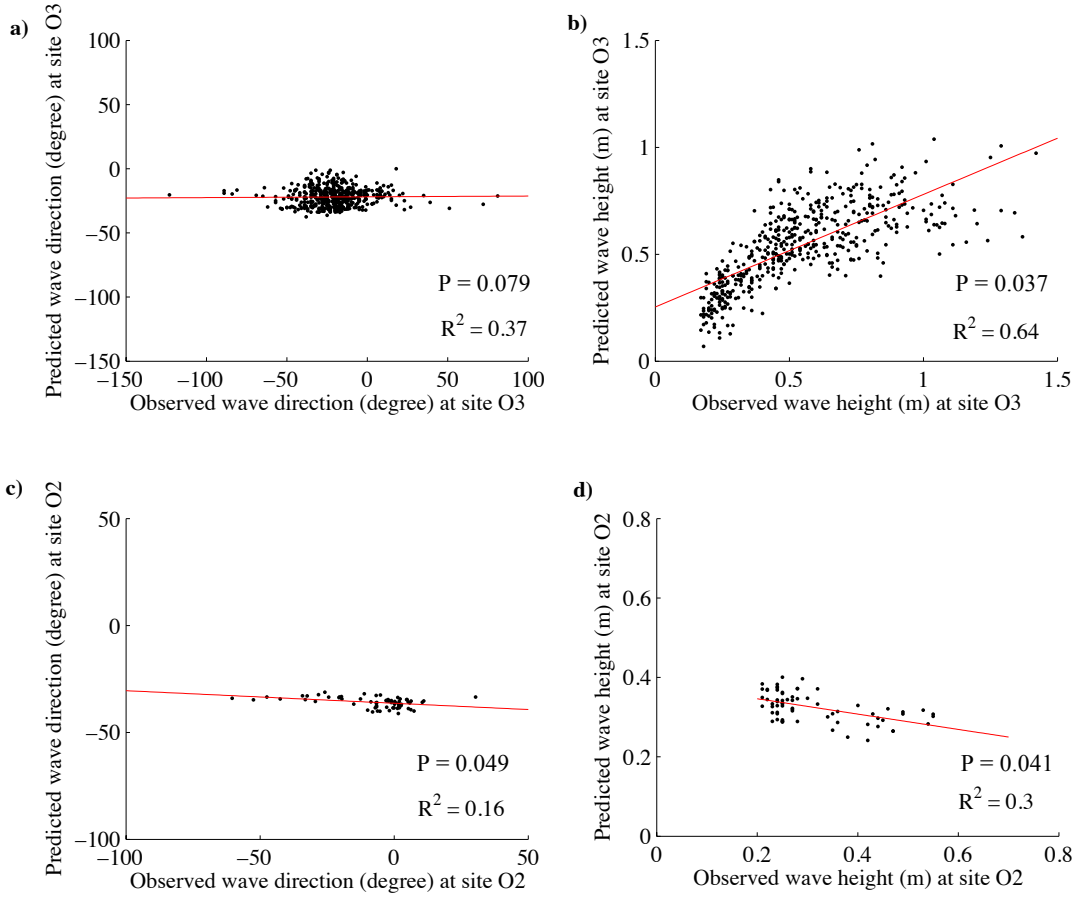

Figure 4.7. Scatter plots of predicted wave height and directions using Zanuttigh and Andersen's (2010) and Zanuttigh and Van der Meer's (2008) approaches versus observations collected during Field Experiment 1 at sites O3 and during Field Experiment 2 at O2.

In order to evaluate the effect of reflection on wave characteristics at areas more exposed to the incident waves in Okains Bay, the data from Field Experiment 2 were used as an input to Eq. 4.7 to 4.9 (Figure 4.7). As discussed in chapter 3, Eq. 3.10 and 3.11 were applied to remap waves for site O1 using wave input data from site B collected during Field Experiment 2. The predicted wave direction at site O1 predominantly approached from 45° to the shoreline (Figure 4.7a). This direction was within the approaching wave directional sector for site O2, which was 345° to 50° to the shoreline. Note that since site O2 was close to the entrance of the bay, waves with a higher range of directions could directly approach and dominate the area compared to site O3.

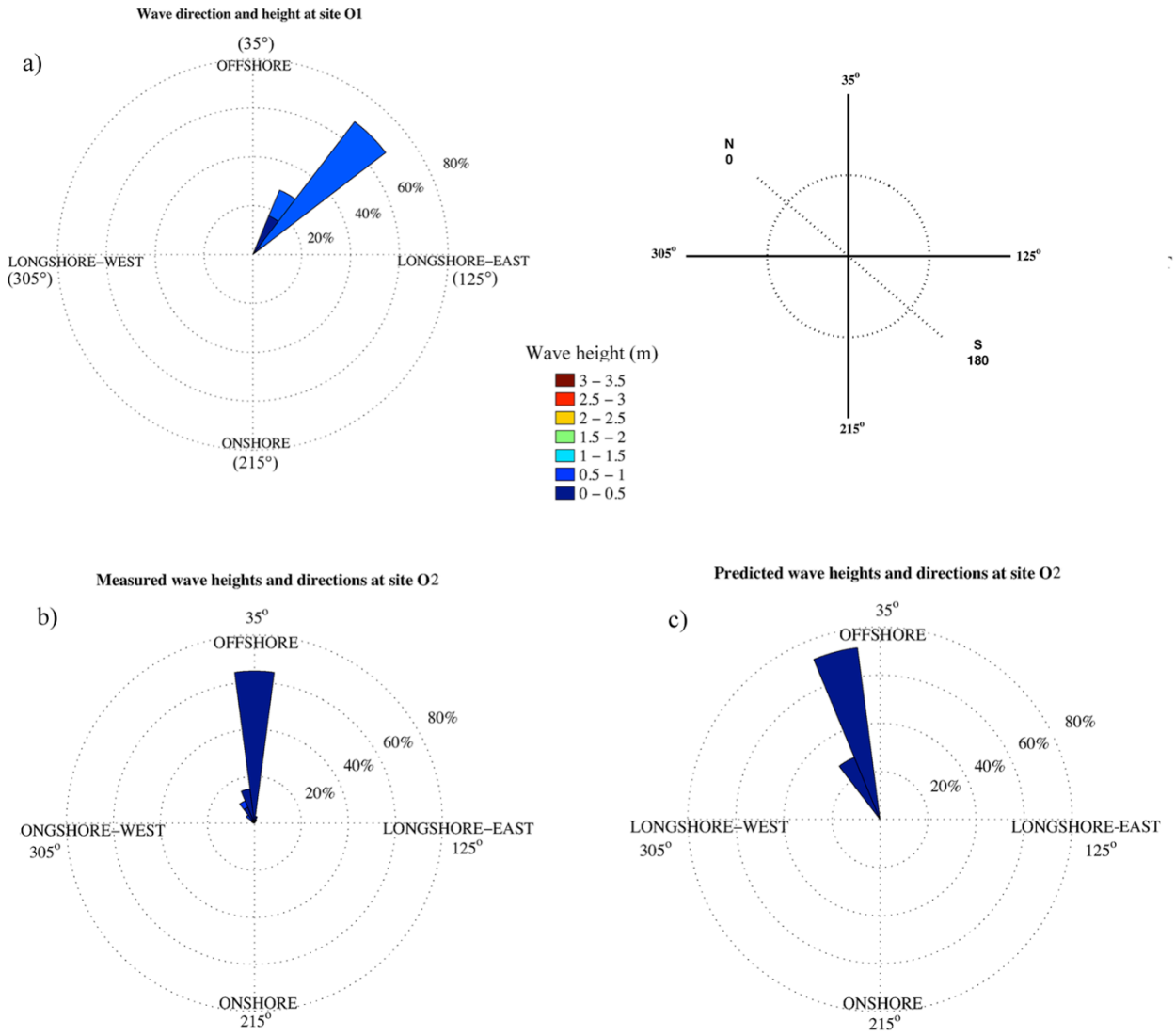

Figure 4.8. Predicted reflected wave data for site O2 versus observations collected during the Field Experiment 2 at sites O1 and O2 (a, b and c). Directions are shown relative to the Okains Bay beach orientation.

Reflection has a minor effect on combined waves at site O2. As depicted in Figure 4.8c, the predicted wave reflection at site O2 predominantly approached at an angle of 330° to the shoreline, which was different from the observations (Figure 4.8b). The MAE and IOA calculated for predicted and observed wave directions at site O2 were 30.1 and 0.07° respectively. These values suggest that the effect of reflection on combined waves at site O2 was considerably reduced because this area was more exposed to direct incident waves.

Reflected waves also had a minor effect on the wave heights of combined waves at site O2. Reflected wave heights predicted by Zanuttigh and Van der Meer's (2008), and Zanuttigh and Andersen's (2010) approach poorly correlated with the observations at site O2 with an R^2 of 0.3. IOA calculated for predicted wave height and observed wave height was about 0.1. This poor prediction indicates that the combined wave height was mainly influenced by direct incident waves. These findings are similar to the results of section 4.3.1, when waves approached the model pocket beach at an angle close to shore normal (Table 4.4).

In addition to the influence of direct incident waves on combined waves at site O2, another possible reason to decrease the effect of reflection at this site could be explained by Eq. 4.11. Based on the geometry of Okains Bay, if the reflected wave direction, θ, was between 270° and 310°, the reflected wave could propagate towards site O2. However, the prediction shows that the reflected wave direction was predominantly approaching from 330° to the shoreline, which is greater than θ. Therefore, reflected waves could not directly propagate towards site O2 and influenced the wave characteristics.

From the results of the experimental model of Zanuttigh and Van der Meer (2008), and Zanuttigh and Andersen (2010), it can be concluded that in pocket beaches, the importance of reflection on combined waves depends on the direction of incident waves and the length of the headlands. The effect of reflection on combined waves decreases: a) if waves approach at an angle close to shore normal, b) if the length of the downcoast headland is shorter and, c) if the area is exposed to direct incident waves.

4.3.3. Numerical modelling of wave processes in Okains Bay

The second approach to evaluating the effect of reflection on wave characteristics in Okains Bay was to use the SWAN wave model. In this study, SWAN model results were first validated against observations recorded during all three field experiments in Okains Bay, and then the importance of reflection in different sites inside the bay was assessed. Note that for more realistic simulations, all possible factors influencing wave characteristics in Okains Bay, such as reflection and diffraction from the headlands, were taken into account.

Table 4.6. Comparison of IOA and MAE of wave characteristics predicted by SWAN at sites O2, O3, O4 and O5 during all three field experiments.

Field Experiment	Site	IOA (H)	MAE (H)	IOA (T)	MAE (T)	IOA (dir)	MAE (dir)
1	O3	0.86	0.22	0.85	1.12	0.92	9.48
2	O2	0.9	0.093	0.76	1.02	0.09	12.7
2	O4	0.74	0.031	0.87	0.56	-	-
2	O5	0.78	0.04	0.84	0.61	-	-
3	O3	0.85	0.16	0.81	0.87	0.71	8.54
3	O5	0.74	0.15	0.73	1.12	-	-

4.3.3.1. Validation of SWAN wave model

Field Experiment 1 was used to compare the results of the SWAN wave model with observations at site O3, where its indentation was about 1.5 km. As depicted in Figure 4.9, SWAN slightly overestimated wave heights with an average of 0.14 m. However, the comparison of wave height between predictions and observations showed that SWAN predictions were reasonably correlated to observations at site O3 with an R^2 of 0.79 (Figure

4.10a). As shown in Table 4.6, IOA and MAE calculated for the predicted and observed wave heights were 0.86 and 0.22 respectively. These values indicate the SWAN model can predict wave heights at site O3 inside Okains Bay with an acceptable level of accuracy.

SWAN can also reasonably predict wave periods at site O3 inside Okains Bay. The results showed that SWAN-estimated wave periods at site O3 were reasonably correlated to the observations with an R^2 of 0.78 (Figure 4.10b). IOA and MAE calculated for the predicted and observed wave periods were 0.92 and 9.48 (Table 4.6). Similar to the results of wave heights, this suggests that the SWAN model can be used to predict wave periods with an acceptable level of accuracy inside the bay.

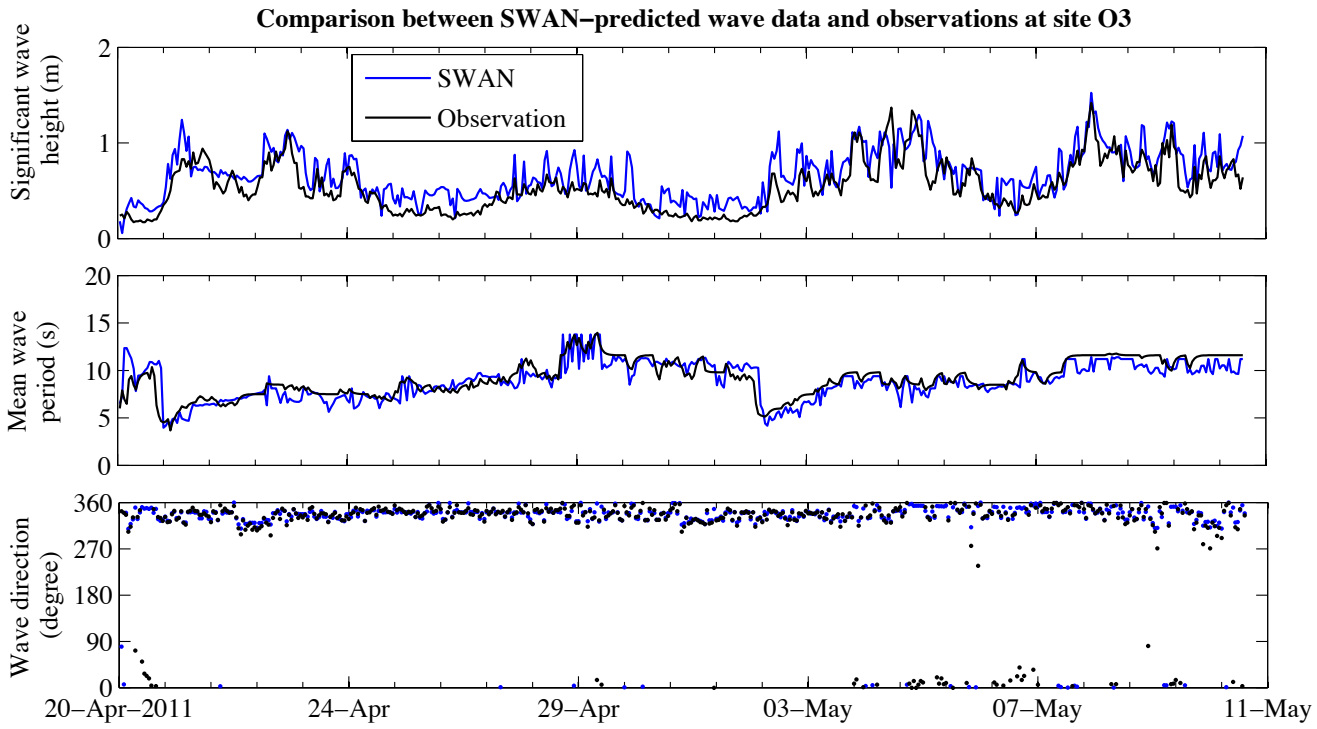

Figure 4.9. Comparison between predicted wave data using SWAN model and observations recorded during Field Experiment 1 at site O3.

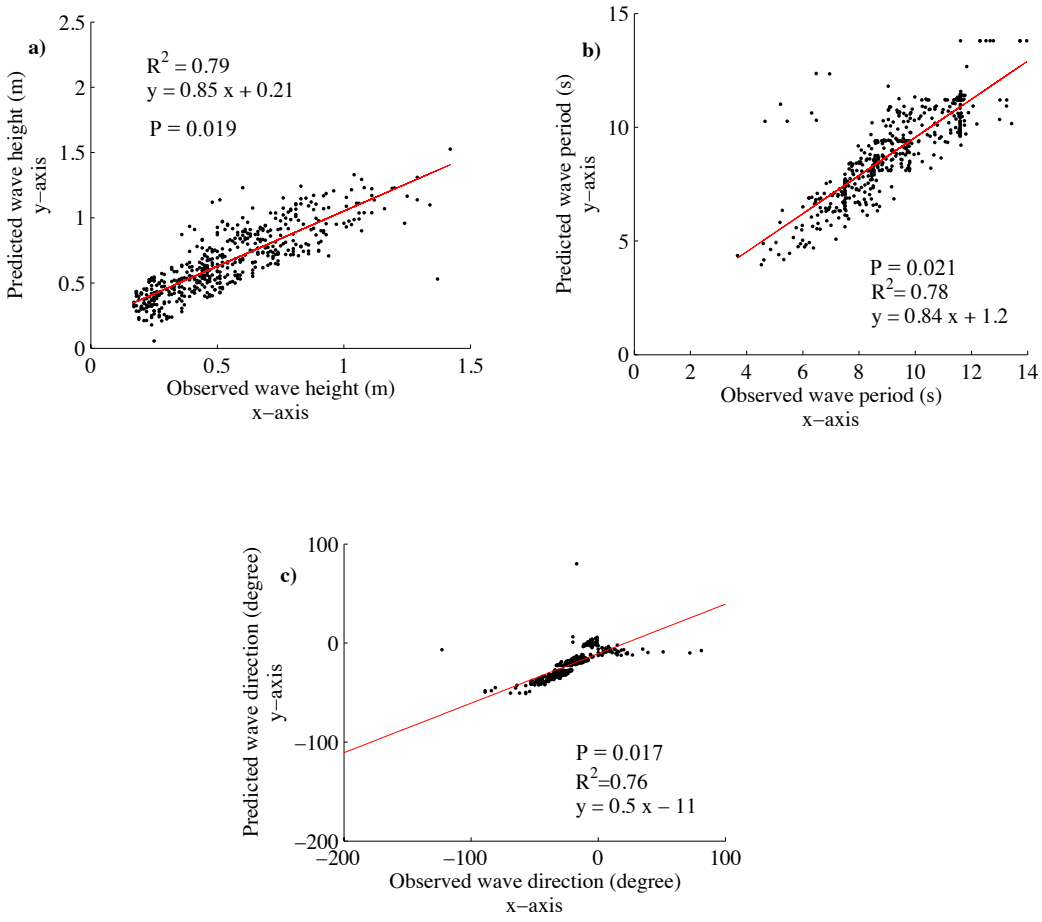

Figure 4.10. Scatter plots of predicted wave height, period and directions using SWAN wave model against observations collected during Field Experiment 1at site O3.

SWAN was found to reasonably predict wave directions at site O3 (Figure 4.11a and b). A scatter plot analysis showed that SWAN predictions were reasonably correlated to observations at site O3 with an R^2 of 0.76 (Figure 4.10c). IOA and MAE calculated for the predicted and observed wave directions are 0.86 and 0.22 respectively (Table 4.6), suggesting that SWAN can be reliably used to estimate wave direction at site O3.

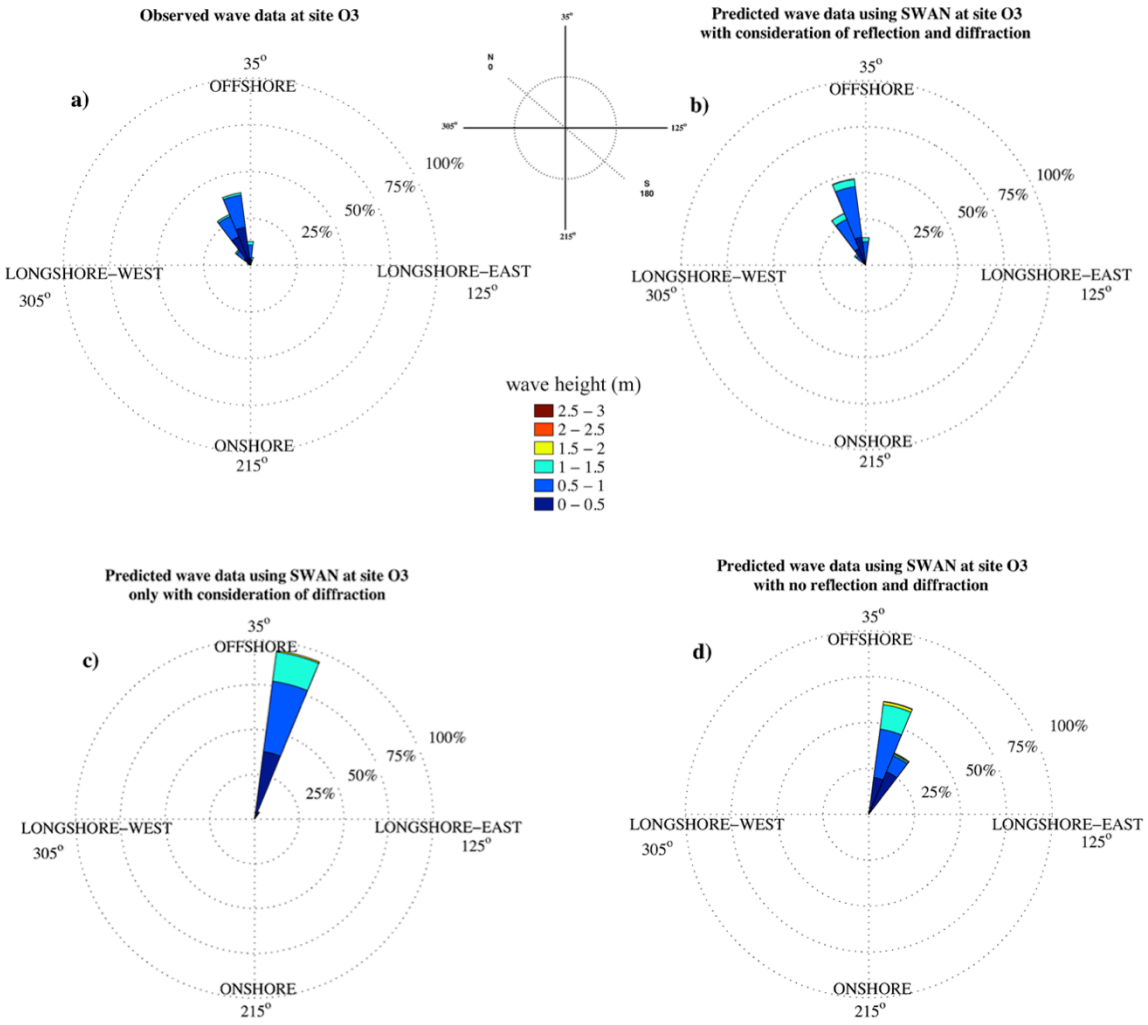

Figure 4.11. Rose plot showing wave heights and directions of SWAN predictions and observations collected during Field Experiment 1at site O3.

Field Experiment 2 was used to compare the results of the SWAN model with observations at site O2, with an indentation of about 0.5 km relative to the entrance of the bay, and also at sites O4 and O5, with an indentation of about 2 km (Figure 4.12). A comparison between the SWAN predicted wave heights and observations at site O2 showed that predictions were reasonably correlated to observations with an R^2 of 0.77 (Figure 4.13a). IOA and MAE calculated for the predicted and observed wave heights at site O2 were 0.9 and 0.093 (Table 4.6). A good correlation between predicted wave heights and observations was also found at sites O4 and O5 with an R^2 of 0.7, IOA of 0.79 and MAE of 0.031 (Figure 4.14a and c and Table 4.6). This indicates that the SWAN model can be used to predict wave heights at sites O2, O4 and O5 with an acceptable level of accuracy.

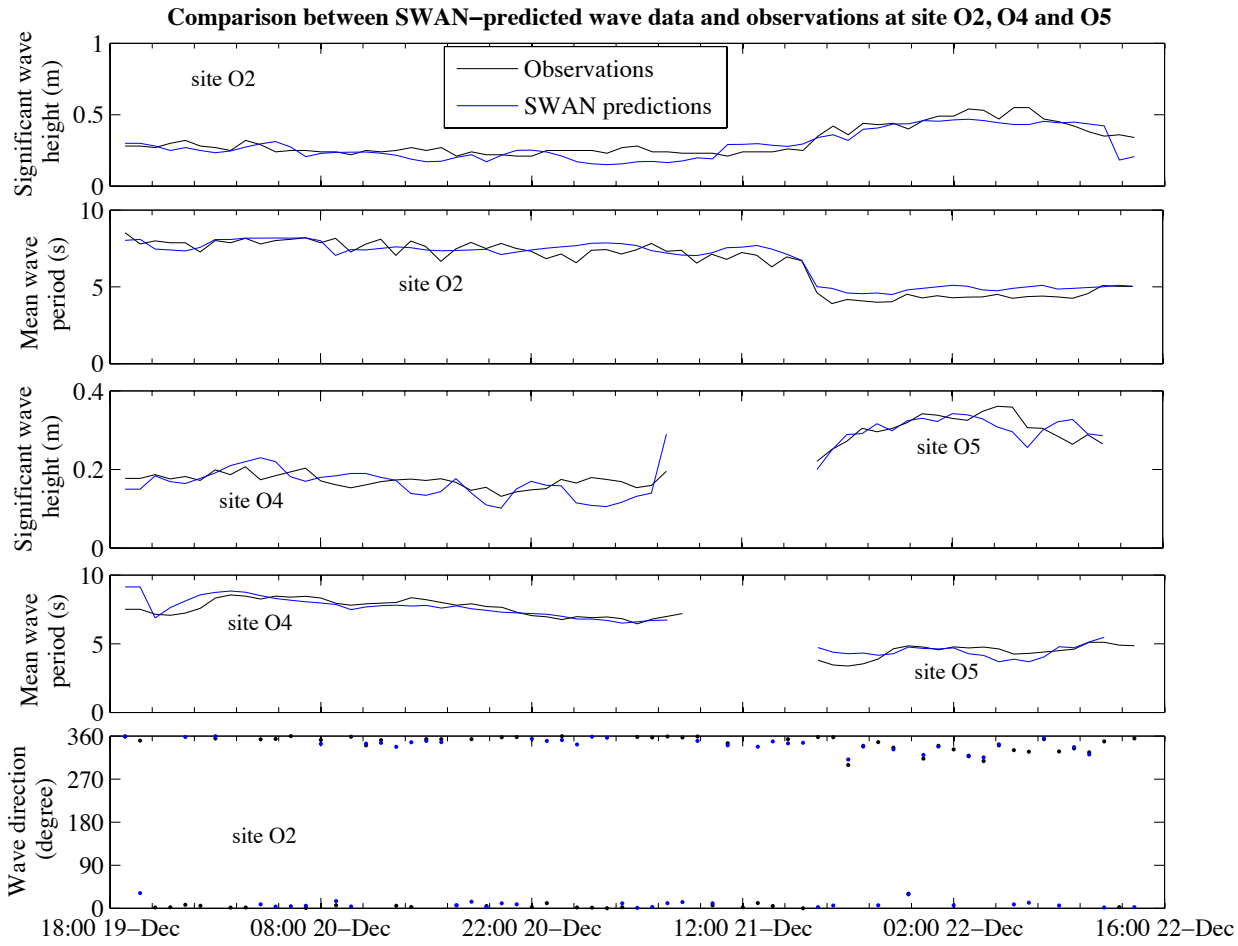

Figure 4.12. Comparison between predicted wave data using SWAN wave model and observations recorded during Field Experiment 2 at sites O2, O4 and O5.

As shown in Figure 4.12, the SWAN model was found to reasonably estimate wave periods at sites O2, O4 and O5 inside Okains Bay. The results indicated that SWAN-estimated wave periods at site O2 are correlated to the observations with an R^2 of 0.77 (Figure 4.13b), IOA of 0.93 and MAE of 1.02 (Table 4.6). The results also stated that there was a good correlation between predicted wave periods and observations at sites O4 and O5 with an R^2 of 0.79 (Figure 4.14b and d). IOA calculated for the predicted and observed wave periods at sites O4 and O5 was 0.87 and 0.84 respectively (Table 4.6). This indicates that the SWAN model was found to reasonably predict wave period at sites O2, O4 and O5.

Wave directions at site O2 can also be reasonably estimated using the SWAN wave model (Figure 4.12 and 4.15a and b). The comparison of predicted wave directions and observations showed that the SWAN results are correlated to observations at site O2 with an R^2 of 0.69 (Figure 4.13c). Despite having a moderate coefficient of determination, IOA and MAE calculated for the predicted and observed wave directions are 0.76 and 12.7 respectively (Table 4.6). This suggests that SWAN can reasonably estimate wave direction at site O2.

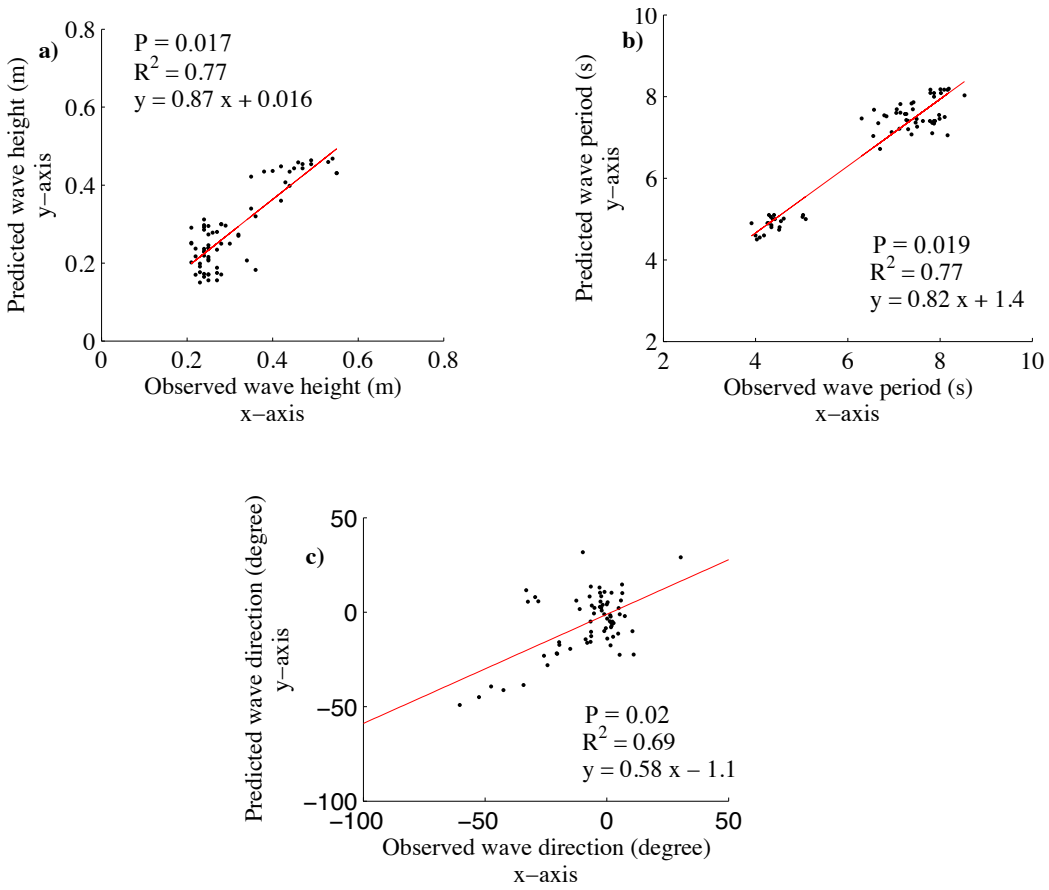

Figure 4.13. Scatter plots of predicted wave height, period and directions using SWAN versus observations collected during Field Experiment 2 at site O2.

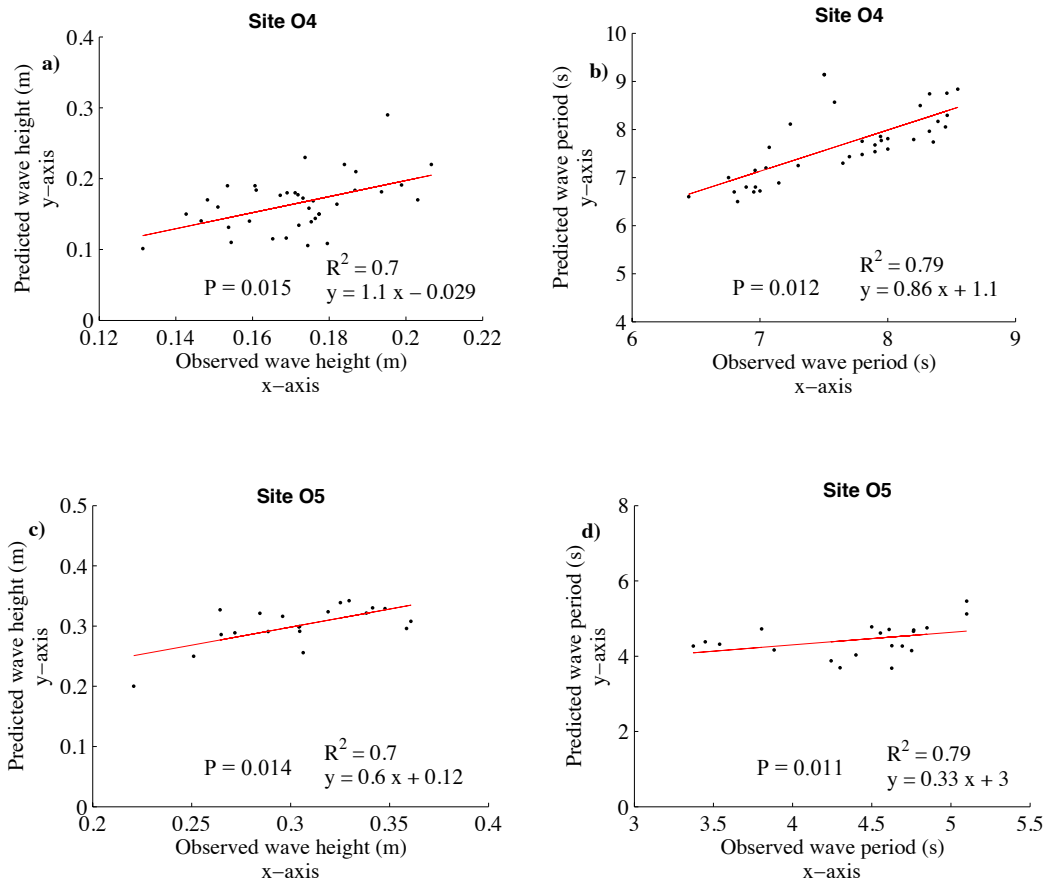

Figure 4.14. Scatter plots of predicted wave height, period and directions using SWAN versus observations collected during Field Experiment 2 at sites O4 and O5.

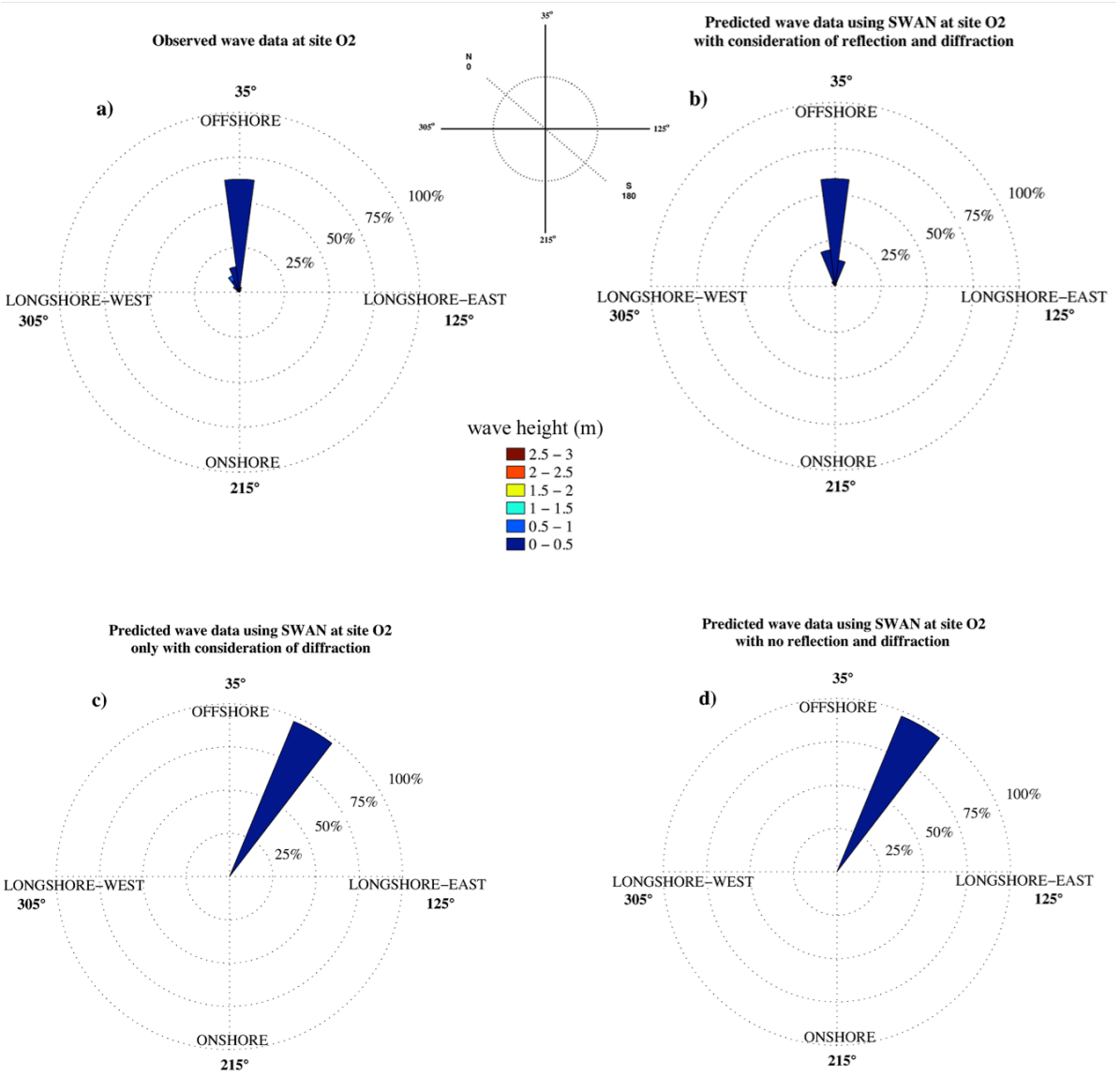

Figure 4.15. Rose plot showing wave heights and directions of SWAN predictions and observations collected during Field Experiment 2 at site O2.

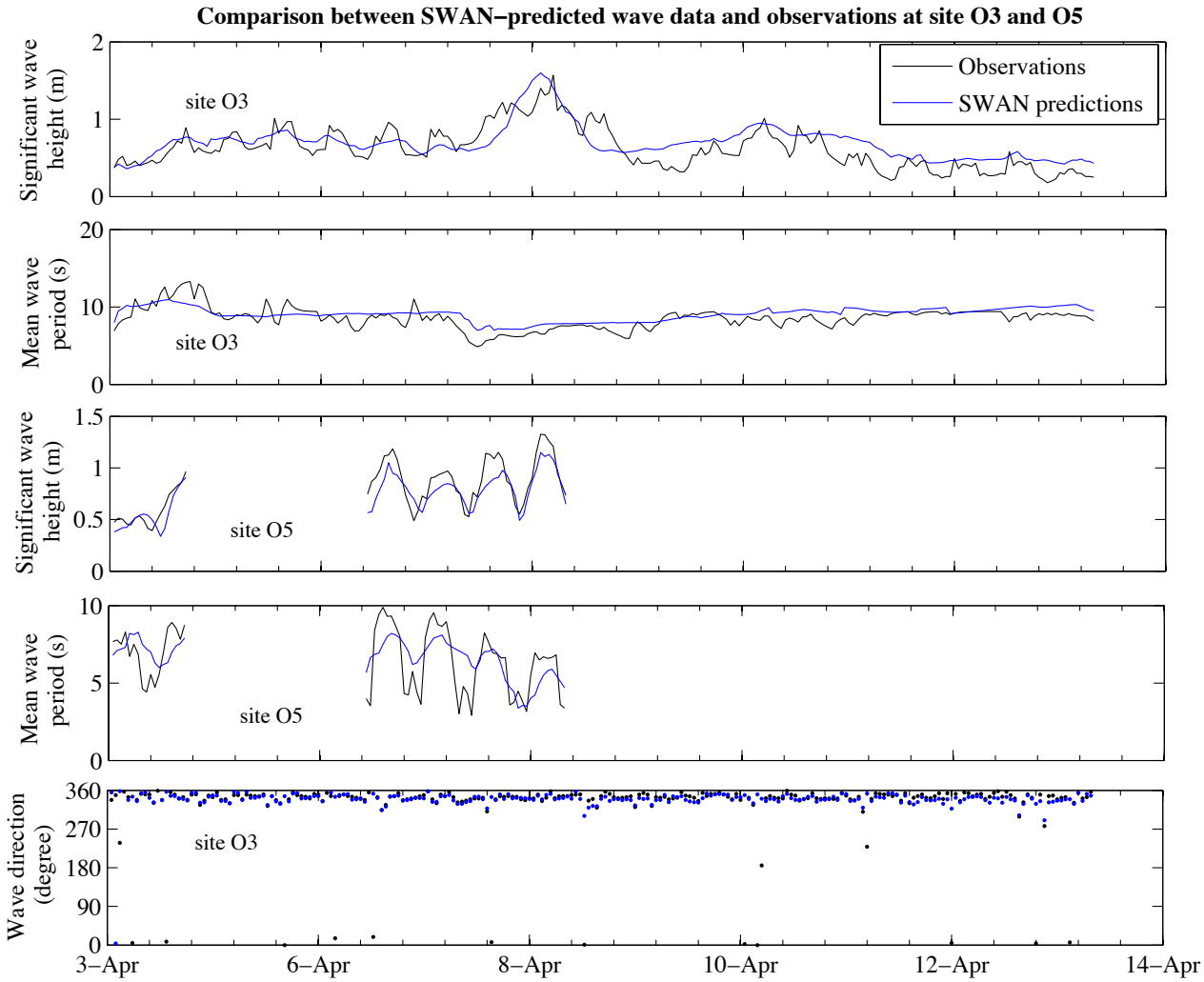

Figure 4.16. Comparison between predicted wave data using SWAN and observations recorded during Field Experiment 3 at site O3 and O5.

SWAN was also applied to simulate waves inside Okains Bay at sites O3 and O5 during Field Experiment 3 (Figure 4.16). The comparison of wave height between the results of SWAN and observations at sites O3 and O5 showed that the predictions were reasonably correlated to observations with an R^2 of 0.76 and 0.84 respectively (Figure 4.17a and 4.18a). IOA calculated for the predicted and observed wave heights at sites O3 and O5 were 0.85 and 0.77 with MAE of 0.16 and 0.15 respectively (Table 4.6). These values indicate that SWAN can predict wave heights at Okains Bay at sites O3 and O5 with an acceptable level of accuracy.

Wave periods can be reasonably estimated using SWAN at sites O3 and O5. The results indicate that SWAN-estimated wave periods at site O3 were correlated to the observations with an R^2 of 0.73 (Figure 4.17b) with IOA and MAE of 0.81 and 0.87 respectively (Table 4.6). The results also state that predicted wave period for site O5 were correlated to the observations with an R^2 of 0.81 (Figure 4.18b) with IOA and MAE of 0.73 and 1.12 respectively (Table 4.6). The correlations indicate that SWAN can reasonably produce wave periods for sites O3 and O5.

Wave directions can also be reasonably estimated using SWAN for site O3 (Figure 4.16 and Figure 4.19b). A comparison between the results of SWAN and observations showed that predicted wave directions were correlated to observations at site O3 with an R^2 of 0.55 (Figure 4.17c). Although the coefficient of determination (R^2) was moderate, IOA and MAE calculated for the predicted and observed wave directions were 0.71 and 8.54 respectively (Table 4.6). This suggests that SWAN can be used to estimate wave direction at site O3 with an acceptable level of accuracy.

From the comparison of the SWAN predictions against the observations recorded during all three field experiments, SWAN was found to reasonably produce the wave characteristics inside Okains Bay, when reflection and diffraction effects in the model configuration are taken into account. In order to examine whether reflection could play an important role in influencing wave characteristics in Okains Bay, two more simulations were separately run for Field Experiments 1 and 2. In the first simulation, the reflection effect was turned off in the model configuration, and in the second simulation, both reflection and diffraction effects were turned off to examine whether or not reflection dominates diffraction in pocket beaches.

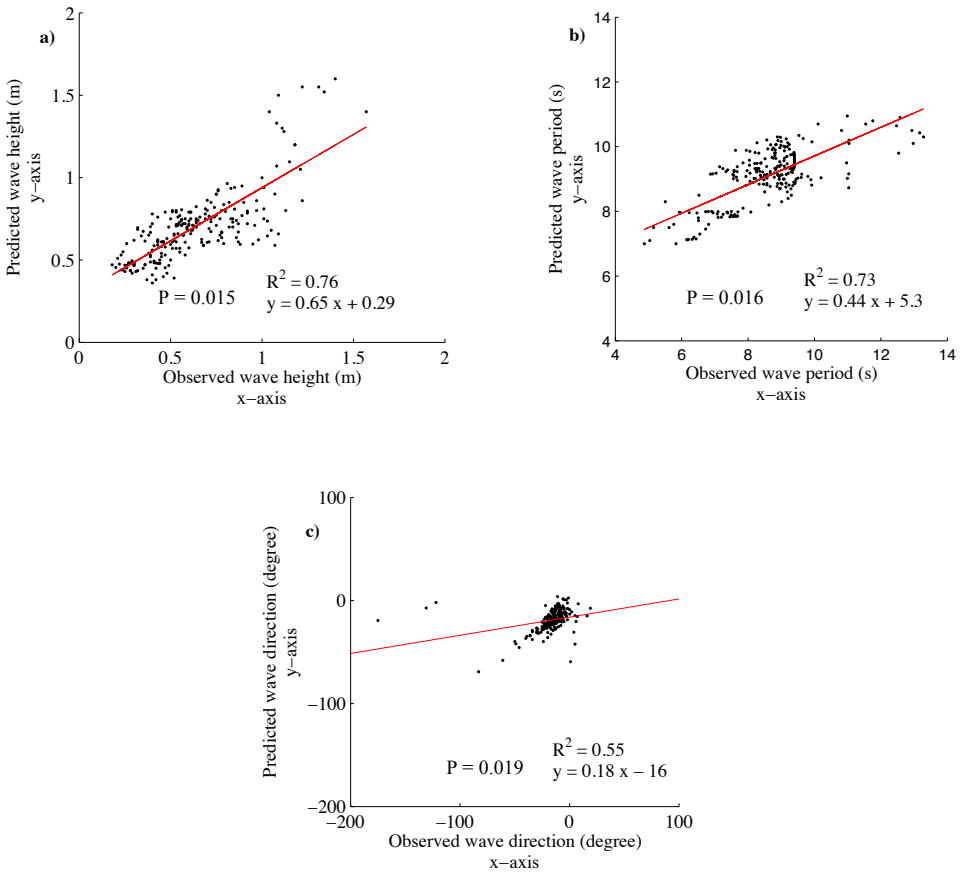

Figure 4.17. Scatter plots of predicted wave height, period and directions using SWAN versus observations collected during Field Experiment 3 at site O3.

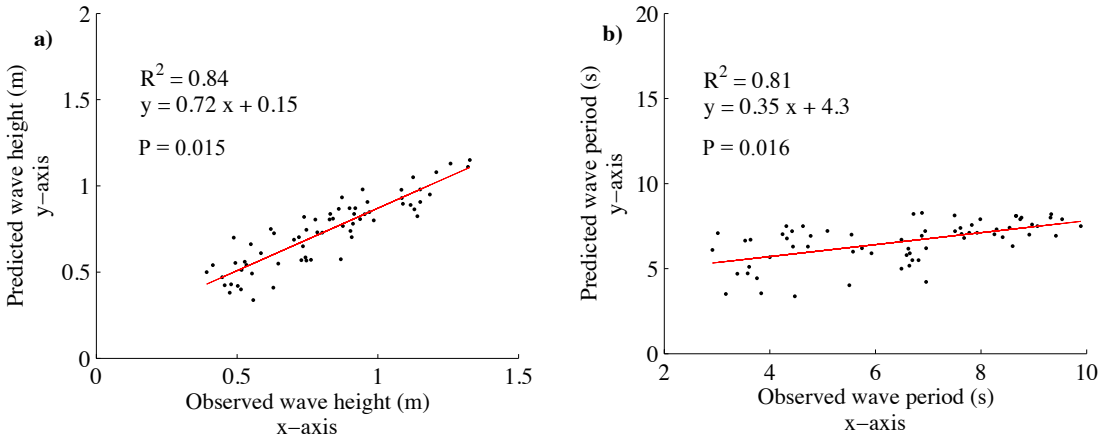

Figure 4.18. Scatter plots of predicted wave height, period and directions using SWAN versus observations collected during Field Experiment 3 at site O5.

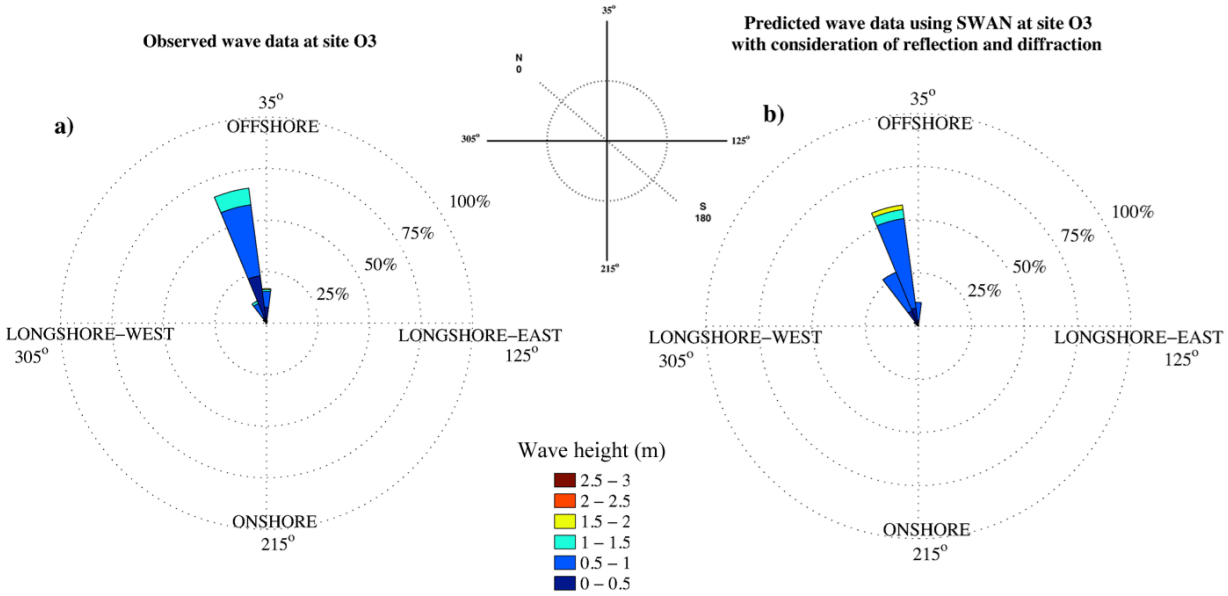

Figure 4.19. Rose plot showing wave heights and directions of SWAN predictions and observations collected during Field Experiment 3 at site O3.

Table 4.7. Comparison of IOA and MAE of wave characteristics predicted by SWAN when diffraction was only considered during all three field experiments at sites O2, O3, O4 and O5.

Field Experiment	Site	IOA (H)	MAE (H)	IOA (T)	MAE (T)	IOA (dir)	MAE (dir)
1	O3	0.61	0.36	0.63	1.74	0.34	39.05
2	O2	0.8	0.072	0.76	1.08	0.55	38.13
2	O4	0.35	0.069	0.36	0.87	-	-
2	O5	0.3	0.062	0.31	0.89	-	-
3	O3	0.68	0.22	0.76	1.12	0.32	40.68
3	O5	0.37	0.31	0.64	2.63	-	-

4.3.3.2. Evaluation of the importance of reflection in Okains Bay

In the previous section, SWAN was found to produce wave characteristics inside Okains Bay with an acceptable level of accuracy. In this section, SWAN will be used to evaluate the importance of reflection inside the bay. The first model experiment was carried out without consideration of reflection in Okains Bay using wave input data collected during Field Experiments 1 and 2. The results showed that predicted wave heights and periods for site O3 were moderately correlated to the observations collected during Field Experiment 1 with an R^2 of 0.49 and 0.47 respectively (Figure 4.20a and b). IOA and MAE calculated for predicted wave height and periods versus observations shown in Table 4.7 also indicate that the predictions poorly fit the observations in comparison to the simulations in which reflection was taken into account (section 4.3.3.1 and Table 4.6).

Similar results were also found for predicted wave heights and periods for sites O4 and O5 using wave input data collected during Field Experiment 2. The results indicated that predictions were poorly correlated to observations (Figure 4.21). IOA and MAE calculated for predictions and observations shown in Table 4.7 also indicate that the predictions poorly fit the observations, if reflection is not considered in the model.

However, SWAN was found to reasonably estimate wave heights and periods for site O2 without consideration of reflection. The comparison between the SWAN results and observations recorded during Field Experiment 2 at site O2 showed that predictions were reasonably correlated to observations with an R^2 of 0.69 and 0.7 respectively (Figure 4.21a and b). As shown in Table 4.7, IOA and MAE calculated for predictions and observations also indicate that the predictions reliably fit the observations. However, the correlation was slightly weaker than that found for the simulations in which reflection was considered (section 4.3.3.1 and Table 4.6). The results state that reflection influences the wave characteristics at site O2, but this effect appears to be less compared to sites O3, O4 and O5, which are located further into the bay. Therefore, it can be concluded that the effect of reflection on wave heights and periods would be more accentuated in areas further into the bay towards the shoreline. However, those areas more exposed to direct incident waves (e.g. site O2) would be less affected by reflection.

When the reflection effect was not taken into account, the SWAN-predicted wave directions were notably different from observations collected during Field Experiment 1 at site O3. The results show that predicted wave directions were poorly correlated to observations with an R^2 of 0.23 (Figure 4.20c). IOA and MAE calculated for predictions versus observations were 0.34 and 39.05 (Table 4.7), indicating poor estimations using SWAN with no reflections effect. Figures 4.10c and 4.20c indicate how significant the predominant wave directions at site O3 would change, if reflection was not taken into account. Predicted wave directions approached predominantly from 15°, while the predominant observed wave directions approached from 330° and 345°. When reflection was not taken into account, this considerable change in the wave directions is more noticeable compared to predicted wave heights and periods. Therefore, it can be concluded that reflection could more influence wave directions inside Okains Bay relevant to wave heights and periods.

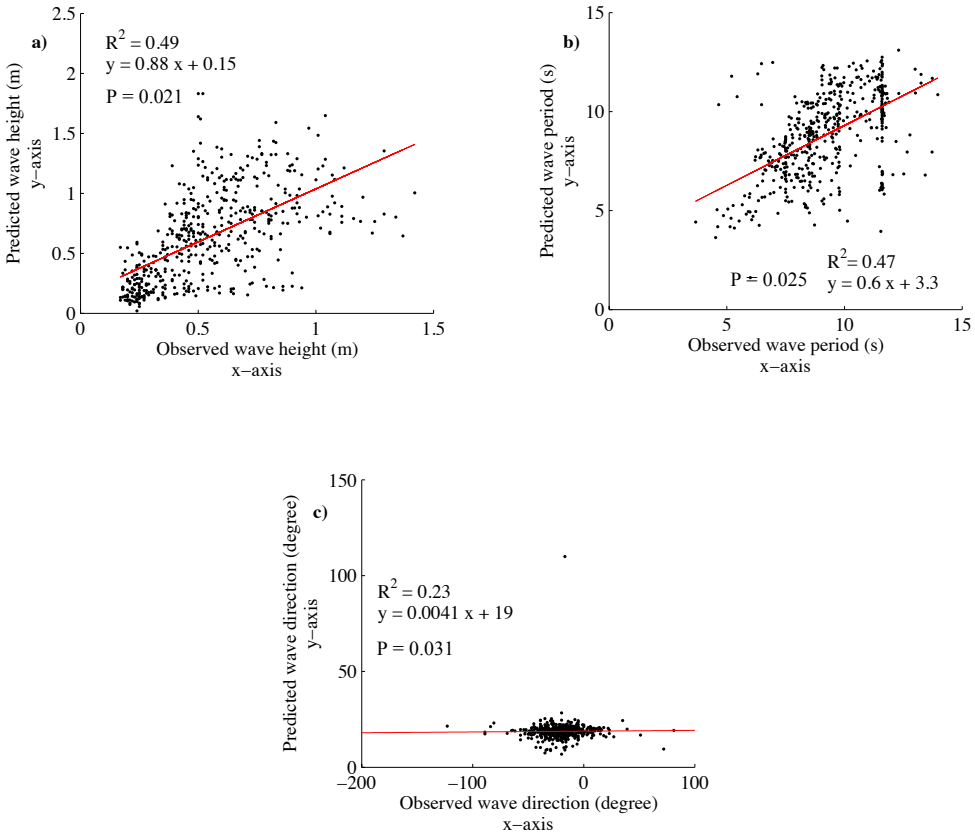

Figure 4.20. Scatter plots of predicted wave height, period and directions using SWAN without consideration of reflection versus observations collected during Field Experiment 1 at site O3.

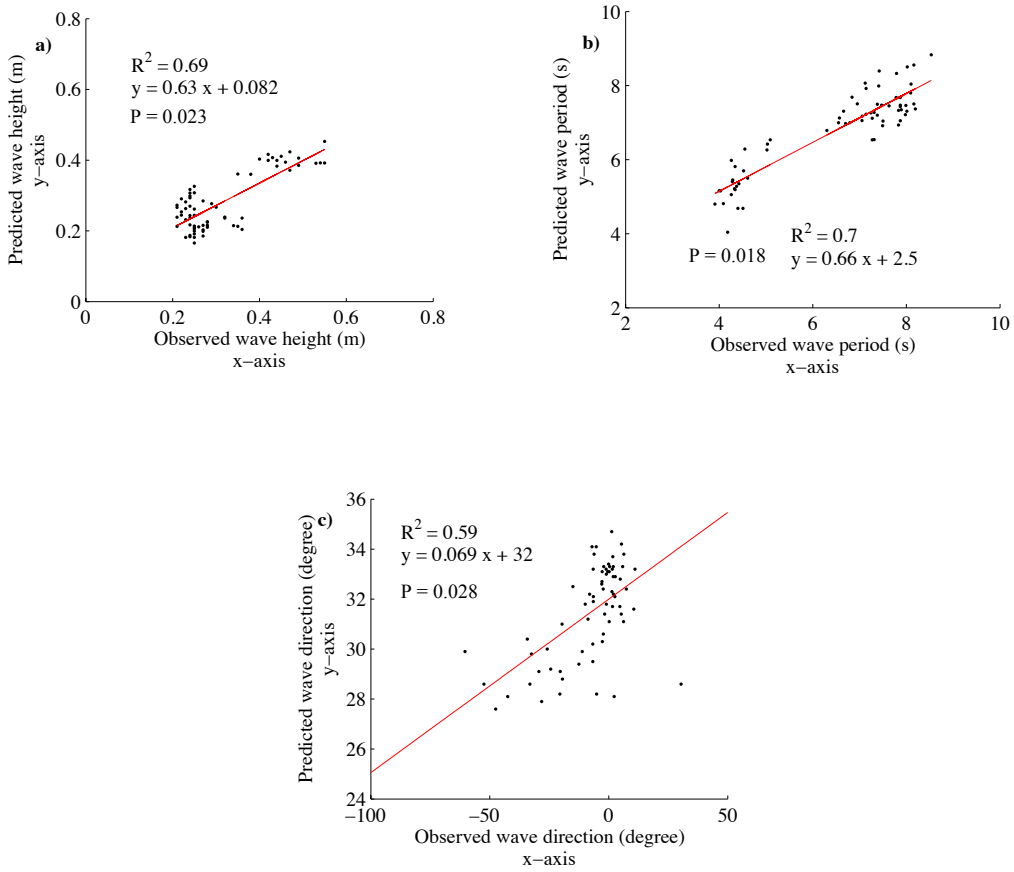

Figure 4.21. Scatter plots of predicted wave height, period and directions using SWAN without consideration of reflection versus observations collected during Field Experiment 2 at site O2.

Similar results were also found at site O2 during Field Experiment 2. The results showed that there was a moderate correlation between predicted wave directions and observations with an R^2 of 0.59. IOA and MAE calculated for predictions versus observations were 0.55 and 38.13 (Figure 4.21c and Table 4.7). Also as depicted in Figure 4.15c, the difference between predominant predicted wave direction and observed wave directions recorded at site O2 was 30°. This shows that the predictions poorly fit the observations, so it can be inferred that reflection could change the wave direction at site O2.

However, the reflection effect at site O2 is less important than the other areas further into the bay. The comparison between the results of SWAN without consideration of reflection at sites O2 and O3 shows that there was a better fit between predictions and observations at site O2 relevant to site O3. The coefficient of determination, R^2, at site O2 is 0.62 versus

0.23 at site O3 and the IOA calculated for site O2 was 0.55, while IOA calculated for site O3 was 0.34. Also as depicted in Figure 4.11c, the difference between predominant predicted wave direction and predominant observed wave directions recorded at site O3 was about 30° to 45°, while this difference for site O2 was less than 30°. Therefore, it can be concluded that reflection tends to influence wave characteristics less in areas close to the entrance of Okains Bay than other areas further into the bay where they are sheltered from approaching incident waves by the headlands.

The second model experiment was carried out in order to examine whether diffraction is as important as reflection inside Okains Bay and could change wave characteristics. In the model configuration both reflection and diffraction were turned off during simulations. The results showed that predicted wave heights and periods were poorly correlated to observations collected during Field Experiment 1 at site O3 with an R^2 of 0.45 and 0.39 respectively (Figure 4.23a and b). IOA calculated for predicted wave heights and periods versus observations were 0.59 and 0.6 with MAE of 0.38 and 1.89 respectively (Table 4.8). This indicates the correlation was slightly weaker than when the diffraction was taken into account.

Table 4.8. Comparison of IOA and MAE of wave characteristics predicted by SWAN without consideration of reflection and diffraction during all three field experiments at sites O2, O3, O4 and O5.

Field Experiment	Site	IOA (H)	MAE (H)	IOA (T)	MAE (T)	IOA (dir)	MAE (dir)
1	O3	0.59	0.38	0.6	1.89	0.31	41.78
2	O2	0.79	0.078	0.75	1.21	0.53	39.06
2	O4	0.18	0.067	0.31	0.97	-	-
2	O5	0.15	0.064	0.28	0.93	-	-
3	O3	0.62	0.25	0.75	1.14	0.27	31.57
3	O5	0.35	0.44	0.57	3.57	-	-

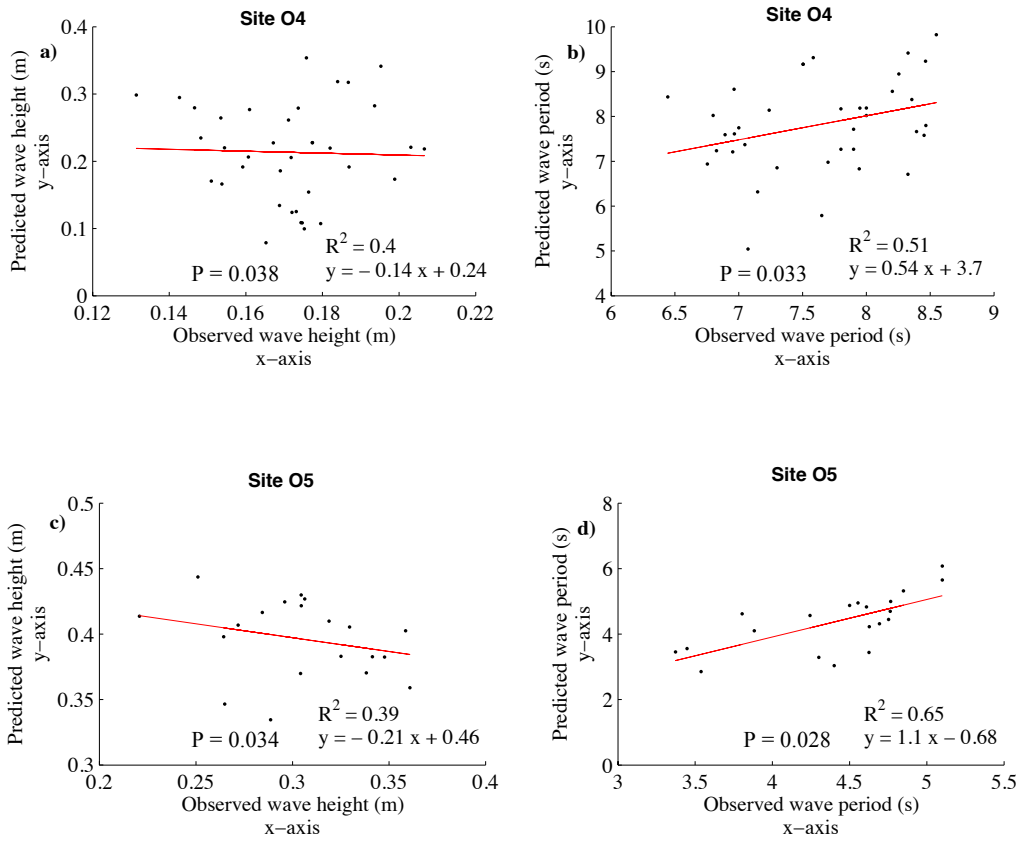

Figure 4.22. Scatter plots of predicted wave height and period using SWAN without consideration of reflection versus observations collected during Field Experiment 2 at sites O4 and O5.

However, SWAN could reasonably estimate wave heights and periods for site O2 without consideration of reflection and diffraction. The comparison between the SWAN results and observations recorded during Field Experiment 2 at site O2 showed that predicted wave heights and periods were reasonably correlated to observations with an R^2 of 0.69 and 0.7 respectively (Figure 24a and b). As shown in Table 4.8, IOA and MAE calculated for predictions versus observations also indicate that the predictions reliably fit the observations. However, the correlations were slightly weaker than those of simulations when only diffraction was considered. The results state that besides reflection, diffraction influences the wave characteristics at site O2, but this effect appears to be less compared to areas (e.g. site O3) further into bay.

Similar to the results of the first model experiment, when both reflection and diffraction effects were not taken into account, the SWAN-predicted wave directions were notably different from observations collected during Field Experiment 1 at site O3. The results state

that predicted wave directions were poorly correlated to the observations with an R^2 of 0.18 (Figure 4.23c). IOA and MAE calculated for predicted wave directions versus observations were 0.31 and 41.78 respectively (Table 4.8), indicating weak estimations using SWAN with no diffraction and reflection effects.

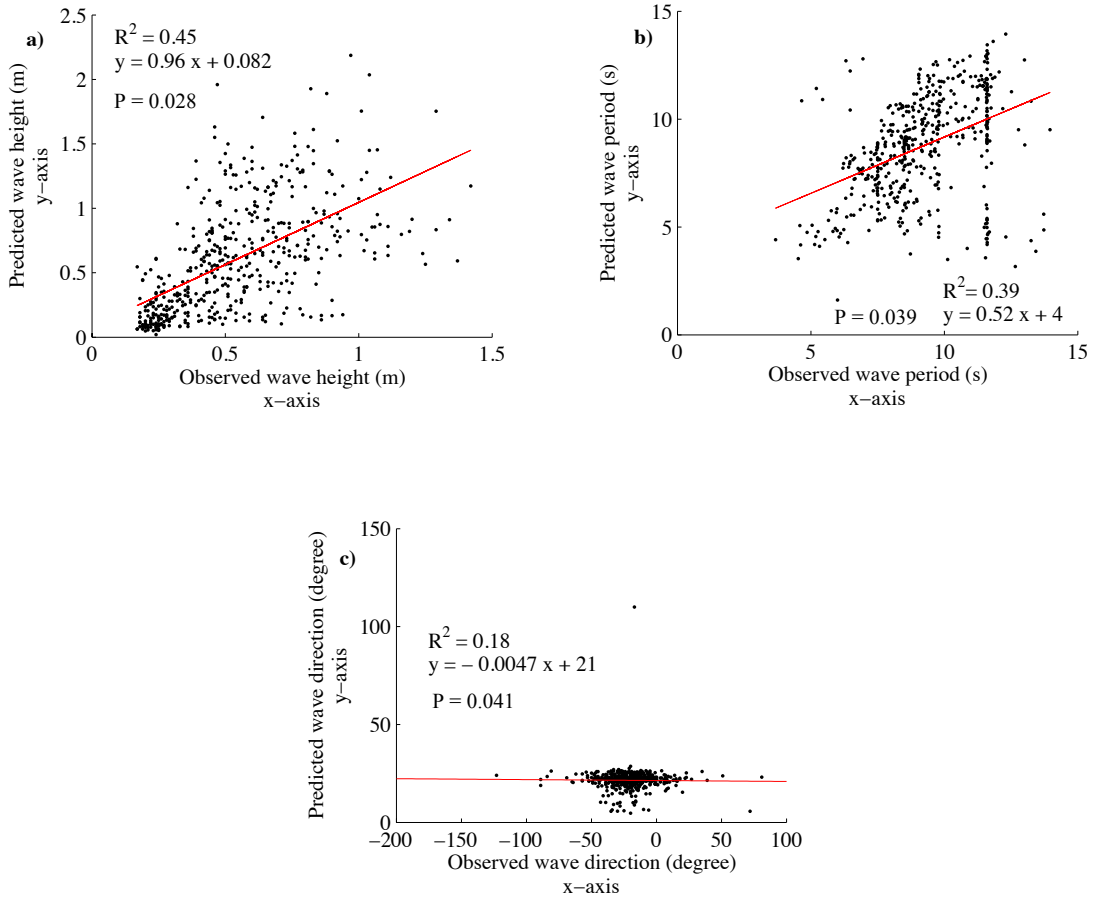

Figure 4.23. Scatter plots of predicted wave height, period and directions using SWAN without consideration of reflection and diffraction versus observations collected during Field Experiment 1 at site O3.

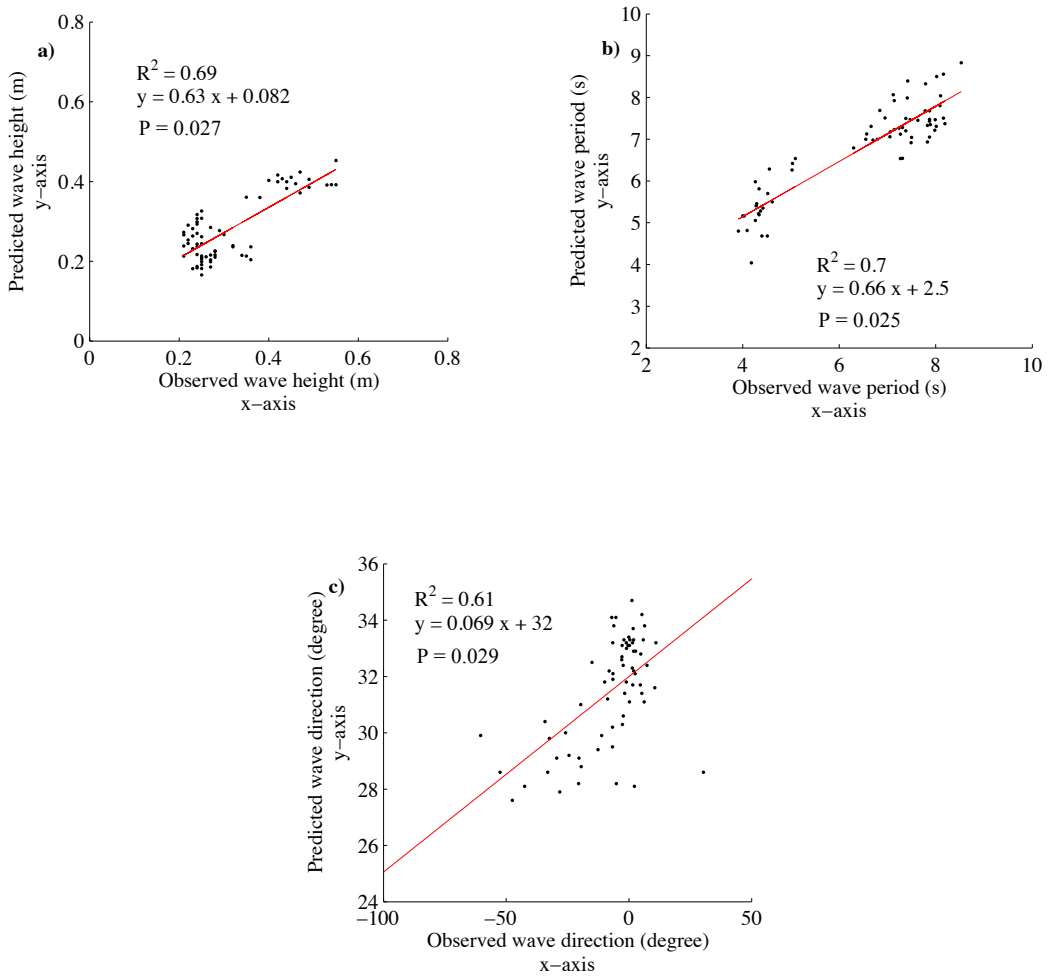

Figure 4.24. Scatter plots of predicted wave height, period and directions using SWAN without consideration of reflection and diffraction versus observations collected during Field Experiment 2 at site O2.

With no reflection and diffraction, similar results were also found during Field Experiment 2 at sites O4 and O5. The results indicate that predicted wave heights and periods at sites O4 and O5 were poorly correlated to observations (Figure 4.25). IOA and MAE calculated for predictions versus observations shown in Table 4.8 also indicate that the predictions poorly fit the observations at these two sites inside the bay.

As shown in Figure 4.11c and d, the predominant wave directions at site O3 changed slightly when diffraction was not taken into account. The SWAN predictions indicate that wave directions approached from 15° to the shoreline followed by 30°, whereas the

predicted wave directions with consideration of only diffraction show that waves predominantly approached from 15° to the shoreline. This slight change in wave directions is more noticeable than predicted wave heights and periods when diffraction was not taken into account. Therefore, it can be concluded that diffraction could more slightly influence wave directions than wave heights and periods inside the bay.

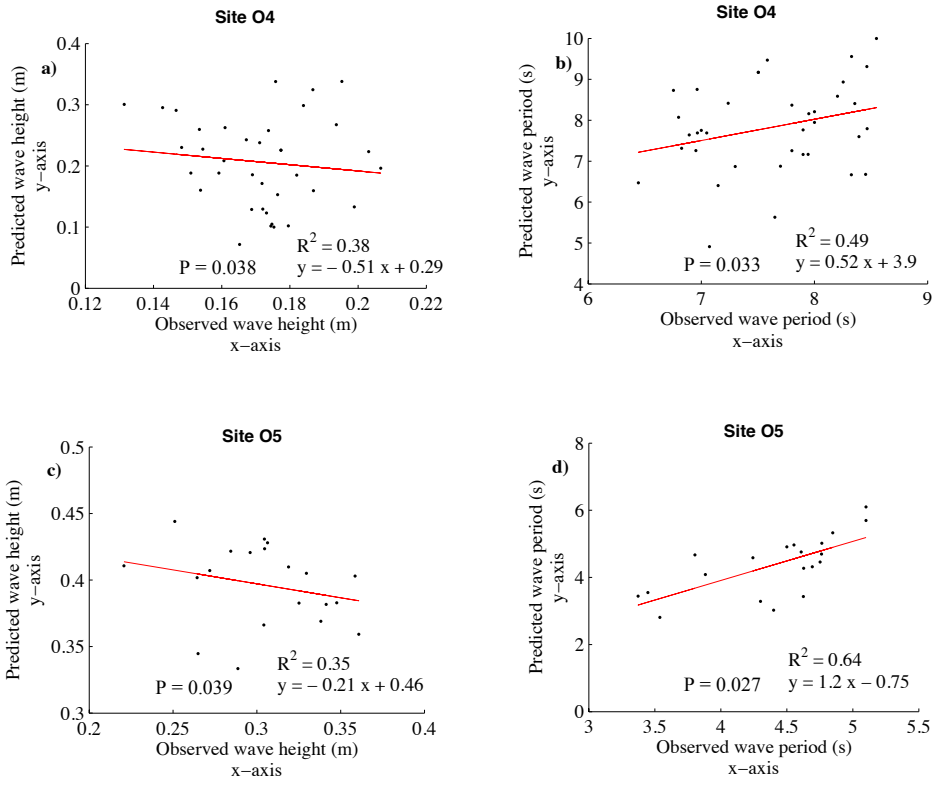

Figure 4.25. Scatter plots of predicted wave height and period using SWAN without consideration of reflection and diffraction versus observations collected during Field Experiment 2 at sites O4 and O5.

Similar results were also found at site O2 during Field Experiment 2. The results showed that there was a moderate correlation between predicted wave directions and observations with an R^2 of 0.61 (Figure 4.24c). IOA and MAE calculated for predictions versus observations were 0.53 and 39.06 (Table 4.8). Also as depicted in Figure 4.14c and d, predominant predicted wave direction was the same as when the diffraction was taken into

account with only a few degrees change in the wave direction. This states that diffraction could slightly change the wave direction at site O2, which indicates that this area is more exposed to direct incident waves.

From the SWAN results, it can be concluded that diffraction slightly affects wave characteristics at site O2 compared to the areas further into the bay. The comparison between the results of SWAN without consideration of diffraction and reflection at sites O2 and O3 shows that the predictions better fit observations at site O2 compared to site O3. The coefficient of determination, R^2, at site O2 was 0.61 but it was 0.18 at site O3. Also IOA calculated for predictions for site O2 versus observations was 0.53, while it was 0.31 for site O3. Therefore, it can be concluded that diffraction is less important in areas close to the entrance of the bay than other areas further into the bay. Note that both sites O2 and O3 were closer to the downcoast headland than the upcoast headland, so diffraction has a minor effect on wave characteristics compared to those areas in proximity to the upcoast headland.

Comparison between the model experiments with and without reflection and diffraction effects indicate that reflection could importantly influence wave characteristics compared to diffraction inside Okains Bay in areas closer to the downcoast headland. Since both sites O2 and O3 were closer to the downcoast headland, reflection from the downcoast headland had a greater influence on waves than diffraction from the upcoast headland. It was expected that the diffraction gradually dominated the area towards the upcoast headland. However, this study is more focused on the importance of reflection on wave characteristics in pocket beaches than the diffraction effect. Our knowledge of wave diffraction from the upcoast headland is adequate because diffraction has been widely studied in embayed beaches (Thomas et al., 2011; Harley and Turner, 2008; Reniers et al., 2004; da Fontoura Klein and de Menezes, 2001); however, the importance of reflection has been poorly documented in pocket beaches and it needed more studies to improve our knowledge of reflection on wave characteristics inside natural pocket beaches.

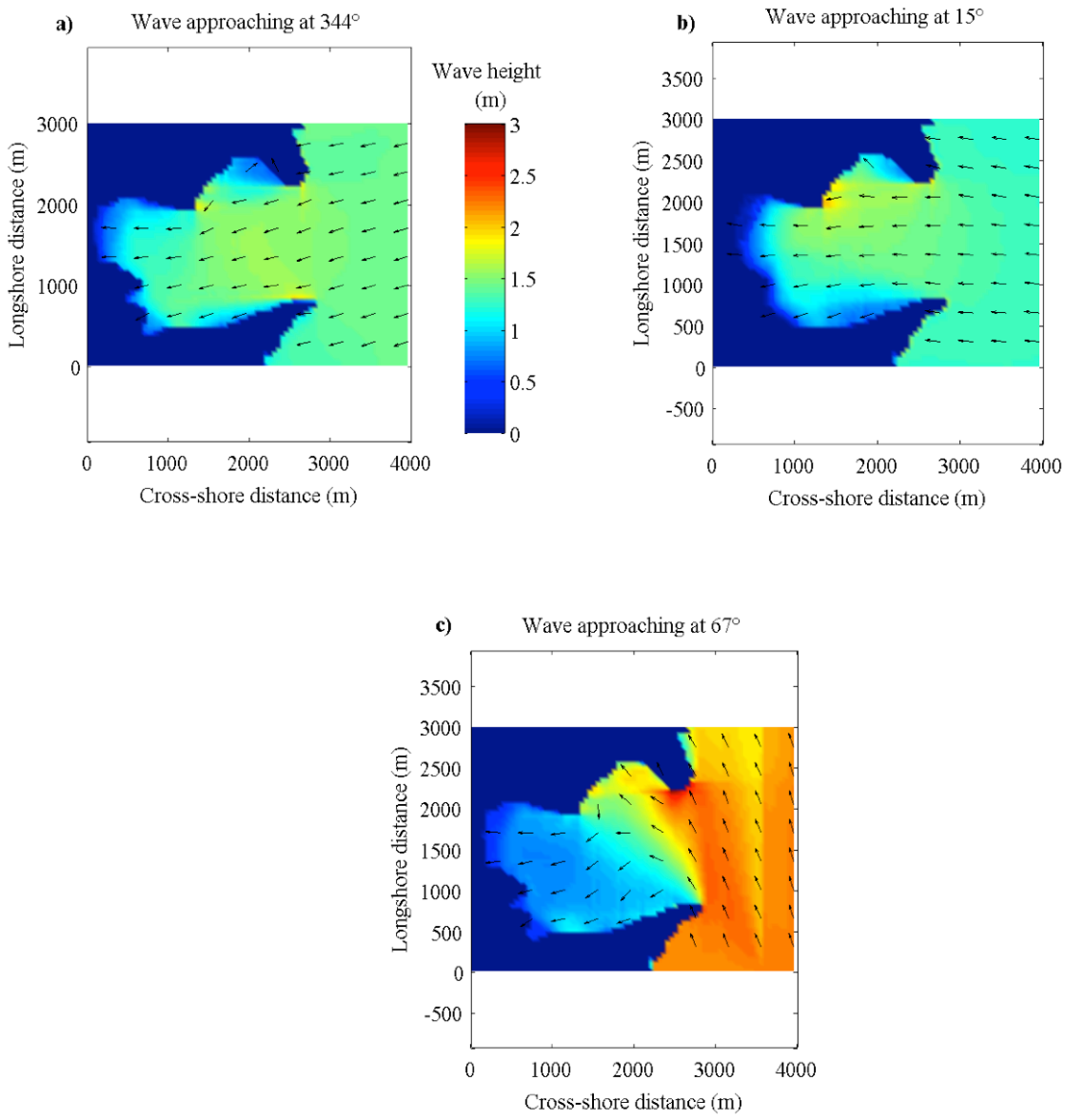

Figure 4.26. Comparison of wave reflection in Okains Bay with waves approaching from 15°, 67° and 344° to the shoreline, extracted from the results of SWAN wave model.

4.4. Discussion

The results of this study showed that reflection could play an important role in controlling wave characteristics in pocket beaches. As discussed in chapter 2, the observations inside Okains Bay suggested that the reflection effect could importantly influence the wave directions inside Okains Bay, especially in areas close to the downcoast headland. The experimental and numerical approaches used in this study proved that reflection may significantly change wave characteristics, particularly wave directions.

In the first step of this study, the reflection effect was calculated for monochromic waves using the experimental method of Zanuttigh and Van der Meer (2008), and Zanuttigh and Andersen (2010). Although the analysis was based on simple mathematics, it gave an initial idea on how reflection could importantly influence wave characteristics in pocket beaches.

More sophisticated mathematical analyses using SWAN demonstrated the importance of reflection in Okains Bay. The results of the model showed that if waves approach from an angle greater than the limited directional sector of Okains Bay, reflection could significantly alter wave characteristics inside the bay. However, this effect was not observed when reflection was deactivated in the model. The model validation against observations recorded at different locations inside the bay indicated that the model could reasonably estimate wave characteristics when reflection is taken into account. Therefore, the results of the model prove that the analysis based on the experimental method is reliable, even though it is based on simple mathematics, that is, reflection plays an important role in controlling wave characteristics in Okains Bay, an example pocket beach.

Further analysis using SWAN showed that reflection was less important in areas close to the entrance of the bay. In areas more exposed to direct incident waves, refraction and shoaling prevail over other factors, such as reflection and diffraction. Therefore, reflection has less effect on wave characteristics, especially on wave heights and periods.

However, the reflection effect gradually dominates the area further into the bay. For example, both experimental methods and model experiments showed that reflection was less important at site O2 which was closer to the entrance of the bay compared to other areas further into the bay, such as site O3. The findings could extend to all pocket beaches with different lengths of headlands and indentations. If a pocket beach has a small indentation, the bay is more exposed to direct incident waves, so refraction and shoaling prevail over other factors, but if the indentation is longer, reflection dominates the area.

The intensity of reflection on wave characteristics inside pocket beaches depends on the approaching wave directions. The reflection effect reduces when waves approach from an angle close to normal. As depicted in Figure 4.26, waves with angles of 344° or 15° to the shoreline have a minimum reflection effect compared to waves approaching at 67°. The results are similar to the findings discussed in section 4.3.1 (see Table 4.2 to 4.4). The intensity of reflection is also shown in Eq. 4.8 and 4.9, developed by Zanuttigh and

Andersen (2010). If waves approach perpendicular to the headland, the reflection coefficient is at its maximum.

More studies still need to be carried out to classify the intensity of reflection based on approaching wave directions. The current study showed that the effect of reflection on wave characteristics could vary depending on approaching wave directions. Further research needs to be done to collect more wave data approaching from longshore to normal. This range of wave directions could provide adequate information as an input to SWAN to simulate waves inside a pocket beach. The results could be used to classify the intensity of the reflection effect on wave characteristics based on approaching incident wave direction.

4.5. Conclusion

In this study, the importance of reflection in pocket beaches was discussed using the SWAN model and the experimental approach developed by Zanuttigh and Van der Meer (2008) and Zanuttigh and Andersen (2010). In this study, the experimental approach was first used to examine reflection for monochromic waves in a simplified model pocket beach. Then this approach was applied to Okains Bay using wave input data collected during Field Experiments 1 and 2. Finally, SWAN was used to simulate waves inside Okains Bay with and without consideration of reflection and diffraction.

The results of both experimental and numerical models were validated against observations. The comparison between the predictions and observations recorded throughout Field Experiments 1, 2 and 3 indicate that Zanuttigh and Van der Meer's (2008), and Zanuttigh and Andersen's (2010) approaches, and also SWAN can reasonably predict reflected waves inside Okains Bay. SWAN predictions were more precise as the model is designed to simulate waves with more realistic results.

Both models showed that reflection could play an important role in controlling wave characteristics in Okains Bay, an example pocket beach. The results stated that reflection could significantly affect wave characteristics, especially wave directions inside the bay. When the reflection effect was deactivated in SWAN, there was a considerable difference

between the predominant predicted wave directions and predominant observed wave directions around 30° to 45°. This indicates how significantly reflection could change wave directions inside the bay.

The intensity of reflection on wave characteristics inside Okains Bay depends on the indentation of the bay. The reflection gradually decreases in areas closer to the entrance of the bay; that is, areas with a smaller indentation are less affected by reflection. That is because this area is more exposed to direct incident waves, and refraction and shoaling could prevail over other factors in controlling wave characteristics. For instance, the results showed that reflection has less effect on waves observed at site O2, which is closer to the entrance of the bay, relative to waves collected at site O3 located further into the bay.

SWAN results indicated that diffraction was not as important as reflection in areas closer to the downcoast headland. When diffraction was deactivated in the SWAN model, wave estimations changed slightly compared to the predictions carried out when both reflection and diffraction were taken into account. However, diffraction had a greater influence on wave patterns in areas in proximity to the upcoast headland.

This chapter mainly focused on highlighting the effect of reflection on wave characteristics in Okains Bay. Chapter 5 evaluates the current system inside Okains Bay and also examines the importance of tides and local winds on controlling nearshore currents.

Part II: Nearshore current processes in pocket beaches

Chapter 5: Nearshore current observations in Okains Bay

This chapter first discusses existing knowledge of the nearshore current processes in open coast and embayed beaches. Then observations collected from different depths in Okains Bay are used to highlight the differences between the nearshore currents in pocket beaches and those in open coast and embayed beach settings. In this chapter, the effects of local winds and tides on nearshore currents were also discussed. This chapter contributes field-based findings towards addressing thesis aim 3 and also towards the 'currents' aspects of thesis aims 1 and 2.

5.1. Introduction

Nearshore currents, particularly in the surf zone, are one of the most commonly studied subjects in coastal engineering, since changes in shoreline profiles and morphological features are basically attributed to currents (Muir Wood and Fleming, 1981; Héquette *et al.*, 2013). In coastal areas, nearshore sediment transport is defined as the movement of sediment in the longshore or cross-shore directions under the nearshore currents generated by winds, tides, and especially incoming waves. Therefore, obtaining more information on nearshore currents in any type of coastal environment leads to a better understanding of the processes driving sediment transport in that area. This chapter explores nearshore currents in Okains Bay under different sea conditions using an array of oceanography instruments. This study also serves to explain the differences between nearshore currents in pocket beaches and open coast beaches.

5.1.1. Wave generated currents in the surf zone

Knowledge of nearshore current mechanisms leads to a better understanding of the mechanisms of sediment transport, since the turbulence of waves generally suspends sediment, allowing currents to then carry it in different directions (Soulsby, 1997). Therefore, in beaches exposed to waves, wave-driven currents play a key role in controlling sediment transport. When waves approach shorelines and break, they can generate three 'end member' types of current system inside the surf zone: longshore currents; cell circulation or rip currents; and bed return flow.

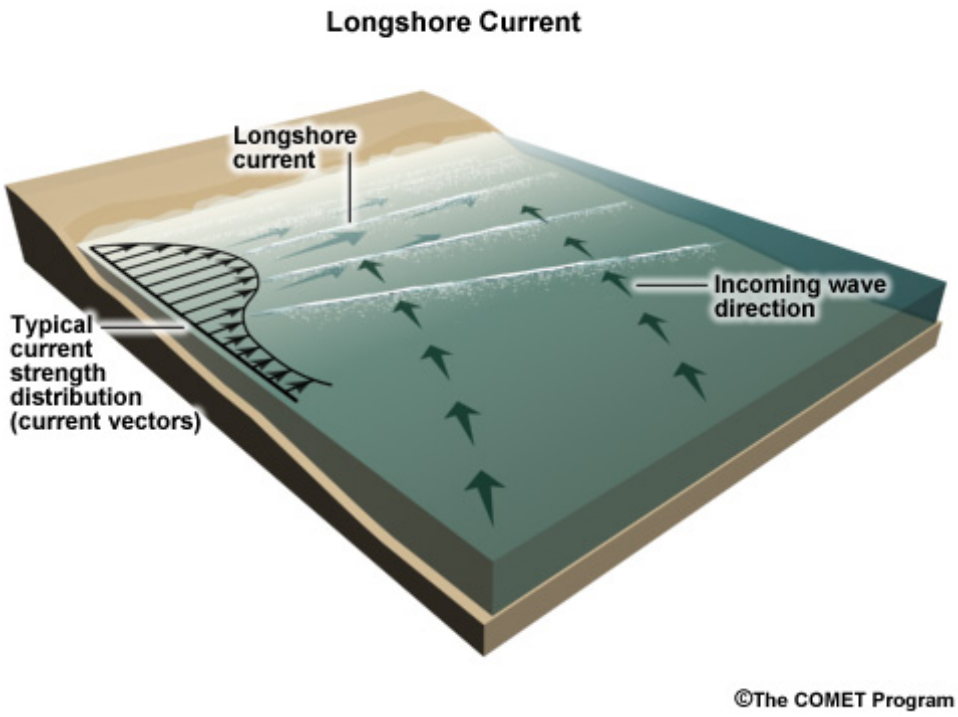

Figure 5.1. Longshore current structures (Comet Program, 2012).

Broken oblique-approach waves frequently induce longshore currents (Figure 5.1). Wave-induced longshore currents mostly occur in the nearshore and their velocity quickly declines outside the surf zone (Komar, 1998). This type of current system is a key driver of long-term beach erosion, so understanding of longshore currents is vital. The velocity of these currents (v_l) may be calculated when the bottom frictional force and onshore gradient of radiation stress are in equilibrium (Longuet-Higgins, 1970a, b), as follows:

$$v_l = \frac{5\pi}{8} \frac{\tan\beta}{c_f} u_m \sin\alpha_b \tag{5.1}$$

where c_f is the frictional coefficient, which, according to field measurements by Komar and Miller (1975), ranges from approximately 0.017 to 0.018, $\tan\beta$ is beach slope (°), α_b is wave angle at breaker point (°), and u_m is the maximum orbital velocity (ms^{-1}).

Although this model was used as the basic theory, it has a major weakness to predict the longshore currents in the actual surf zone. This model is based on regular monochromatic waves, while in reality waves are irregular and break at different points (multi breakpoints) (Short, 1999). Thornton and Guza (1989) developed Longuet-Higgins's (1970a, b) model under random waves to predict longshore currents, shown as:

$$v_l = \frac{3\pi}{8}\frac{B_0^{1/2} f_p^{1/2}}{c_f <\gamma>^4}\frac{\sin\alpha}{C}\frac{H_{rms}^6}{h^{9/2}} \tag{5.2}$$

where B_0 is the wave shape factor, f_p is peak wave frequency (hz), γ is the breaker index, C is wave celerity (ms^{-1}), α is wave angle, H_{rms} and h are the local root mean square wave height (m), and the local mean water depth (m). This model can successfully be applied to a plane-slope beach, but failed to predict longshore currents with an acceptable level of accuracy in barred beaches (Short, 1999). That is because the model only takes into account the local depth and wave height.

Komar (1998) also points out that another important factor in generating wave-induced longshore currents occurs when breaker wave heights change alongshore, so the elevation of wave set-up varies in this direction. In this case, a flow tends to move from areas of higher wave set-up to areas of lower wave set-up parallel to the shore. The resultant longshore current velocity is given by:

$$v_l = 1.7\sqrt{gH_b}\,\sin\alpha_b\,\cos\alpha_b - a\sqrt{gH_b}\,\frac{\partial H_b}{\partial y} \tag{5.3}$$

$$a = \frac{\pi\sqrt{2}}{C_f\gamma^{5/2}}\left(1+\frac{\gamma^2}{8}\right) \tag{5.4}$$

where H_b is breaker wave height (m), g is gravitational acceleration (ms^{-2}), and the term $\partial H_b / \partial y$ is the alongshore variation of the wave height (m). This formula calculates the maximum speed for wave-induced longshore currents, which occurs midway between the breaker line and shoreline.

In existing longshore current equations, including Eq. 5.1 to 5.3, it is assumed that longshore currents are generated by waves, while these currents could be generated or significantly affected by winds or tides (Nelson, 2009). However, these equations are not able to consider these effects on longshore currents. Therefore, these effects must be taken into account separately.

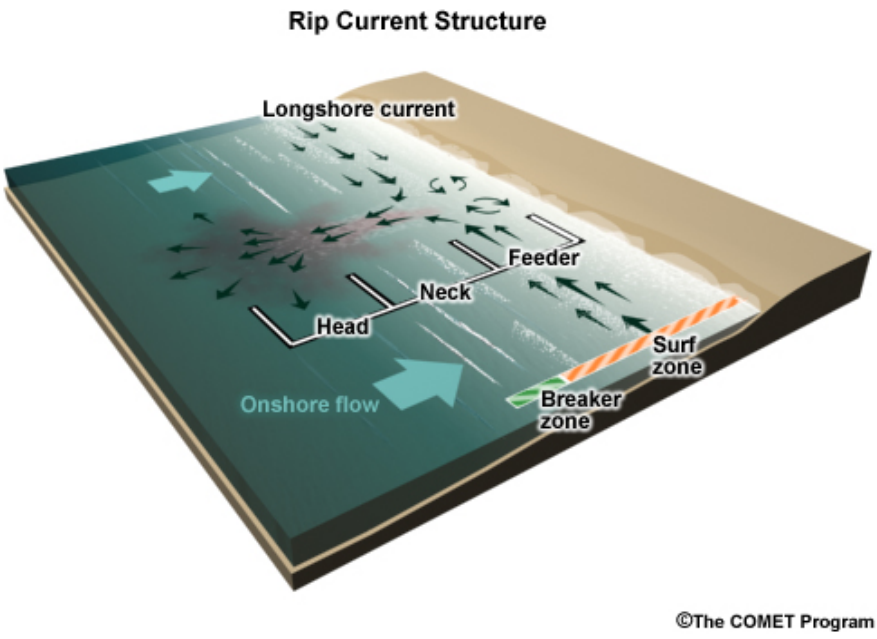

Figure 5.2. Rip current structure (Comet Program, 2010).

Rip currents or cell-circulation are another type of wave-induced nearshore current system, driven by relatively shore-normal waves (Komar, 1998; Short, 1999). This system appears when two longshore currents in opposite directions converge and generate an offshore moving current. These currents move in the offshore direction through the breaker zone. At the rip

heads, the seaward-moving currents spread out and feed into a shoreward return flow (Figure 5.2) (Shepard and Inman, 1950). Rip currents generally occur in intermediate sandy beaches, which are formed from medium sized sands (Nielson, 2009). The space between two rip currents normally extends approximately two to five times the distance between the shoreline and the breakpoint. This spacing tends to enlarge when wave heights increase and/or the beach profile flattens. In order to calculate the mean rip current velocity, V_{rip}, Aagaard *et al.* (1997) show that:

$$V_{rip} = \left(Q_{drift} + Q_{roller}\right)\left({}^{\lambda}/_{R_0}\right)$$

$$Q_{drift} = {}^{CBH^2}/_{h} \qquad (5.5)$$

$$Q_{roller} = {}^{A}/_{T}$$

where Q_{drift} and Q_{roller} are the rip current discharge and the wave roller mass transport respectively, λ is the distance between two rip channels (m), R_a is the cross sectional area of the rip current (m), C is wave celerity (ms^{-1}), B is a wave profile coefficient (l/12 for saw-tooth bores), H is wave height (m), $A = 0.9H^2$ is the area of the surface roller (m^2) (Fredsøe and Deigaard, 1992), T is wave period (s).

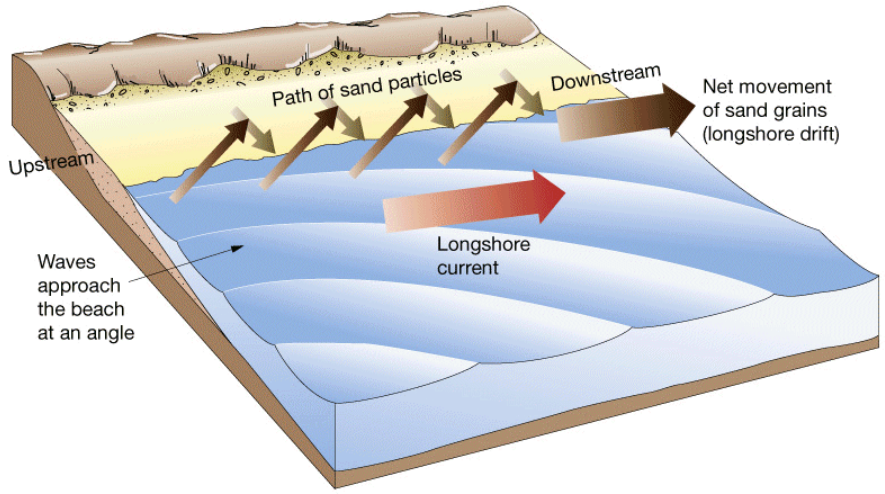

Figure 5.3. Longshore sediment transport concept (Pearson Prentice Hall, 2005).

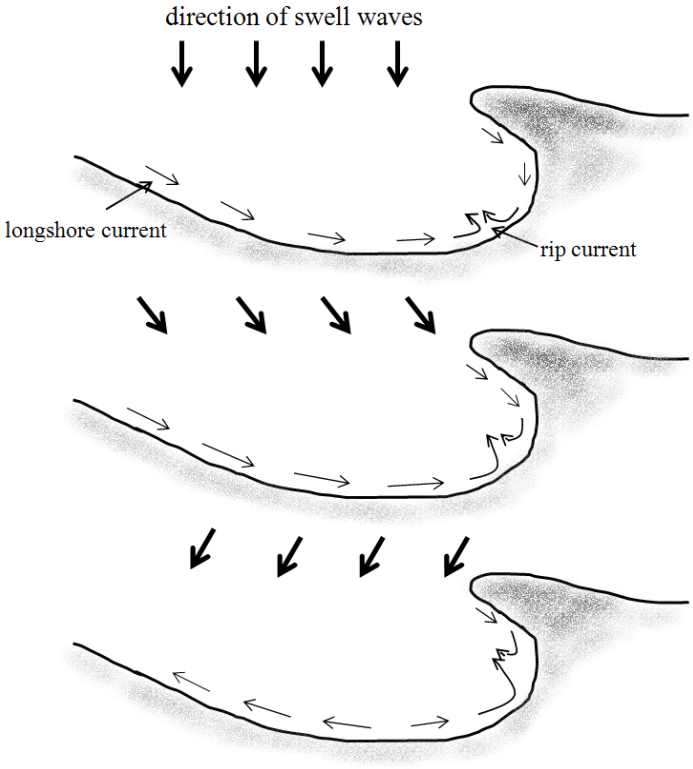

Figure 5.4. Structure of nearshore currents in embayed beaches under different approaching wave directions (Silvester and Hsu, 1999).

5.1.2. Nearshore currents in embayed and pocket beaches

The nearshore current processes in embayed and pocket beaches differ from those in open coast beaches due to the existence of headland(s). Klein *et al.* (2002) studied short-term beach rotation processes in embayments. They pointed out that nearshore currents, especially longshore currents, are attributable to the orientation of headlands and angle of approaching waves. They also stated that rip currents formed in proximity to the headland play an important role in morphological changes. Loureiro *et al.* (2012) studied the influence of megarips on erosion in high-energy beaches enclosed by two headlands. The results demonstrated that megarips had an important influence on the profile erosion in the bays.

They also showed that normal waves generated a single megarip in the center of the bay, whereas oblique waves drove two megarips in proximity of the headlands.

Silvester and Hsu (1999) also studied current processes in embayed beaches with different approaching wave directions (Figure 5.4). The upcoast headland plays an important role in controlling currents and in generating rip currents. Diffraction from the headland causes the longshore current to be generated around the headland. This current moves in the opposite direction to normal wave-generated longshore currents, with the opposing longshore currents converging, and generates an offshore current or rip currents. The location of the rip current depends on the approaching swell waves (Figure 5.4).

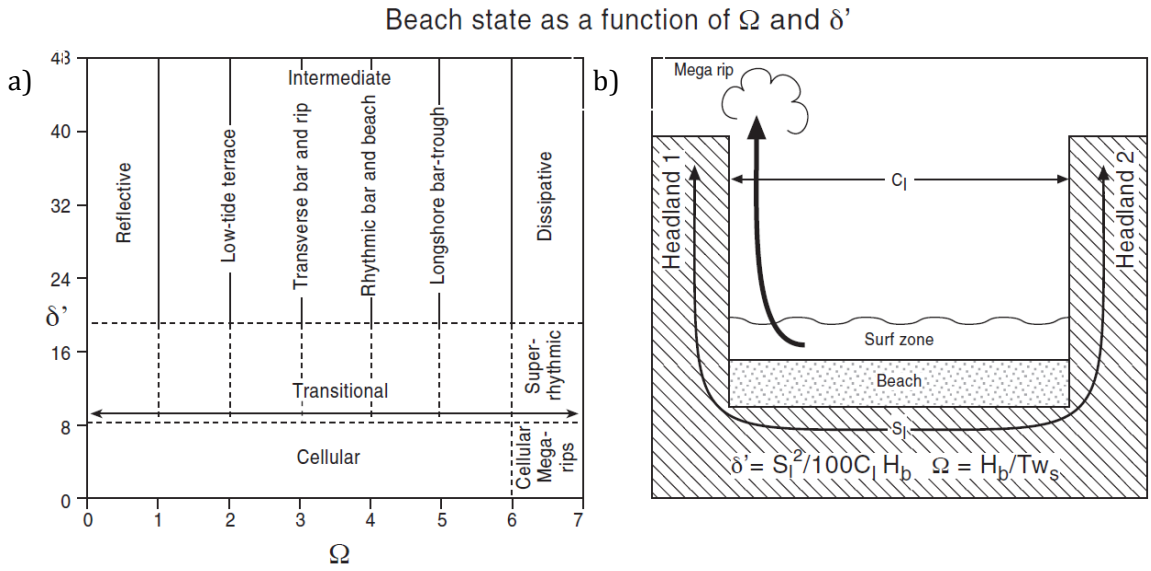

Figure 5.5. The dimensionless fall velocity plotted against the dimensionless embayment scaling parameter (a), definition sketch of the dimensionless embayment scaling parameter for a beach with 0.01 beach slope (b) (Short, 1999 p. 236). Note that S_l is the length of the shoreline of an embayment, which extends from the end of the surf zone at the upcoast headland side to the end of the surf zone at the downcoast headland side of the bay.

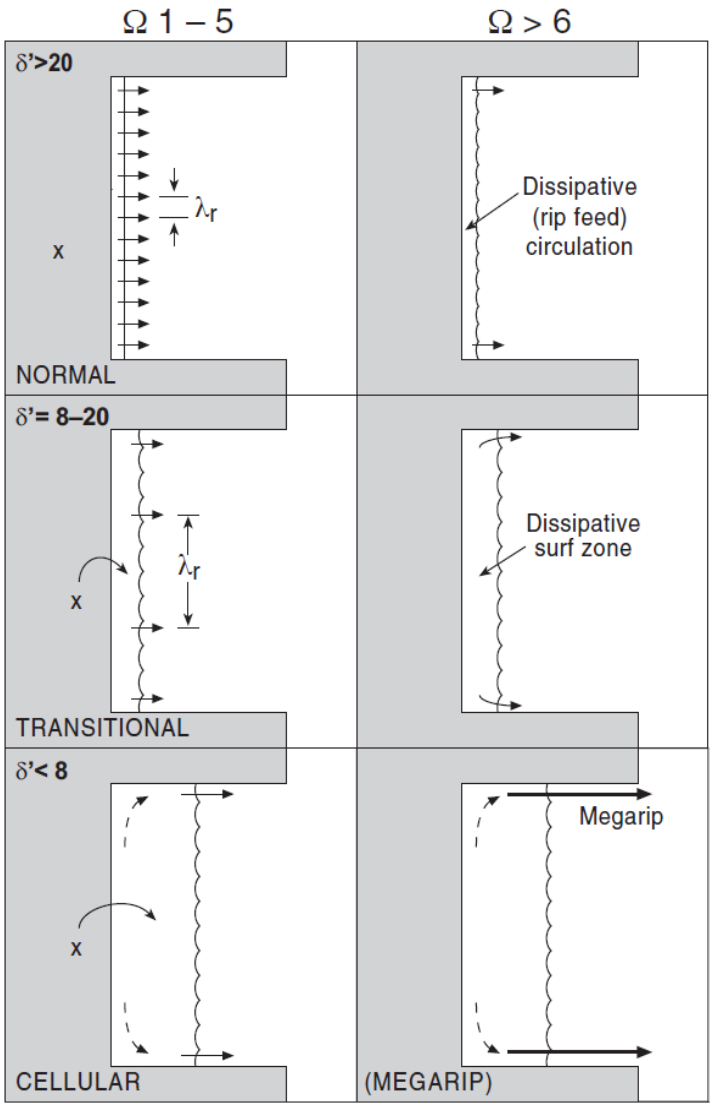

Figure 5.6. Surf zone circulation system classification scheme according to the dimensionless fall velocity and the dimensionless embayment scaling parameter (Short, 1999 p. 237).

Short (1999 and 2010) studied current systems in embayed and pocket beaches, and showed how bay characteristics can influence and change the nearshore currents. According to current circulations, Short (1999) divided beaches into open coast beaches and embayments. In order to define the type of headland-enclosed bay beaches, the dimensionless embayment scaling parameter is used (δ') (Figure 5.5) (Short 1999, 2010):

$$\delta' = \frac{S_1^2}{C_1 H_b} \tan \beta \tag{5.6}$$

where S_1 is the length of the shoreline of an embayment (m), which extends from the end of the surf zone at the upcoast headland side to the end of the surf zone at the downcoast headland side of the bay, C_1 is the distance between headlands at the entrance as in Figure 5.5b (m), H_b is the breaking wave height (m), and β is the beach slope (degree). If $\delta' > 20$, the area has normal beach circulation and the headlands do not affect the current system; if $8 < \delta' \leq 19$, the area has transitional circulation and the currents are influenced by the shape and size of the embayment; and if $\delta' \leq 8$, the area has cellular circulation and the shape and size of the embayment significantly affect the currents. The later circulation scenario could represent the case of current system in pocket beaches (Prof A. Short, University of Sydney, Coastal Scientists, pres. comm. 28/07/2010).

The dimensionless fall velocity (Ω) is also used to describe the state of the beach as reflective or dissipative, and to precisely define the surf zone circulation system (Figure 5.5a and 5.6), given as:

$$\Omega = \frac{H_b}{T w_S} \tag{5.7}$$

where w_s is sediment fall velocity (ms^{-1}), T is the wave period (s). In this equation, breaking wave height and period, and sediment size are the key components to define the state of a beach regardless of its type, such as open coast or headland-enclosed bay beaches (Figure 5.5.a). It can, therefore, be inferred that two-headland bay beaches, including pocket beaches, may be classified as having either dissipative or reflective beach profiles without consideration of the length of the headlands or of the shoreline.

Eq. 5.6 is based on the deep water wave energy distribution along the shoreline in embayments. As depicted in Figure 5.5b, this equation shows that the space between two headlands, beach slope, width of the surf zone and breaking wave height are the key components to influence the current system in such environments. In this equation, S_1 is the sum of the shoreline length and the length of each headland from the shoreline to the end of the surf zone, not to the end of headlands (Prof A. Short, University of Sydney, Coastal Scientists, pres. comm. 28/07/2010); that is, the effect of the length of headlands on the

current system was not taken into account. This equation also indicates that the direction of approaching waves does not affect the current system in two headland bay beaches. This raises the question of whether or not there is any relationship between the lengths of the headlands and current circulation type.

Moreover, since in this equation, other factors such as breaking wave height, beach slope and the distance between two headlands, are taken into account, there might be two different headland-bay beaches with the same type of current circulation system, but completely different headland lengths. As discussed in Part I, the length of the upcoast headland is important in filtering approaching waves in Okains Bay. This filtering could potentially cause a different current system inside the bay compared to a pocket beach with a shorter upcoast headland and thus greater exposure to incident waves. If it is demonstrated that the width of the surf zone varies according to the length of headlands, then Eq. 5.6 could also be used to topographically classify the beach planform type into headland-enclosed bay beaches, embayed and pocket beaches.

5.1.3. The effect of winds and tides on nearshore currents in open coast beaches

Wind effects

Many studies (Gallop *et al.*, 2011; Port *et al.*, 2010; Curtiss *et al.*, 2009; Whitford and Thornton, 1993; Sonu, 1972; Shepard and Inman, 1950a) have shown that waves are not the only factor in shaping nearshore currents, especially longshore currents. Huberts (1986) measured the effect of wind on longshore currents at Duck, North Carolina. He showed that under conditions with high winds in the nearshore area blowing in the same direction as the wave-induced current, the longshore current velocities were two to three times larger than current velocities measured under low wind speed conditions. Similar effects of wind on alongshore currents were observed by Curtiss *et al.* (2009), Grunnet *et al*. (2005), and Masselink and Pattiaratchi (1998). The results also indicated that the opposing wind could slow nearshore longshore current velocities.

An offshore-blowing wind (offshore wind) is also a factor in controlling offshore-directed surface currents: it tends to reinforce seaward flowing surface currents, such as rip currents, enabling them to move further seaward beyond the breaker zone (Dalrymple *et al.*, 2011;

Scott *et al.,* 2009; King, 1972). During storms, onshore-blowing winds (onshore winds) influence onshore-flowing surface currents and can increase water level set-up (Hequette and Hill, 1993). During steady state conditions, the onshore mass transport of surface water is offset by downwelling near the shoreline and offshore bed return flow. Thus, an increase in the velocity of an onshore wind can result in an increase in the bed return flow. It can, therefore, be inferred that the velocities of these types of currents could be correlated to wind conditions. This correlation is interpreted by adding a surface wind stress component to the momentum equation in the longshore direction and by integrating it throughout the surf zone (Whitford and Thornton, 1993).

Beneath the ocean surface, wind tends to influence nearshore currents, especially in those beaches where local wind-generated waves prevail. Strong onshore wind stress results in sea surface set-up, thereby increasing hydrostatic pressure gradients and causing an offshore-directed near bottom current or undertow (Hequette and Hill, 1993). However, if the wind blows in an offshore direction, the near-bottom current can change to flow onshore (Komar, 1999). Onshore and offshore winds could noticeably influence the nearshore currents in pocket beaches, even for moderate winds, when incident waves approach at a direction greater than a pocket beach direct wave approach sector; that is, waves may lose energy after diffraction and reflection, making wind induced currents relatively more important inside the bay.

Tide effects

In addition to incident waves and local winds, tides also tend to influence onshore and offshore directed flows in coastal areas (Guan *et al.*, 2009; Pond and Pickard, 1983) and can generate currents in both deep and shallow waters (Soulsby, 1997). Similar to winds, tides can directly and indirectly affect wave-generated nearshore currents (Short, 1999). Further, temporary changes in the position of the surf, swash and shoaling zones over a tidal cycle, significantly affect the hydrodynamics and morphodynamics of the beaches (Masselink and Short, 1993; Short, 1999). An early study by Shepard *et al.* (1941) based on daily tidal ranges, found no obvious correlation between spring/neap tides and rip currents. They, however, pointed out that the instantaneous level of these tides might affect rip currents. For instance, at low tide, when the water depth is shallow, rip current velocities are stronger.

Low tidal levels also frequently change either the position of rip currents or their orientation across the surf zone (Mackenzie, 1958). The rip currents sometimes return to their previous positions during high tidal levels. When sea levels falls over tidal cycles, rip currents will be reinforced and may reach their maximum velocities (Mackenzie, 1958; Brander and MacMahan, 2001; MacMahan *et al.*, 2006). This decrease in sea level could result in the development of rip currents on some beaches, while on other beaches rip currents could be formed at high tidal levels (Cook, 1970).

Tides also influence bed return flow (seaward) and longshore currents. Russell *et al.* (1991) monitored suspended sediment transport in a macro-tidal beach during a storm and found that bed return flow velocities increased during the ebb tides. This effect was also observed by Dean (1973), Goodwin (1996), and Ranasinghe and Pattiaratchi (2003).

Given their effects on nearshore currents, tides tend to influence sediment transport mechanisms in beaches, especially in macro-tidal beaches. However, this effect might be masked when the energy released by waves is significant (King, 1972). In order to determine whether a beach is dominated by tides or not, Masselink and Short (1993) introduced the dimensionless relative tide range parameter (*RTR*):

$$RTR = TR / H_b \tag{5.8}$$

where TR is tidal range (m). If the value of RTR is greater than 15, tides dominate the area. If RTR is less than 3, waves are the dominant factor. The RTR may be applicable to pocket beaches, but no studies have so far examined the application of this equation to such environments and whether or not it needs any modification in such beaches, due to significant wave climate restrictions. Pocket beaches are more likely to be tidal dominated, compared to open coast beaches, since headlands reduce $H_{b,}$ after waves are diffracted and reflected from the headlands. It is also possible that *TR* increases in long bays due to the geometry of the bay. More research needs to be carried out in order to investigate this idea further.

5.1.4. The effect of tides on nearshore currents in embayments

Wind effects

Notwithstanding the similarity of the actual mechanisms of generating wind-driven currents in embayments and open beaches, local winds can play a crucial role in the hydrodynamics and morphodynamics of embayed and pocket beaches. Cooper *et al*. (2004) studied the effect of storms on embayed beaches dominating by high energy waves. The results showed that winds, especially their directions, have an important influence on morphological changes in embayedments.

Local winds can drive strong nearshore currents in areas not exposed to incident waves (Dehouck *et al.,* 2009). In some cases, local winds may even generate stronger mean current velocities than waves in embayed or pocket beaches (Dehouck *et al.*, 2009; Sedrati and Anthony, 2007; Storlazzi and Field, 2000; Hegge, 1996). For instance, Dehouck *et al.* (2009) found that winds generate mean cross-shore and longshore current velocities twice those of high energetic swell waves in embayed beaches. They also suggested that, since waves approaching shorelines in a shore-normal direction drive relatively weak longshore currents, the wind blowing parallel to the shore significantly enhances the longshore currents. However, this cannot be the case in pocket beaches, enclosed by high rocky headlands. In such environments, longshore winds either rarely pass over the headlands and enter the bay, or their direction turns to onshore/offshore in order to enter the bay. These changes in local wind directions will be discussed later in this chapter.

Wind can also affect currents close to the bed in embayed beaches. Storlazzi and Griggs (2000), when considering the effect of El Nino-Southern Oscillation events, stated that onshore winds tend to drive strong bottom currents in a seaward direction in embayed beaches. It can, therefore, be generally inferred that onshore near-surface transported water is balanced by offshore near bottom flow in such environments (Storlazzi and Jaffe, 2002); that is, an increase in onshore water movement caused by wind results in an increase in bed return flow. However, the importance of winds in pocket beaches is poorly documented and more studies need to be carried out in order to better understand the effect of wind in nearshore currents and sediment transport mechanisms in pocket beaches.

Tidal effects

Tidal currents might appear to influence nearshore currents in embayments. Small variations in water level, such as micro tides, could potentially move the position of the surf zone a few hundred meters seaward in gently sloping environments. Few studies have been conducted on the effect of tidal currents on nearshore wave-induced currents in embayed and pocket beaches, especially in micro-tidal beaches (Klein *et al.*, 2001; Vousdoukas *et al.*, 2009). Researchers have focused more on macro-tidal embayments (Dehouck *et al.*, 2009). The general findings including the effect of tides on longshore and cross-shore currents are similar to the findings in meso- and macro-tidal open coast beaches, as outlined in Section 5.1.3.2 (Dehouck *et al.*, 2009; Anthony *et al.*, 2004; Wright *et al.*, 1982). Although most studies conducted on the morphodynamics and hydrodynamics of embayed and pocket beaches have addressed the importance of tidal currents on nearshore currents (Dehouck *et al.*, 2009; Masselink and Pattiaratchi 2000; Storlazzi and Griggs; Storlazzi and Jaffe, 2002; Hegge *et al.*, 1996), the effect of tidal currents on nearshore currents and sediment transport processes are still poorly documented, especially in micro-tidal pocket beaches. Therefore, studies on both reflective and dissipative micro-tidal pocket beaches are needed to examine the importance of tides on nearshore current processes in such environments.

5.2. Methodology

The approach used in this chapter fits within the 'field experiment', 'currents' boxes on the left-hand side of the thesis methodology diagram illustrated in Figure 1.6.

5.2.1. Study site

Similar to the wave observation approach, Okains Bay was selected as an example pocket beach in order to study the nearshore current system. As discussed in chapter 2, this bay contains a shoreline of about 750 m, embayed between approximately 2 km of natural rocky headlands. The shoreline is oriented at 35° to true north so the bay is relatively exposed to high-energy swell waves from the Pacific Ocean to the east. However, the headlands function to limit the waves that approach and enter directly into the bay. Okains Bay is classified as a dissipative beach with a foreshore gradient of 1:60 and a backshore gradient of 1:90

(Dingwall, 1974). The wave climates outside Okians Bay was discussed earlier in section 2.2.1.

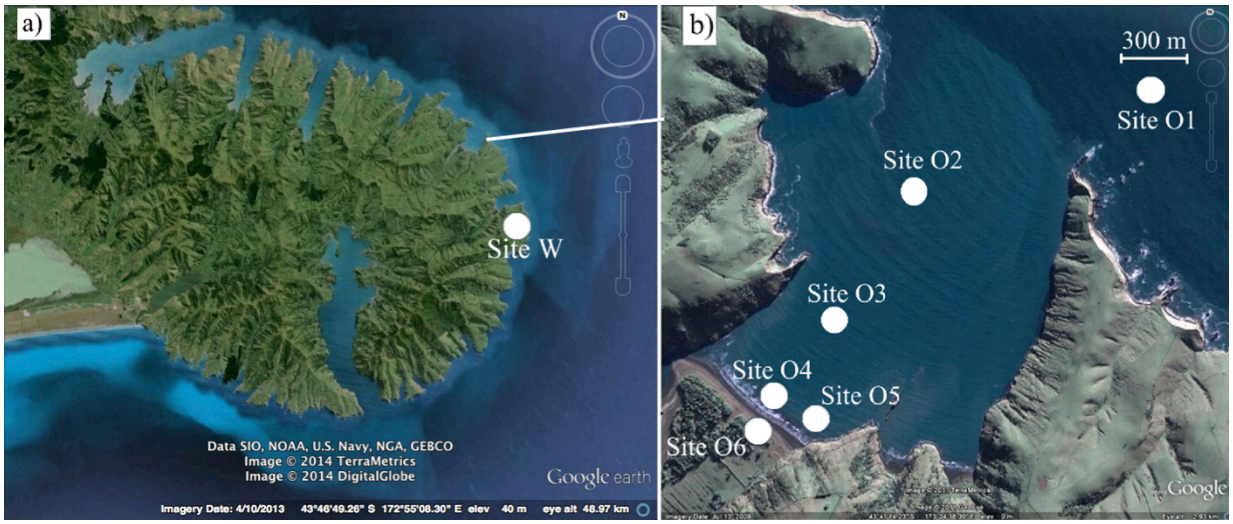

Figure 5.7. NIWA wind station deployed at -43.746S 173.119E, shown as site 'W' in Banks Peninsula, New Zealand (a) and field instruments deployment sites in Okains Bay (b), located on Banks Peninsula (modified from Google Earth, 2012).

Information on local winds in Okains Bay is inadequate, but the data are available for larger scale synoptic patterns (Banks Peninsula). Banks Peninsula has prevailing northeast and southwest, followed by winds coming from the northwest, while easterly and southerly winds also blow in this area (Dingwall, 1974; NIWA, 2012). Note that winds in this area are predominantly from the northeast and southwest during summer (URS 2001). Due to orographic effects in the vicinity of Banks Peninsula, the valleys act as channels and wind direction changes accordingly. Therefore, winds mostly blow in offshore or onshore directions on beaches in Banks Peninsula, including Okains Bay (Dingwall, 1974). Additionally, orographic effects cause the wind speed to increase at the beaches (Dingwall, 1974).

Studies in Banks Peninsula showed that tides drive the strongest currents off the peninsula (Dingwall, 1974; Reynolds-Fleming and Fleming, 2005). The flood streams appear to move

to the north, while the ebb streams set to the south (Dingwall, 1974). However, the direction of tidal currents frequently changes according to the sea and weather conditions.

A strong oceanic current moving towards the north also influences the area outside Okains Bay. This current, called the Southland Current, originates from the subtropical convergence zone west of New Zealand (Chiswell, 1996; Reynolds-Fleming and Fleming, 2005). The pathway of this current is along the continental shelf through Foveaux Strait and around the south-tip of New Zealand. It then flows along the east side of the South Island's continental shelf break and finally reaches Bank Peninsula. However, this understanding is large scale so that we can infer little about the influence of the Southland Current off Okains Bay.

5.2.2. Methods

This study employs field experiments to better understand the nearshore current circulations in Okains Bay during different sea and weather conditions. Similar to the wave observations discussed in chapter 2, three individual field measurements were carried out to collect current data, local wind data and tidal currents.

Field Experiment 1 was accomplished between 20th April and 11th May, 2011 in two locations: inside Okains Bay at site O3 in high tide water depth of almost 6 m, and off Okains Bay at site O1 in high tide water depth of 12 m. During the field experiment, two units of Acoustic Doppler Current Profiler (ADCP) were deployed at sites O1 and O3. An upward-facing 600 kHz ADCP at site O1 was used to collect tidal ranges and also currents from 1 m above the bed for every 1 m water column to the surface. A downward-facing 1200 kHz ADCP was also deployed at site O3 to collect tidal ranges and also currents from approximately 2 m below the water surface for every 0.5 m of water column to about 10 cm above the bed. This study focuses on determining the current system close to the bed in order to better understand the sediment transport pathway in Okains Bay, as example pocket beach. Therefore, a downward-facing ADCP was deployed inside Okains Bay. The configuration of each instrument is shown in Table 5.1.

Table 5.1. Information on instrument deployments for all three field experiments.

Field Experiment	Instrument name	Instrument frequency (kHz)	Deployment period	Water depth (below surface) (m)	Sampling rate	Site
1	ADCP	600	20/April/2011 to 11/May/2011	12	every 1 min	O1
	ADCP	1200	20/April/2011 to 11/May/2011	5	every 1 min	O3
2	Inter Ocean S4	-	19/December/2011 to 22/December/2011	8	2 Hz	O2
	ADV	-	19/December/2011 to 21/December/2011	2.8	6 Hz	O4
	ADV	-	21/December/2011 to 22/December/2011	2.8	6 Hz	O5
	Weather Station	-	21/December/2011 to 22/December/2011	-1	every 10 min	O6
3	ADCP	1200	3/April/2011 to 13/April/2011	12	every 1 min	O3
	ADV	-	3/April/2011 to 4/April/2011	2.8	6 Hz	O5
	ADV	-	6/April/2011 to 8/April/2011	2.8	6 Hz	O5
	Weather Station	-	6/April/2011 to 8/April/2011	-1	Every 10 min	O6

Field Experiment 2 was conducted from 19th Dec to 22nd Dec 2011. An InterOcean S4ADW current meter was deployed at site O2 in high tide water depth of 8 m. The S4 was used to measure currents and tidal ranges approximately 1 m above the bed (Table 2.2). In shallower areas inside the surf zone, an Acoustic Doppler Velocimeter (ADV) was also deployed in high tide water depth of about 2.5 m at two sites: O4 and O5. The ADV was deployed for 35 hours at site O4 and then it was shifted to site O5 for 18 hours. The ADV was used to collect tidal ranges and currents around 10 cm above the bed. Throughout the measurements, a HOBO H21 weather station was also deployed on the beach at site O6 to collect wind speed and direction inside Okains Bay (Figure 5.7b). The S4, ADV and wind station configurations are shown in (Table 5.1). In order to compare the wind data collected in Okains Bay with larger scale synoptic patterns, wind data collected by NIWA at -43.746S 173.119E was used (Figure 5.7a), which was the nearest site to the bay.

Field Experiment 3 was carried out between 3rd and 13th April 2012. A 1200 kHz upside-facing ADCP was deployed at site O3 throughout the period of the measurements. The upward-facing ADCP collected tidal ranges and also currents from 1 m above the bed for every 0.5 m water column to the surface. The ADV was also deployed at O5 for 2 days and 16 hours to collect tidal currents and currents around 10 cm above the bed. As in Field Experiment 2, the weather station was deployed on the beach at site O6 to collect wind speed and direction inside the bay (Figure 5.7b). The ADCP, ADV and wind station configurations are shown in (Table 5.1). The wind data collected in Okains bay were compared to wind data collected at the top of a hill [-43.746S 173.119E] (Figure 5.7a), collected by NIWA, representing a larger scale synoptic pattern of wind in Banks Peninsula.

Throughout all the field experiments, observed current data were collected at sampling rates ranging from 6 Hz to 1 sample every min (Tables 5.1 to 5.3). In order to simplify the comparison of currents collected with different sampling rates, all the data were averaged to every 10 min. Note that it is common to collect or average wind and current data with an interval of 10 to 20 min in coastal studies for the purpose of time series analysis (Austin and Masselink, 2006; Allard *et al.*, 2008; Austin *et al.*, 2010).

In this study, two approaches were used to examine the effect of local winds and tidal currents on nearshore currents inside and outside Okains Bay. The Utide Matlab Function approach (Matte *et al.*, 2013; Codiga, 2011) was first used to remove the tidal currents from the observed currents. In order to increase the accuracy of confidence interval estimates in tidal

analysis, it is important to remove sub-tidal (i.e. non-tidal, low frequency) signals from the raw data (Dr D. Codiga, University of Rhode Island Bay, Marine Research Scientist, pres. comm. 22/01/2012). Therefore, a low-pass filter with a cutoff of frequency of 3 hours was applied to all data using WaveLet, a toolbox in Matlab. Afterwards, the Utide Matlab Functions were applied to separate the tidal components in both longshore and cross-shore directions from the observed currents inside and outside Okains Bay.

Linear regression analysis using the SPSS was also applied to examine the effect of local winds on nearshore currents inside Okains Bay. When the tidal currents were removed from the observed currents, the filtered currents showed only the influence of incident waves and local winds. In this study, the local winds and the currents were first plotted in a time series to examine the records for a correlation between the current speed and the wind speed at some lag (Dr E. Moltchanova, University of Canterbury, Statistician, pres. comm. 15/01/2014). The x (cross-shore) and y (longshore) components were also plotted separately to examine whether there was a better correlation between these decomposed sea and wind flows rather than the total current and wind vectors.

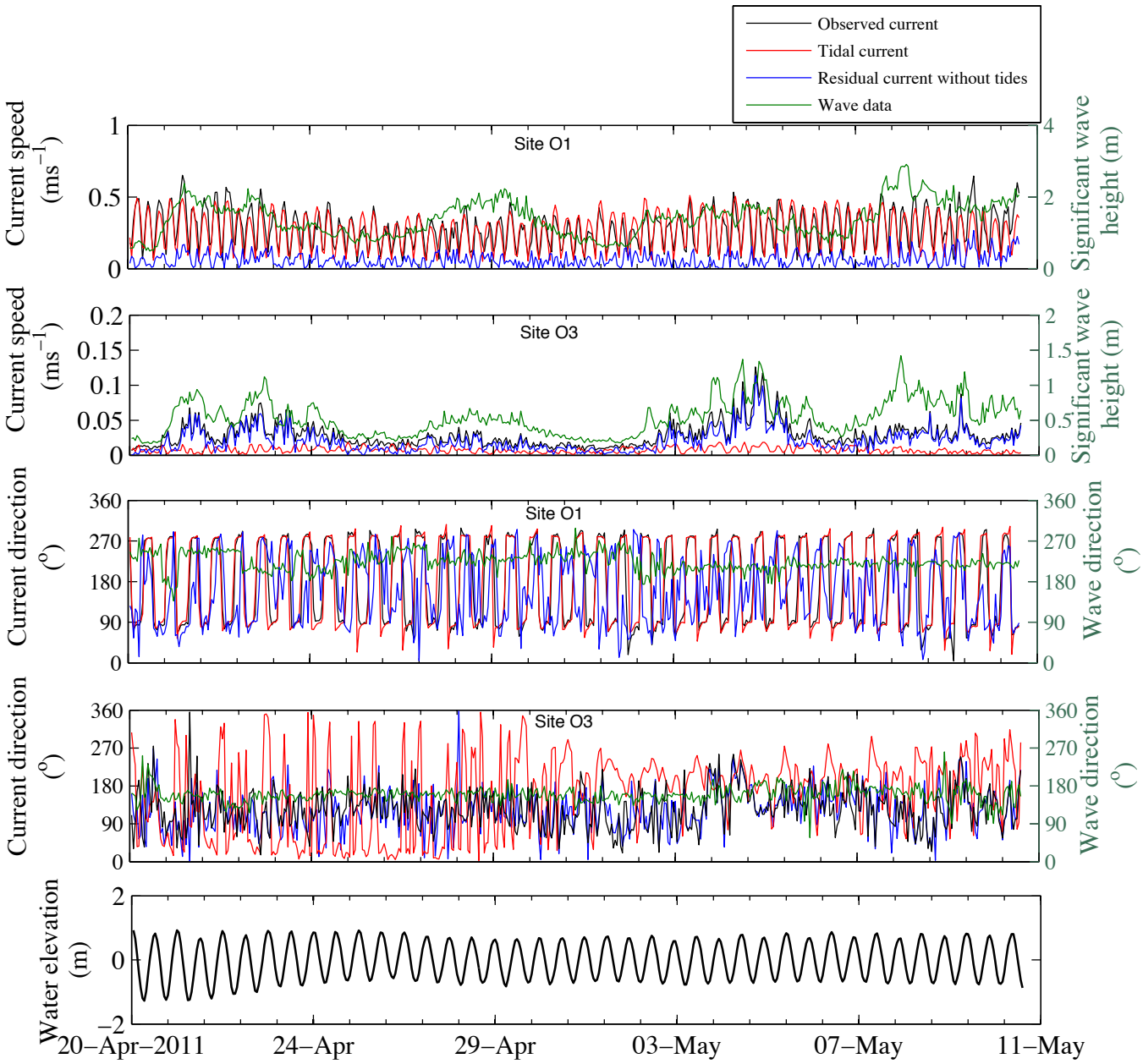

Figure 5.8. Comparison of wave and different types of currents observed during Field Experiment 1 at sites O1 and O3. Note that the current and wave directions are shown 'to' and relative to the Okains Bay beach orientation. Water elevation is relative to the water depth below the water surface collected at site O1.

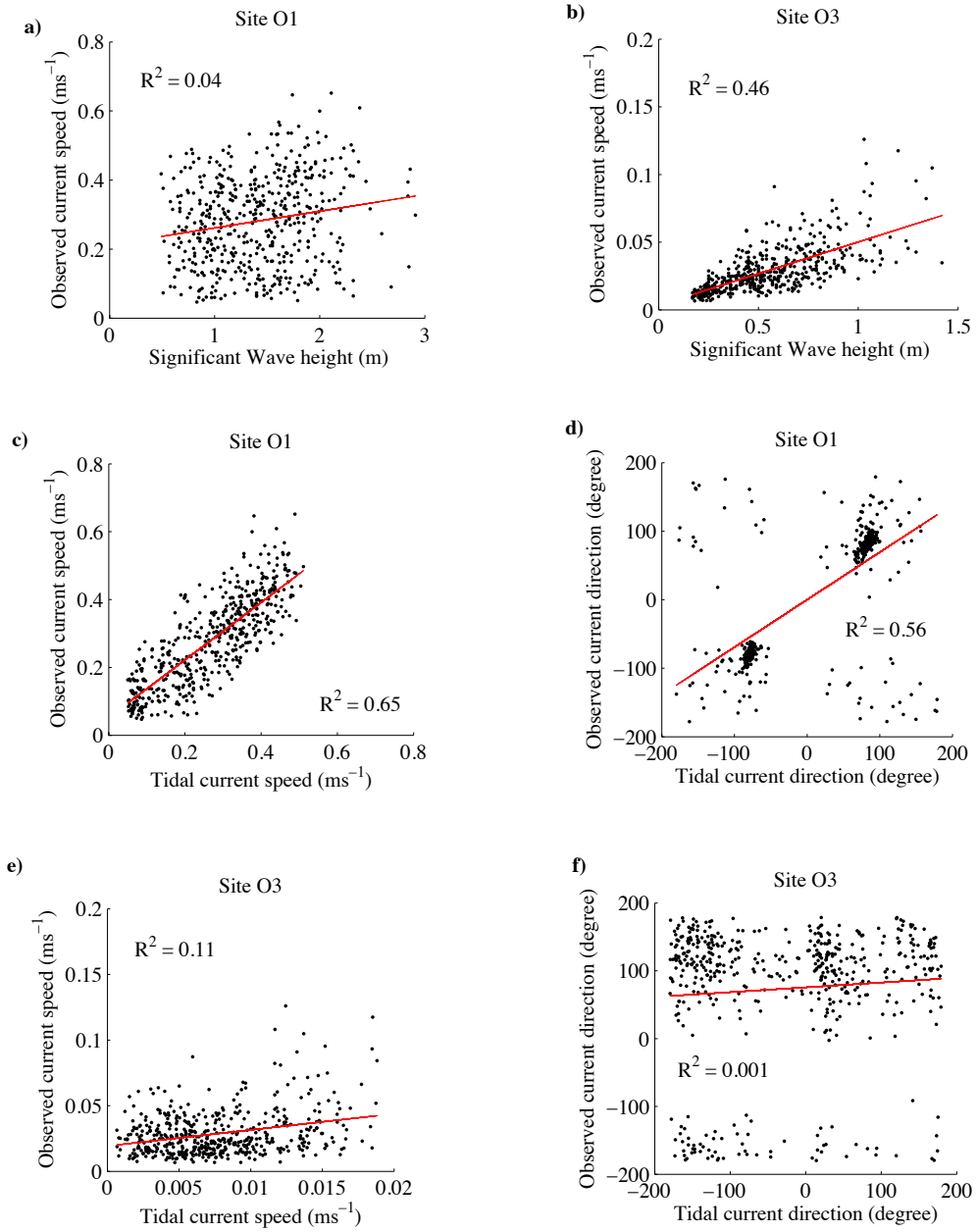

Figure 5.9. Scatter plots shown the correlation between wave height and observed currents (a and b), and also between observed currents and tidal currents (c to f) collected during Field Experiment 1 at sites O1 and O3.

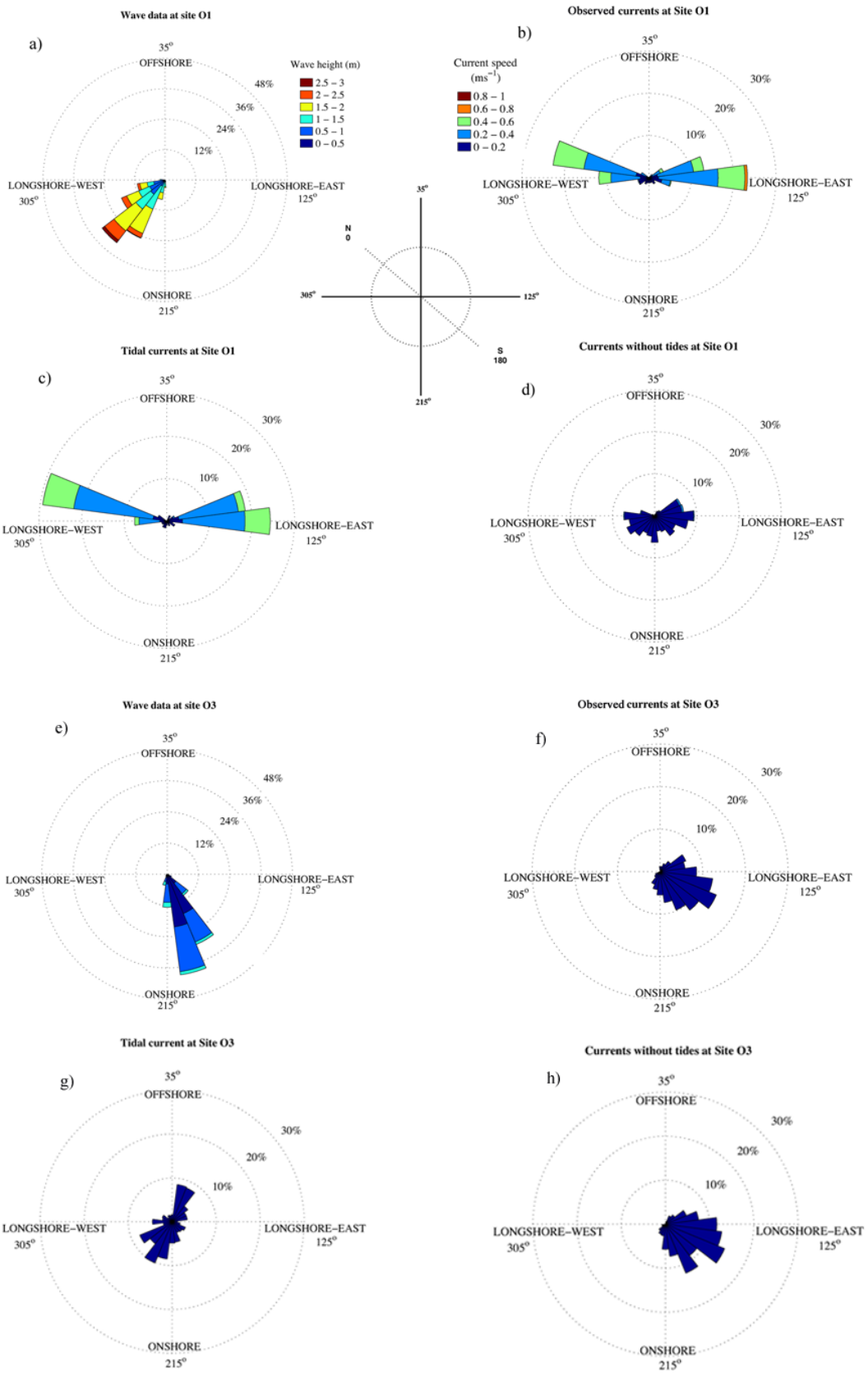

Figure 5.10. Rose plot showing wave data, observed and tidal currents collected during Field Experiment 1 at sites O1 and O3. Note that current and wave directions are shown 'to' and relative to the Okains Bay beach orientation.

5.3 Results of nearshore current observations in Okains Bay

In this section, the current and wind data obtained from an array of instruments at sites O1, O2, O3, O4, O5 and O6 at Okains Bay during three individual experiments between 20th April 2011 and 4th April 2012 are discussed. This study helps to improve our understanding of current circulation in Okains Bay and, subsequently, in pocket beaches during different sea conditions. The results also serve to examine the influence of tidal currents and local winds on nearshore currents in different depths inside and outside Okains Bay.

5.3.1. Field Experiment 1

During this field experiment the speed of currents close to the bottom recorded at site O1 showed the presence of strong currents off Okains Bay. The observed current speed at this site varied between about 0.05 ms^{-1} and 0.65 ms^{-1} with an average of 0.28 ms^{-1} (Figure 5.8).

Waves collected off Okains Bay at site O1 had a minor effect on observed currents recorded at the same site (Figure 5.8). The results of linear regression analysis indicated that the observed currents were poorly correlated to significant wave height at site O1 with R^2 of 0.04 (Table 5.2 and Figure 5.9a). A time series plot of observed wave and current directions also indicated that there was no correlation between these two components (Figure 5.8). The predominant wave direction approached from 225° to the shoreline (Figure 5.10a), while currents predominantly moved to 90° and 285° to the shoreline (Figure 5.10b). As expected, recorded waves at site O1 with a maximum significant wave height of 2.9 m were unlikely to be a strong influence on currents at about 11 m below the water surface. This result indicates that currents near the bed at this site are largely influenced by other factors, such as tides.

The tidal analysis using the Utide Matlab Function (Codiga, 2011) showed a strong effect of tides on currents near the bed off Okains Bay (Figure 5.8). The scatter plot analysis indicated that the observed currents were reasonably correlated to tidal currents at site O1 (Table 5.2 and Figure 5.9c and d). Time series analysis also indicated that the predominant tidal current directions moved to 90° and 285° to the shoreline (Figure 5.10c). These directions were similar to the predominant current directions at the same site (Figure 5.10b), but with different frequencies. The results demonstrate the influence of the Southland Current (the strong tidal

currents off Banks Peninsula, studied by Dingwall (1974) and Reynolds-Fleming and Fleming (2005)) on currents off the bay.

After removing the tides from observed currents, the residual currents were relatively slow. The current speed varied between 0.0002 ms^{-1} and 0.26 ms^{-1} with an average of 0.062 ms^{-1} (Figure 5.8). The predominant current direction moved to 90°, 105°, 155°, 180° and 270° to the shoreline (Figure 5.10d).

Table 5.2. Comparison of correlation coefficient (R^2) and P-value for observed wave height, observed currents and tidal currents at sites O1 and O3 during Field Experiment 1.

Site	Component 1	Component 2	R^2	P-value
O1	Observed current speed	Significant wave height	0.04	0.51
	Observed current speed	Tidal current speed	0.65	0.041
	Observed current direction	Tidal current direction	0.56	0.051
O3	Observed current speed	Significant wave height	0.46	0.048
	Observed current speed	Tidal current speed	0.11	0.21
	Observed current direction	Tidal current direction	0.001	0.66

Observations of currents inside Okains Bay showed that the current system was different from that off Okains Bay, which was mainly influenced by tidal currents. The observations indicated relatively weak currents close to bed at site O3. The current speed at this site varied between 0.007 ms^{-1} and 0.13 ms^{-1} with an average of 0.06 ms^{-1} (Figure 5.8).

Current speed inside Okains Bay at site O3 was mainly influenced by incident waves. The time series analysis showed that 71% of the time, when there was an increase in the

significant wave height at site O3, current speed was also reinforced accordingly (Figure 5.8). This effect is more obvious at the peak of significant wave height. However, 58% of the time a reduction in the significant wave height resulted in a current speed decrease (Figure 5.8). A linear regression analysis also indicated that the observed currents were moderately correlated to significant wave height at site O3 with an R^2 of 0.45 (Table 5.2 and Figure 5.9b). In contrast to the observations at site O1, since site O3 is located at a shallower depth (6 m), a notable influence of waves on currents was observed close to the bed. The results indicated that currents at site O3 were mainly generated by waves and other factors, including tides and local winds, and that there could be a secondary factor controlling currents inside the bay.

A time series plot of wave and observed current directions showed poor correlation between these two components (Figure 5.8). However, the predominant wave and current directions moved to the same quadrant towards the shoreline (Figure 5.10e and f). The predominant wave directions were 150° and 165° to the shoreline, while currents predominantly moved to 105° and 120° to the shoreline.

The tidal analysis showed tidal currents were relatively weak at site O3 (Figure 5.8). The results showed that the observed currents were poorly correlated to tidal currents at site O3 (Table 5.2 and Figure 5.9e and f). The results also pointed out that the predominant tidal current directions moved to 15° and 210° to the shoreline, which were completely different from the observed current direction at the same site (Figure 5.10f and g). This demonstrates that the Southland Current and tidal currents have limited effect on nearshore currents collected at site O3 beyond the breaking zone inside Okains Bay.

However, the tidal effect could be important when the significant wave height decreases. As depicted in Figure 5.8, when wave heights were reduced to below 0.5 m between 1st and 2nd of May, observed currents were also reduced. During that period, the differences between tidal and observed currents reached their minimum (about 0.005 m). This suggests that when wave height, as the main factor in generating currents, decreases, tidal currents could become a major factor in controlling nearshore currents inside the bay.

After removing the tides from observed currents, the residual currents were relatively equal to the observed currents recorded at site O3. The residual current speed varied between 0.0001 ms^{-1} and 0.11 ms^{-1} with an average of 0.02 ms^{-1} (Figure 5.8). The observed current direction predominantly moved to 120° to the shoreline and this angle did not change after removing

the tidal effect (Figure 5.12f and h), although it slightly affected the frequency of other directions. This indicates that tides have a limited effect on nearshore currents beyond the breaking zone inside the bay.

In general, the results showed that waves could play an important role in controlling nearshore currents inside the bay. These findings could be also observed in open coast beaches with the same incident wave conditions. However, what makes pocket beaches unique is the effect of headlands on wave heights and directions. As discussed in chapter 2 (section 2.3.1 and 2.3.3), wave heights notably decrease when waves enter the bay as a result of diffraction. This would reduce the effect of waves on nearshore currents inside pocket beaches compared to open coast beaches with the same offshore incident waves.

Additionally, as discussed in sections 2.3.1 and 4.3.2, wave direction is mainly influenced by reflection from the downcoast headland inside Okains Bay. If the headlands do not exist, such as cases in open coast beaches, wave directions at the same depth as site O3 would be influenced mainly by refraction and shoaling. Therefore, waves reach this site from different directions and result in generating currents moving to different directions.

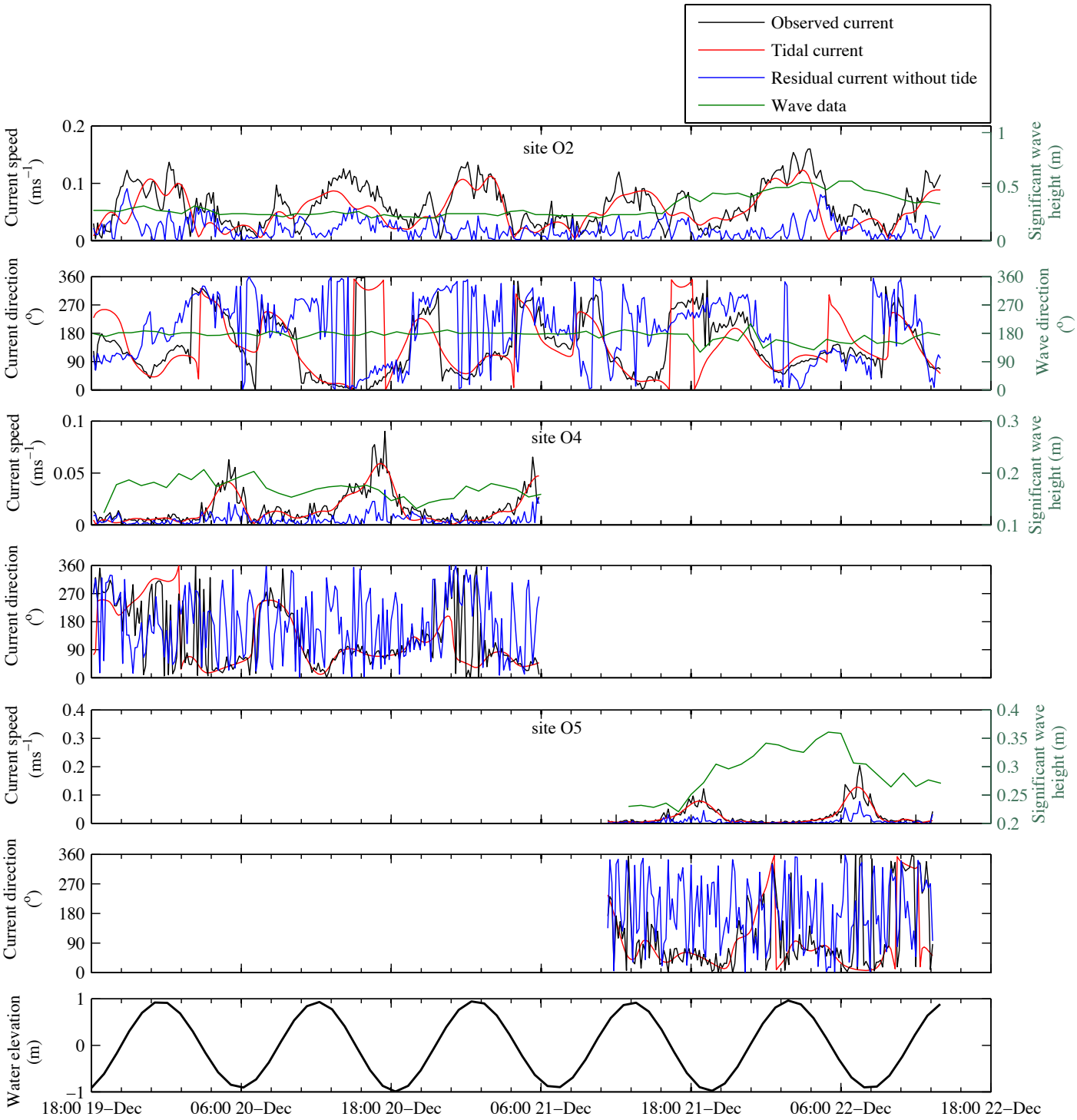

Figure 5.11. Comparison of different types of current data versus wave data collected during Filed Experiment 2 at sites O2, O4 and O5. Note that current and wave directions are shown 'to' and relative to the Okains Bay beach orientation. Also water elevation is relative to the water depth below the water surface collected at site O2.

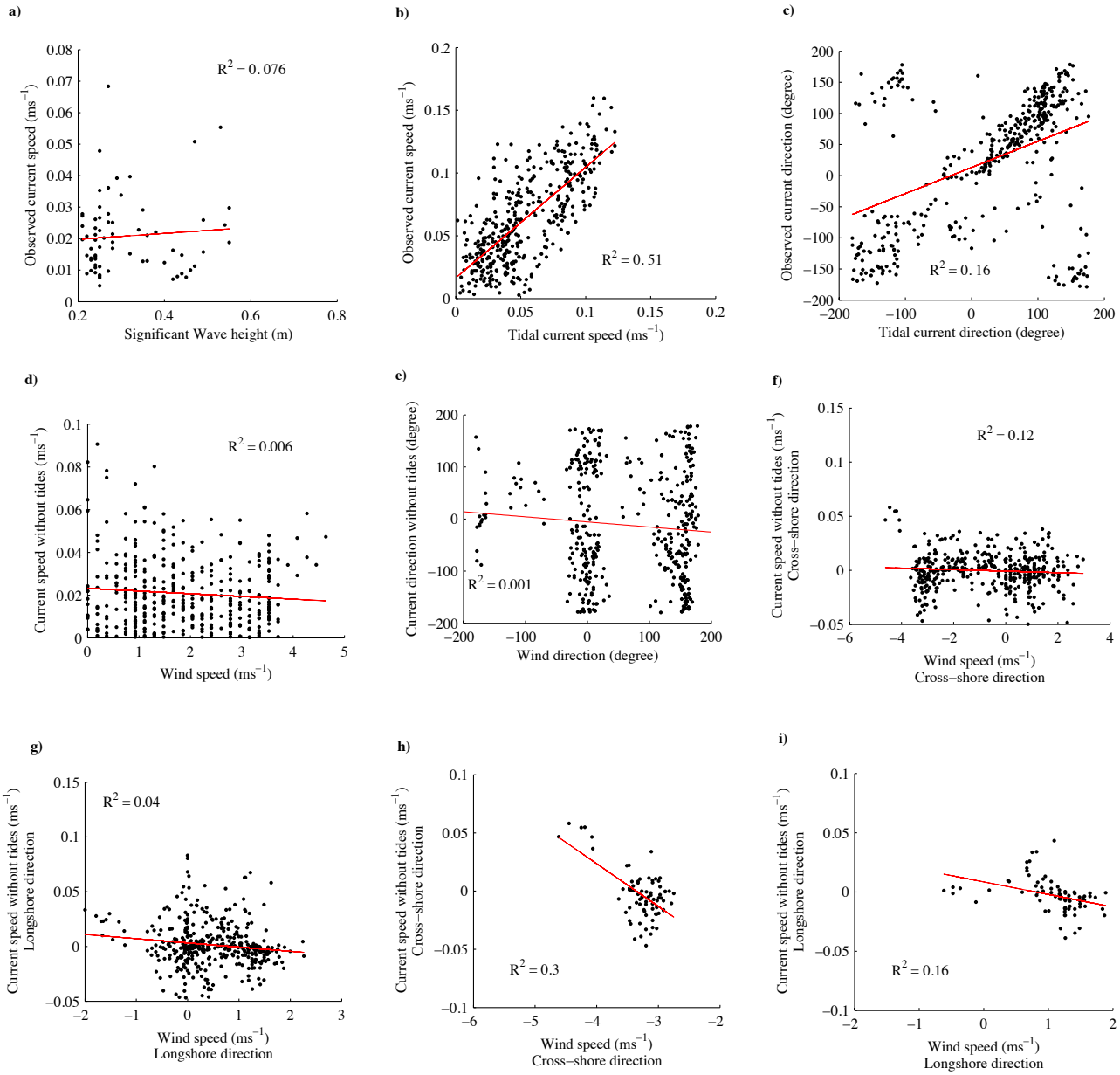

Figure 5.12. Scatter plots shown the correlation between wave height and observed currents (a), between observed currents and tidal currents (b to c), between wind and residual currents (d to g), and between residual currents and wind speed exceeding 3.5 ms^{-1} (h and i). The observations were recorded during Field Experiment 2 at site O2.

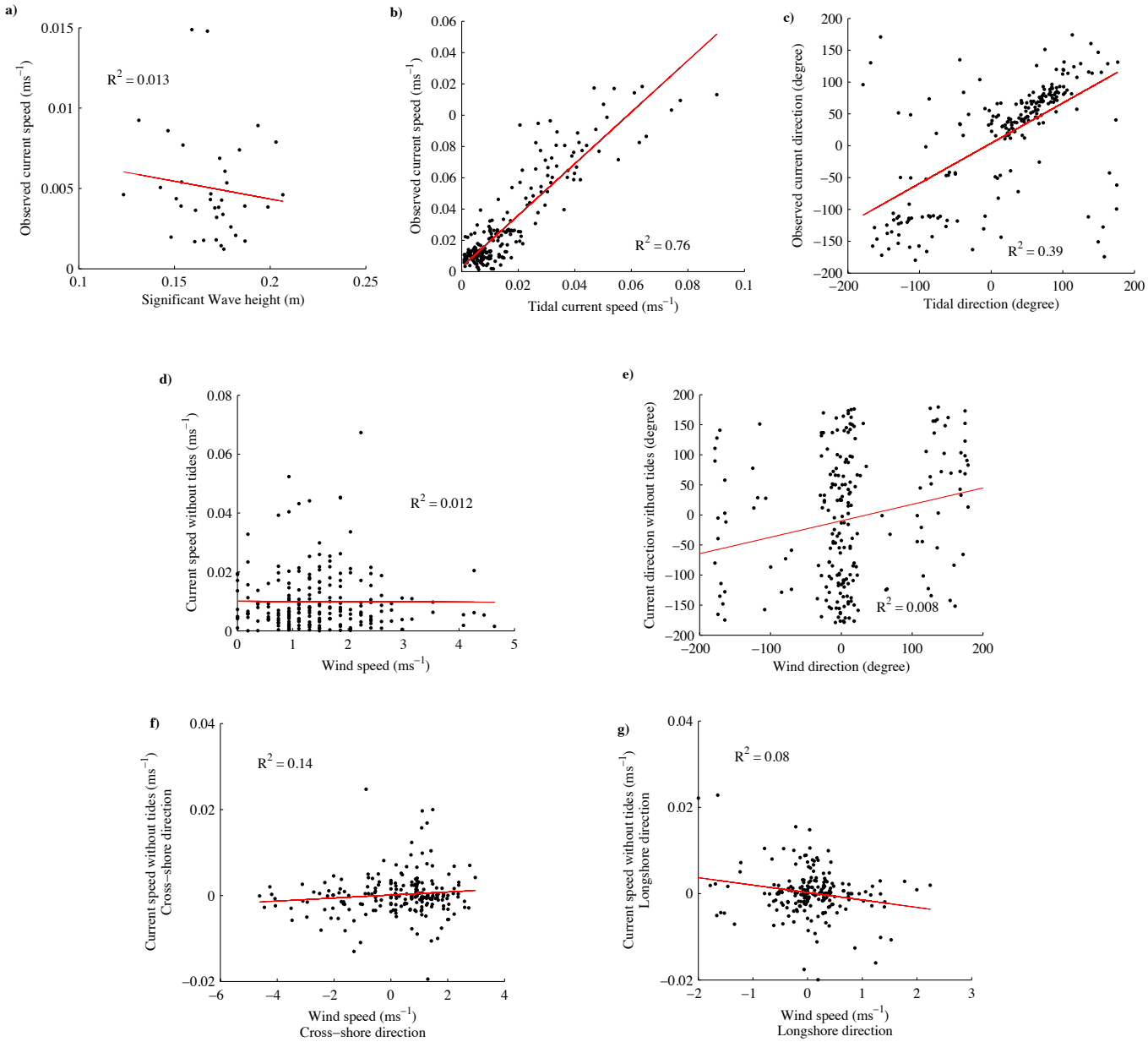

Figure 5.13. Scatter plots shown the correlation between wave height and observed currents (a), between observed currents and tidal currents (b to c), and also between wind and residual currents (d to g). The observations were recorded during Field Experiment 2 at site O4.

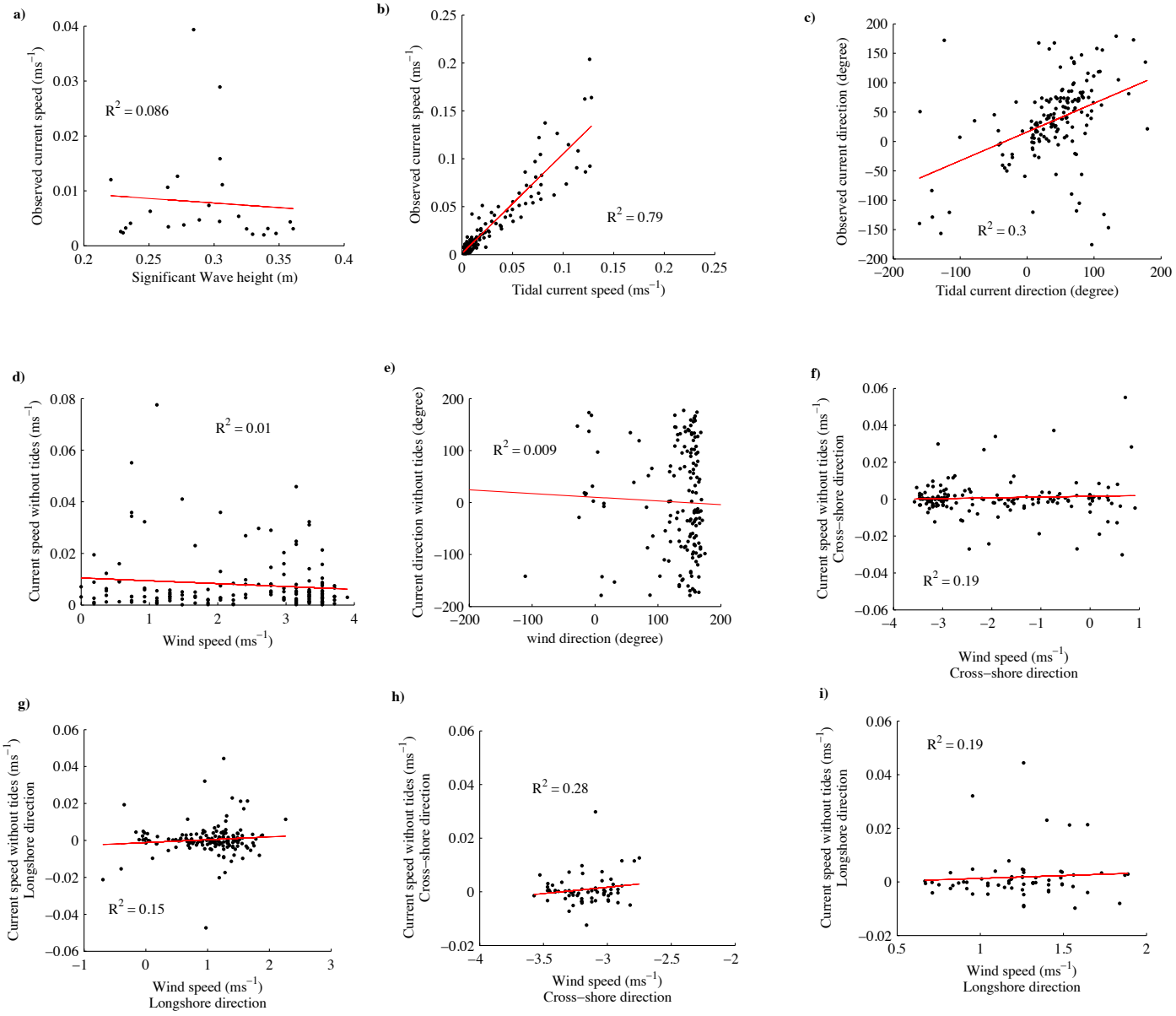

Figure 5.14. Scatter plots shown the correlation between wave height and observed currents (a), between observed currents and tidal currents (b to c), between wind and residual currents (d to g), and between residual currents and wind speed exceeding 3.5 ms^{-1} (h and i). The observations were recorded during Field Experiment 2 at site O5.

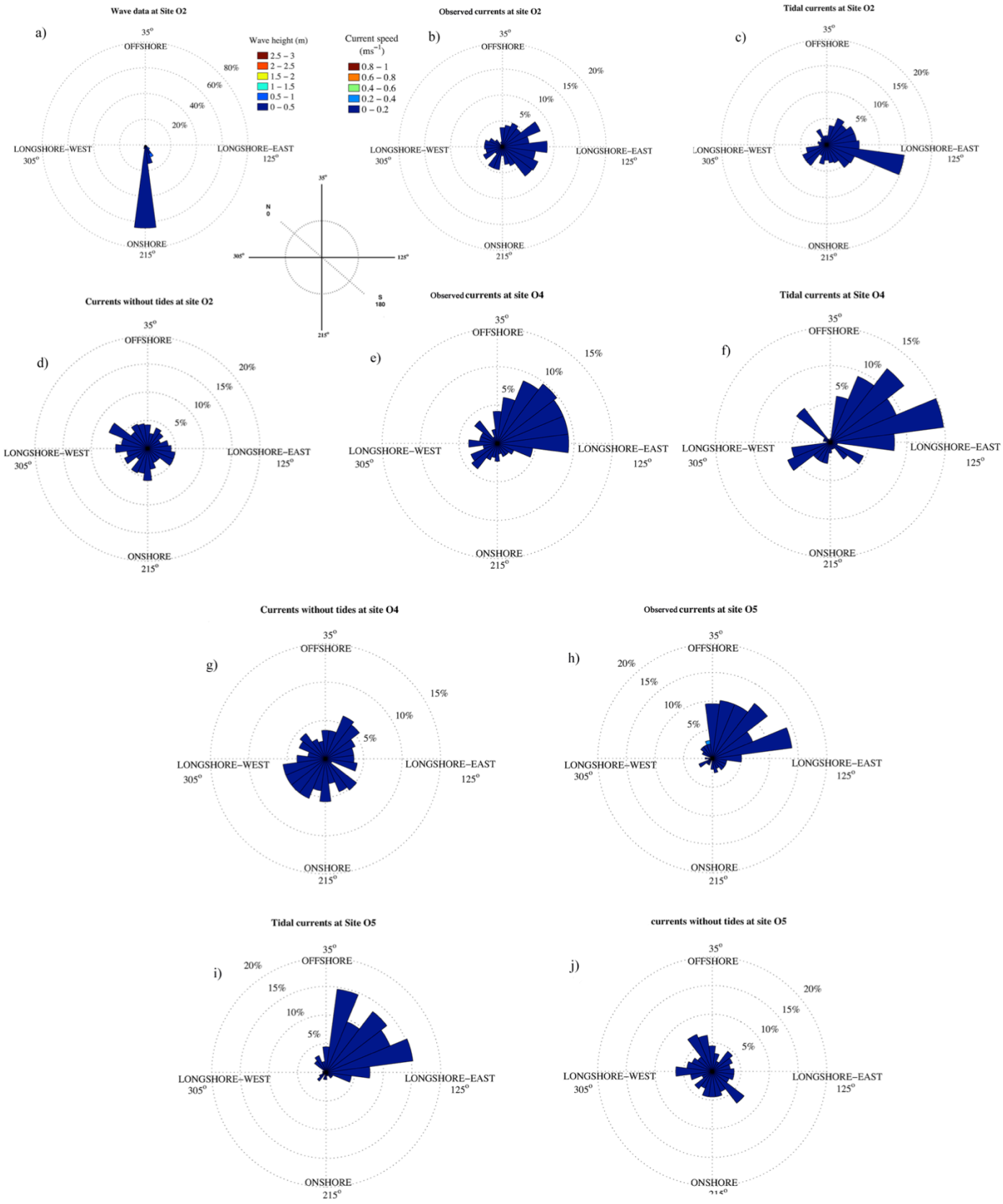

Figure 5.15. Rose plot showing wave data, observed and tidal currents collected during Field Experiment 2 at sites O2, O4 and O5. Note that current and wave directions are shown 'to' and relative to the Okains Bay beach orientation.

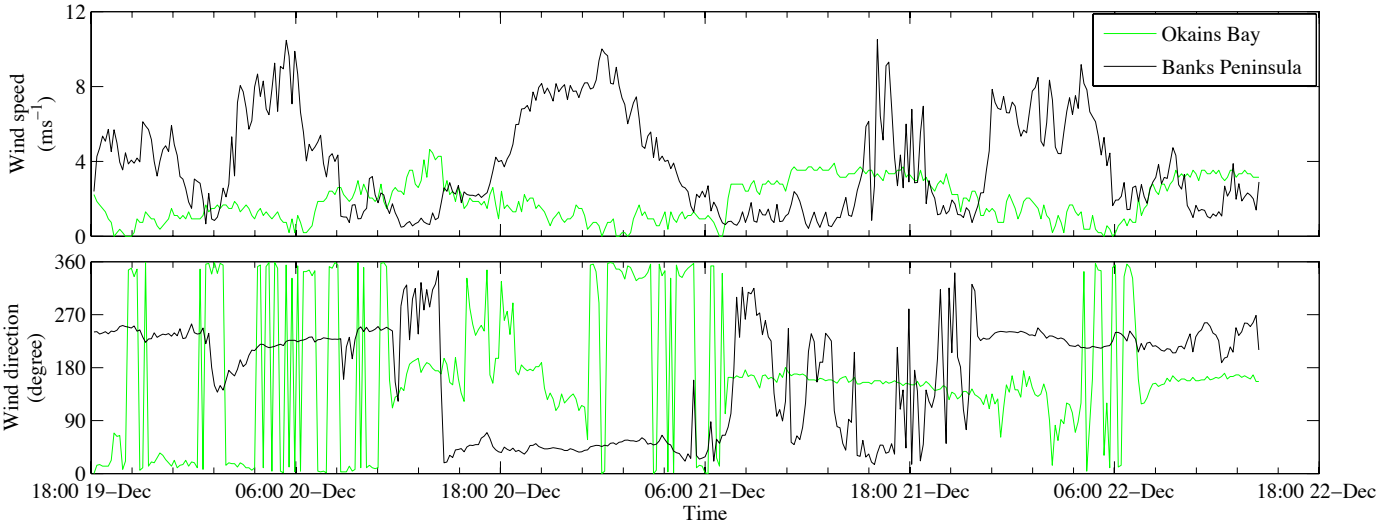

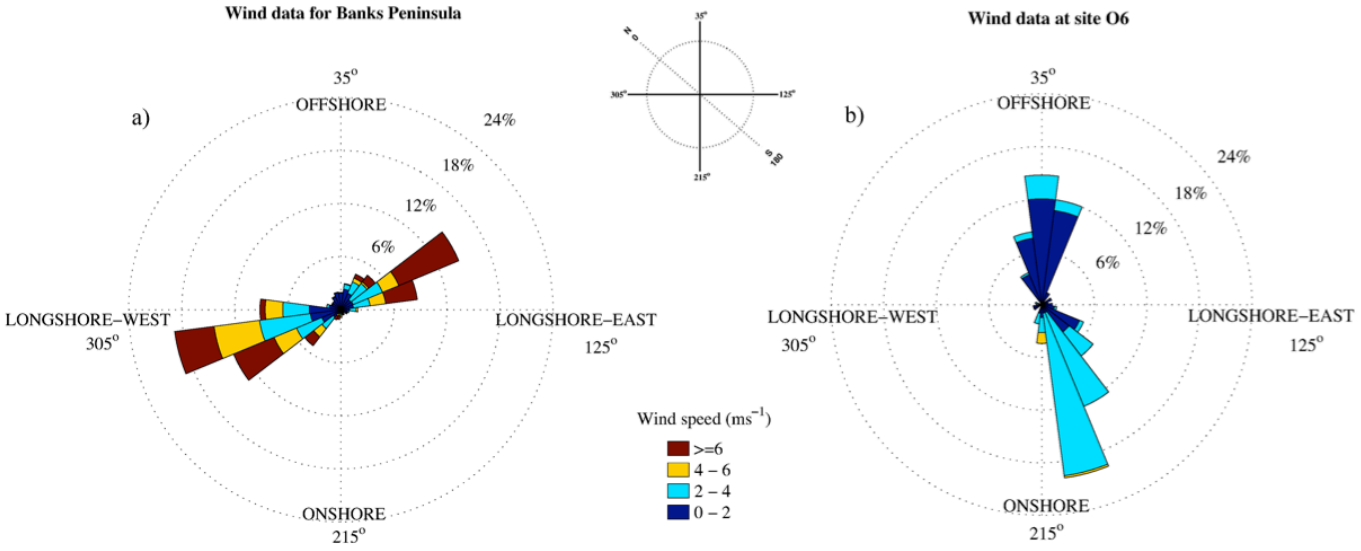

Figure 5.16. Comparison of observed local winds recorded during Filed Experiment 2 at site O6 inside Okains Bay versus wind data recorded at site W [-43.746S 173.119E] representing wind patterns in Banks Peninsula. Note that wind directions are shown 'to' and relative to the Okains Bay beach orientation.

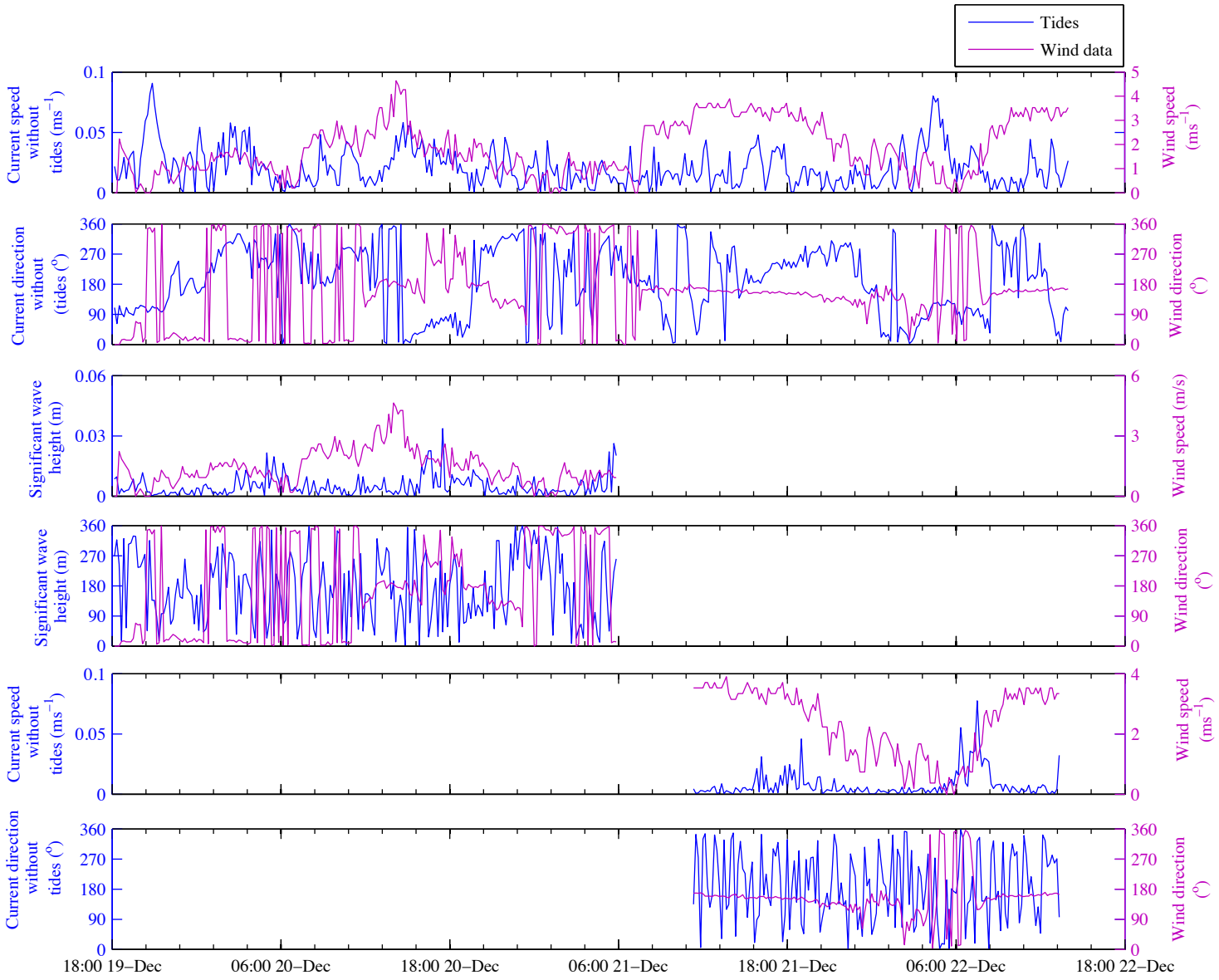

Figure 5.17. Comparison of different types of current data versus wind data collected during Filed Experiment 2 at sites O2, O4 and O5. Note that current and wind directions are shown 'to' and relative to the Okains Bay beach orientation. Also water elevation is relative to the water depth below the water surface collected at site O2.

Table 5.3. Comparison of correlation coefficient (R^2) and P-value for observed wave height, currents, tidal currents and wind data collected during Field Experiment 2 at sites O2, O4 and O5.

Site	Component 1	Component 2	R^2	P-value
O2	Observed current speed	Significant wave height	0.076	0.31
	Observed current speed	Tidal current speed	0.51	0.043
	Observed current direction	Tidal current direction	0.16	0.11
	Observed current speed	Wind speed	0.006	0.29
	Observed current direction	Wind direction	0.001	0.38
O4	Observed current speed	Significant wave height	0.46	0.048
	Observed current speed	Tidal current speed	0.11	0.21
	Observed current direction	Tidal current direction	0.001	0.66
	Observed current speed	Wind speed	0.012	0.26
	Observed current direction	Wind direction	0.008	0.35
O5	Observed current speed	Significant wave height	0.46	0.048
	Observed current speed	Tidal current speed	0.11	0.21
	Observed current direction	Tidal current direction	0.001	0.66
	Observed current speed	Wind speed	0.01	0.27
	Observed current direction	Wind direction	0.009	0.34

5.3.2. Field Experiment 2

During this field experiment significant wave heights were small, and varied between 0.21 m to 0.55 m at site O2 (Figure 5.11). The observations also showed relatively weak currents at site O2. The observed current speeds at this site varied between 0.003 ms^{-1} and 0.16 ms^{-1}, with an average of 0.063 ms^{-1}. Currents collected inside the surf zone at site O4 were also

slow, varying between 0.0009 ms^{-1} and 0.09 ms^{-1}, with an average of 0.016 ms^{-1} (Figure 5.11). Currents were also collected inside the surf zone at site O5 in proximity to the upcoast headland (Figure 5.11). The observations showed that the currents were relatively slow and varied between 0.001 ms^{-1} and 0.2 ms^{-1}, with an average of 0.03 ms^{-1}.

In contrast to observations at site O3 during Field Experiment 1, waves collected during Field Experiment 2 at sites O2, O4 and O5 had a minor effect on observed currents (Figure 5.11). Linear regression analysis showed that there was a poor correlation between currents and wave height at each site (Table 5.3 and Figure 5.12a to 5.14a). Similarly, there was a poor correlation between wave directions and current directions (Figure 5.15). For instance, the predominant wave direction at site O2 was normal, while currents predominantly moved to 60°, 90° and 120° to the shoreline (Figure 5.15a and b). The results indicated that currents near the bed at different sites inside the bay during low energy waves were largely influenced by other factors, such as tides.

Previously, during Field Experiment 1, it was suggested that when waves are small, tides could largely influence the currents beyond the breaking zone. As shown in Figure 5.11, since during Field Experiment 2 wave heights were relatively small, the observations showed that the currents at sites O2, O4 and O5 primarily fluctuated because of tides. The tidal analysis using the Utide Matlab Function (Codiga, 2011) showed a strong effect of tides on currents inside the bay. The results indicated that the observed currents reasonably correlated with tidal currents at sites O2, O4 and O5 (Table 5.3 and Figure 5.12b to 5.14b). A time series analysis showed that the current speed collected at site O2 consistently increased during high tide and it decreased during low tides (Figure 5.11), while a reverse effect was observed at sites O4 and O5. This indicates that observed currents inside the bay in a deeper area beyond the breaking zone, were largely influenced by flood currents, whereas currents collected inside the surf zone were mainly influenced by ebb currents.

The tidal analysis also showed that tides could influence current directions inside the bay (Figure 5.11 and Figure 5.15). The results indicated that the predominant directions of tidal currents were similar to those of observed currents at site O2, O4 and O5, but with different frequencies. However, a linear regression analysis showed a poor correlation between tidal and observed current directions (Figure 5.12 to 5.14).

The findings suggest that regardless of the depth of water, if Okains Bay is dominated by low energy waves, tides could importantly influence the currents. As shown during Field Experiment 1, observed currents at site O3 were mainly influenced by the incident waves. However, during Field Experiment 2, currents collected at site O2 were largely affected by tides as the area was dominated by low energy waves. Although the water depth at site O2 was deeper than that at site O3, when incident wave heights decreased, the effect of tides on currents increased. This process could be the same as open coast beaches, but in pocket beaches, if incident waves approach at an angle greater than the pocket beach direct wave approach sector, wave heights could decrease as a result of diffraction. Tides could, consequently, play an important role in controlling nearshore currents inside the bay.

After removing the tides from observed currents, the residual currents were relatively slow (Figure 5.11). The residual currents tended to move to both onshore and offshore directions, while the observed currents and tidal currents tended to move more longshore to the east at site O2 and to an offshore direction at sites O4 and O5 (Figure 5.15).

As discussed earlier in section 5.1, nearshore currents could possibly be influenced by local winds (Gallop *et al.*, 2012). Wind data collected at site O6 showed that local winds considerably changed inside Okains Bay relative to the wind data at site W which represents the wind patterns in Banks Peninsula (Figure 5.16). The wind data in Banks Peninsula scale indicated that winds were predominantly blowing at 60° and 255° relative to the shoreline. However, wind data recorded in Okains Bay showed the predominant wind directions were moving to 0° and 165° relative to the shoreline (Figure 5.15); that is, winds were mostly moving to offshore and onshore directions. The onshore and offshore movements of local winds indicate that the headlands act as a channel and cause winds to shift to offshore or onshore directions.

The comparison of local winds between Okains Bay at site O6 and Banks Peninsula scale at site W also showed that wind speed considerably decreased (Figure 5.16). The average of wind speed at site W was 3.85 ms^{-1}, while it was about 1.87 ms^{-1} at site O6. This indicates that in addition to changes in wind directions, wind speed also notably changed due to orographic affect.

In order to evaluate the effect of local winds on nearshore currents inside Okains Bay, the tidal currents were first removed from the observed currents collected at different sites.

Afterwards, the correlation between the currents and local winds were studied. An initial comparison showed that the residual currents at sites O2, O4 and O5 were poorly correlated to local winds at site O6 (Table 5.3 and Figure 5.12 to 5.14 and 5.17). However, the correlation between wind and residual currents were slightly improved when cross-shore and longshore components were considered. The scatter plot analysis showed that the correlation between winds and currents was stronger in cross-shore direction than longshore direction (Figure 5.12 to 5.14). These correlations in cross-shore and longshore directions were even stronger when wind speed increased above 3.5 ms^{-1}. The results indicated that cross-shore components of the currents were more affected by local winds than the longshore components of the currents inside the bay. That is because the predominant wind directions inside Okains Bay during Field Experiment 2 were moving to offshore and onshore directions. Therefore, the local winds tend to influence currents more in cross-shore directions and this effect could be further accentuated when wind speed was stronger. Note that throughout Field Experiment 2 at site O4, wind speed rarely exceed 3.5 ms^{-1}, so there was inadequate data to examine the effect of stronger winds on nearshore currents.

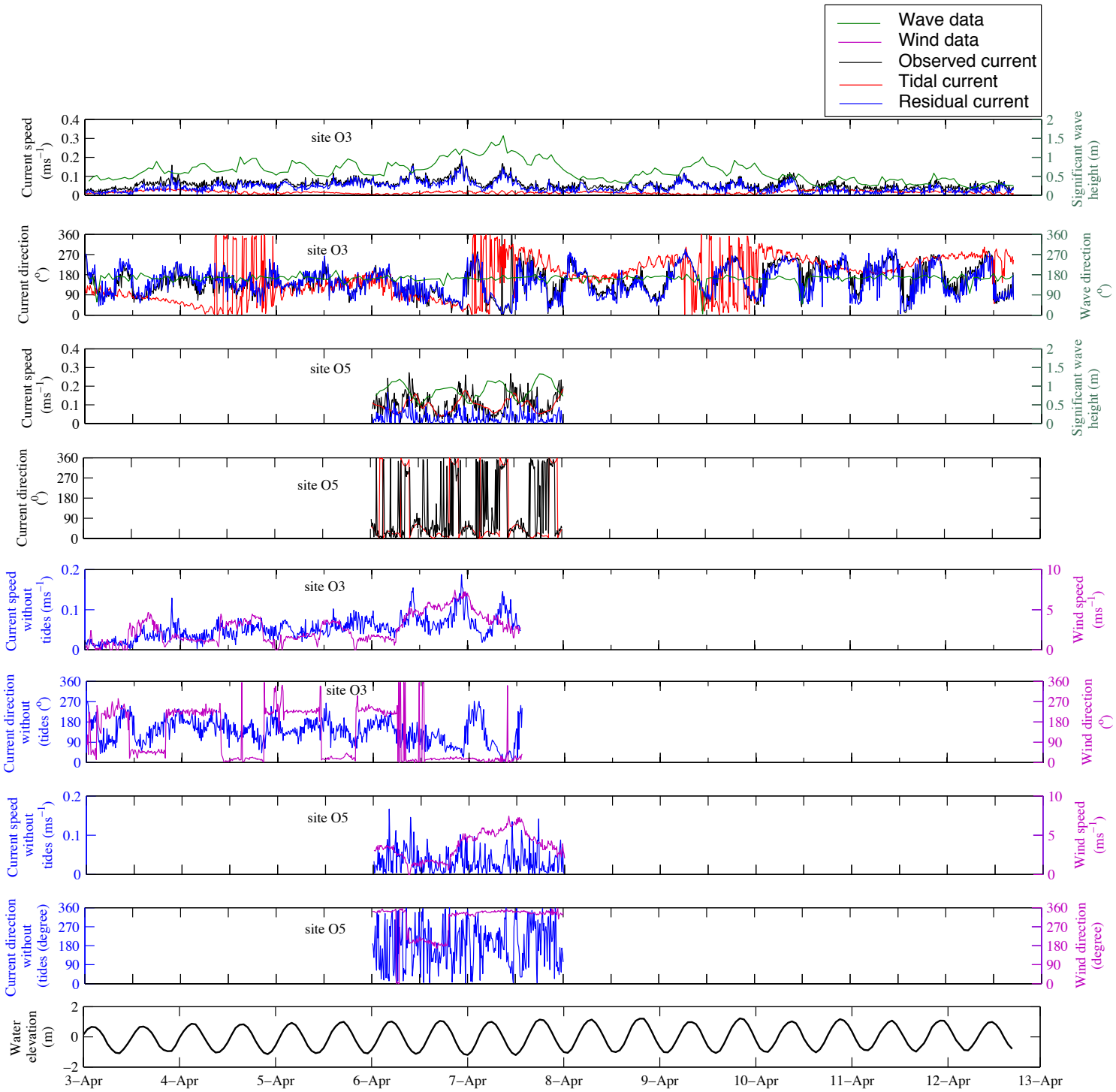

Figure 5.18. Comparison of different types of current data, collected during Filed Experiment 3 at sites O3 and O5, versus wave and wind data. Note that current, wind and wave directions are shown 'to' and relative to the Okains Bay beach orientation. Also water elevation is relative to the water depth below the water surface collected at site O3.

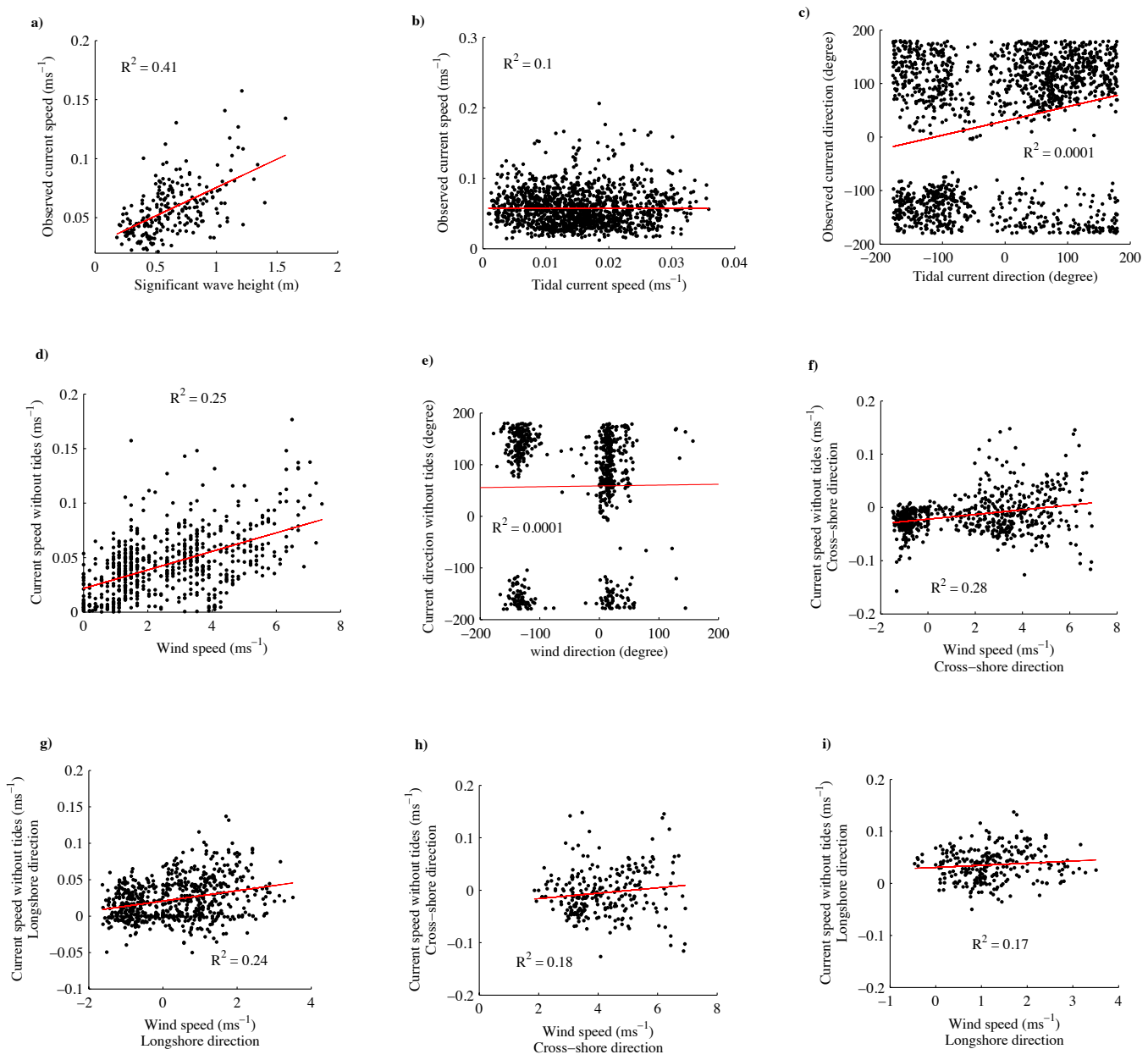

Figure 5.19. Scatter plots shown correlations between wave height and observed currents (a), between observed currents and tidal currents (b and c), between wind and residual currents (d to g), and between residual currents and wind speed exceeding 3.5 ms^{-1} (h and i). The observations were recorded during Field Experiment 3 at site O3.

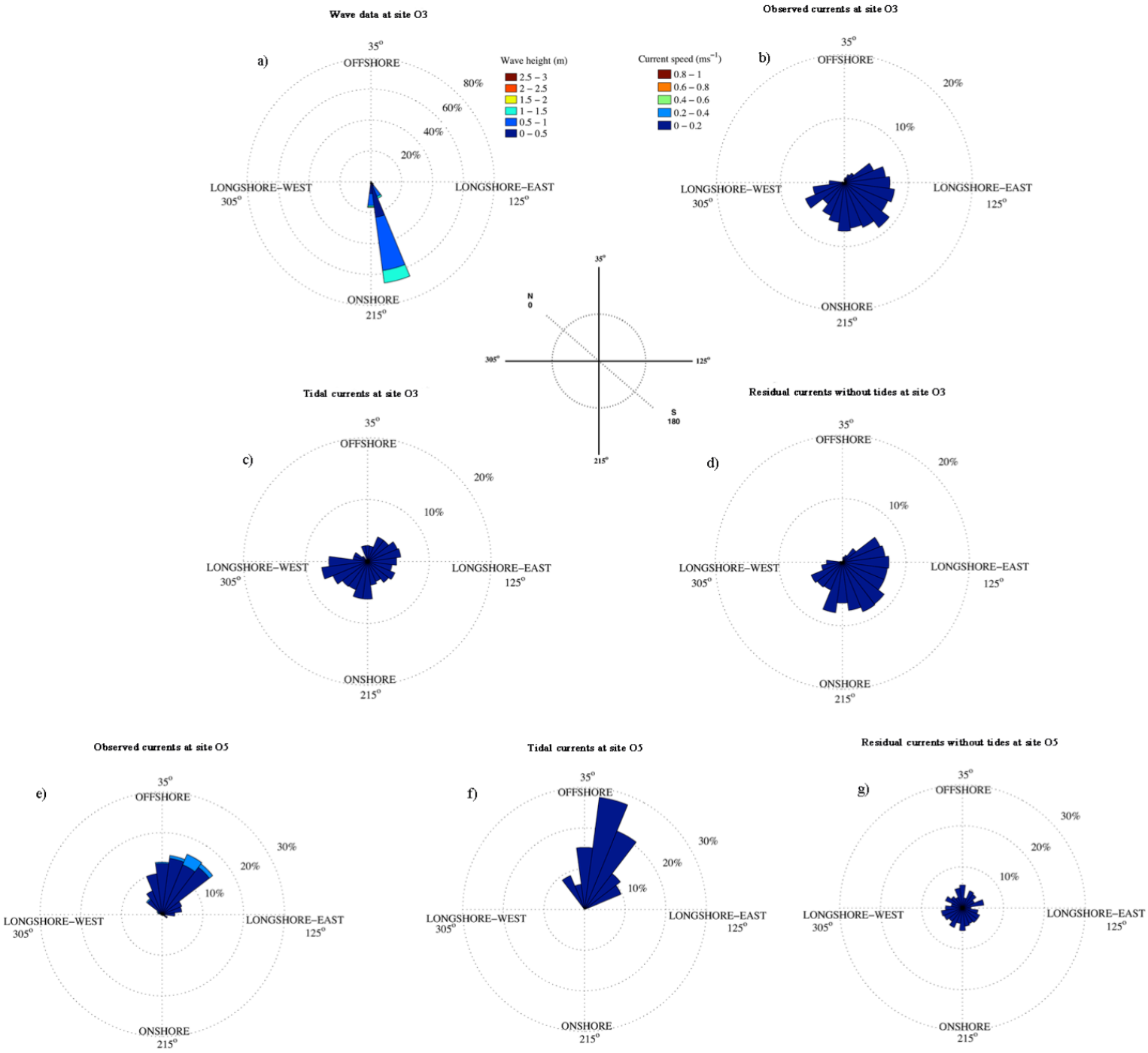

Figure 5.20. Rose plot showing wave data, observed and tidal currents collected during Field Experiment 3 at sites O3 and O5. Note that current and wave directions are shown 'to' and relative to the Okains Bay beach orientation.

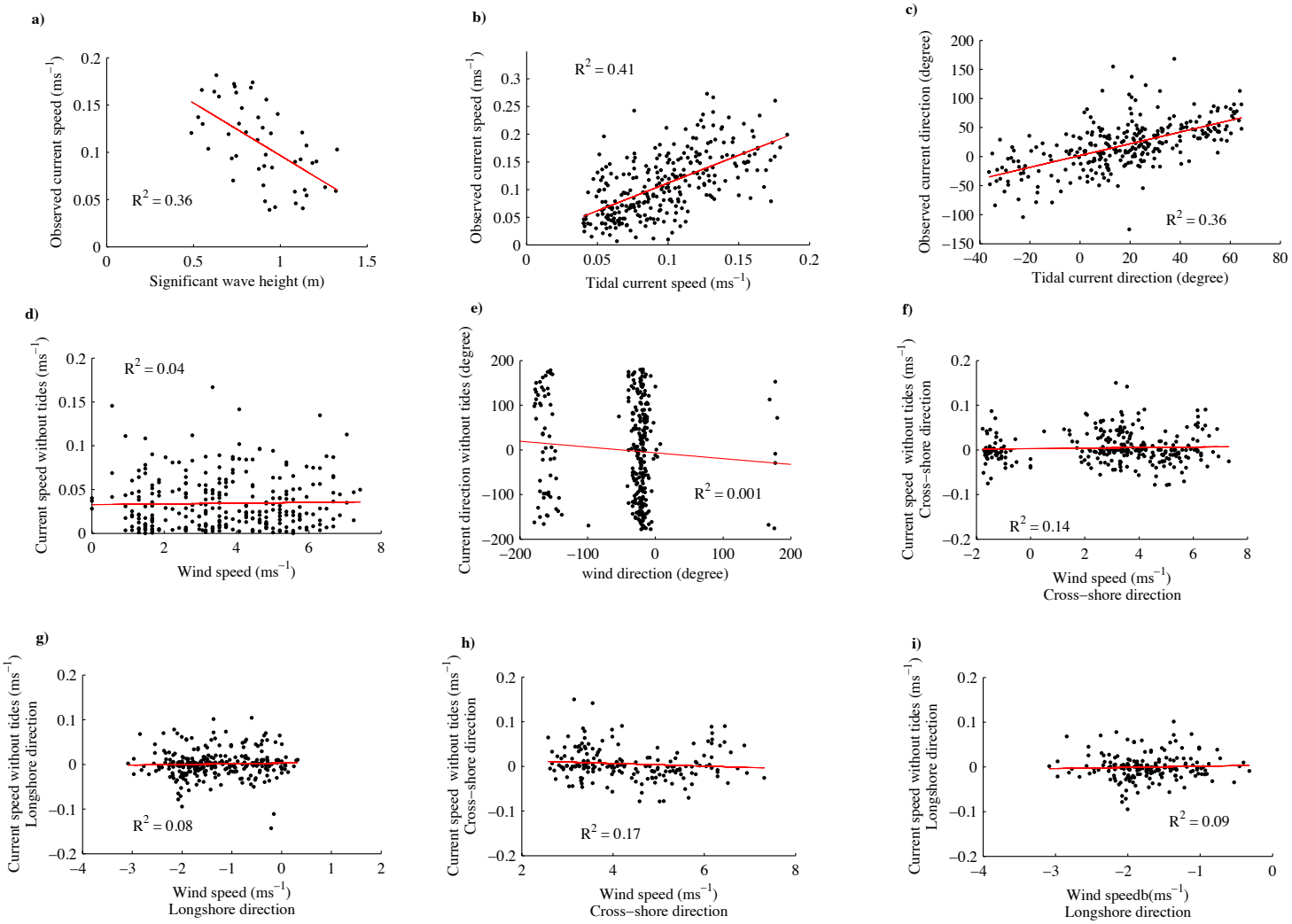

Figure 5.21. Scatter plots shown correlations between wave height and observed currents (a), between observed currents and tidal currents (b and c), between wind and residual currents (d to g), and between residual currents and wind speed exceeding 3.5 ms^{-1} (h and i). The observations were recorded during Field Experiment 3 at site O5.

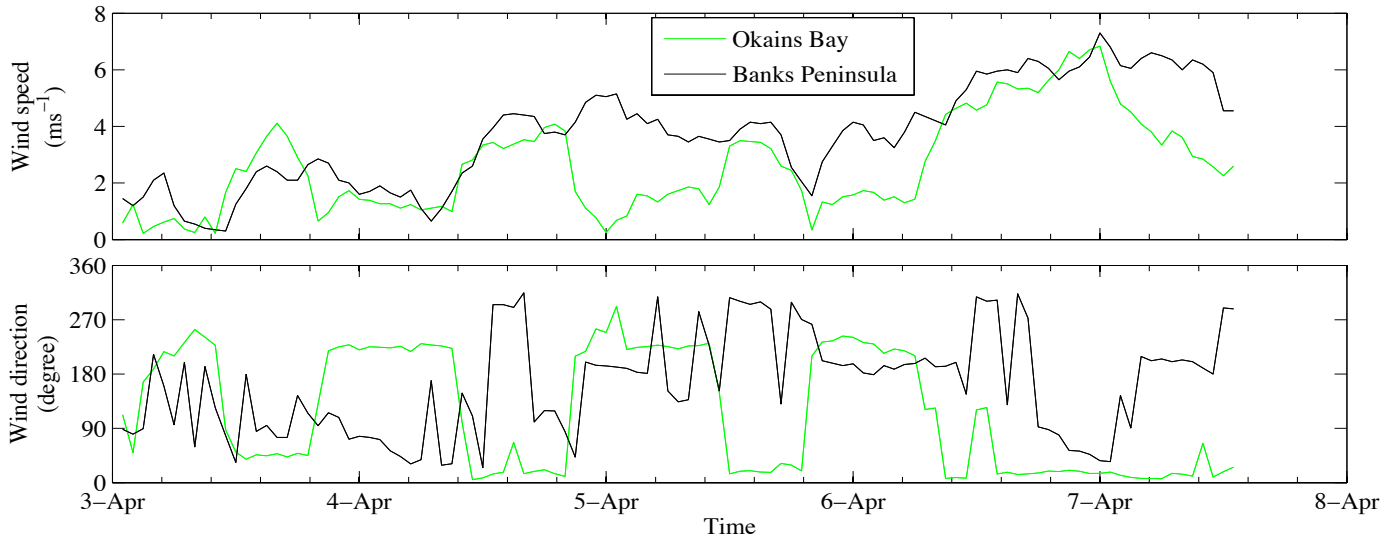

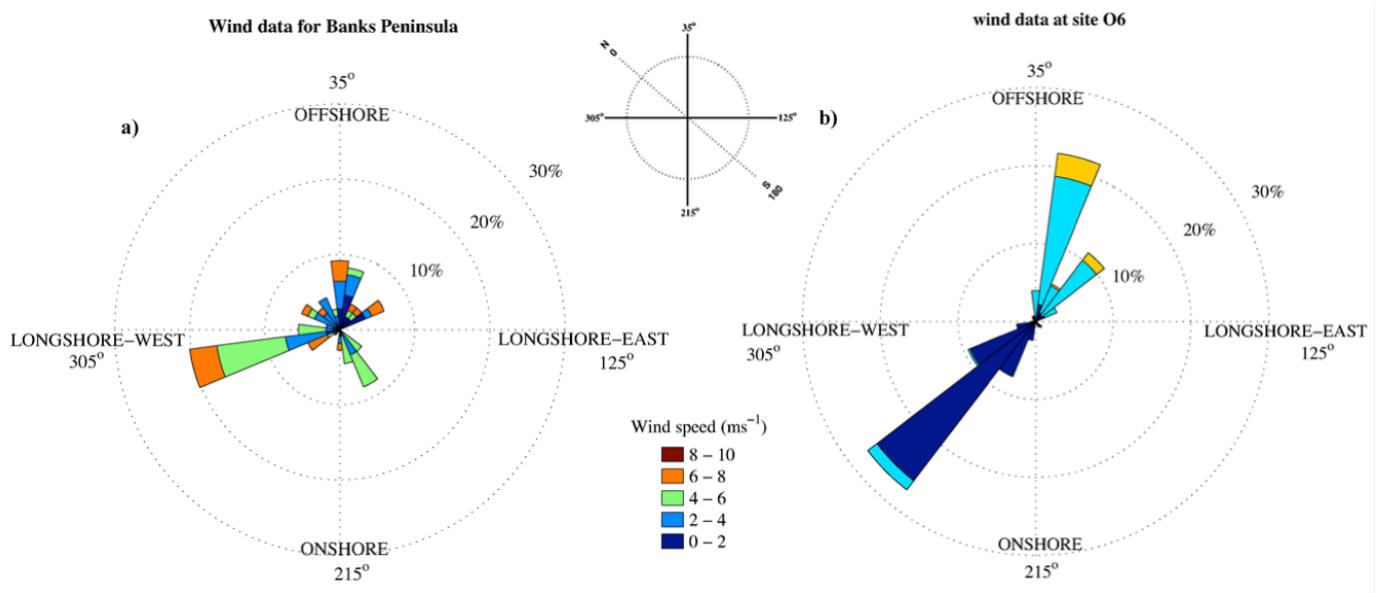

Figure 5.22. Comparison of observed local winds recorded during Filed Experiment 3 at site O6 inside Okains Bay versus wind data recorded at site W [-43.746S 173.119E] representing wind patterns in Banks Peninsula. Note that wind directions are shown 'to' and relative to the Okains Bay beach orientation.

Table 5.4. Comparison of correlation coefficient (R^2) and P-value for observed wave height, currents, tidal currents and wind data collected during Field Experiment 3 at sites O3 and O5.

Site	Component 1	Component 2	R^2	P-value
O3	Observed current speed	Significant wave height	0.41	0.04
	Observed current speed	Tidal current speed	0.1	0.12
	Observed current direction	Tidal current direction	0.0001	0.63
	Observed current speed	Wind speed	0.25	0.052
	Observed current direction	Wind direction	0.01	0.29
O5	Observed current speed	Significant wave height	0.36	0.049
	Observed current speed	Tidal current speed	0.41	0.03
	Observed current direction	Tidal current direction	0.36	0.042
	Observed current speed	Wind speed	0.04	0.19
	Observed current direction	Wind direction	0.01	0.25

5.3.3. Field Experiment 3

During Field Experiment 3, significant wave heights at site O3 ranged from 0.18 m to 1.57 m with a mean of 0.62 m, which were relatively higher than those collected during Field Experiment 2. The observations recorded at this site indicated weak currents beyond the surf zone (Figure 5.18). The observed current speed at this site varied between about 0.012 ms^{-1} and 0.21 ms^{-1} with a mean of 0.057s ms^{-1}. However, observations recorded at site O5 inside the surf zone showed that currents were relatively moderate and stronger compared to those collected at site O3. The observed current speed at this site varied between about 0.007 ms^{-1} and 0.27 ms^{-1} with a mean of 0.11 ms^{-1} (Figure 5.18).

The observations showed that current speeds inside Okains Bay beyond the surf zone were mainly influenced by incident waves. The time series analysis showed that 66% of the time when there was an increase in the significant wave height at site O3, current speed was also reinforced accordingly (Figure 5.18). Also 59% of the time a reduction in the significant wave height caused the current speed to decrease. The results of linear regression analysis indicated that the observed currents were moderately correlated to significant wave height but there was a poor correlation between waves and current directions (Figure 5.19a and Table 5.4). However, the diagrams depicted in Figure 5.20a and b indicated that the predominant wave and current directions were in the same quadrant towards the shoreline; that is, the predominant wave direction was propagating to 165° relative to the shoreline, while currents were predominantly moving to 105° and 135° (Figure 5.20a and b). The results suggest the importance of incident waves on currents close to bed at site O3 when significant wave height is over 0.6 m. Similar results were also found during Field Experiment 1 inside Okains Bay at site O3, when the significant wave heights were over 0.54.

The effect of waves on currents would gradually decrease towards the shoreline as the headlands filter a higher range of approaching incident wave directions. The observations collected inside the surf zone at site O5 showed that currents were less influenced by incident waves compared to the currents collected at site O3 (Figure 5.18). A linear regression analysis indicated that current speed moderately correlated to wave height with R^2 of 0.36 (Figure 5.21a and Table 5.4). Note that wave directions were not collected at site O5 and as discussed earlier, it was assumed that waves approached relatively in shore normal (see Short, 1999; Woodroffe, 2002). With this assumption, wave directions and predominant current directions were moving in an opposite direction (Figure 5.20e), indicating the influence of other factors in controlling currents inside the surf zone.

The tidal analysis showed tidal currents were relatively weak at site O3 (Figure 5.18). The analysis indicated that the observed currents were poorly correlated to tidal currents at site O3 (Figure 5.19b and c and Figure 5.20 b and c). However, as expected the tidal effect on currents increased in the surf zone at site O5. The analysis indicated that the current speed at site O5 consistently increased during low tide and decreased during high tides (Figure 5.18). The analysis indicated that the observed currents moderately correlated to tidal current at site O5 (Figure 5.21b and c and Table 5.4). The results also showed that tides could significantly change the current directions at site O5 (Figure 5.20e and f). The predominant observed

current directions were 30° and 45° relative to the shoreline and the tidal current directions were predominantly moving to 15° and 30° relative to the shoreline. The results suggest that tides could alter the observed current at site O5 inside Okains Bay.

After removing the tides from observed currents, the residual currents were relatively equal to the observed currents recorded at site O3 (Figure 5.18). The residual current speed varied from about 0.00006 ms^{-1} to 0.19 ms^{-1} with a mean of 0.042 ms^{-1}. The predominant residual current directions were moving to 150°, 165° and 195° relative to the shoreline (Figure 5.20d). This states that the predominant observed current directions changed slightly after removing the tidal effect, although the currents were predominantly moving to the same quadrant towards the shoreline.

Similarly, the residual currents at site O5 were also slow, varying between approximately 0.00001 ms^{-1} and 0.17 ms^{-1}, with a mean of 0.034 ms^{-1} (Figure 5.18). The residual currents at site O5 were predominantly moving to 135° and 330° relative to the shoreline (Figure 5.20g). Therefore, the results indicated that tides had a greater effect on currents inside the surf zone compared to those recorded beyond the surf zone. The findings could be similar to open coast beaches and could be a depth related effect. However, what makes the pocket beach environments different from open coast beaches is the way waves are filtered by headlands, resulting in accentuating the tidal effect on currents inside the bay. Areas close to the shoreline, including the surf zone, are more sheltered from a higher range of approaching incident waves. Therefore, it is expected that other factors, such as tides or local winds, have a greater impact on currents than approaching waves.

As discussed earlier during Field Experiment 2, currents can be influenced by local winds inside Okains Bay. Wind data collected during Field Experiment 3 at site O6 showed that local winds changed considerably inside Okains Bay relative to the wind data recorded at site W, representing the wind patterns in Banks Peninsula (Figure 5.22). The wind data in Banks Peninsula scale indicated that winds were predominantly blowing 255° relative to the shoreline. However, wind data recorded in Okains Bay showed the predominant wind directions were moving to 15° and 210° relative to the shoreline (Figure 5.22a and b); that is, winds were mostly blowing in offshore and onshore directions. Similar to wind observations during Field Experiment 2, the onshore and offshore movements of local winds indicate that the headlands act as a channel and force the wind to shift to offshore or onshore directions, which is similar to the findings of Dingwall (1974).

The comparison of local winds between Okains Bay at site O6 and Banks Peninsula scale at site W also showed that wind speed considerably decreased (Figure 5.22). The average of wind speed at site W was 3.7 ms^{-1}, whereas it dropped to 2.5 ms^{-1} at site O6. This indicates that in addition to changes in wind directions, wind speed also changes due to orographic affect.

The residual currents calculated for site O3 and O5 were evaluated against local wind data collected at site O6 in order to examine the effect of winds on currents inside Okains Bay. An initial comparison showed that the residual currents at sites O3 and O5 poorly correlated with local winds at site O6 (Table 5.4 and Figure 5.19 and 5.21). However, the correlation between wind and residual currents were slightly improved when cross-shore and longshore components were considered. The analysis showed that the correlation between the winds and currents was stronger in the cross-shore direction than longshore direction (Figure 5.19 and 5.21). These correlations in cross-shore and longshore directions were even stronger only for site O5 when wind speed increased above 3.5 ms^{-1}. Similar to the findings during Field Experiment 2, the results indicated that cross-shore components of the currents were more affected by local winds than the longshore components, as the local wind directions inside the bay were predominantly moving to offshore and onshore directions.

Generally, the correlation between residual currents and local winds were relatively week inside Okains Bay. If the area is dominated by incident waves or tides, local winds typically have less effect on currents. However, what makes pocket beaches unique in terms of local winds is the predominant wind direction inside the bay. Owing to the influence of headlands, wind direction changes to offshore or onshore directions inside the bay, regardless of the direction of wind outside the bay. Therefore, local winds tend to influence currents more in a cross-shore direction. However, there is no orographic effect in open coast beaches and wind direction does not change considerably when they move towards the shoreline. Therefore, local winds could influence currents in both longshore and cross-shore directions depending on the local wind direction.

5.4. Discussion

In pocket beaches, incident waves can play an important role in controlling nearshore currents close to the bed. The results indicated that waves over 0.5 m inside Okains Bay beyond the surf zone significantly influenced currents close to the bed. This feature is similar to open coast beaches. However, as discussed in chapter 2, if waves approach from an angle greater than the pocket beach direct wave approach sector, wave heights could significantly decrease inside the bay. Therefore, their effects on nearshore currents close to the bed would be reduced and the effect of other factors, such as tides and local winds, could prevail over waves. This could be a unique feature occurring only in pocket beaches as the headlands filter the approaching incident waves and could create a shadow zone in areas close to the shoreline.

The tidal analysis showed that tides influenced currents beyond the surf zone only when waves were small. However, the analysis inside the surf zone indicated that tides notably affected the currents when approaching incident wave heights varied from low to high. Since Okains Bay is sheltered by two long headlands, waves with a limited range of direction directly approached the surf zone. Therefore, this area was mostly a tide-dominated area. However, in adjacent open coast beaches, waves approaching from a wide range of directions could still dominate the surf zone and influence the currents.

The analysis also showed that currents outside Okains Bay were mainly influenced by tides. Throughout the observations recorded outside Okains Bay, wave energy varied from low to high. However, waves had a limited effect on currents close to the bed at a depth of 12 m. Based on the observations in this area, it is impossible to conclude this notable effect of tides on currents outside the bay is unique to Okains Bay or, in general, to pocket beaches. This is because, as discussed earlier, the Southland Current (Chiswell, 1996; Reynolds-Fleming and Fleming, 2005), moves towards the north and influences the currents outside pocket beaches located in Banks Peninsula, including Okains Bay.

The observations showed that local winds tended to blow predominantly in offshore and onshore directions inside Okains Bay. Since the bay is located in a valley with a hill cress elevation of around 500 m above sea level (measured using a GPS navigation tool), the topography acts as a channel and shifts the wind directions. Therefore, it appeared that the local winds blew at angles close to offshore and onshore directions inside the bay, which is

similar to the findings of Dingwall (1974). However, due to the orographic effect of Banks Peninsula, the speed of wind moving to an offshore direction decreased when it reached the bay.

The local winds tended to influence currents more in cross-shore directions. Since the predominant wind directions were in offshore and onshore directions, their cross-shore component was more effective in influencing the currents than the longshore component. The analysis of the observations demonstrated that the correlation between cross-shore winds and cross-shore residual currents were stronger than that of longshore components. This effect was accentuated when the wind was stronger. It can be concluded that local winds tend to influence currents in cross-shore directions in pocket beaches. However, in open coast beaches both longshore and cross-shore components of local winds could equally be important in controlling nearshore currents, as the area is completely open to local winds from a wide range of directions.

5.5. Conclusion

This chapter discussed the primary factors found to control the nearshore currents close to bed in Okains Bay. Observations indicated that incident waves could influence the currents in shallower water depth inside the bay, but tides were the primary influence in deeper waters outside the bay. Studies by Dingwall, (1974) and Reynolds-Fleming and Fleming (2005) showed the existence of strong tidal currents off the peninsula. This strong current was also recorded during Field Experiment 1 outside the bay at site O1. Regardless of variation in significant wave heights at this site, tidal currents were the main influence on the observed currents close to the bed.

The analysis also indicated that tides could influence the observed currents inside the bay. Once waves reached a certain height, they were an important influence on the currents. Results showed that if the wave heights were above 0.5 m, currents inside the bay were mainly influenced by waves. However, when the wave heights dropped below 0.5 m, other factors, such as tides, prevail over waves to influence the currents inside the bay. This feature

could also be observed in open coast beaches, but what makes pocket beaches unique is the effect of headlands on wave heights and directions. Wave heights can notably decrease when waves enter the bay, as a result of diffraction. This reduces the effect of waves on nearshore currents inside pocket beaches and accentuates the effect of tides compared to adjacent open coast beaches.

Observations of local winds showed that winds were predominantly moving in offshore and onshore directions. The orographic effect in the vicinity of Banks Peninsula caused winds to shift markedly, and when they entered the bay, they predominantly blew in cross-shore directions. Observations indicated this effect could reduce the speed of the winds. This feature makes pocket beaches unique in terms of local winds and their effects on currents.

The cross-shore components of the local winds were more effective than longshore components in influencing the currents. The analysis showed that the correlation between cross-shore components of local winds and currents were stronger than those of longshore components. Although this effect was accentuated when the wind speed increased over 3.5 ms^{-1}, analysis indicated that the winds had a minor effect on the observed currents compared to the effect of waves and tides.

The next chapter will focus on the nearshore current modelling in Okains Bay using the XBeach model. The results will be used to better understand the special variation in the current system, including rip currents, during different sea and weather conditions.

Chapter 6: Numerical modelling of nearshore currents in Okains Bay

This chapter discusses the numerical modelling of the current systems within Okains Bay using the XBeach model. Current systems were examined under different sea conditions with consideration of the local winds and tides. First, the results of the model were validated versus observations, then, the model was used to examine the current systems inside the bay. This chapter contributes theoretical results towards thesis aim 3 and towards the current-related aspects of thesis aims 1 and 2.

6.1. Introduction

Knowledge about the formation of nearshore currents under incident waves and tides in pocket beaches with long headlands and micro-tidal regimes is poorly documented. The majority of numerical and physical modelling studies on currents in topographically constrained settings have focused on embayed beaches, mainly with the goal of evaluating shoreline changes (Daly *et al*., 2014; Van de Lageweg *et al*., 2013; Daly *et al*., 2013; Uda *et al.*, 2010; Weesakul *et al.*, 2010; Ranasinghe *et al.*, 2004; Silvester and Hsu, 1999; Hsu *et al.*, 1989). Numerical studies of nearshore currents, validated by observations, in pocket beaches are scarce (Castelle and Coco, 2012; Silva *et al.*, 2010).

As discussed in chapter 5, Short (1999) introduced the dimensionless embayment scaling parameter to determine the type of current system in headland-enclosed bay beaches (see Eq. 5.6). Wave direction is not taken into account in this parameter. The wave studies in Chapters 2 and 4 showed that offshore wave directions have an important control on hydrodynamic conditions within the bay, including wave directions and heights. These changes in the wave direction in combination with wave heights may potentially influence the current circulation, especially the rip currents in proximity to the headlands or toporips. For instance, Silva *et al.* (2010) studied nearshore current circulation in a pocket beach in Spain using a numerical model. The results showed that two onshore currents were formed close to the headlands inside the surf zone. The currents gradually turned to the centre of the shoreline in opposing directions, to form the feeder currents of a rip current. Silva *et al.* (2010) also indicated that incident wave directions could influence the current circulations, especially the magnitude of the currents inside the bay.

Castelle and Coco (2012) studied the behaviour of nearshore currents, in particular the morphodynamics of rip channels, using a nonlinear morphodynamic model (detailed in Castelle *et al.*, 2012; Castelle and Ruessink, 2011) in simplified model pocket beaches. They

reproduced normal, transitional and cellular circulation systems by changing the geometry of the pocket beaches. Castelle and Coco (2012) also found that when waves approached obliquely to the shoreline, the rip spacing became larger. A toporip was also formed regardless of the direction of incident waves. That is because the center of the shoreline is more exposed to the incident waves so wave heights are higher compared to the sheltered areas close to the upcoast headland. Therefore, the alongshore gradients in wave height causes water to move towards the headland and form toporips.

The results of this research to date indicate that the results of Castelle and Coco's (2012) studies may be less applicable to pocket beaches where the length of the headlands is larger than that of the shoreline and the indentation number is higher. This is because, in such pocket beaches, like in Okains Bay, reflected waves can dominate more of the area inside the bay, including the shadow zone, as discussed in Chapters 2 and 5. In such settings, wave reflection can reduce the size of the shadow zone and alongshore gradients in wave height may not be the primary factor in generating toporips. Also, similar to Silva *et al.*'s (2010) studies, the rip current could shift towards the centre of the shoreline in these settings with longer headlands.

Castelle and Coco (2012) did not analyse the effect of tides on nearshore currents. Since wave heights can noteably decrease due to headland sheltering in long, shallow bays, the effects of tides on currents can be accentuated, as discussed in Chapter 5. In order to refine current theories regarding the nature of the current systems in pocket beaches, it is necessary to take into account the tidal ranges. Hence, this chapter includes a focus on numerical studies of tide effects on nearshore currents.

6.2. The XBeach model

Over the last few decades, several 1D, 2D and 3D coastal numerical models have been developed for hydrodynamic and morphodynamic purposes, such as simulating wave transformation, nearshore currents, sediment transport and overwashing. XBeach is one of the advanced 2D hydrodynamic, morphodynamic models. It was mainly developed to improve our understanding of morphological concepts including dune erosion, overwashing and breaching (Roelvink *et al.*, 2010). This is an open source model initially developed by the Engineer Research Development Centre of the United States Army Corps of Engineers (USACE-ERDC), later improved by Prof. Damo Roelvink of UNESCO-IHE, Dr. Ad Reniers of

University of Miami, Jaap van Thiel de Vries, Robert McCall of Delft University of Technology, Dr. Ap Van Dongeren and Jamie Lescinski of Deltares. In this model, short wave propagation, nonstationary shallow water, sediment transport and continuity equations were designed to take into consideration the hurricane and storm conditions. XBeach can be solely applied for hydrodynamic and morphodynamic simulations of small-scale coastal areas (Roelvink *et al.*, 2010). This model can also be used in conjunction with Morphos-3D project, initiated by USACE-ERDC, to couple the model to wind, wave and surge models to provide the boundary conditions. Note that XBeach can be run for a maximum of eleven days.

The short wave propagation equation used in the XBeach model is based on a developed time-dependent wave action balance solver (Roelvink *et al.*, 2010), shown as

$$\frac{\partial A}{\partial t}+\frac{\partial C_x A}{\partial x}+\frac{\partial C_y A}{\partial y}+\frac{\partial C_\theta A}{\partial \theta}=-\frac{D}{\sigma} \tag{6.1}$$

where

$$A(x,y,\theta)=\frac{S_w(x,y,\theta)}{\sigma(x,y)} \tag{6.2}$$

and where D shows the wave dissipation due to wave breaking, θ is the angle of incidence with respect to the x-axis, C_x, C_y and C_θ are wave action propagation speeds in cross-shore (x), longshore directions (y) and in θ-space respectively. S_w is the wave energy in each directional bin, and σ is the intrinsic wave frequency. Eq. 6.1 and 6.2 enable the model to calculate wave refraction effects and to make waves vary in cross-shore and longshore directions, time and also over the directional space. The simulation of the propagation and dissipation of wave groups can also be done using the short wave propagation equations, given by:

$$\frac{\partial u}{\partial t}+u\frac{\partial u}{\partial x}+v\frac{\partial u}{\partial y}-fv-v_h\left(\frac{\partial^2 u}{\partial x^2}+\frac{\partial^2 u}{\partial y^2}\right)=\frac{\tau_{sx}}{\rho h}-\frac{\tau_{bx}}{\rho h}-g\frac{\partial \eta}{\partial x}+\frac{F_x}{\rho h} \tag{6.3}$$

$$\frac{\partial v}{\partial t}+u\frac{\partial v}{\partial x}+v\frac{\partial v}{\partial y}-fu-u_h\left(\frac{\partial^2 v}{\partial x^2}+\frac{\partial^2 v}{\partial y^2}\right)=\frac{\tau_{sy}}{\rho h}-\frac{\tau_{by}}{\rho h}-g\frac{\partial \eta}{\partial y}+\frac{F_y}{\rho h} \tag{6.4}$$

$$\frac{\partial \eta}{\partial t}+\frac{\partial hu}{\partial x}+\frac{\partial hv}{\partial x}+w=0 \tag{6.5}$$

where h is the water depth, u and v are velocities in x and y directions, τ_{bx} and τ_{by} are the bed shear stresses, τ_{sx} and τ_{sy} are the wind stresses, g is the gravity acceleration, η is the water level, F_x and F_y are wave-induced stresses, ρ is the water density and w is the groundwater infiltration and exfiltration velocity. A roller energy balance is applied to the XBeach model to take into consideration the effect of energy redistribution from breaking waves to foam. The roller energy balance and wave action/energy balance are combined and the dissipation of wave energy is used as a source term for roller energy balance:

$$\frac{\partial E_{roller}}{\partial t} + \frac{\partial c_x E_{roller}}{\partial x} + \frac{\partial c_y E_{roller}}{\partial y} + \frac{\partial c_\theta E_{roller}}{\partial \theta} = -D_{roller} + D_{waves} \qquad (6.6)$$

where E_{roller} is the roller wave energy calculated according to Reniers (2004).

A feature highlighting XBeach is the prediction of mean wave direction without the use of a separate model, so several wave groups can propagate in different directions. The short wave propagation equation also takes into account the full wave-current interaction.

XBeach uses the Generalised Lagrangean Mean (GLM) method for the calculation of the depth-average bed return current (undertow), and thus its effect on bed shear stresses and sediment transport (Roelvink *et al.*, 2010). To this end, velocities in Eq. 6.3 to 6.5 are replaced with Lagrangean velocities. The numerical calculations of the long-wave run-up and backwash on the beach have been modified according to the momentum-conserving form of Stelling and Duinmeijer's (2003) approach.

The XBeach model has been widely used for hydrodynamic and morphodynamic applications, such as dune erosion, overwash and breaching (e.g. Chien et at., 2008; McCall 2010a, 2010b; Roelvink *et al.*, 2009; Van Dongeren *et al.*, 2009; Lindemer et at., 2010). For example, the effects of storm on beaches, dunes and barrier islands were studied and modelled using XBeach by Roelvink *et al.* (2009). The results of the model have also been validated using analytical, laboratory and fieldwork data sets. XBeach was found to simulate dune erosion, overwash and breaching with a high level of accuracy. Comparison between the results of the model and fieldwork indicates that XBeach is capable of precisely predicting incident and infragravity band waves, especially in the inner surf zone.

Orzech *et al.* (2008) used XBeach to study the effect of alongshore rip channel migration and mega-cusp migration on sediment transport at Fort Ord, near Monterey, California. Three years

of fieldwork data, collected by a video, was used to validate the application of XBeach. Then flows and sediment transport patterns were simulated by XBeach using wave data recorded in 15 m water depth. The comparison between the model results and the dune retreat measurements for a particular period of time showed good agreement.

Erosion and overwashing of a section of Santa Rosa Island, Florida, caused by hurricane Ivan (2004), was studied by McCall *et al.* (2010b). XBeach was used to examine the effect of the hurricane on hydrodynamics and morphodynamics in a 2D spatial domain. The results were compared with post-storm data and they demonstrated that the XBeach performed well in simulating complex run-up and some morphological features, including overwash, foredune erosion, back barrier deposition and washover fans. The results also indicated that small changes in the hydraulic boundary conditions of the XBeach model insignificantly affected the morphological regime.

Lindemer *et al.* (2010) carried out some research on the effect of Hurricane Katrina on the morphological changes in the Chandeleur Islands, located 161 km east of New Orleans, Louisiana. XBeach was used to predict the amount of erosion and accretion under hurricane conditions. Although the bathymetry and topography results of the model showed that the island erosion pattern was similar to post-storm survey data, the model underestimated the amount of erosion. This underestimation may have been attributable to an error in the initial input bathymetry / topography, in forcing conditions, or in physical processes not taken into account in XBeach, including bio-physical processes.

Jamal *et al.* (2011) investigated and modified the application of XBeach in gravel beaches in order to evaluate morphological responses. They used the sediment transport equations with Soulsby's (1997) current- and wave-induced sediment transport equations; Eulerian Velocity in sediment movement equations was replaced by Lagrangean Velocity; and Packwood's (1983) pragmatic model of infiltration was included in the unsaturated area of the wash region. Comparisons between the results of the model and field experiment showed an acceptable level of accuracy.

More research on the application of the XBeach model to dune erosion, overwash and breaching can be seen in the studies of Lindemer *et al.* (2008), Vitorino *et al.* (2010), Aarninkhof *et al.* (2010), Baart *et al.* (2010), Chien and Roelvink (2007), Roelvink *et al.* (2007), Eshleman (2009) and Chien (2007). Note that a precise prediction of sediment transport using XBeach relies on accurate predictions of nearshore currents. Literature on

XBeach (Jamal *et al.*, 2011; Lindemer *et al.*, 2010; McCall *et al.*, 2010b) pointed out that the model is capable of simulating nearshore currents in different coastal environments.

Numerical studies in embayed or pocket beaches using XBeach are scarce. For instance, Strauss *et al.* (2010) used XBeach to model beach nourishment and evaluate the stability of the current beach profile at Palm Beach, Gold Coast, Australia, which is an example embayed beach. Comparisons between field data and the results of the model showed that XBeach was found to reasonably estimate erosion of the upper beach and dunes during different storm conditions.

XBeach could not be used to accurately simulate waves in embayed or pocket beaches. That is because the wave equations used in XBeach are not taken into account reflection and diffraction. Therefore, XBeach may not accurately predict nearshore currents and sediment transport inside embayed or pocket beaches. The results of this study in Chapters 2 to 4 indicated that reflection and diffraction play an important role in controlling wave characteristics in Okains Bay, an example pocket beach. In order to address this issue, SWAN was used to simulate waves inside the bay with consideration of reflection and diffraction. Then the results of SWAN were used as wave data inputs into the XBeach model to simulate nearshore currents.

6.3. Methodology

Similar to the wave simulation discussed in Chapter 4, Okains Bay was chosen to study the numerical modelling of near shore currents. The study area was defined as being 4 km in the cross-shore direction and 3 km in the longshore direction (Figure 4.3b). The bathymetry of Okains Bay is also shown in Figure 4.3c. The XBeach model (version v1.20.3606, released in 2014) was applied to examine the current system inside the bay during different wave conditions.

The first part of this study was to validate the results of XBeach with observations recorded at sites O2, O3, O4 and O5 during all three field experiments, discussed earlier in Chapter 5. The model was run with the same time step of all field experiments. The spin-up time of one tidal cycle was applied for the simulations. The duration of the simulations was the same as Field

Experiments 2 and 3; however, it was only the first eleven days for Field Experiment 1 as XBeach can be run for a maximum of eleven days. The reason that the first eleven days was chosen was that the maximum of the tidal range during the full moon and the minimum of the tidal range during a new moon was recorded during this period. Also throughout this period, a variation of wave heights and directions were collected.

SWAN wave data were used as an input to the XBeach model to simulate nearshore currents in Okains Bay. As discussed in Chapter 4, SWAN was used to simulate waves inside the bay using the observations recorded at site O1. The results of SWAN for each field experiment was then used as an input to XBeach model in order to improve the accuracy of predicted currents inside the bay. Uniform and rectangular grids were chosen for these simulations. The grid configuration used in this model is shown in Table 6.1.

After the validation of the model, three scenarios were considered to better understand the current system under incident waves and tides. As shown in Table 6.2, the first category was used to examine how the current system could change inside the bay according to incident wave directions. The purpose of the second category was to evaluate the effect of tides on the current system during low energy waves. Water elevation as a separate input file was added to the Xbeach. These water elevations were hourly data and obtained from the ADCP at site O3. Note that in this study waves below 0.5 m in height at a depth of 12 m were considered as low energy waves and waves above 2 m height were considered as high energy waves. The third category was used to examine whether tides could prevail over high energy waves to generate currents when waves approach at an angle close to the longshore direction.

Table 6.1. Configuration grid for XBeach simulations.

Simulation duration	Grid description	Grid (Easting x Northing)	Cell grid size (m)	
			dx	dy
20/April/2011 to 01/May/2011	small resolution grid	80 x 60	50	50
19/December/2011 to 22/December/2011	small resolution grid	80 x 60	50	50
3/April/2011 to 13/April/2011	small resolution grid	80 x 60	50	50

Table 6.2. Summary of the 2D XBeach experiments in Okains Bay.

Category number	Description	Number of simulations	Wave height (m)	Wave direction (degree)	Purpose
1	Wave direction effect on currents	3	2	Normal, 45° and 315°	To examine the effect of wave direction on current system
2	Tides controlling currents	3	0.3	Normal, 45° and 315°	To examine the effect of tides on current system during low energy waves
3	Waves directions versus tides in controlling currents	3	2	45° and 60°	To examine if tides mainly control currents when waves approach close to a longshore direction

SWAN was used first to simulate waves inside the bay for each scenario using the same model configuration explained in Chapter 4. Each simulation lasted 12 hours to cover approximately a tidal cycle. Afterwards, the simulated waves were used as an input to the XBeach to simulate the current system. The tidal range for all simulations was 2 m relative to mean sea level. Note that XBeach is a 2D model and currents are averaged over depth.

6.4. Numerical modelling of the current system inside Okains Bay

XBeach was applied to Okains Bay to remap the current system inside the bay during different sea conditions and tidal stages. In this study, XBeach results were first validated against observations recorded during three field experiments in Okains Bay. Afterwards, the current system was analyzed via simulations run with different approaching wave directions. The importance of tides on currents was also assessed, especially inside the surf zone.

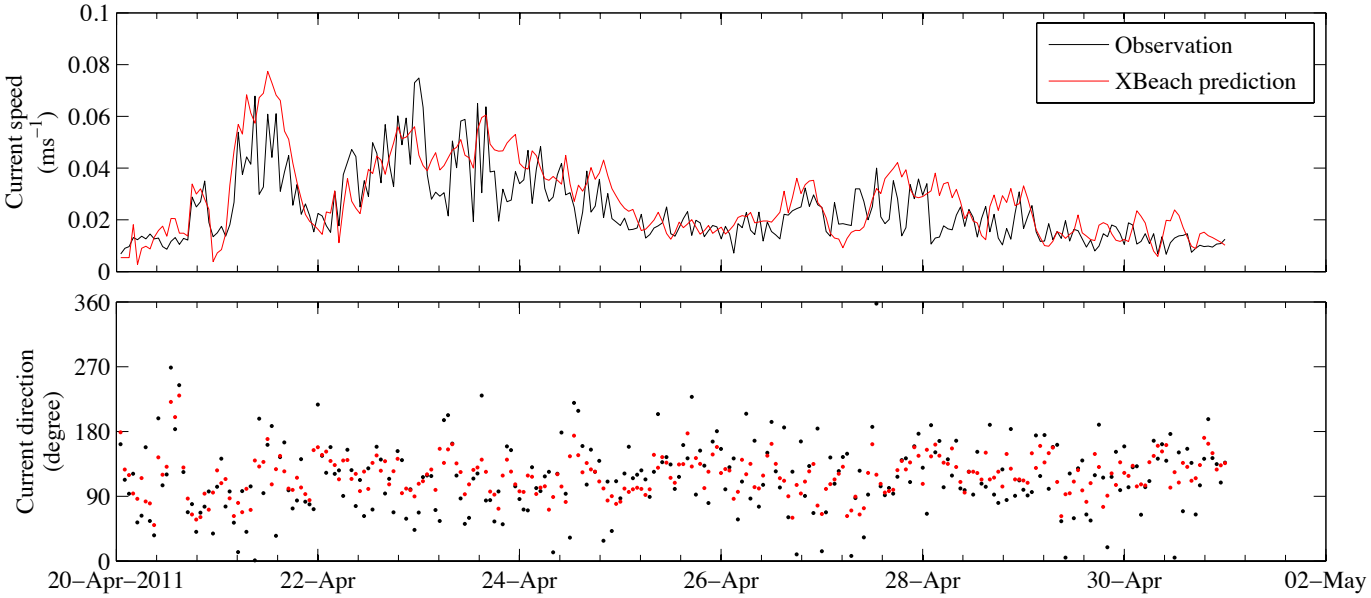

Figure 6.1. Time series comparison between observed versus XBeach simulated currents for site O3 during the first eleven days of Field Experiment 1.

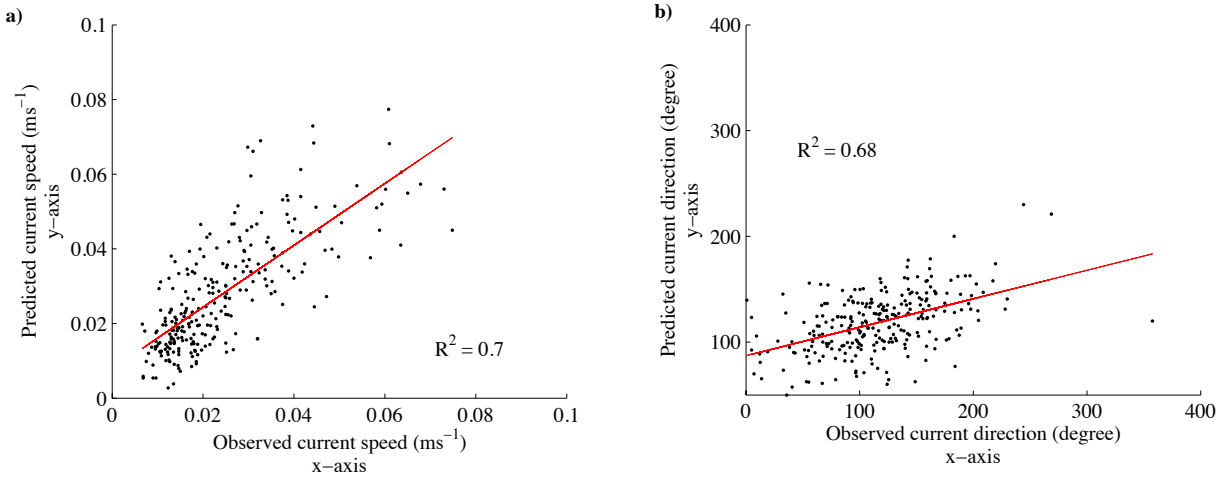

Figure 6.2. Scatter plots of current speeds (a) and directions (b) generated by observations versus XBeach predictions for site O3 during the first eleven days of Field Experiment 1.

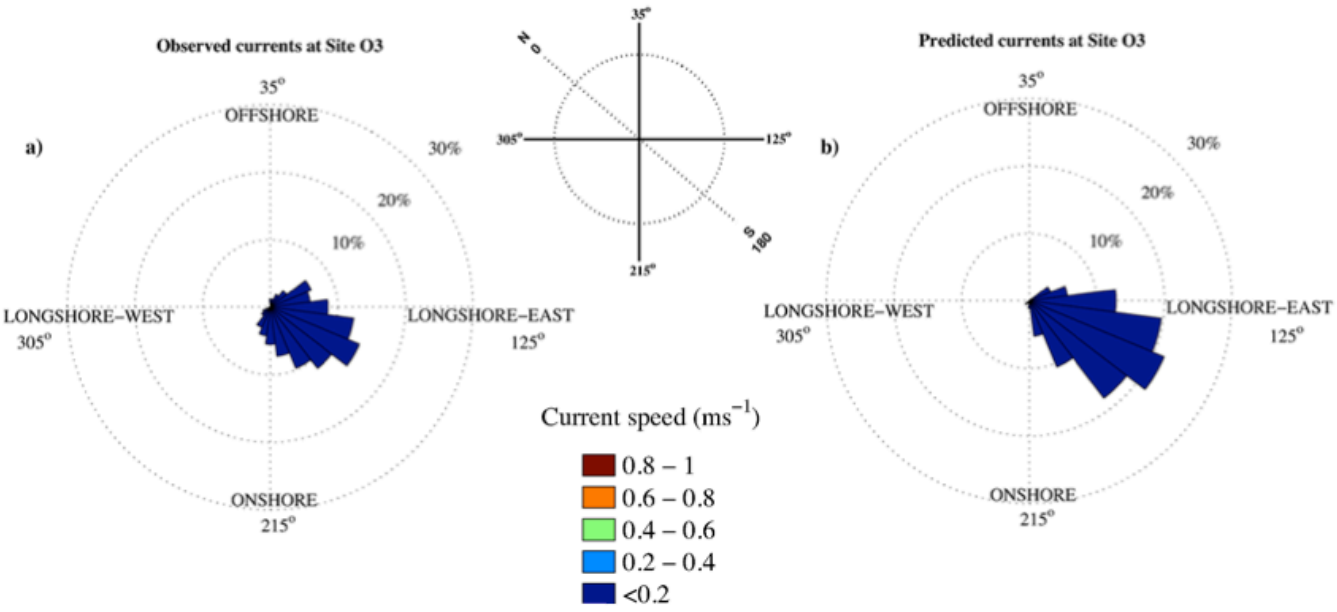

Figure 6.3. Rose plots showing current speed and directions generated by observations and XBeach predictions at site O3 for the first eleven days of Field Experiment 1.

Table 6.3. Comparison of IOA, MAE, R^2 and p-value of observed versus predicted currents for sites examined during Field Experiment 1 to 3.

Field Experiment	Site	IOA (speed)	MAE (speed)	R^2 (speed)	p-value (speed)	IOA (dir)	MAE (dir)	R^2 (dir)	p-value (dir)
1	O3	0.84	0.012	0.7	0.007	0.7	31.12	0.68	0.01
2	O2	0.9	0.032	0.8	0.004	0.89	25.11	0.79	0.006
2	O4	0.87	0.011	0.69	0.043	0.79	28.6	0.67	0.029
2	O5	0.91	0.25	0.71	0.023	0.62	38.4	0.69	0.011
3	O3	0.83	0.018	0.69	0.032	0.86	27.6	0.77	0.008
3	O5	0.8	0.035	0.67	0.047	0.79	23.38	0.61	0.044

6.4.1. Validation of XBeach predictions versus observations

The first eleven days of Field Experiment 1 were chosen to validate the results of the model at site O3. During this period, the current speeds varied between the weakest (0.027 ms^{-1}) and strongest currents (0.078 ms^{-1}) observed in this study. The tidal ranges also varied between 1.35 m during the new moon and 2.19 m during the full moon. As depicted in Figure 6.1, XBeach slightly overestimated the current speeds, but the trends in the predicted current strengths and directions were similar to the observations. A linear correlation between the XBeach results and field observations at site O3 produced an R^2 value of 0.7 (Figure 6.2a). As shown in Table 6.3, the Index of Agreement (IOA) and Mean Absolute Error (MAE) calculated for the predicted and observed currents were 0.84 and 0.012 respectively. Note that since XBeach is a 2D model, it uses depth-averaged currents, while the observed currents were collected from a distinct point close to the bed. Therefore, it is expected that there would be some level of discrepancy between predictions and observations. Despite this, results indicate that XBeach can reasonably simulate the currents at site O3 inside Okains Bay using input wave data from the SWAN model.

Current directions at site O3 could also be reasonably estimated using XBeach. In contrast to current speed, XBeach was found to slightly underestimate the current directions (Fig 6.1). This reduced the range of predicted current directions compared to the observations, thereby producing an increase in the frequency of particular directions. As shown in Figure 6.3, predicted current directions were predominantly moving towards 155° followed by 145°, which matches the observed directions, but with higher frequencies. The frequencies of predicted directions for angles between 215° and 245° were considerably reduced.

Linear regression analysis revealed a correlation between current directions predicted via XBeach versus observations at site O3 with an R^2 of 0.68 (Figure 6.2b). IOA and MAE calculated for the predicted versus observed wave directions were 0.7 and 22.12 respectively (Table 6.3), suggesting that XBeach can reasonably estimate current direction at site O3. As with current speed, XBeach uses depth-averaged current directions, which causes predictions to differ slightly from observations.

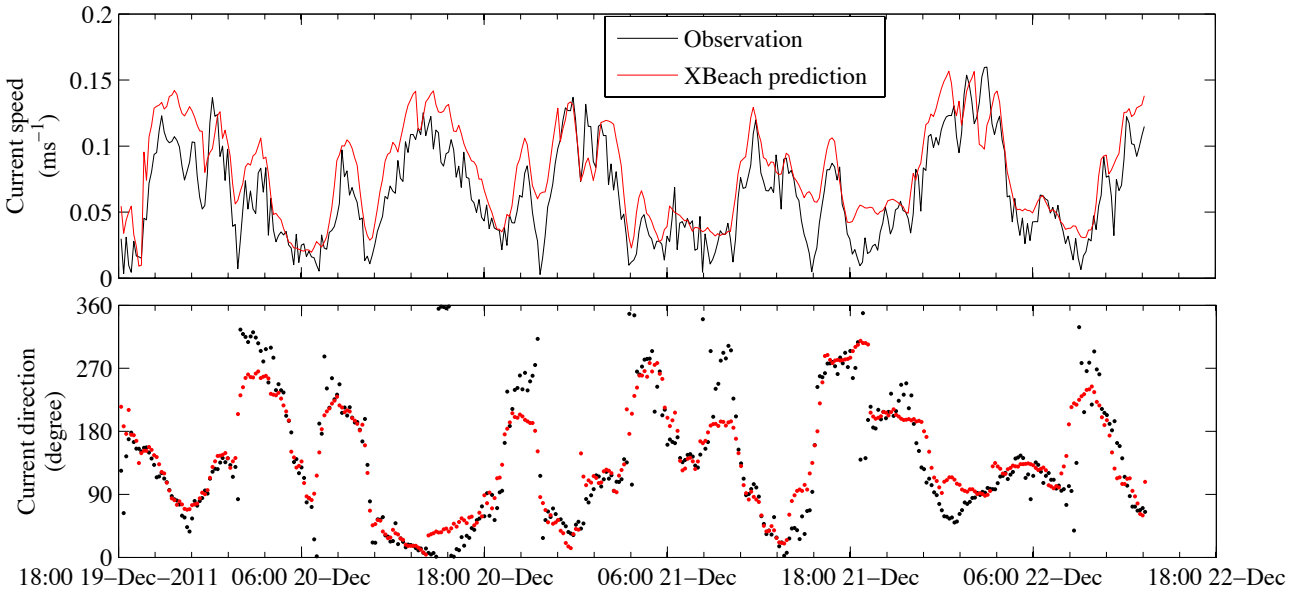

Figure 6.4. Time series comparison between observed versus XBeach simulated currents for site O2 during the first eleven days of Field Experiment 2.

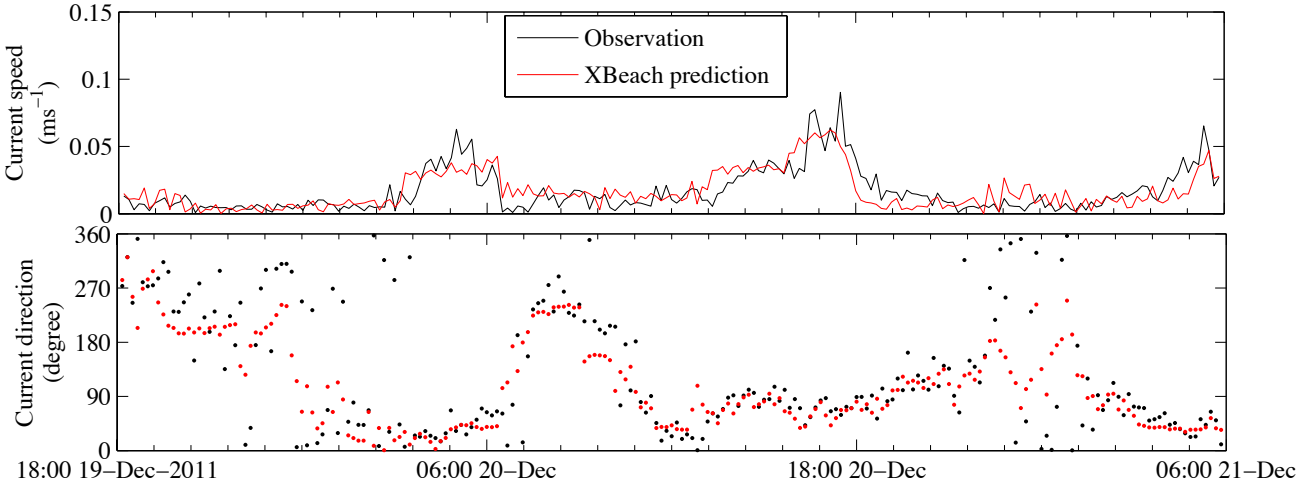

Figure 6.5. Time series comparison between observed versus XBeach simulated currents for site O4 during the first eleven days of Field Experiment 2.

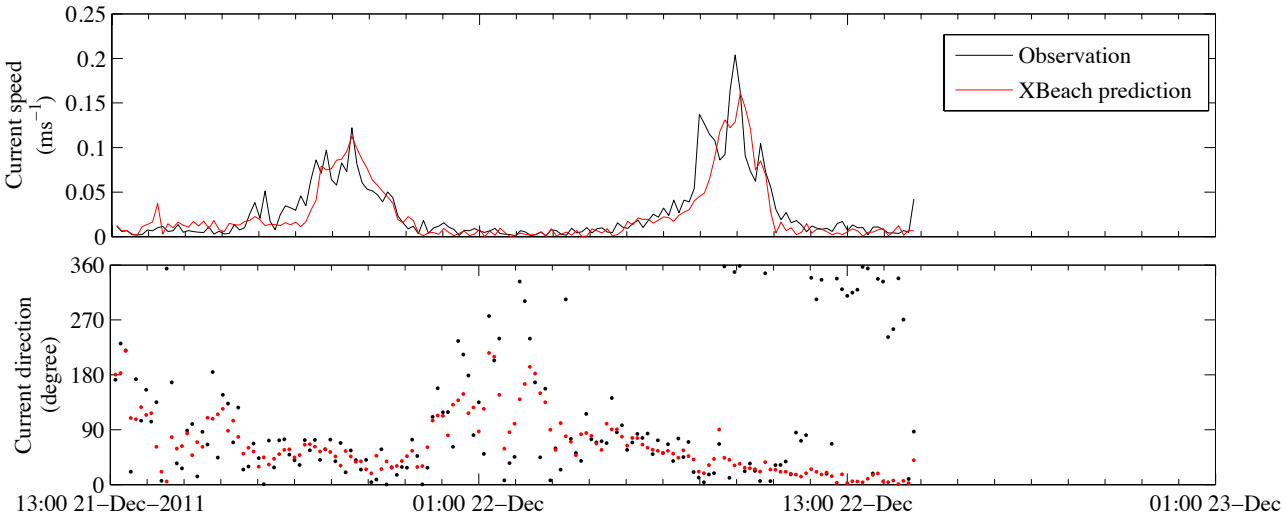

Figure 6.6. Time series comparison between observed versus XBeach simulated currents for site O5 during the first eleven days of Field Experiment 2.

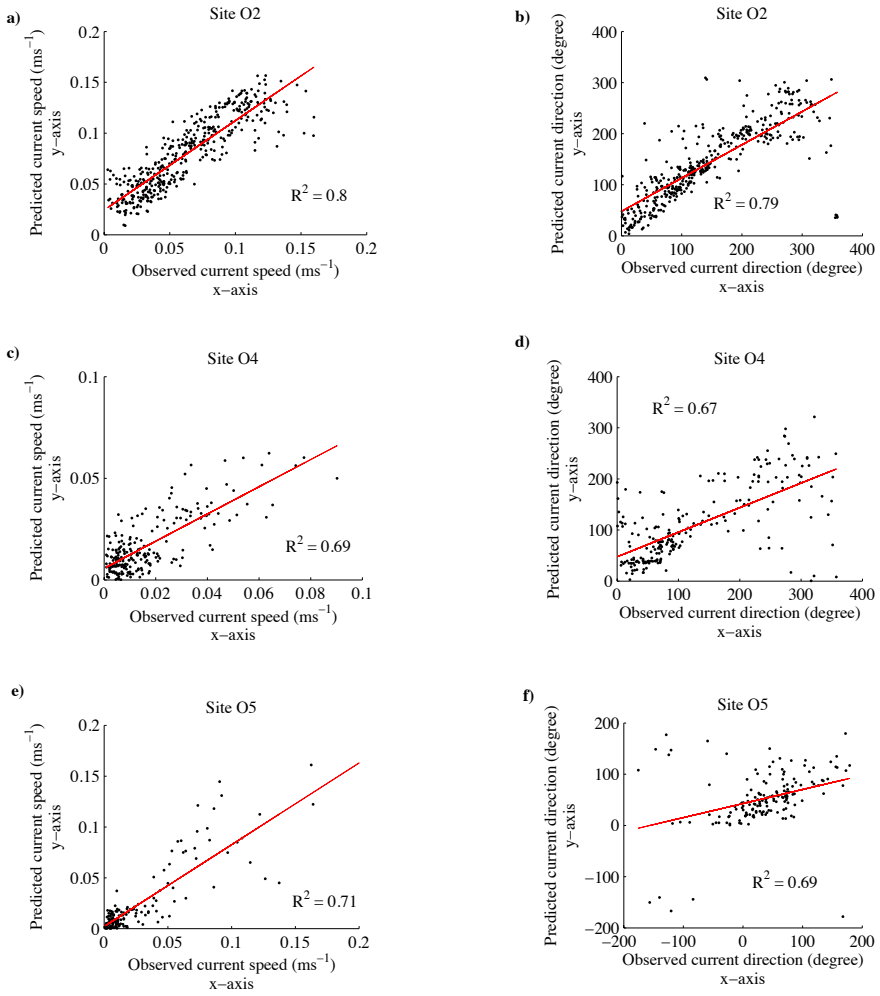

Figure 6.7. Scatter plots of predicted current speeds (a, c and e) and directions (b, d and f) observed in the field versus predicted using XBeach for sites O2, O4 and O5 during Field Experiment 2.

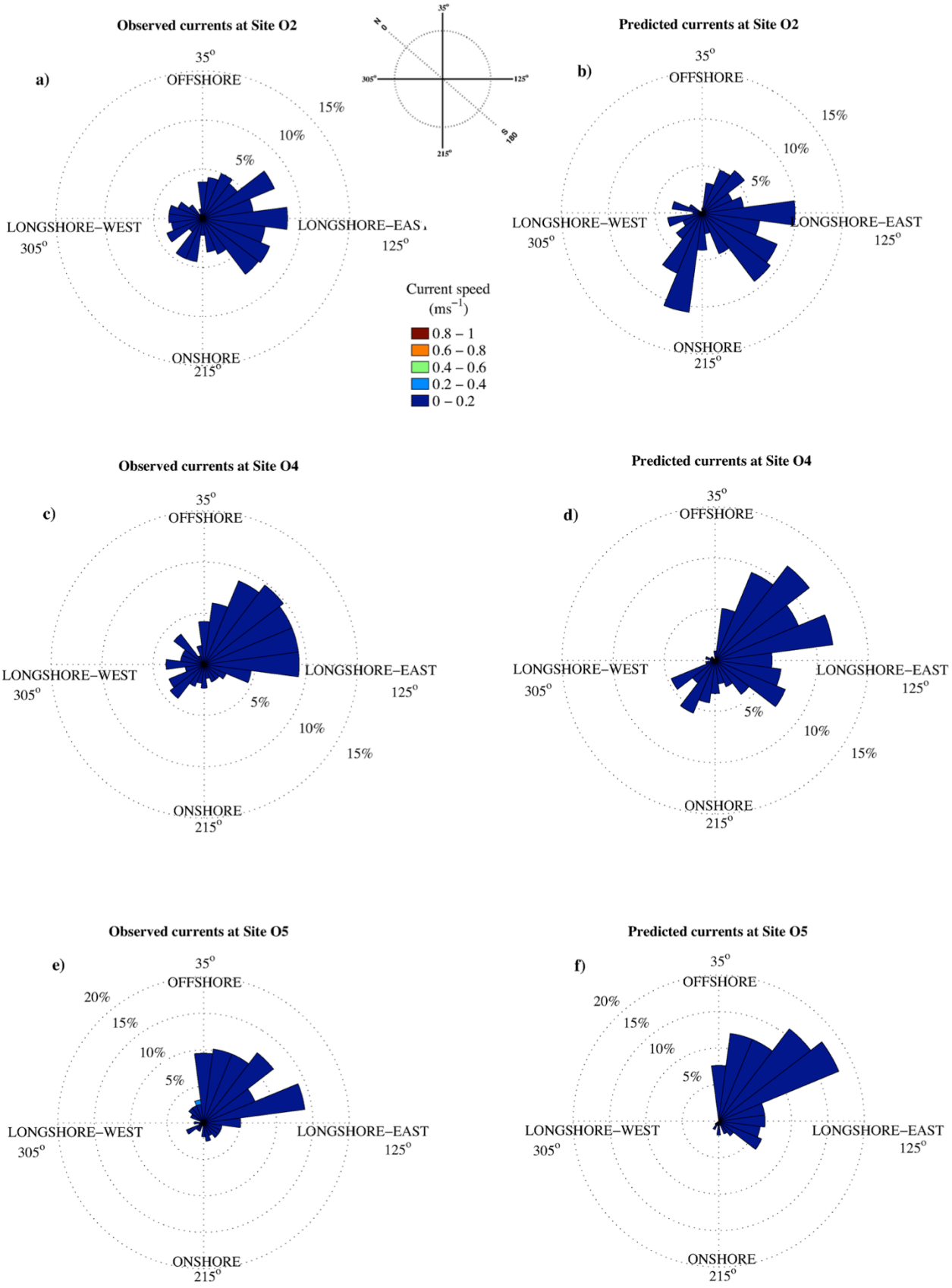

Figure 6.8. Rose plots showing current speeds and directions observed versus those predicted using XBeach for sites O2, O4 and O5 during Field Experiment 2.

Observation data from Field Experiment 2 were used to validate the results of the model seaward of the breaking zone at site O2 and also inside the surf zone at sites O4 and O5. As discussed in Chapter 5, during this short period the wave heights were small (varied from 0.2 m to 0.6 m) and tidal currents mainly influenced the nearshore currents. The tidal range was about 1.8 m when the moon was in its third quarter phase. As depicted in Figures 6.4 to 6.6, a time series analysis revealed very similar trends in both the observed and predicted current speeds and directions. Regression analysis also showed that the predictions reasonably correlated with observations at sites O2, O4 and O5 (Table 6.3 and Figure 6.7). IOA and MAE, calculated for the predicted and observed current speeds at each site are shown in Table 6.3. From the comparisons and statistical analysis, it can be inferred that XBeach was found to reasonably produce the current speeds for areas seaward of the breaking zone and also inside the surf zone.

Predicted current directions were found less accurate than the predicted current speeds (Fig 6.8). This consequently reduced the range of predicted current directions compared to observations, so the frequency for some directions increased. Although this increase can be seen clearly in Figure 6.8, the predominant directions of predicted currents were similar to those of the observations. For instance, XBeach was found to overpredict directions between 215° and 245° for site O2, and to underpredict directions between 305° and 360° for site O4, and between 215° and 345° for site O5. That is because XBeach uses depth-average calculations, whereas observations were obtained from a distinct depth of water. However, this discrepancy between observations and predictions was expected.

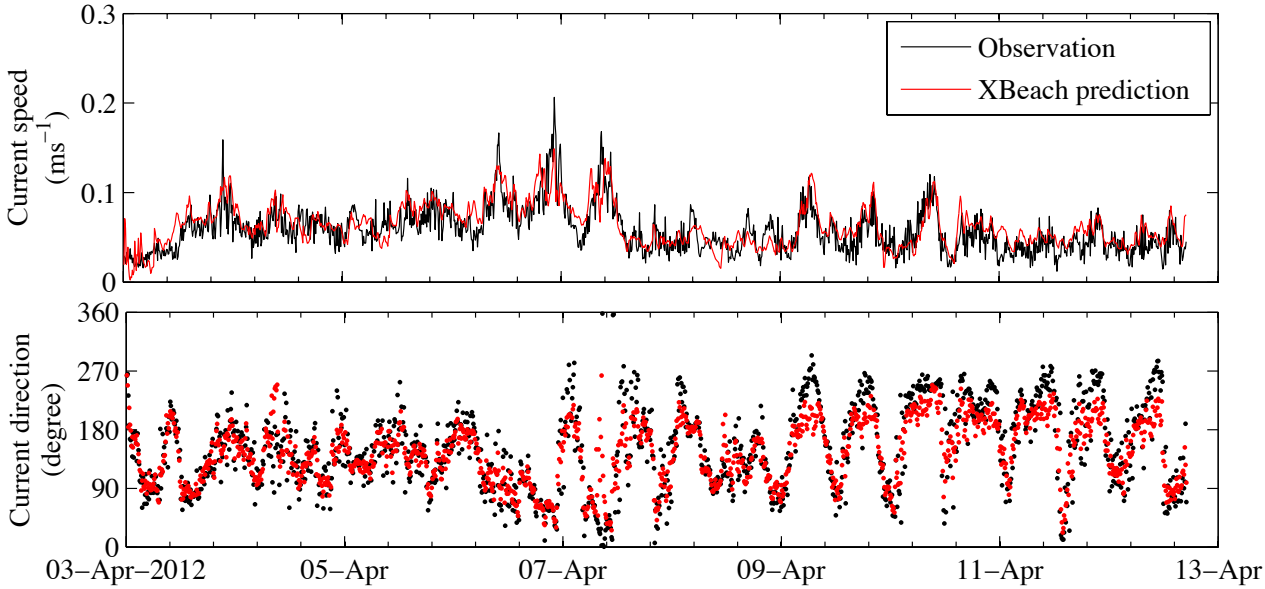

Figure 6.9. Time series comparison between observed versus XBeach simulated currents for site O3 during the first eleven days of Field Experiment 3.

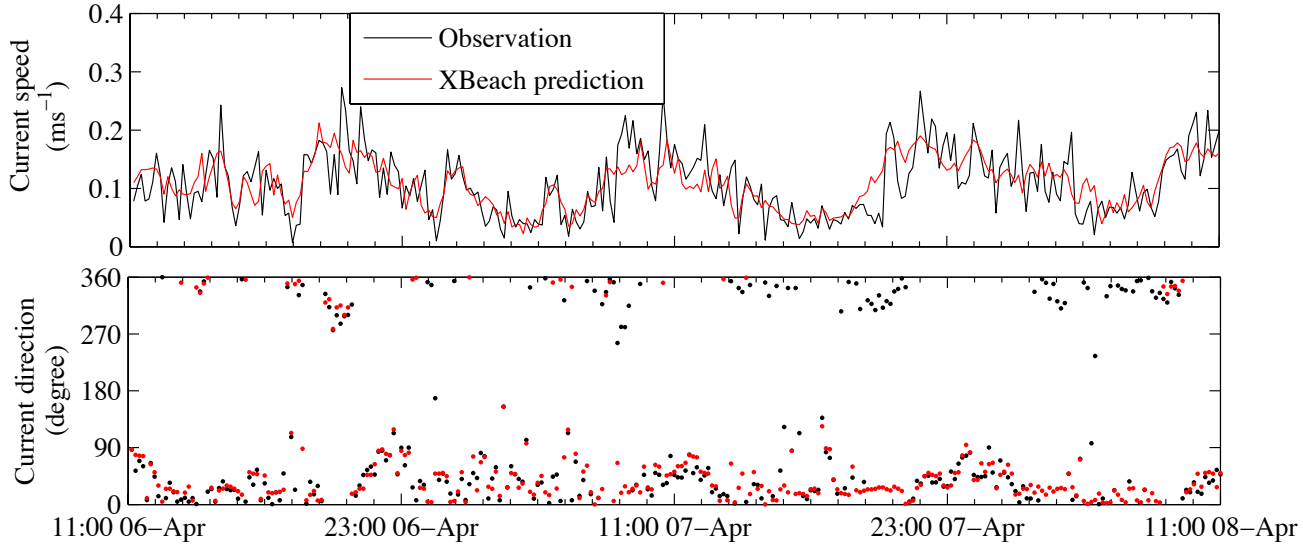

Figure 6.10. Time series comparison between observed versus XBeach simulated currents for site O5 during the first eleven days of Field Experiment 3.

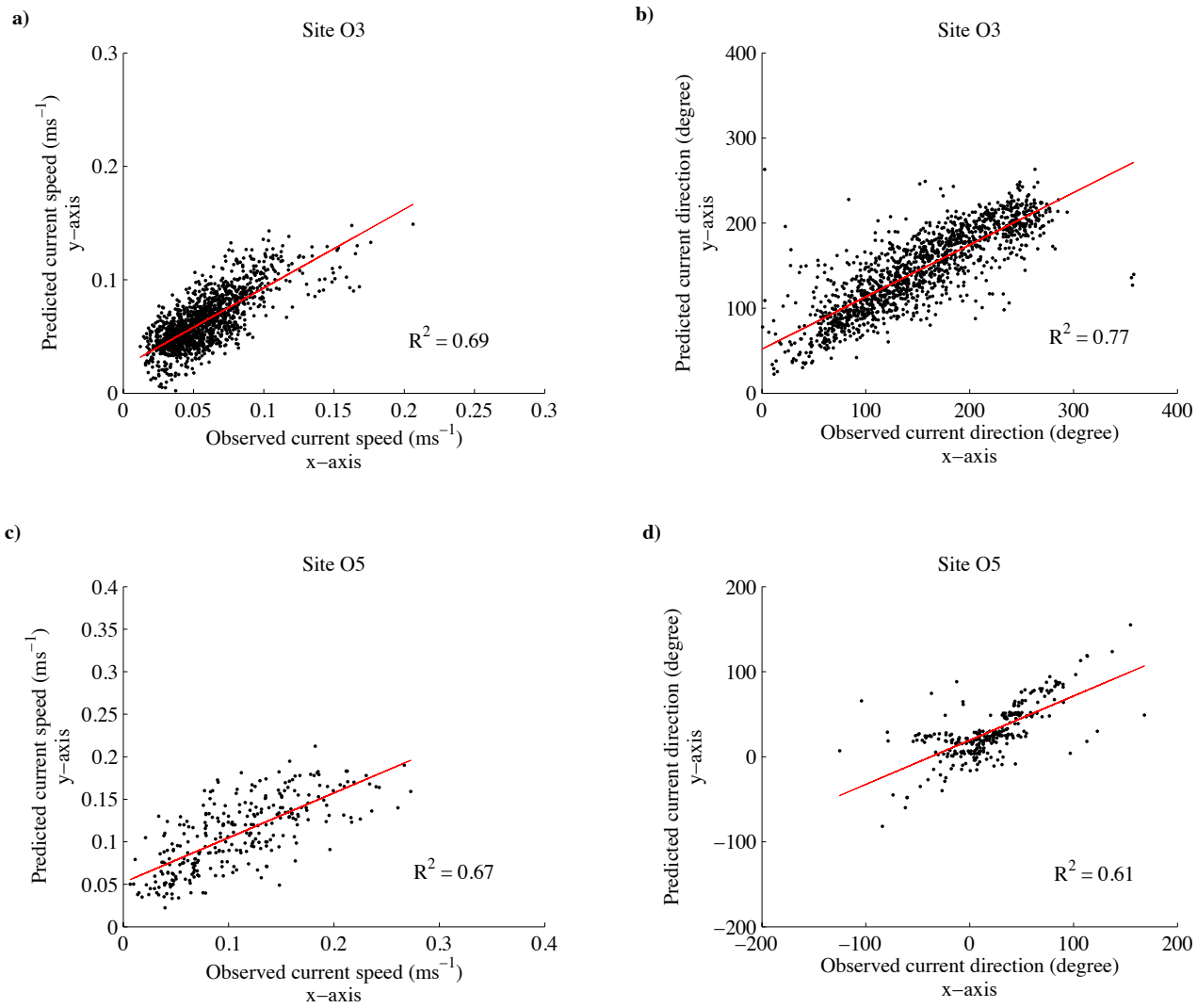

Figure 6.11. Scatter plots of predicted current speeds (a and c) and directions (b and d) observed in the field versus predicted using XBeach for sites O3 and O5 during Field Experiment 3.

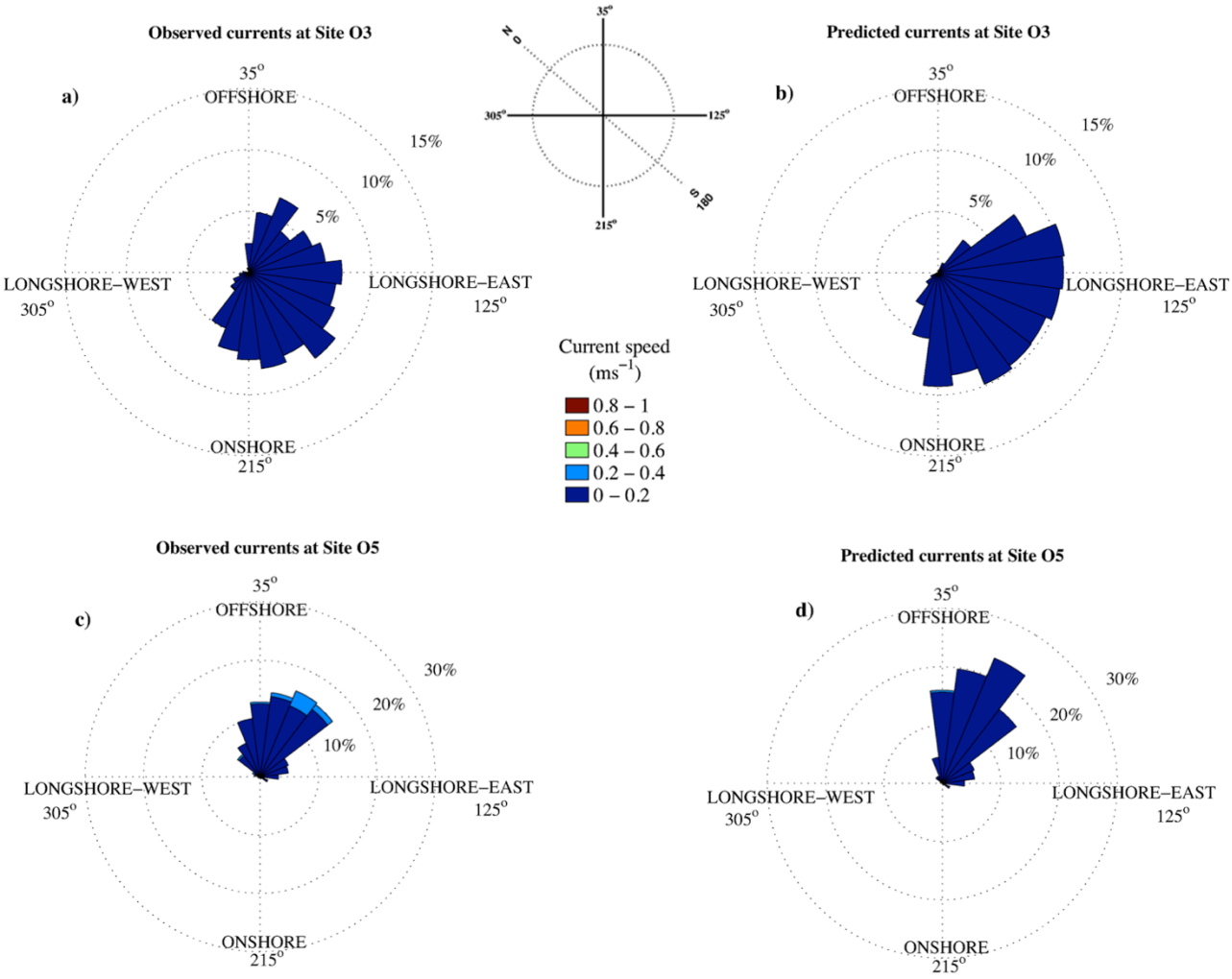

Figure 6.12. Rose plots showing current speeds and directions observed versus those predicted using XBeach for sites O3 and O5 during Field Experiment 3.

The results of the model were also validated against observations recorded during Field Experiment 3 for sites O3 and O5. As discussed in Chapter 5, the wave heights were higher inside the bay, particularly inside the surf zone, compared to during the previous two field experiments. The tidal range varied between about 1.8 m, when moon was in its third quarter phase, and 2.2 m during the full moon. As depicted in Figures 6.9 to 6.10, time series analysis shows that the trend in the predicted current speeds was similar to that of the field observations. Regression analysis shows that the predictions were correlated to observations at sites O3 and O5 with R^2 values of .69 and 0.67 respectively (Figures 6.11a and c). IOA and MAE, calculated for the predicted and observed currents at each site, are shown in Table 6.3.

From the comparisons and statistical analysis, it can be inferred that XBeach can reasonably remap the current speeds for areas seaward of the breaking zone and also inside the surf zone, when wave heights are relatively high, especially inside the surf zone.

Current directions at these sites were reasonably estimated using XBeach. The comparison of predicted current directions and observations showed that XBeach predictions correlated to observations at sites O3 and O5 with R^2 values of 0.77 and 0.61 respectively (Table 6.3 and Figure 6.11b and d). IOA and MAE calculated for the predicted and observed wave directions are shown in Table 6.3. Similar to the predictions during Field Experiments 1 and 2, XBeach tended to slightly underestimate the higher current directions (Figs 6.9 and 6.10). This caused the range of predicted current directions to be reduced relative to that of the observations. Therefore, the results of XBeach showed that predicted currents more frequently moved in lower directions. This increase in the frequency of low angle current directions can clearly be seen in Figure 6.12, but the predominant directions of predicted currents are similar to those of observations. Note that the aim of this study is not to accurately predict currents, but to improve the general knowledge of current systems in pocket beaches. Since the trends of observations and predictions are very similar and also predicted currents reasonably correlated to observations, XBeach can be used to reliably simulate the current circulation inside the bay during different sea conditions and tidal ranges.

As discussed earlier, since XBeach uses depth-average currents and the observations were measured at a distinct depth of water, this discrepancy between observations and predictions was expected. These suggest that current speeds and directions could vary considerably from lower levels of water depth to the surface. Therefore, the mass transport near the bed currents could be offset by surface water. Local winds could be one main reason why current speeds and directions changed at different levels of water column. When winds blow, the surface currents begin to change (see Dalrymple *et al.*, 2011; Hequette and Hill, 1993). However, these changes in surface currents could not reach or considerably change the currents close to the bed, depending on the water depth and the strength of local winds.

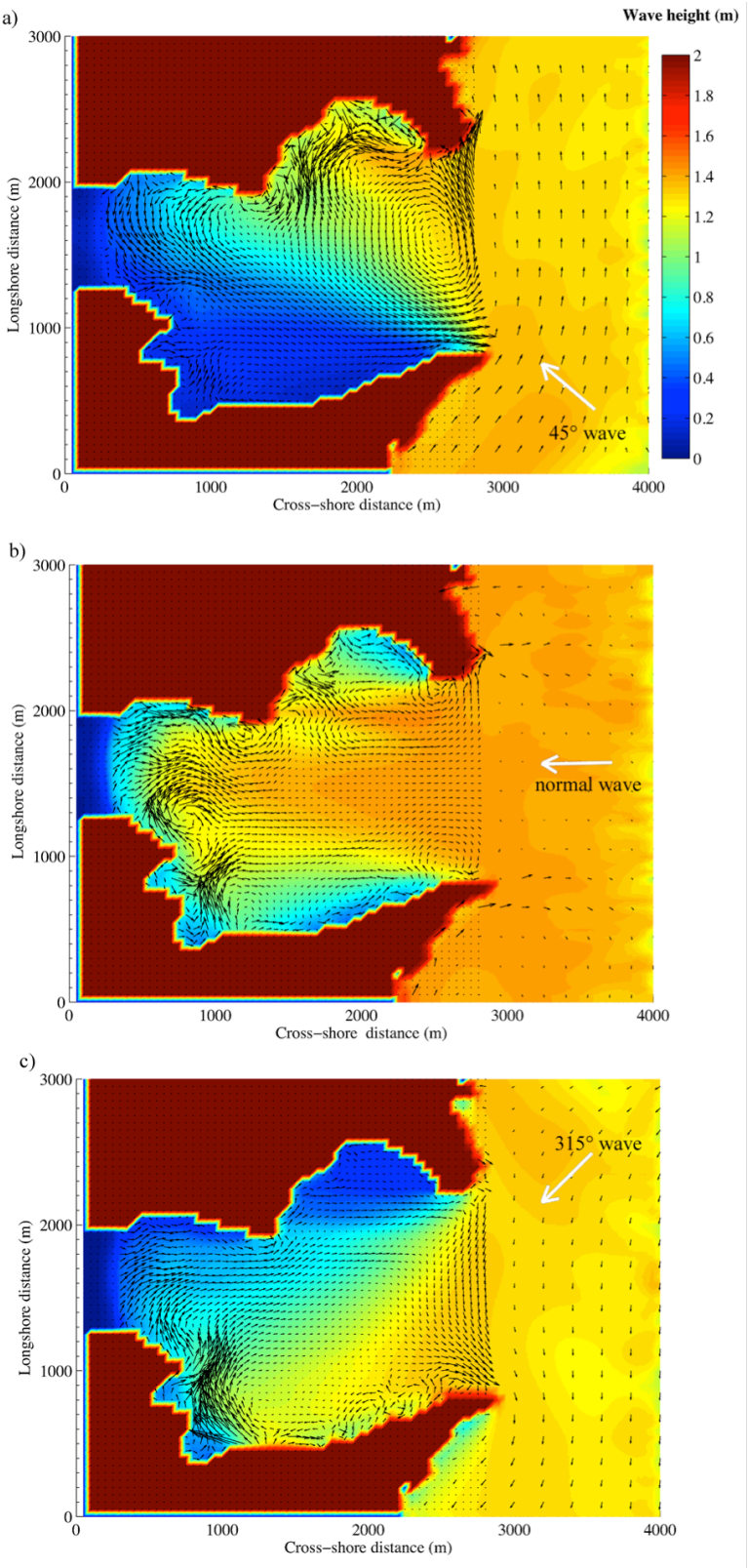

Figure 6.13. Comparison of XBeach simulated current systems inside Okains Bay when a 2 m height wave approaches from angles of 45° (a), normal (b) and 315° (c) to the central bay shoreline (shown by a while arrow). The black arrows indicate the current directions (arrow length = current velocity). Land is also shown in red. The simulations were during flood currents. Note that more arrows were used inside the bay to clearly show the current circulations inside the bay relative to current circulation outside the bay.

6.4.2. Analysis of current systems inside Okains Bay

In order to better understand the current systems that exist inside Okains Bay during different incident wave conditions, XBeach was run for seven cases in three categories (see Table 6.2). The purpose of the simulations in the first category (XBeach Experiment 1) was to determine how the current system inside the bay could change according to different wave approach directions. Results indicated that when waves approached from the upcoast headland at an angle of 45° to the central bay shoreline, currents tended to move towards the shoreline in proximity to the downcoast headland (Figure 6.13a). Then, they gradually turned towards a longshore direction inside the surf zone and moved towards the upcoast headland. Finally, in areas close to the upcoast headland the currents headed in an offshore direction and formed a rip current or 'toporip'. This current system is similar to the cellular current system described by Short (1999) for headland enclosed bay beaches. As depicted in Figure 6.13a, the currents seaward of the breaking zone were relatively weak compared to inside the surf zone and moved towards a seaward direction in proximity to the upcoast headland. In areas close to the bay mouth, the currents became stronger again.

However, when approaching waves came from a shore normal direction, the current system completely changed inside the surf zone. Cross-shore currents were formed in areas close to the upcoast headland, moving towards the shoreline (Figure 6.13b). They gradually turned to a longshore direction, which was opposite to the direction of the currents when incident waves approached from 45° to the central bay shoreline. Currents then turned to an offshore direction in the center of the shoreline and formed a rip current similar to the findings of Loureiro *et al*. (2012). A toporip also formed in proximity to the downcoast headland. The reason why longshore currents moved from the upcoast to the downcoast headland could be due to the non-uniform depth contours (Figure 4.3b) and the geometry of the bay, especially due to the asymmetric headlands. Similar to the previous experiment, currents in deeper areas seaward of the surf zone moved in an offshore direction. These currents were relatively weak compared to the surf zone currents.

When incident waves approached at an angle of 315° to the central bay shoreline, the currents inside the surf zone were fairly similar to when simulated waves approached at a normal angle. Although the downcoast headland sheltered a large area inside the surf zone from incident waves, the effect of waves played a key role in controlling the current system. Wave-driven currents moved in a cross-shore direction towards the shoreline in proximity to the upcoast

headland (Figure 6.13c). Then they gradually turned towards a longshore direction, moving towards the downcoast headland. In deeper areas inside the surf zone, longshore currents turned towards an offshore direction in the centre of the shoreline to form a rip current. However, in shallower surf zone areas, longshore currents moved towards the downcoast headland to form a toporip. In this experiment, the current system resembled that when waves approached normally, except that the rip current and toporip were weaker.

The results of XBeach Experiment 1 confirm that variations in the wave height inside the surf zone of Okains Bay are the main driver of the formation of longshore currents. When waves approach oblique to the central bay shoreline, they cannot equally propagate across the entire bay due to headland sheltering. Therefore, wave heights across the side of the bay exposed to the incident waves are higher than across the other side (the shadow zone) (Figure 6.13a and c). This causes water to move from areas with higher waves to those with lower waves, thus forming longshore currents. Under these conditions, longshore currents formed inside the bay are always in a reverse direction to those of wave-generated longshore currents on adjacent open coasts.

During XBeach Experiment 1 the input open-coast-incident wave height was 2 m and tides had less effect on the current system inside Okains Bay. As discussed in Chapter 5, the field observations indicated that the effect of tides was accentuated when wave heights inside the bay in areas seaward of the surf zone were less than 0.3 m. The dominance of tidal currents could also be seen in the results of the model using input data from Field Experiment 2 when wave heights were small. As depicted in Figures 6.4 to 6.6, when wave heights dropped below 0.3 m, the currents at three sites inside the bay were clearly influenced by tides. In order to better understand the current system of pocket beach bays during low energy waves, XBeach Experiment 2 was carried out as summarized in the second category shown in Table 6.2.

The results of XBeach Experiment 2 showed that the current system across the entire bay was influenced by tides. The predominant current direction during one complete tidal cycle was in a cross-shore direction towards the shoreline. That is, the flood current prevailed over ebb currents inside the bay when waves were small (6.14 a to c). The results would be expected to vary in other pocket beaches with different beach slopes and geometries, particularly, headland sizes.

However, the direction of approaching waves could slightly offset the ebb currents. When waves approached at angles of 45° and 315° to the central bay shoreline (Figure 6.14a and c),

due to the headland sheltering effect, wave heights decreased considerably and reached below 0.15 m inside the bay and had less effect on flood currents. In contrast, when waves approached normal to the central shoreline, the effect of diffraction and reflection reached their minimum. Waves were only affected by shoaling and refraction, thereby losing less of their energy. In this case, wave-driven currents slightly reduced the effect of flood currents (Figure 6.14b). This raises the question of whether or not tidal currents dominate the pocket beaches only during low wave energy conditions. What if moderate to high energy waves approached at angles close to perpendicular to the headlands? To answer this question, XBeach Experiment 3 (Table 6.2) was carried out.

XBeach Experiment 3 indicates that when a high energy wave approached at an angle close to perpendicular to the upcoast headland, the bay's current system can be dominated by tides. As depicted in Figure 6.15a, when waves approached at an angle of 45°, they reached a larger area inside the bay after diffraction and reflection. As discussed earlier, waves are overall the dominant factor in controlling the current system inside the bay. However, when the waves approached at an angle of 60°, they propagated to smaller areas as diffraction prevailed over reflection (Figure 6.15b). Consequently, the current system of areas close to the entrance of the bay, which is exposed to the waves, is mainly influenced by waves. However, tides considerably influence the current system of the rest of the bay, especially the surf zone. It can be inferred that in addition to low energy waves, the effect of tides on currents could be accentuated if high energy waves approach at a large, oblique angle to the central bay shoreline.

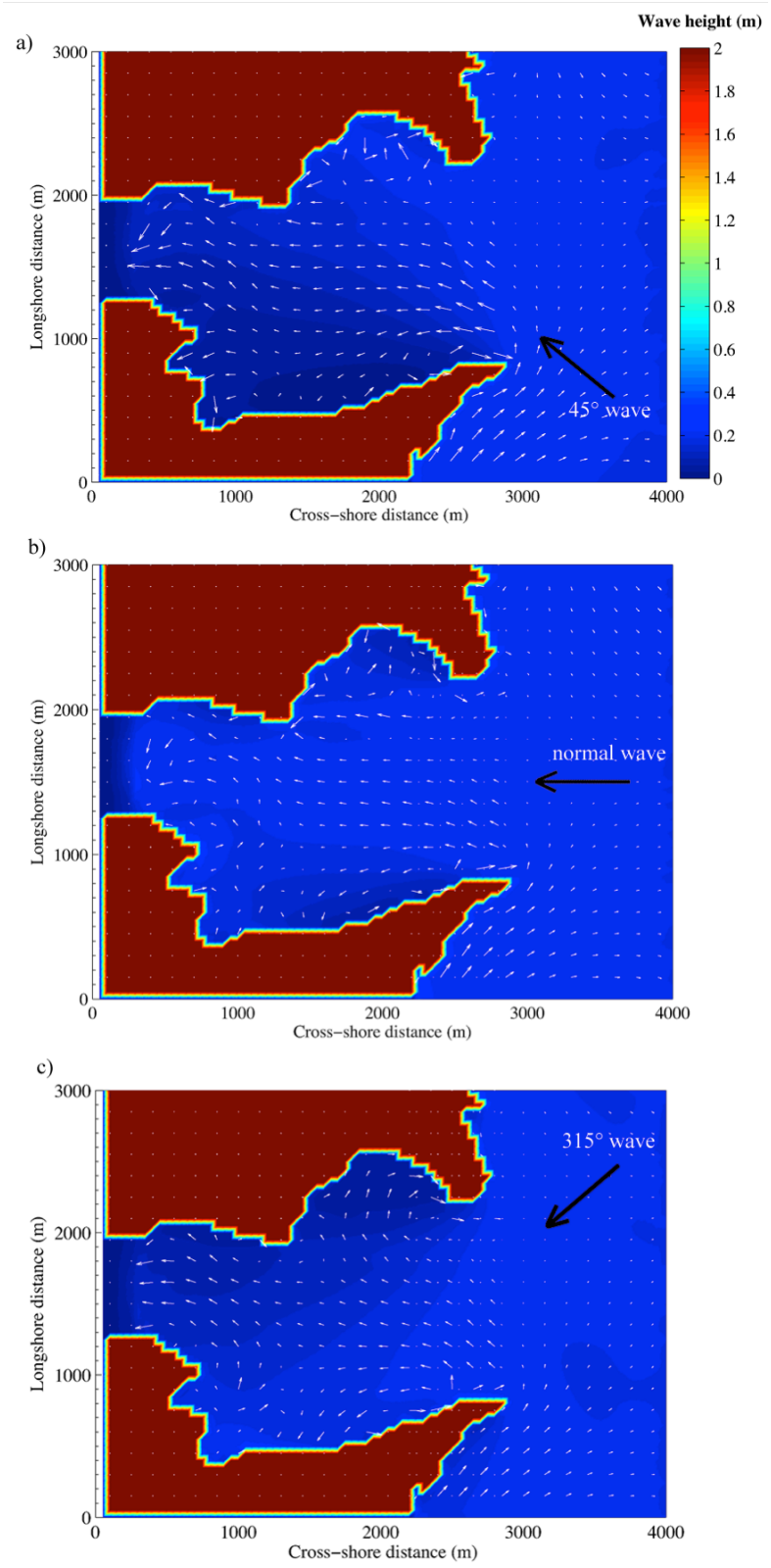

Figure 6.14. Comparison of simulated current systems produced inside Okains Bay when a 0.3 m high offshore wave approaches at angles of 45° (a), normal (b) and 315° (c) to the central bay shoreline (shown by a black arrow). The while arrows indicate the current directions (arrow length = current velocity). Land is also shown in red. The simulations were during flood currents. Note that more arrows were used inside the bay to clearly show the current circulations inside the bay relative to current circulation outside the bay.

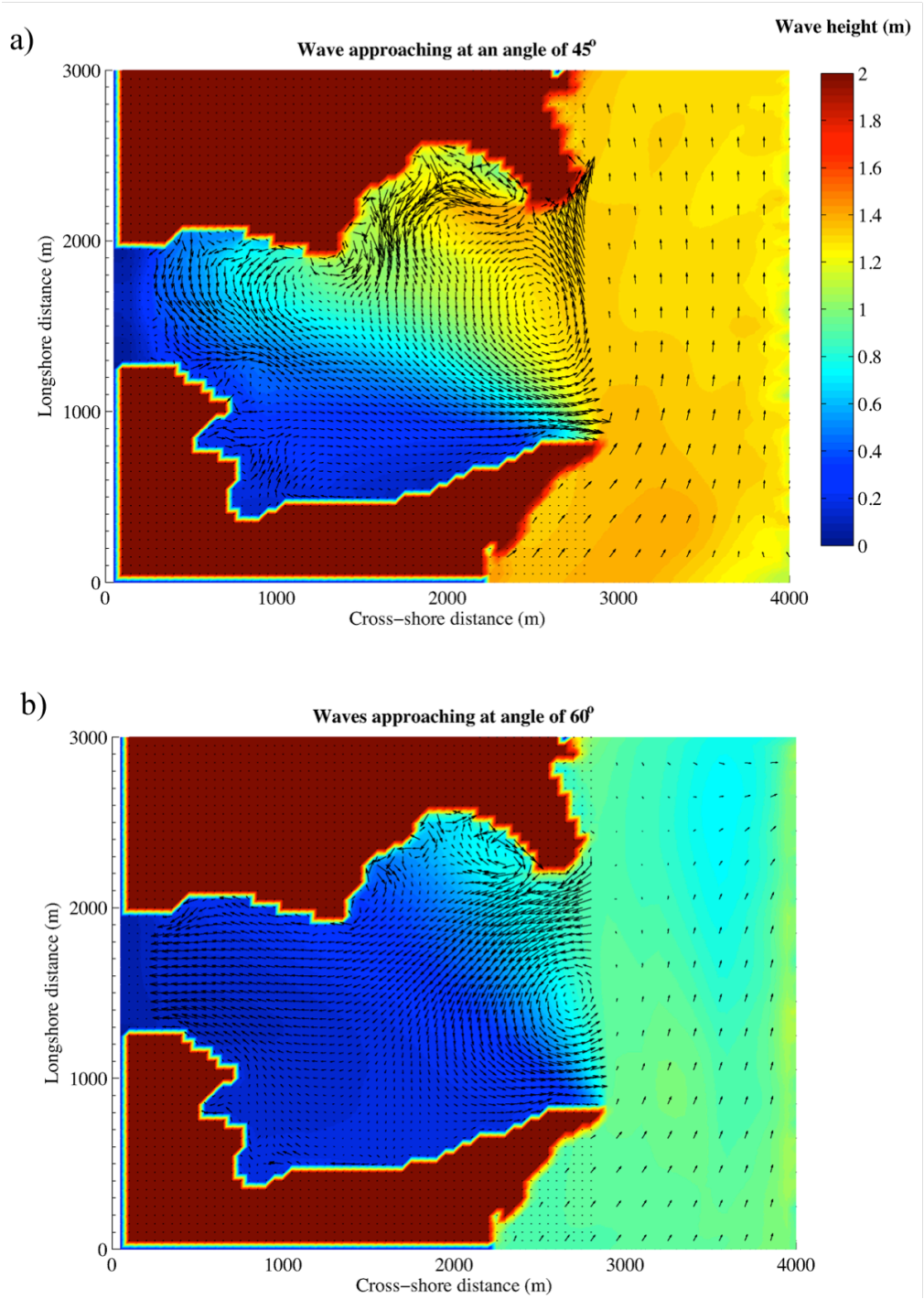

Figure 6.15. Comparison of simulated current systems produced inside Okains Bay when a 2 m height offshore wave approaches at angles of 45° (a) and 60° (b) to the central bay shoreline. The black arrows indicate the current directions (arrow length = current velocity). Land is also shown in red. The simulations were during flood currents. Note that more arrows were used inside the bay to clearly show the current circulations inside the bay relative to current circulation outside the bay.

6.5. Discussion

As discussed in Chapter 5, Short (1999) indicated a general concept for determining what sort of current circulation system existed in different headland-enclosed bay beaches based on a dimensionless embayment scaling parameter (see Eq. 5.6). In this parameter, wave direction was not taken into account, while the wave studies in Chapters 2 and 4 give evidence that incident wave directions outside the bay could notably change the wave characteristics inside the bay. Chapter 5 shows that these changes in the wave height and direction can influence the current circulation, especially the formation of rip currents in proximity to the headlands. The results of the modelling experiments detailed in this chapter showed that if currents inside the bay are mainly influenced by incident waves, changes in the wave directions are an important influence on the current system.

Model results showed that during high energy waves, when waves approach oblique or normal to the central bay shoreline, the current system consists of a longshore current influenced by headlands and a rip current in the center of the shoreline or toporips in proximity to headlands. These results are similar to the findings of Short (1999), and Castelle and Coco (2012). This study showed that the current system within a bay, especially, the location of the rip current or toporip varies based on the direction of waves, while wave direction is not taken into account as a dimensionless embayment scaling parameter introduced by Short (1999).

However, if approaching wave directions increase to an angle close to perpendicular to the headlands, the dependancy of the pocket beach current system on incident waves appears to markedly decrease. There is a corresponding increase in the effect of tides on the current system and this effect can be accentuated in the surf zone and shallower depths. As discussed in Chapter 4, when wave approach angles increase, waves become mainly diffracted inside the bay, thereby losing considerable energy. The effect of reflection also reduces, so waves are reflected to a smaller area inside the bay. Accordingly, the wave heights inside the bay decrease dramatically, and the influence of tides gradually increases to the point where they are the main factor in generating pocket beach currents.

The feature that tides prevail over waves in generating currents under certain conditions makes pocket beaches different from adjacent open coast beaches. Since there is no dominant headland or obstacle in open coast beaches, high energy waves approaching from a wide range of angles can reach the shoreline, allowing waves to persist as the main factor in generating currents. Accordingly, changes in wave directions are unlikely to increase the tide

range parameter, RTR, (discussed in Chapter 5) to the point where tides can dominate the area. However, in pocket beaches, if waves approach at angles greater than pocket beach direct wave approach sector, wave heights decrease notably inside the bay as a result of diffraction. Therefore, RTR could increase to a level that tides will dominate the area. Note that in embayed beaches if waves only approach from the upcoast headland, tides could prevail over waves in generating currents inside the bay.

Field and model results showed that during low energy waves, the current systems are mainly driven by tides in micro-tidal pocket beaches. The results of this study indicate that currents predominantly moved towards the shoreline when incident wave heights outside the bay were retatively small regardless of the wave approach directions. This suggests that flood currents prevail over ebb currents in Okains Bay. This could also be the case for other dissipation pocket beaches with two headlands that are almost twice as large as the shoreline. When the wave heights increase and also waves approach at angles close to normal to the central bay shoreline, the effects of tides on currents decrease. This reduction starts in areas close to the entrance of the bay where the pocket area is exposed to incident waves and then it eventually moves towards the shoreline and the shadow zone.

It can be concluded that in pocket beaches where waves predominantly approach from angles close to perpendicular to the headlands, tidal currents will be the main factor in controlling the current system and, consequently, beach morphology. However, more studies are needed to evidence the relationship between the pocket beach current system identified in this thesis with geomorphic and sediment transport processes.

6.6. Conclusion

This chapter focused on the numerical modelling of current systems in a micro-tidal pocket beach setting. A combination of SWAN and XBeach simulations were used to numerically examine the importance of tides and incident waves as driving processes of nearshore current systems. In this study, the results of XBeach were first validated against field obvservations. Then XBeach was used to simulate three scenarios in Okains Bay to better understand the effect of wave directions on current systems. The results were also used to examine if tides could function as an important influence on the currents inside the bay during the absence of high energy waves.

The results of XBeach were compared to the observations at sites O2, O3, O4 and O5 inside Okains Bay. The model was run for three field experiments as discussed in Chapter 5. In order to consider wave reflection and diffraction, the SWAN model was first applied to simulate waves inside the bay. Then the results were used as an input to the XBeach model to simulate currents. Since XBeach is a 2D model, it is designed to average the currents over the depth of the water column. This understandably causes the correlation between model results and observation to be slightly less than if it was a 3D model. However, comparisons between the results of the model and observations indicated that XBeach can reliably predict the current systems inside Okains Bay under different wave conditions and tidal ranges.

The second part of this chapter discussed the importance of wave direction and tides on the current system inside the bay. Three scenarios shown in Table 6.2 were used to examine: a) how the current system could change based on incident wave direction, and b) under what conditions the current system would be influenced mainly by tides versus waves. The results showed that when high energy waves approach oblique to the central bay shoreline, a longshore current is generated in an opposite direction to what would be the case for wave-generated longshore currents in open coast beaches. This current moves from one side of the bay to the other and forms a toporip in proximity to upcoast or downcoast headlands. However, if waves approach normally, a longshore current forms a rip current in the centre of the shoreline.

This study has found that inside pocket beaches, such as Okains Bay, the current system is mainly influenced by tides during low energy wave conditions. The results showed that if waves approached oblique to the central bay shoreline, wave heights considerably decreased owing to diffraction and reflection. However, if waves approached normal to the shoreline, the

effect of diffraction and reflection reached their minimum, and shoaling and refraction only affected waves. Therefore, wave-driven currents slightly reduced the overall influence of tidal currents inside the bay.

The results also showed the effect of tides on nearshore currents might be accentuated during high energy waves under certain approach angles. When waves approached at an angle close to perpendicular to the headlands, they were mainly diffracted from the upcoast headland. Waves were also reflected from the downcoast headland to an area inside the bay. Therefore, wave heights inside the bay notably decreased, and tides prevailed over waves as a driver of the current system.

More studies need to be carried out to define the critical wave heights and directions in the relationships established here. It is possible that waves with heights over 2 m and directions close to perpendicular to the headlands could prevail over tides to generate currents inside the bay. Therefore, more observations and simulations are needed to establish a quantitative relationship between tidal range and wave characterisitics in different pocket beach configurations.

Chapter 7: Discussion and conclusion

This chapter summarises the findings of this research in relation to my thesis aims.

7.1. Introduction

The overarching purpose of this study was to explore wave and current processes operating within a micro-tidal pocket beach hydrodynamic environment. This included the roles of headland effects on waves such as filtering and reflection, the roles of tides and local winds and also an evaluation of the relevance of embayed beach models for pocket beach environment applications. The methods and results of this study can be used, not only to better understand energy levels, beach dynamics and therefore, sensible development strategies in natural pocket beaches, but also to avoid the problem of water level rise and reflected waves causing scour and destabilization of coastal structures in artificial pocket beach environments. The general theoretical literature on pocket beaches is inconclusive on several vital questions within the factors influencing waves and currents inside pocket beaches. This study aimed to address four of these research question topic areas:

1) To examine the effects on pocket beach wave and current environments of interactions between wave approach and the two headlands, including the filtering of waves entering the bay, and the operation of refraction and diffraction processes;

2) To examine the influence on pocket beach wave and current environments of the reflection of waves off the downcoast headland within a pocket beach bay;

3) To establish whether or not tides and local winds operate as important influences on the wave and nearshore current environment inside pocket beach bays, and

4) To conduct a preliminary review of the applicability to pocket beaches of existing embayed beach equilibrium shoreline equations and models based on an understanding of the similarities and differences between their hydrodynamic process environments.

About 51% of coastlines worldwide are confined by one or two headlands, forming headland-bay beaches (Ojeda and Guillen, 2008). Pocket beaches are a subcategory of two-headland-bay beaches, bounded between two natural or artificial longshore constraints such as groins, breakwaters, rocky headlands, peninsulas and/or reefs. In such environments, waves can approach the shoreline directly from a narrow range of directions, depending on

the length of the headlands (Figure 7.1). Some incident waves are significantly influenced by reflection and diffraction, caused by the headlands (Dehouck *et al*., 2009). The majority of studies have been carried out in areas confined by one headland or two short headlands so that the length of headlands, in most cases, are shorter than those of the shoreline (e.g. Hsu and Evans, 1989; Hsu *et al*., 2008; Klein *et al*., 2002, 2010; Dehouck *et al*., 2009; Short, 1999, 2010). The hydrodynamics and morphodynamics of pocket beaches with headlands that are long relative to their shoreline length and surf zone extent are poorly documented. A field site confined by long headlands, relative to shoreline length, and with a micro-tidal regime and relatively narrow surf zone provided an excellent opportunity to investigate and contribute to this theoretical gap in our understanding of confined beaches.

Owing to the perception that pocket beaches typically have relatively stable shorelines compared to open coast beaches, the creation of artificial pocket beaches has recently been recommended for many eroding coastlines around the world as a tool to stabilize the shoreline (Ojeda and Guillen, 2008). Artificial pocket beaches have been also used to shelter beaches from high energy waves in order to create calm sea conditions inside bays for purposes such as the construction of jetties, wharfs or the extension of airport runways into the water. However, wave reflection from coastal structures is a serious issue since this process can dramatically increase energy level and sediment scour, thereby encouraging structure destabilization (Zanuttigh and Van der Meer, 2008). Therefore, there is need for further research on the hydrodynamics of pocket beaches, with a particular focus on reflection.

This study was carried out in two parts. The first part synthesized the findings of field and SWAN modelling experiments to answer the first two research questions. This part examined the importance of reflection, diffraction and refraction on wave characteristics inside pocket beaches and showed how wave processes inside a pocket beach differs from those in embayed and open coast beaches. This part focused on wave processes inside and outside of Okains Bay, an example pocket beach. Three field experiments were used to examine the important factors in controlling wave characteristics inside the bay. An array of instruments, including two ADCPs, one InterOcean S4AWD current meter, one ADV, one RBR xr-620 CTD and one HOBO H21 weather station, were deployed at different depths and locations to measure wave characteristics, currents, tides and local winds inside and outside the bay (see Tables 2.1 to 2.3 and 5.1). This study employed experimental equations

developed by Zanuttigh and Andersen (2010) and Zanuttigh and Van der Meer (2008), and also the SWAN model to simulate waves when they enter the bay and compared these simulations to field observations.

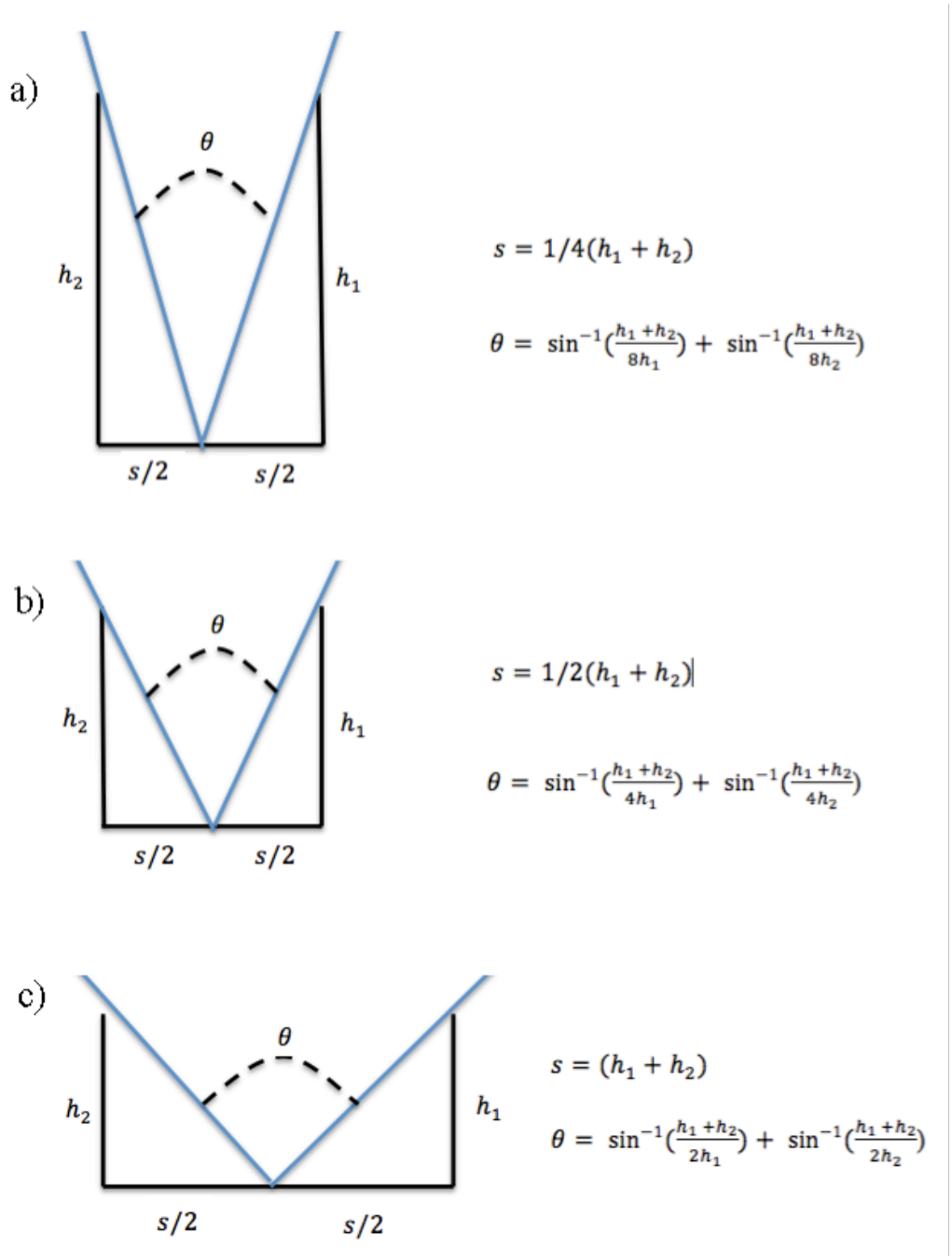

Figure 7.1. A diagram showing wave approaching direction sector of a pocket beach varies based on the ratio between the length of the shoreline and headlands. When headlands are longer than the shoreline length (a), waves can approach the shoreline directly from a narrower range of direction compared to when the shoreline length is longer than the headlands (c).

The second part synthesized the findings of field and XBeach modelling experiments to answer the third research questions. This part evaluated the importance of local winds and tides on nearshore currents in micro-tidal pocket beaches where incident waves are filtered by headlands and affected by reflection and diffraction. Initially, field data recorded during three field experiments, were employed to investigate how important local winds and tides were as an influence on nearshore currents inside the bay under conditions when incident waves varied from low to high energy levels. Then, the XBeach model was used to examine the type of current system that could realistically occur inside the pocket beach bay in response to different incident wave heights and approach directions outside the bay. Throughout Chapter 2 to 6, the differences between pocket, embayed and open coast beaches were discussed. However, this chapter will answer the last research question which is whether or not existing embayed beach equilibrium shoreline equations and models could be applicable to pocket beach environments.

The study area chosen for this research was Okains Bay, located on the north-eastern side of the extinct and partially eroded volcanic Banks Peninsula on the east coast of New Zealand's South Island (Figure 2.1). Tidal range in this area varied between 1.38 m and 2.35 m during neap tides and spring tides respectively (Land Information New Zealand, 2012). The dominant offshore waves, as measured at the Canterbury wave buoy (site B), approach the outer limits of the bay from the southwest and south (Gorman et al., 2003). Mean significant wave height at this site was reported as around 2 m with a maximum significant wave height of 7 m. Mean and maximum wave periods were also reported about 7.39 s and 12.9 s respectively. Beaches in Banks Peninsula experience prevailing northeast and southwest winds, followed by easterly and southerly winds.

7.2. Discussion and conclusions

The first research question that this thesis set out to address was to examine the effects on pocket beach wave and current environments of interactions between wave approach and the two headlands, including the filtering of waves entering the bay, and the operation of refraction and diffraction processes. The results of this study showed that in contrast to open coast beaches but similar to embayed beaches, if waves approach obliquely to the upcoast

headland, they will be diffracted into the bay. Field experiments showed that waves with an angle greater than the directional sector of Okains Bay (25° to 70° relative to true north) were influenced by diffraction, thereby considerably losing the wave energy and, subsequently, decreasing the wave heights inside the bay. The reduction in wave heights would theoretically increase when waves approach at an angle closer to longshore. For instance, when wave directions at site O1 during the period between 27th April and 2nd May increased to an angle towards longshore with a range between 60° and 120° to the shoreline, the wave heights inside the bay significantly decreased with an average of 0.7 m.

A SWAN model experiment was also carried out in order to examine whether diffraction is as important inside Okains Bay and could change wave characteristics. In the model configuration both reflection and diffraction were turned off during simulations. The results showed that predicted waves were poorly correlated to observations. For example, the predicted wave heights and directions were correlated to observations collected during Field Experiment 1 at site O3 with an R^2 of 0.45 and 0.18 respectively. This indicates that the correlation was slightly weaker than when the diffraction was taken into account (an R^2 of 0.49 and 0.23 respectively). However, waves in areas closer to the entrance of the bay were less affected by the upcoast headland and refraction was the main influence on wave characteristics. For instance, the results of the model demonstrated waves are less influenced by diffraction at site O2. The predicted wave heights and directions were reasonably correlated to observations with an R^2 of 0.69 and 061 respectively. It can be concluded that when waves are not filtered by the headlands, wave processes inside the bay is similar to open coast beaches and the effect of headlands on waves will be accentuated when waves approach the bay with an angle greater than the directional sector of that pocket beach.

The second research question that this thesis set out to address was to examine the influence on pocket beach wave and current environments of the reflection of waves off the downcoast headland within a pocket beach bay. The analyses indicated that, in additional to the effects of dispersion, development of wave asymmetry, shoaling, refraction and diffraction, the changes in the wave heights and directions were significantly influenced by wave reflection processes inside the bay. Wave directions varied significantly between outside versus inside the bay. The results of this study showed that waves inside the bay approached predominantly *from* the direction of the downcoast headland, whereas incident waves outside the bay predominantly approached the bay in directions heading *towards* the downcoast headland. For instance, during Field Experiment 1, waves collected inside

Okains Bay were approaching at angles of 345° to the shoreline, while waves outside the bay were approaching at angles of 30° relative to the shoreline. This phenomena was examined using SWAN simulations with and without the consideration of reflection. The results indicated that when wave reflection was not taken into account waves predominantly approached at angles of 15° to the shoreline, which was different from the observations (345°). However, when reflection was taken into account, the SWAN predictions closely matched the observations inside the bay.

The reflection effect was accentuated when waves could not enter the bay directly. Areas further inside the bay towards the shoreline were influenced more by reflection effect compared to areas closer to the entrance of the bay. For instance, when incident waves predominantly approached Okains Bay at angles of 45°, waves at site O2 (close to the entrance of the bay) predominantly approach normal to the shoreline, whereas waves at site O3 (further inside the bay towards the shoreline) predominantly approached at angles of 345° to the shoreline, which came from the downcoast headland. The importance of this reflection effect makes pocket beaches unique in terms of wave processes, compared to embayed beaches where diffraction dominates, or to open coast beaches where refraction and shoaling dominate. In essence, this study shows that reflection becomes an important influence on beach hydrodynamics where there is both an upcoast headland 'filter' of oblique wave approaches and a downcoast headland to bounce the waves that manage to enter the bay off.

Reflection effects on the pocket beach hydrodynamics change based on approaching wave direction. The intensity of reflection effects on wave characteristics inside pocket beaches depends on the approaching wave directions. Reflection effects reduce when waves approach from angles close to parallel to headlands and then increase if waves approach from angles close to perpendicular to headlands. For instance, the results showed that reflection effect of waves became greater when the incident wave directions increased from 20° to 50° and then to 70° to the shoreline. Note that it was assumed that the shoreline is at 90° to headlands. It can be inferred that if waves approach perpendicular to the downcoast headland, the reflection coefficient will reach its maximum, which can be also explained by Eq. 4.8 and 4.9.

This study also sought to answer the question whether or not tides and local winds operate as important influences on the wave and nearshore current environment inside pocket beach

bays (thesis aim 3). The results of this study indicated that waves and tides can be the primary drivers of nearshore currents close to the bed inside micro-tidal pocket beaches, depending on incident wave conditions. If wave heights inside the bay are higher than 0.5 m, waves are the primary driver of nearshore currents. However, if wave heights drop below 0.5 m, tides gradually dominate over other waves. This process may also happen in open coast beaches if incident wave heights drop to a certain point, but what makes micro-tidal pocket beaches different from open coast beaches is the way that the headlands filter deep water waves. There could be high energy waves moving towards a pocket beach, but they may not enter the bay directly as headlands filter approaching waves. The results of model experiments showed that when a 2 m incident wave approached 45° to the shoreline (the shoreline is at 90° to headlands), some parts of the bay were exposed to direct approaching waves, so currents were driven by waves. However, the other parts were filtered by the headlands, wave heights decreased to below 0.5 m, so the dimensionless relative tide range parameter (see Masselink and Short, 1993) increased to a certain point. As a result, tides dominated over waves to drive nearshore currents inside the bay. It can be inferred that those areas inside micro-tidal pocket beaches where exposed to direct approaching waves, currents are driven by waves, while currents in areas further into the bay, which are filtered by the headlands, are mainly generated by tides.

Changes in the current circulation system within a pocket beach are related to the incoming directions of offshore waves. I found that through field and modelling experiments in chapters 5 and 6, incident wave direction was an important influence on the current system in pocket beaches. The results of this study outlined in Chapter 6 showed that if high energy waves approach oblique or normal to the shoreline, the current system consists of longshore currents influended by headlands plus a rip current in the center of the shoreline or a toporip in proximity to headlands. The location of the rip current or toporip varies based on the direction of appoaching incident waves. For example when incident waves approached 45° to the upcoast headland, toporip formed in proximity to the downcoast headland. However, when incident waves approached 45° to the downcoast headland, toporip formed in proximity to the upcoast headland.

Short (1999) showed that current circulation type in headland-enclosed bay beaches can be determined by the dimensionless embayment scaling parameter (see Eq. 5.6). Wave direction was not taken into account in Short's parameter. As discussed earlier, the current

study demonstrates that changes in the wave heights and directions inside the bay vary based on approaching wave directions. This occurs because reflection and diffraction coefficients are proportional to approaching wave directions. These changes in wave characteristics, in turn, influence the current circulation system, especially the formation of the rip currents in proximity to the headlands. We can therefore conclude from my research that it is important to consider wave directions in the determination of current system type inside pocket beaches. It can also be inferred that the dimensionless embayment scaling parameter is not able to accurately determine the current system in pocket beaches with two long headlands.

Another aspect of my thesis aim 3 was to investigate the influence of local winds on nearshore currents within pocket beach environments. Before answering to this question, it was important to examine the local wind behavior in a pocket beach environment, which could lead to better understanding of how winds could influence the nearshore currents. The results of this study showed that another feature that makes some pocket beaches different from open coast beaches is the tendency of local winds to blow predominantly in offshore and onshore directions. For example, during Field Experiment 2, local winds collected on the beach inside the bay at site O6 predominantly below normal to the shore and at 165° to the shore, while wind directions at Banks Peninsula scale at site W predominantly moved in directions towards 60° and 255° to the shoreline. The localized on-offshore channeling of the beach scale wind occurred because the bay is located in a valley, so orographic effects acted to channel and shift the wind directions to angles close to offshore and onshore directions inside the bay. The results also showed that wind speeds also notably changed due to the orographic effects. For instance, during Field Experiment 2, the average of wind speed at site W was 3.85 ms^{-1}, while it was reduced to 1.87 ms^{-1} at site O6. These results are similar to Dingwall's (1974) findings in some pocket beaches in the same region. Therefore, it is expected that local winds influence (strengthen or weaken) cross-shore currents more than longshore currents in pocket beaches. However, it is important to note that this effect cannot happen in artificial pocket beaches, as the breakwaters or artificial headlands are not built as high as natural headlands. This effect might not also be observed in natural pocket beaches where the headland heights are low. In these cases, local winds easily blow over the headlands and enter the bay from a longshore direction. Therefore, the results of this study show that the wind field and aeolian influences on hydrodynamic currents varies between artificial and certain types of natural pocket beach.

The results of this study reinforce the idea that in pocket beach settings with elevated headland topography the local winds influence currents more in cross-shore directions. Since the predominant wind directions blew at angles close to offshore and onshore directions, the cross-shore components of local winds was a more effective influence on currents than the longshore components. For instance, during Field Experiment 2, waves were small at site O2 (Hs < 0.6 m) and the currents were driven primarily mainly by tides. The overall correlation between the cross-shore components of local winds and currents at site O2 was weak, with an R^2 of 0.12, but this was stronger than the correlation of the longshore components (R^2 of 0.04). When wind speeds exceeded 3.5 ms^{-1}, these correlations improved in both cross-shore and longshore directions, with R^2 of 0.3 and 0.12 respectively. The results suggest that local winds influence the hydrodynamic currents of pocket beaches with elevated topography more likely in a cross-shore direction since the winds predominantly blow in an offshore or onshore direction.

However, in open coast beaches both longshore and cross-shore components of local winds could equally be important in controlling nearshore currents, as the area is completely open to local winds from a wide range of directions. For example, many studies (e.g. Gallop *et al*., 2011; Curtiss *et al.,* 2009; Hubertz 1986) showed local winds importantly influenced longshore currents than cross-shore currents as those areas dominated by relatively longshore winds. Other studies (e.g. Dalrymple *et al*., 2011; Scott *et al.,* 2009; King, 1972) indicated that cross-shore local winds regardless of the directions they initially blow in at higher levels, importantly influenced cross-shore currents compared to longshore currents. However, the results of this study indicated that local winds tended to influence cross-shore currents more than longshore currents in pocket beaches, since local winds were shifted to a cross-shore direction by topographic channeling.

Local winds are a secondary factor influencing nearshore currents in pocket beaches. The results of this study showed that during low energy waves, the currents were primarily driven by tides, with a coefficient of determination of 0.51. However, there was also a weak correlation between winds and currents under these conditions, with a maximum of R^2 of 0.12 when wind speeds were less than 4.2 ms^{-1}. When wave heights increased during Field Experiment 3 (Hs < 1.57 m), the currents were primarily driven by incident waves (R^2 of 0.41), and tides had a minor effect on currents (R^2 of 0.1). During this period, local winds were less than 6.3 ms^{-1}, but the correlation between local winds and currents remained weak

with an R^2 of 0.28. This indicates that local winds act as a secondary factor in influencing the currents in pocket beaches when the area is primarily dominated by the influence of waves or tides. However, if wind speeds increase to a certain level (e.g. over 6 ms^{-1}), wind can become an important secondary moderator of the nearshore currents inside pocket beaches. There is a need to study further the effect of strong local winds on nearshore currents within pocket beach environments.

The last research question that this study set out to address was to conduct a preliminary review of the applicability to pocket beaches of existing embayed beach equilibrium shoreline equations and models based on an understanding of the similarities and differences between their hydrodynamic process environments (thesis aim 4). This study indicated that reflection processes significantly change the characteristics of the wave environments, particularly wave directions inside pocket beaches. As a result, other processes which are in turn affected by waves, such as current systems, sediment transport pathways and shoreline planforms, can differ from those that would result from the same offshore wave conditions in embayed and open coast beaches. This means in addition that Applying experimental and numerical models developed for embayed or open coast beaches may result in inaccurate predictions for pocket beaches, if wave reflection effects are not taken into account.

As shown in other research on one-headland-bay beaches or in two-headland bay beaches with a short downcoast headland (e.g. Loureiro *et al*., 2013; Hsu *et al*., 2008; Klein *et al*., 2002, 2010), the planforms of beaches are significantly influenced by the predominant incident waves. The theoretical shoreline curvature of such beaches in static equilibrium has been widely predicted using the state-of-the-art parabolic shape equation (Hardaway and Gunn 2010; Jackson and Cooper, 2010; Hsu *et al.,* 2008; Hsu and Evans, 1989). Although one-headland bay beach concepts were used to originally develop the parabolic shape equation, it has recently been suggested that this method can be applied to two-headland-bay beaches or pocket beaches (Hsu et al. 2008; Hardaway and Gunn, 2010). This study confirms that this method is applicable when there are two diffraction points; that is, when waves approach predominantly from both headlands (Hsu et al., 2008). Therefore, under these circumstances the parabolic shape equation is applied separately for each headland to predict the curvature in two parts. If pocket beaches have only one diffraction point, like in the case of Okains Bay, Hsu *et al*. (2008) recommended using the same approach as embayed beaches. In this approach the downcoast headland effect is not taken into account,

while the result of this study indicated that downcoast headland plays an important role in controlling wave characteristics inside the bay. Therefore, the results of this study indicate that the parabolic shape equation or indeed any other equation developed for one-headland bay beaches may not be able to predict the shoreline curvature to an acceptable level of accuracy in such pocket beaches (Figure 7.2).

Figure 7.2. Predicted curvature of the Okains Bay shoreline in static equilibrium (a) based on the parabolic shape model, where (b) indicates the distance between the point where waves become diffracted by the upcoast headland and the point where the downcast headland intersects the shoreline; and (c) indicates the wave crests' direction of approach (i.e. the wave orthogonal).

A glance at the shorelines of pocket beaches with two long headlands using the Google Earth suggests that the shorelines tend to be parallel to the predominant approaching wave crest, like Okains Bay and the adjacent pocket beaches. The results of this study indicated that waves inside the bay in areas seaward of the breaking zone propagate normal to or at angles close to normal to the shore, regardless of the offshore wave directions. This finding

is similar to the situations described in Woodroffe (2002). This makes pocket beaches different from embayed and open coast beaches in terms of wave directions inside the bay, since in the later situations waves can approach from a wide range of directions. This difference could explain why the planform of embayed beaches consists of a highly curved shoreline close to the headland, followed by a gentle curvature in the middle of the shoreline, and a straight shoreline towards the downcoast limit of the beach (Klein et al., 2010), but in pocket beaches like Okains Bay, the shoreline is gently curved in proximity to both headlands, while the middle section of the shoreline is relatively straight, owing to the directions of waves inside the bay.

From this study, it can be concluded that waves and tides are primary factors, and local winds are secondary factor, in controlling the current systems of topographically constrained micro-tidal pocket beaches. Wave characteristics inside pocket beaches are proportional to deep water wave directions. Wave heights and directions inside the bay are under certain wave approach conditions influenced significantly by reflection and diffraction, with consequent changes indicated in the current systems. In order to study the hydrodynamics and morphodynamics of micro-tidal pocket beaches, it is necessary to consider waves, tides and local winds, even during conditions with high energy waves. However, in micro-tidal open coast beaches, current systems are primarily driven by waves, while tides and moderate local winds have less importance in terms of current system drivers or modifiers.

This thesis also contributes to the theoretical definition of pocket beaches by showing that the shoreline control exerted by the downcoast headland is via wave reflection processes. That is, previous definitions of pocket beaches acknowledged that these environments are defined by the presence of both and upcoast and a downcoast headland which influenced the shoreline shape. Embayed beach research indicated that the specific processes whereby the upcoast headland influenced the shoreline were wave diffraction and reflection. This is confirmed by the field and modelling results of this thesis. The exact nature of the process influence of the downcoast headland was not understood. This thesis contributes to pocket beach theory by showing that wave reflection is the key processes by which the downcoast headland influences the pocket beach shoreline, and it outlines conditions under which this reflection influence vary. Sediment trapping may be another influence of downcoast headlands, where they operate like a groyne. However, this thesis indicates that wave reflection is of paramount importance.

7.3. Limitations of this study

The study has offered an evaluative perspective on wave processes and nearshore currents within pocket beaches. However, the study encountered a number of limitations, which need to be considered. An important limitation in this study is the number of study sites. This study focused on one particular pocket beach. This pocket beach was characterised by fine sands and a gentle beach slope and the long shore constraints provided by topographically elevated headlands. Therefore, all findings in this research are limited to dissipative beaches with topographically elevated constraints. If two or more pocket beaches with different bay characteristics, including headland size, beach slope and sand size, are studied in the future, then the findings could extend to different types of pocket beaches. Owing to a limited budget and time, this was not the case for the present study.

Another limitation in this study is the length of observations. This study employed three field experiments collected throughout a year. During Field Experiment 1, the length of collected data was adequate, but no wind data were collected, as measuring local winds was not in the initial plan. During Field Experiment 2 and 3, waves, currents and local winds were collected at different sites inside the bay. However, due to the difficulty of collecting data inside the surf zone, currents were recorded for a maximum of 2 days at a time. This reduced the chance of measuring currents when local winds were strong. If strong wind condition data were collected in this study, the results could have shown a stronger correlation between the cross-shore components of local winds and currents.

7.4. Areas for further research

Gaps in our understanding of pocket beach environments are extensive and multifaceted. This thesis has focused on two key area of the functioning of these environments: wave and current processes. Examining sediment transport systems, in particular, was beyond the scope of this thesis. To further deepen our understanding of the hydrodynamics and morphodynamics of pocket beaches, there is a need for more case studies to allow further assessment of how the length of the downcoast headlands could influence the stability of the shoreline. This study showed that reflection effects have important influence on wave characteristics and, consequently, on nearshore currents inside pocket beaches. Therefore,

more field data and modelling studies could lead to develop an equation (similar to the parabolic shape equation) to predict the curvature of the shoreline with consideration of the downcoast headland length under different wave conditions, especially wave directions. This could also help to classify current circulation systems in pocket beaches based on the ratio between the length of the headlands and shoreline with consideration of incident wave approach directions.

Reference:

Aagaard, T., Greenwood, B., Nielsen, J., 1997. Mean currents and sediment transport in a rip channel. *Marine Geology*, vol. 140, no. 1: pp. 25–45.

Aarninkhof, S., J. van Dalfsen, J. Mulder, and D. Rijks. 2010. Sustainable development of nourished shorelines. *PIANC MMX Congress, Liverpool, UK.*

Abbott, M.B., Petersen, H.M., Skovgaard, O., 1978. On the numerical modelling of short waves in shallow water. *Journal of Hydraulic Research*, Vol. 16, no. 3: pp. 173–204.

Abreu, M., Larraza, A., Thornton, E., 1992. Nonlinear transformation of directional wave spectra in shallow water. *Journal of Geophysical Research,* Vol. 97, no. C10: pp. 15579-15589.

Abul-Azm, A.G., Williams, A.N., 1997. Oblique wave diffraction by segmented offshore breakwaters. *Ocean engineering,* no. 24: pp. 63–82.

Airy, G., 1845. Tides and waves. *Encyc. Metrop,* Vol. 192: pp. 241–396.

Anastasiou, S., Sylaios, G., 2013. Nearshore wave field simulation at the lee of a large island. *Ocean Engineering,* no. 74: pp. 61–71.

Allard, R., Dykes, J., Hsu, Y.L., Kaihatu, J., Conley, D., 2008. A real-time nearshore wave and current prediction system. *Journal of Marine Systems*, vol. 69, no. 1: pp. 37–58.

Allsop, N.W.H., Hettiarachchi, S.S.L., 1989. Wave reflections in harbours; the design, construction and performance of wave absorbing structures. *Report OD 89*.

Anthony, E.J., Dolique, F., 2004. The influence of Amazon-derived mud banks on the morphology of sandy headland-bound beaches in Cayenne, French Guiana: a short-to long-term perspective. *Marine Geology* vol. 208, no. 2: pp. 249–264.

Austin, M., Scott, T., Brown, J., Brown, J., MacMahan, J., Masselink, G., Russell, P., 2010. Temporal observations of rip current circulation on a macro-tidal beach. *Continental Shelf Research*, vol. 30, no. 9: pp. 1149–1165.

Austin, M.J., Masselink, G., 2006. Observations of morphological change and sediment transport on a steep gravel beach. *Marine Geology*, vol. 229, no. 1: pp. 59–77.

Argyrous, G., 2011. Statistics for research: with a guide to SPSS. *Sage Publications Ltd. University of New South Wales*, 608 p.

Baart, F., T. Van der Kaaij, M. Van Ormondt, A. Van Dongeren, M. Van Koningsveld, and J. Roelvink. 2009. Real-time forecasting of morphological storm impacts: a case study in the Netherlands, *Journal of coastal research*: pp. 1617-1621.

Battjes, J.A., 1974. Computation of set-up, longshore currents, run-up and overtopping due to wind-generated waves. *Department of Civil Engineering, Delft University of Technology*: 74 p.

Battjes, J.A., 1974. Surf similarity. *Coastal Engineering Proceedings 1*, no. 14: pp. 136-149.

Bird, E.C.F., 2000. Coastal geomorphology: an introduction. *Wiley Online Library*, 332 p.

Brandenburg, P.G.F. 2010. Scale dependency of dune erosion models: performance assessment of the DUROS and XBeach model for various experiment scales. *Msc. thesis, Water Engineering & Management, University of Twente, The Netherlands.*

Brander, R.W., MacMahan, J.H., 2011. Future challenges for rip current research and outreach. *Rip Currents: Beach Safety, Physical Oceanography and Wave Modelling*: pp. 1–29.

Boccotti, P., 2000. Wave mechanics for ocean engineering. *Access Online via Elsevier*, vol. 64.

Booij, N., Holthuijsen, L.H., Ris, R.C., 1996. The“ SWAN” wave model for shallow water. *Coastal Engineering Proceedings 1*, no. 25: pp. 184-196.

Booij, N., Ris, R.C., Holthuijsen, L.H., 1999. A third-generation wave model for coastal regions: 1. Model description and validation. *Journal of Geophysical Research: Oceans (1978–2012),* no. 104: pp. 7649–7666.

Bryan, K. R., Foster, R., and MacDonald, I., 2013. Beach Rotation at Two Adjacent Headland-Enclosed Beaches. Journal of Coastal Research, no. 65: pp. 2095-2100.

Calabrese, M., Di Pace, P., Buccino, M., 2009. Wave reflection at rubble mound breakwaters ranging from submerged to exposed. *Proc. Coastal Eng, World Scientific, Hamburg*.

Castelle, B., Coco, G., 2012. The morphodynamics of rip channels on embayed beaches. *Continental Shelf Research,* vol. 43: pp. 10–23.

Castelle, B., Marieu, V., Coco, G., Bonneton, P., Bruneau, N., Ruessink, B.G., 2012. On the impact of an offshore bathymetric anomaly on surf zone rip channels. *Journal of Geophysical Research, Earth Surface*, vol. 117, no. f1: pp. 1-20.

Castelle, B., Ruessink, B.G., 2011. Modeling formation and subsequent nonlinear evolution of rip channels: Time-varying versus time-invariant wave forcing. *Journal of Geophysical Research, Earth Surface*, vol. 116, no. f4: pp. 1-15.

Chien, N.Q., and D. Roelvink. 2007. Application of the cut-cell finite volume method in a 2-D hydrodynamic model. *Vietnam Estuary Workshop, Hochiminh, Vietnam: pp. 48-66.*

Chien, N.Q., D. Roelvink, E. Commitee, and I.M. van der Wegen. 2007. Simulating shoreline retreat in a 2-D hydromorphologic model. *Msc. Theses, Institute of UNESCO-IHE for water education, Delft, The Netherlands*.

Chiswell, S.M., 1996. Variability in the Southland Current, New Zealand. *New Zealand journal of marine and freshwater research*, vol. 30, no. 1: pp. 1–17.

Cialone, M.A., Kraus, N.C., 1987. A Numerical model for shoaling and refraction of third-order stokes waves over an irregular bottom. *Misc.Pap., CERC 87-10, US Army Eng. WES, CERC*.

Codiga, D.L., 2011. Unified tidal analysis and prediction using the UTide Matlab functions. *Graduate School of Oceanography, University of Rhode Island*.

Cook, D.O., 1970. The occurrence and geologic work of rip currents off southern California. Marine geology, vol. 9, no. 3: pp. 173–186.

Cooper, J. A. G., and Alonso, I., 2006. Natural and anthropic coasts: challenges for coastal management in Spain. *Journal of Coastal Research*, pp. 1-7.

Cooper, J. A. G., Jackson, D. W. T., Navas, F., McKenna, J., and Malvarez, G., 2004. Identifying storm impacts on an embayed, high-energy coastline: examples from western Ireland. *Marine Geology*, Vol. 210, no. 1: pp. 261-280.

Cowell, P., Roy, P., Zeng, T., Hennecke, W. and Thom, B., 1996. Regional predictions of climate change impacts. In *Australian Coastal Management Conference, Coast to Coast,* Vol.96*:* pp. 185-193.

Curtiss, G.M., Osborne, P.D., Horner-Devine, A.R., 2009. Seasonal patterns of coarse sediment transport on a mixed sand and gravel beach due to vessel wakes, wind waves, and tidal currents. *Marine Geology*, vol. 259, no. 1: pp. 73–85.

D' Angremond, K., Van Der Meer, J.W., De Jong, R.J., 1996. Wave transmission at low-crested structures. *Coastal Engineering Proceedings 1*, no. 25: pp. 254-269.

Da Fontoura Klein, A.H., Benedet Filho, L., Schumacher, D.H., 2002. Short-term beach rotation processes in distinct headland bay beach systems. *Journal of Coastal Research: pp.* 442–458.

Da Fontoura Klein, A.H., de Menezes, J.T., 2001. Beach morphodynamics and profile sequence for a headland bay coast. *Journal of Coastal Research*: pp. 812–835.

Dalrymple, R.A., MacMahan, J.H., Reniers, A.J., Nelko, V., 2011. Rip currents. *Annual Review of Fluid Mechanics*, no. 43: pp. 551–581.

Dalrymple, R.A., Martin, P.A., 1990. Wave diffraction through offshore breakwaters. *Journal of waterway, port, coastal, and ocean engineering, no.* 116: pp. 727–741.

Daly, C. J., Bryan, K. R., Roelvink, J. A., Klein, A. H. F., Hebbeln, D., & Winter, C., 2011. Morphodynamics of embayed beaches: the effect of wave conditions. In *Proceedings of the 11th International Coastal Symposium,* pp. 1003-1007.

Daly, C. J., Bryan, K. R., and Winter, C., 2014. Wave energy distribution and morphological development in and around the shadow zone of an embayed beach. *Coastal Engineering*, no. 93: pp. 40-54.

Davidson-Arnott, R., 2010. Introduction to coastal processes and geomorphology. *Routledge, Cambridge University Press.*

Davidson, M.A., Bird, P.A.D., Bullock, G.N., Huntley, D.A., 1996. A new non-dimensional number for the analysis of wave reflection from rubble mound breakwaters. *Coastal engineering*, no. 28: pp. 93–120.

de Abreu, C.F. 2010. Morphological behaviour of a non-equilibrium coastal profile. *PhD thesis, Delft University of Technology*.

Dean, R.G., 1973. Heuristic models of sand transport in the surf zone, in: First Australian Conference on Coastal Engineering, 1973: Engineering Dynamics of the Coastal Zone. *Institution of Engineers, Australia*: 215 p.

Dean, R.G., 1974. Evaluation and development of water wave theories for engineering application. *US Coastal Engineering Research Centre*.

Dean, R.G., Dalrymple, R.A., 1991. Water wave mechanics for engineers and scientists. *Prentice-Hall.*

Dehouck, A., Dupuis, H., Sénéchal, N., 2009. Pocket beach hydrodynamics: the example of four macrotidal beaches, Brittany, France. *Marine geology*, vol. 266: no. 1: pp. 1–17.

Demirbilek, Z., Lin, L., Wilson, D., Rosati, J., 2012. WaveNet: A Web-based metocean data access, processing and analysis tool. *Engineer Research and Development Centre Vicksburg Ms Coastal and Hydraulics Lab.*

Dingwall, P.R., 1974. Bay-head sand beaches of Banks Peninsula, New Zealand. *Memoir, NZ Oceanographic Institute,* Vol. 15: 63 p.

Ecan, 2014. About the wave buoy and how it works. *Web. 1 April. 2014.‹http://ecan.govt.nz /ser-vices/online-services/monitoring/coastal-monitoring/wave-buoy/Pages/about-wave-buoy.aspx›.*

Eckart, C., 1952. The propagation of gravity waves from deep to shallow water. *In Gravity Waves*, Vol. 1: pp. 156-175.

Engineers, U.A.C.O., 1984. Shore protection manual. *Army Engineer Waterways Experiment Station, Vicksburg*, MS. 2v.

Engineers, U.A.C.O., 2002. Coastal engineering manual. *Engineer Manual 1110*: pp. 2–1100.

Ergin, A., Williams, A.T., and A., Micallef, 2006. Coastal Scenery: Appreciation and Evaluation. *Journal of Coastal Research,* vol. 22, no. 2: pp. 958-964.

Eshleman, J. 2009. Storm hazard analyst GIP position: Evaluation coastal hazards for NPS lands in southern California. *National Park Service, Denver, Colorado.*

Fenton, J.D., 1985. A fifth-order Stokes theory for steady waves. *Journal of waterway, port, coastal, and ocean engineering*, no. 111: pp. 216–234.

Finnegan, W., Goggins, J., 2012. Numerical simulation of linear water waves and wave–structure interaction. *Ocean Engineering*, no. 43: pp. 23–31.

Fredsøe, J., Deigaard, R., 1992. Mechanics of coastal sediment transport. *World Scientific*.

Galappatti, G., and C. Vreugdenhil. 1985. Depth-integrated Model for Suspended Sediment Transport. *Journal of Hydraulic Research JHYRAF*, vol. 23 no. 4: pp. 1-16.

Gallop, S.L., Bosserelle, C., Pattiaratchi, C., Eliot, I., 2011. Hydrodynamic and morphological response of a perched beach during sea breeze activity. *Journal of Coastal Research*: pp. 75–79.

Gallop, S.L., Verspecht, F., Pattiaratchi, C.B., 2012. Sea breezes drive currents on the inner continental shelf off southwest Western Australia. *Ocean Dynamics*, vol. 62, no. 4: pp. 569–583.

Goda, Y., & Suzuki, T., 1976. Estimation of incident and reflected waves in random wave experiments. *Coastal engineering proceedings*, *1*(15).

Goodwin, P., 1996. Predicting the stability of tidal inlets for wetland and estuary management. *Journal of Coastal Research*: pp. 83–101.

Gorman, R.M., Bryan, K.R., Laing, A.K., 2003a. Wave hindcast for the New Zealand region: nearshore validation and coastal wave climate. *New Zealand Journal of Marine and Freshwater Research*, Vol. 37, no. 3: pp. 567–588.

Gorman, R.M., Bryan, K.R., Laing, A.K., 2003b. Wave hindcast for the New Zealand region: Deep-water wave climate. *New Zealand Journal of Marine and Freshwater Research*, Vol. 37, no. 3: pp. 589–612.

Grunnet, N.M., Ruessink, B.G., Walstra, D.-J.R., 2005. The influence of tides, wind and waves on the redistribution of nourished sediment at Terschelling, The Netherlands. *Coastal engineering*, vol. 52, no. 7: pp. 617–631.

Guan, X., Ou, H.-W., Chen, D., 2009. Tidal effect on the dense water discharge, Part 2: A numerical study. *Deep Sea Research Part II: Topical Studies in Oceanography*, vol. 56, no. 13: pp. 884–894.

Hardaway, C.S., and Gunn, J.R., 2010. Design and performance of headland bays in Chesapeake Bay, USA. *Coastal Engineering,* Vol. 57, no. 2: pp. 203-212.

Hargreaves, J.C., Carter, D.J.T., Cotton, P.D., Wolf, J., 2002. Using the SWAN wave model and satellite altimeter data to study the influence of climate change at the coast. *The Global atmosphere and ocean system*, no. 8: pp. 41–66.

Harley, M.D., Turner, I.L., 2008. A simple data transformation technique for pre-processing survey data at embayed beaches. *Coastal Engineering*, no. 55: pp. 63–68.

Hart, D. E., and Bryan, K. R., 2008. New Zealand coastal system boundaries, connections and management. *New Zealand Geographer*, Vol. 64, no. 2: pp. 129-143.

Hegge, B., Eliot, I., Hsu, J., 1996. Sheltered sandy beaches of southwestern Australia. *Journal of Coastal Research*: pp. 748–760.

Héquette, A., Anthony, E.J., Ruz, M.-H., Maspataud, A., Aernouts, D., Hemdane, Y., 2013. The influence of nearshore sand banks on coastal hydrodynamics and sediment transport, northern coast of France, *In Coastal Dynamics*: pp. 334-351.

Héquette, A., Hill, P.R., 1993. Storm-generated currents and offshore sediment transport on a sandy shoreface, Tibjak Beach, Canadian Beaufort Sea. *Marine Geology*, vol. 113, no. 3: pp. 283–304.

Holthuijsen, L.H., 2007. Waves in oceanic and coastal waters. *Cambridge University Press.*

Holthuijsen, L.H., Herman, A., Booij, N., 2003. Phase-decoupled refraction–diffraction for spectral wave models. *Coastal Engineering*, no. 49: pp. 291–305.

Hsu, J.R.C., Benedet, L., Klein, A.H.F., Raabe, A.L.A., Tsai, C.P. and Hsu, T.W., 2008. Appreciation of static bay beach concept for coastal management and protection. *Journal of Coastal Research*, pp. 198-215.

Hsu, J.R.C, and Evans, C.,1989. Parabolic bay shapes and applications. *Ice Virtual Library*, vol. 87 no. 4: pp. 557-570.

Hsu, J.R.C., Jeng, D.S., Tsai, C.P., 1993. Short-crested wave-induced soil response in a porous seabed of infinite thickness. *International Journal for Numerical and Analytical Methods in Geomechanics*, no. 17: pp. 553–576.

Hsu, J.R.C., Yu, M.J., Lee, F.C. and Benedet, L., 2010. Static bay beach concept for scientists and engineers: A review. *Coastal Engineering*, Vol. 57, no. 2: pp. 76-91.

Huang, Y., Weisberg, R.H., Zheng, L., Zijlema, M., 2013. Gulf of Mexico hurricane wave simulations using SWAN: Bulk formula-based drag coefficient sensitivity for Hurricane Ike. *Journal of Geophysical Research: Oceans*, no. 118: pp. 3916–3938.

Hubertz, J.M., 1986. Observations of local wind effects on longshore currents. *Coastal engineering*, vol. 10, no. 3: pp. 275–288.

Jackson, D.W.T., and Cooper, J.A.G., 2010. Application of the equilibrium planform concept to natural beaches in Northern Ireland. *Coastal Engineering,* Vol. 57, no. 2: pp. 112-123.

Jamal, M.H., D.J. Simmonds, V. Magar, and S. Pan. 2011. Modelling infiltration on gravel beaches with an XBeach variant. *Proc.32nd Conf. on Coastal Eng., Shanghai, China*: pp. 1-11.

King, C.A., King, C.A.M., 1972. Beaches and coasts. *Eward Arnold, London:* 570 p.

Klein, A.H., Benedet Filho, L., Schumacher, D.H., 2002. Short-term beach rotation processes in distinct headland bay beach systems. J*ournal of Coastal Research*: pp. 442–458.

Klein, A.H.F., Dias, J., Tessler, M.G., Silveira, L.F., Benedet, L., de Menezes, J.T. and de Abreu, J.G.N., 2010. Morphodynamics of structurally controlled headland-bay beaches in southeastern Brazil: A review. *Coastal Engineering,* Vol. 57, no. 2: pp. 98-111.

Komar, P.D., 1998. Beach processes and sedimentation. *New Jersey Prentice Hall*: 429 p.

Komar, P.D., Miller, M.C., 1975. On the comparison between the threshold of sediment motion under waves and unidirectional currents with a discussion of the practical evaluation of the threshold; reply. *Journal of Sedimentary Research*, vol. 45, no. 1: pp. 362–367.

Le Méhauté, B., 1969. An introduction to hydrodynamics and water waves. *Oceanic Fronts in Coastal Processes 114*, 315 p.

Le Roux, J.P., 2008. An extension of the Airy theory for linear waves into shallow water. C*oastal Engineering*, Vol. 55, no. 4: pp. 295–301.

Lindemer, C., N. Plant, J. Puleo, and D. Thompson. 2008. Modelling Wave Overtopping on the Chandeleur Islands during Hurricane Katrina using XBeach. *AGU Fall Meeting Abstracts*, vol. 1: pp. 1-13.

Lindemer, C., N. Plant, J. Puleo, D. Thompson, and T. Wamsley. 2010. Numerical simulation of a low-lying barrier island's morphological response to Hurricane Katrina. *Coastal Engineering*, vol. 57, no. 11: pp. 985-995.

Liu, P.L.-F., 1994. Model equations for wave propagations from deep to shallow water. *Advances in coastal and ocean engineering*, no. 1: pp. 125–158.

Liu, P.L.-F., Losada, I.J., 2002. Wave propagation modeling in coastal engineering. *Journal of Hydraulic Research,* Vol. 40 no. 3: pp. 229–240.

Loureiro, C., Ferreira, Ó., and Cooper, J. A. G., 2012. Extreme erosion on high-energy embayed beaches: influence of megarips and storm grouping. *Geomorphology*, no. 139: pp. 155-171.

Longuet-Higgins, M.S., 1970a. Longshore currents generated by obliquely incident sea waves: 1. *Journal of geophysical research*, vol. 75, no. 33: pp. 6778–6789.

Longuet-Higgins, M.S., 1970b. Longshore currents generated by obliquely incident sea waves: 2. *Journal of geophysical research*, vol. 75, no. 33: pp. 6790–6801.

Lv, X.C., Wang, D.S., Yuan, D.K., Tao, J.H., 2013. Calibration of SWAN Model for Wave Simulation in Bohai Sea. *Applied Mechanics and Materials*, no. 423: pp. 1344–1350.

MacMahan, J.H., Thornton, E.B., Reniers, A.J., 2006. Rip current review. Coastal Engineering, vol. 53, no. 2: pp. 191–208.

Muttray, M., Oumeraci, H., Oever, E. t, 2006. Wave reflection and wave run-up at rubble mound breakwaters. *Coastal Engineering Conference*: pp. 899-912.

Martino, E., Moreno, L. and Kraus, N., 2003. Engineering guidance for the use of bayed-beach formulations. *Proc. Coast. Sed.. ASCE (2003).*

Masselink, G., 1998. The effect of sea breeze on beach morphology, surf zone hydrodynamics and sediment resuspension. Marine Geology, vol. 146, no. 1: pp. 115–135.

Masselink, G., Hughes, M.G., 2003. Introduction to coastal processes and geomorphology. *Arnold, Hodder Headline Group*.

Masselink, G., Short, A.D., 1993. The effect of tide range on beach morphodynamics and morphology: a conceptual beach model. *Journal of Coastal Research*: pp. 785–800.

Matte, P., Jay, D.A., Zaron, E.D., 2013. Adaptation of Classical Tidal Harmonic Analysis to Nonstationary Tides, with Application to River Tides. *Journal of Atmospheric and Oceanic Technology*, vol. 30, no. 3: pp. 569–589.

McCall, R., N. Plant, and J.T. de Vries. 2010a. The effect of longshore topographic variation on overwash modelling. *Coastal Engineering Processings*, vol. 1, no. 32: pp. 76-91.

McCall, R., J. Van Thiel de Vries, N. Plant, A. Van Dongeren, J. Roelvink, D. Thompson, and A. Reniers. 2010b. Two-dimensional time dependent hurricane overwash and erosion modeling at Santa Rosa Island. *Coastal Engineering*, vol. 57, no. 7: pp. 668-683.

McGranahan, G., Balk, D. and Anderson, B., 2007. The rising tide: assessing the risks of climate change and human settlements in low elevation coastal zones. *Environment and Urbanization,* Vol. 19, no. 1: pp. 17-37.

McCormick, M.E., Kraemer, D.R., 2002. Polynomial approximations for Fresnel integrals in diffraction analysis. *Coastal engineering*, no. 44: pp. 261–266.

McKenzie, P., 1958. Rip-current systems. T*he Journal of Geology*: pp. 103–113.

Mercelis, A.B.P., D. Roelvink, P. Haerens, and K. Trouw. 2010. Application and validation of XBeach for three different field sites. *Coastal Engineering Processings*, vol. 1, no. 32: pp. 112-126.

Miles, J., 1957. On the generation of surface waves by shear flows. *Journal of fluid Mechanics*, Vol. 3 no. 2: pp. 185-204.

Moreno, L.J., and Kraus, N.C., 1999. Equilibrium shape of headland-bay beaches for engineering design. *Coastal Defense Program Madrid (Spain).*

Muir Wood, A., Fleming, C., 1981. Coastal Hydraulics. *Gordon and Breach, New York.*

Nielsen, P.E., 2009. Coastal and estuarine processes. *World Scientific.*

Nicholls, R.J., and Mimura, N., 1998. Regional issues raised by sea-level rise and their policy implications. *Climate Research,* Vol. 11, no. 1: pp. 5-18.

Ojeda, E., and Guillen, J., 2008. Shoreline dynamics and beach rotation of artificial embayed beaches. *Marine Geology,* Vol. 253, no. 1-2: 51-62.

Oliveira, F.S.B.F., and Barreiro, O.M., 2010. Application of empirical models to bay-shaped beaches in Portugal. *Coastal Engineering,* Vol. 57, no. 2: pp. 124-131.

Orzech, M., E. Thornton, A. Reniers, J. Macmahan, and B. O'Reilly. 2008. Modelling Rip Channel and Mega-Cusp Migration With XBeach. *AGU Fall Meeting Abstracts,* vol. 1: pp. 1225-1239.

Ou, S.-H., Liau, J.-M., Hsu, T.-W., Tzang, S.-Y., 2002. Simulating typhoon waves by SWAN wave model in coastal waters of Taiwan. *Ocean Engineering,* no. 29: pp. 947–971.

Packwood, A. 1983. The influence of beach porosity on wave uprush and backwash. *Coastal Engineering,* vol. 7, no. 1: pp. 29-40.

Penney, W.G., Price, A.T., 1952. Part I. The diffraction theory of sea waves and the shelter afforded by breakwaters. Philosophical Transactions of the Royal Society of London. *Series A, Mathematical and Physical Sciences*, no. 244: pp. 236–253.

Pond, S., Pickard, G.L., 1983. Introductory dynamical oceanography. *Gulf Professional Publishing*.

Port, A., Gurgel, K.W., Staneva, J., Schulz-Stellenfleth, J. and Stanev, E.V., 2010. Tidal and wind-driven surface currents in the German Bight: HFR observations versus model simulations. *Ocean Dynamics*, Vol. 61, no. 10: pp. 1567-1585.

Peachey, D.R., 1986. Modeling waves and surf. *ACM Siggraph Computer Graphics*, Vol. 20, no. 4: pp. 65–74.

Postma, G.M., 1989. Wave reflection from rock slopes under random wave attack. *Delft University of Technology, Faculty of Engineering, Delft. M. Sc. thesis*.

Pullen, T., Allsop, N.W.H., Bruce, T., Kortenhaus, A., Schüttrumpf, H., Van der Meer, J.W., 2007. EurOtop wave overtopping of sea defences and related structures: assessment manual.

Ranasinghe, R., Pattiaratchi, C., 2003. The seasonal closure of tidal inlets: causes and effects. *Coastal Engineering Journal*, vol. 45, no. 4: pp. 601–627.

Ranasinghe, R., Symonds, G., Black, K., Holman, R., 2004. Morphodynamics of intermediate beaches: a video imaging and numerical modelling study. *Coastal Engineering*, vol. 51, no. 3: pp. 629–655.

Pattiaratchi, C., Hegge, B., Gould, J., Eliot, I., 1997. Impact of sea-breaze activity on nearshore and foreshore processes in southwestern Australia. *Continental Shelf Research*, Vol. 17, no. 13: pp. 1539-1560.

Rea, C.C., Komar, P.D., 1975. Computer simulation models of a hooked beach shoreline configuration. *Journal of Sedimentary Research*, no. 45: pp. 866–872.

Reniers, A.J., Roelvink, J.A., Thornton, E.B., 2004. Morphodynamic modeling of an embayed beach under wave group forcing. *Journal of Geophysical research*, no. 109: pp. 212-229.

Reynolds-Fleming, J.V., Fleming, J.G., 2005. Coastal circulation within the Banks Peninsula region, New Zealand. *New Zealand Journal of Marine and Freshwater Research*, vol. 39: pp. 217-225.

Roelvink, D. 2007. XBeach Annual Report and Mode Description. Modelling of Hurricane Impacts. *UNESCO-The INST For Water Education Delft (Netherlands)*.

Roelvink, D., A. Reniers, A. Van Dongeren, J. van Thiel de Vries, J. Lescinski, and D. Walstra. 2007. Modelling hurricane impacts on beaches, dunes and barrier islands. *Coastal Engineering*, vol. *56*, no. 11: pp. 1133-1152.

Roelvink, D., A. Reniers, A. van Dongeren, J. van Thiel de Vries, R. McCall, and J. Lescinski. 2009. Modelling storm impacts on beaches, dunes and barrier islands. *Coastal Engineering,* vol. 56 no. 11: pp. 1133-1152.

Roberts, A.J., 1983. Highly nonlinear short-crested water waves. *Journal of Fluid Mechanics*, no. 135: pp. 301–321.

Ruiz de Alegria-Arzaburu, A., J.J. Williams, and G. Masselink. 2010. Application of XBeach to model storm response on a macrotidal gravel barrier. *Coastal Engineering Proceedings*, vol. 1, no. 3: pp. 188-206.

Russell, P., Davidson, M., Huntley, D., Cramp, A., Hardisty, J., Lloyd, G., 1991. The British beach and nearshore dynamics (B-BAND) programme. *In Coastal Sediments*: pp. 371–384.

Scott, T.M., Russell, P., Masselink, G., Wooler, A., 2009. Rip current variability and hazard along a macro-tidal coast. *Journal of Coastal Research SI, vol.* 56: pp. 895–898.

Sedrati, M., Anthony, E.J., 2007. Storm-generated morphological change and longshore sand transport in the intertidal zone of a multi-barred macrotidal beach. *Marine geology*, vol. 244, no. 1: pp. 209–229.

Seelig, W.., 1983. Wave reflection from coastal structures, Balkema. *Proc. Of the Int. Conference on Coastal Structures*, no. 1: pp. 961–973.

Seelig, W.N., Ahrens, J.P., 1981. Estimation of wave reflection and energy dissipation coefficients for beaches, revetments, and breakwaters. *DTIC Document*.

Shepard, F.P., Emery, K.O., La Fond, E.C., 1941. Rip currents: A process of geological importance. *The Journal of Geology*: pp. 337–369.

Shepard, F.P., Inman, D.L., 1950. Nearshore water circulation related to bottom topography and wave refraction. *Transactions, American Geophysical Union*, vol. 31: pp. 196–212.

Sheremet, A., Guza, R. T., Elgar, S., & Herbers, T. H. C., 2002. Observations of nearshore infragravity waves: Seaward and shoreward propagating components. *Journal of Geophysical Research: Oceans,* vol. 107: pp. 1-10.

Short, A., Cowell, P., Cadee, M., Hall, W. and Van Dijk, B., 1995. Beach rotation and possible relation to the Southern Oscillation. *In Ocean Atmosphere Pacific Conference, National Tidal Facility, Adelaide,* pp. 329-334.

Short, A.D., 1999. Handbook of beach and shoreface morphodynamics. *John Wiley & Sons,* 392 p.

Short, A.D., 2010. Role of geological inheritance in Australian beach morphodynamics. *Coastal Engineering,* Vol. 57, no. 2: pp. 92-97.

Silva, P., Bertin, X., Fortunato, A. and Oliveira, A., 2009. Intercomparison of Sediment Transport Formulas in Current and Combined Wave-Current Conditions. *Journal of Coastal Research*, pp.559-563.

Silva, R., Baquerizo, A., Losada, M.Ã. and Mendoza, E., 2010. Hydrodynamics of a headland-bay beach--Nearshore current circulation. *Coastal Engineering,* Vol. 57, no. 2: pp. 160-175.

Silvester, R. and Hsu, J.R.C., 1999. Coastal stabilization-innovative concepts. *World Scientific Pub Co Inc., Singapore*, pp. 68-78.

Silvester, R., 1970. Growth of crenulate shaped bays to equilibrium. *Journal of the Waterways, Harbors and Coastal Engineering Division,* Vol. 96, no. 2: pp. 275-287.

Skjelbreia, L., 1959. Gravity waves: Stokes' third order approximation; tables of functions. *Council on Wave Research, Engineering Foundation*.

Sobey, R.J., 2012. Stokes approximation solution for steep standing waves. *Coastal Engineering Journal*, Vol. 54, no. 2: pp. 76-83.

Sonu, C.J., 1972. Field observation of nearshore circulation and meandering currents. *Journal of Geophysical Research*, vol. 77: pp. 3232–3247.

Sonu, C.J., 1973. Three dimensional beach changes. Journal of Geology, Vol. 81: pp. 42-64.

Sorensen, R.M., 1997. Basic coastal engineering. *Wiley, New York*, 227 p.

Soulsby, R., 1997. Dynamics of marine sands: a manual for practical applications. *Thomas Telford*.

StatisticsNewZealand, 2012. Are New Zealanders living closer to the coast? *Retrieved from http://www.stats.govt.nz/browse_for_stats/population/migration/internal-migration/are-nzs-living-closer-to-coast.aspx.*

Stokes, G.G., 1847. On the theory of oscillatory waves. *Trans Cambridge Philos Soc 8*, pp. 441–473.

Stelling, G., and S. Duinmeijer. 2003. A staggered conservative scheme for every Froude number in rapidly varied shallow water flows. *International journal for numerical methods in fluids*, vol. 43, no. 12: pp.1329-1354.

Stephenson, W.J. 1992. Morphology and morphodynamics of a bay head sand beach, Okains Bay, Banks Peninsula. *A thesis submitted in partial fulfillment of the degree of Master of Science in Geography in the University of Canterbury (Doctoral dissertation, University of Canterbury).*

Storlazzi, C.D., Field, M.E., 2000. Sediment distribution and transport along a rocky, embayed coast: Monterey Peninsula and Carmel Bay, California. *Marine Geology*, vol. 170, no. 3: pp. 289–316.

Storlazzi, C.D., Griggs, G.B., 2000. Influence of El Niño–Southern Oscillation (ENSO) events on the evolution of central California's shoreline. Geological Society of America Bulletin, vol. 112, no. 2: pp. 236–249.

Storlazzi, C.D., Jaffe, B.E., 2002. Flow and sediment suspension events on the inner shelf of central California. Marine Geology, vol. 181, no. 3: pp. 195–213.

Strauss, D., K.D. Splinter, and R. Tomlinson. 2010. Beach nourishment and coastal protection along the Gold Coast, Australia: A case study at Palm Beach. In *Proceedings of Coastal Sediments*: pp. 71-84.

Thomas, T., Phillips, M.R., Williams, A.T., Jenkins, R.E., 2011. Short-term beach rotation, wave climate and the North Atlantic Oscillation (NAO). *Progress in Physical Geography*, no. 35: pp. 333–352.

Thomas, T., Phillips, M.R., Williams, A.T and Jenkins, R.E., 2013. Links between wave forcing and a macro tidal headland bay beach. *Earth Surface Processes and Landforms,* no. 39: pp. 143-155.

The Swan Team, 2013. User manual SWAN Cycle III version 40.91. *Delft University of Technology*.

Thornton, E.B., Guza, R.T., 1989. Wind wave transformation. *Nearshore Sediment Transport, Springer US*: pp. 137–171.

Uda, T., Serizawa, M., Kumada, T. and Sakai, K., 2010. A new model for predicting three-dimensional beach changes by expanding Hsu and Evans' equation. *Coastal Engineering,* Vol. 57, no. 2: pp. 194-202.

URS New Zealand Limited, 2001. Assessment of envi- ronmental effects for Christchurch wastewater discharge. *Christchurch City Council:* 53 p.

Van de Lageweg, W. I., Bryan, K. R., Coco, G., and Ruessink, B. G., 2013. Observations of shoreline–sandbar coupling on an embayed beach. *Marine Geology*, no. *344*: pp. 101-114.

Van der Meer, J.W., Briganti, R., Zanuttigh, B., Wang, B., 2005. Wave transmission and reflection at low-crested structures: Design formulae, oblique wave attack and spectral change. *Coastal Engineering*, no. 52: pp. 915–929.

Van Dongeren, A., A. Bolle, M.I. Vousdoukas, T. Plomaritis, P. Eftimova, J. Williams, C. Armaroli, D. Idier, P. Van Geer, J.V.T. de Vries, and P. Haerens. 2009. Micore: dune erosion and overwash model validation with data from nine European field sites. *Proceedings of Coastal Dynamics*: pp. 1-15.

Vitorino, J., S. Larangeiro, F. Silva, J. Pinto, and S. Almeida. 2010. An operational system for the forecasting of oceanographic conditions in the Nazare Canyon area (W Portugal). *OCEANS 2010 IEEE-Sydney:* pp. 1-5.

Vousdoukas, M.I., Velegrakis, A.F., Dimou, K., Zervakis, V., Conley, D.C., 2009. Wave run-up observations in microtidal, sediment-starved pocket beaches of the Eastern Mediterranean. *Journal of Marine Systems*, vol. 78: pp. S37–S47.

Wang, P., and Kraus, N.C., 2009. Beach profile equilibrium and patterns of wave decay and energy dissipation across the surf zone elucidated in a large-scale laboratory experiment. *Journal of Coastal Research*, pp. 522-534.

Wang, B., Van der Meer, J.W., Otta, A.K., Chadwick, A.J., Horrillo-Caraballo, J., 2005. Reflection of obliquely incident waves at low-crested structures. *Proceedings of Coastal Dynamics*. no. 5: pp. 98-112.

Weesakul, S., Rasmeemasmuang, T., Tasaduak, S., Thaicharoen, C., 2010. Numerical modeling of crenulate bay shapes. *Coastal Engineering*, vol. 57, no. 3: pp. 184–193.

Wiegel, R.L., 1962. Diffraction of waves by semi-infinite breakwater. *Journal of the Hydraulics Division*, no. 88: pp. 27–44.

Wiegel, R. L., 1964. Oceanographical engineering. *Prentice-Hall, Englewood Cliffs, New jersey.*

Wiegel, R.L., 1972. Maximum breaker height. *Journal of the Waterways, Harbors and Coastal Engineering Division*, no. 98: pp. 529–548.

Whitford, D.J., Thornton, E.B., 1993. Comparison of wind and wave forcing of longshore currents. *Continental Shelf Research*, vol. 13, no. 11: pp.1205–1218.

Wiegel, R., 1964. Oceanographical engineering. *Prentice-Hall, Englewood Cliffs, New jersey*.

Weggel, R.J., 1972. Maximum breaker height. J*ournal of the Waterways, Harbors and Coastal Engineering Division*, Vol. 98, no. 4: pp. 529–548.

Williams, A.N., Crull, W.W., 1993. Wave diffraction by array of thin-screen breakwaters. *Journal of waterway, port, coastal, and ocean engineering*, no. 119: pp. 606–617.

Williams, A.N., Vazquez, J.H., Crull, T.W.W., 1995. Oblique-wave diffraction by noncollinear segmented offshore breakwaters. *Journal of waterway, port, coastal, and ocean engineering*, no. 121: pp. 326–333.

Williams, A.T., Ergin, A., Micallef, A., and M.R., Phillips. 2005. The perception of coastal structures: groyned beaches.*Zeitschrift fur Geomorphologie*, no. 141: pp. 111-122.

Williams, A.T., and A., Micallef. 2009. *Beach Management: Principles and Practices*, 445 pp, Earthscan, London.

Woodroffe, C.D., 2002. Coasts: form, process and evolution. *Cambridge University Press*.

Wright, L.D., Nielsen, P., Short, A.D., Green, M.O., 1982. Morphodynamics of a macrotidal beach. *Marine Geology*, vol. 50, no. 3: pp. 97–127.

Yamashita, T., Tsuchiya, Y., 1992. Numerical simulation of pocket beach formation. *Coastal Engineering Proceedings*, vol. 1, no. 23: pp. 2556-2566.

Zanuttigh, B., Andersen, T.L., 2010. Wave reflection in 3D conditions. *Coastal Engineering*, no. 57: pp. 531–538.

Zanuttigh, B., van der Meer, J.W., 2006. Wave reflection from coastal structures, *Coastal Engineering Conference*: pp. 1012-1025.

Zanuttigh, B., van der Meer, J.W., 2008. Wave reflection from coastal structures in design conditions. *Coastal* Engineering, no. 55: pp. 771–779.

Zhang, J., Yang, J., Wen, J., Prislin, I., Hong, K., 1999. Deterministic wave model for short-crested ocean waves: Part I. Theory and numerical scheme. *Applied Ocean Research*, no. 21: pp. 167–188.

Appendix A: Script used for running Utide

```
clear;
clc;
%load currents from file
x=xlsread('currents.xls');

%pick up cross-shore (u) and longshore (v) currents
u(1,:)=x(:,21)/1000;
v(1,:)=x(:,29)/1000;

%pick up water elevations (dep)
dep(1,:)=x(:,12);

%run Utide to analyse tidal currents at cross-shore and
longshore
%directions
a=datenum(2011,4,19,18,00,00)+(1:(1/144):21.39);
coef = ut_solv(a,u,v,-43.6897,'auto','OLS','white');
[u1 v1]=ut_reconstr(a,coef);

%run Utide to analyse water depth (dep1)
clear coef
coef=ut_solv(a,dep,[],-43.6897,'auto','OLS','white');
[dep1]=ut_reconstr(a1,coef);
```

Appendix B: Banks Peninsula Bathymetric map

The bathymetric data were obtained from Land Information New Zealand (LINZ) with a resolution of 3.18 m.